Cell biology of Tumor Protein D54 (TPD54)

Gabrielle Larocque

Thesis submitted for the degree of Doctor of Philosophy
in Medical Sciences

Warwick Medical School, The University of Warwick
December 2017

Contents

List of figures

List of tables

List of abbreviations

2D	Two dimensions
3D	Three dimensions
AAK1	AP2-associated protein kinase 1
ACAP1	Arf-GAP with coiled-coil, ANK repeat and PH domain-containing protein 1
ACSL3	Long-chain acyl-CoA synthetase 3
Akt	RAC-alpha serine/threonine-protein kinase
AP2	Adaptor protein 2
APPL1	Adapter protein containing PH domain, PTB domain and leucine zipper motif 1
Arf6	ADP-ribosylation factor 6
ARH	Autosomal recessive hypercholesterolemia protein
Arp2/3	Actin-related protein 2 and 3
ATM	Ataxia telangiectasia mutated
ATPO	ATP synthase subunit O
BAR	Bin, Amphiphysin, Rvs
BSA	Bovine serum albumin
CCDC53	Coiled-coil domain-containing protein 53
CCS	Clathrin coated structure
CCV	Clathrin-coated vesicles
Ccz1	Vacuolar fusion protein CCZ1 homolog
CD	Cluster of differentiation
Cdc42	Cell division control protein 42 homolog
CGN	cis-Golgi network
CHC	Clathrin heavy chain
CHO	Chinese hamster ovary
Chr	Chromosome
CIMPR	Cation-independent mannose-6-phosphate receptor

CLASP	CLIP-associating protein 1
CLEM	Correlative Light Electron Microscopy
CLIC3	Chloride intracellular channel protein 3
CLIP	CAP-Gly domain-containing linker protein 1
CME	Clathrin-mediated endocytosis
COPA	Coatomer subunit alpha
CORVET	class C core vacuole/endosome tethering complex
CRISPR	Clustered Regularly Interspaced Short Palindromic Repeats
DAB2	Disabled homolog 2
DAPI	4',6-diamidino-2-phenylindole
dKD	Double knockdown
DMEM	Dulbecco Modified Eagle Medium
DNA	Deoxyribonucleic acid
DSCR3	Down syndrome critical region protein 3
ECM	Extracellular matrix
EEA1	Early endosome antigen 1
EGF	Epidermal growth factor
ELISA	Enzyme-linked immunosorbent assay
ER	Endoplasmic reticulum
ERM	Ezrin-radixin-moesin
ESCRT	Endosomal sorting complex required for transport
FA	Focal adhesion
FBS	Foetal bovine serum
FKBP	FK506-binding protein
FN	Fibronectin
FRB	FKBP and rapamycin-binding
GAP	GTPase activating protein
GDI	GDP dissociation inhibitor
GDP	Guanosine diphosphate
GEF	Guanine nucleotide exchange factor
GFP	Green fluorescent protein
GGA	Golgi-localized, gamma ear-containing, ARF-binding protein
GGT	Geranylgeranyl transferase

GLUT4	Glucose transporter type 4
GM130	130 kDa cis-Golgi matrix protein
GST	Glutathione sepharose transferase
GTP	Guanosine-5′-triphosphate
HNRH1	Heterogeneous nuclear ribonucleoprotein H
Hrs	Hepatocyte growth factor-regulated tyrosine kinase substrate
Hsc70	Heat shock cognate 70
ILV	Intraluminal vesicle
IP	Immunoprecipitation
IRES	Internal ribosome entry site
KD	Knockdown
KGF	Keratinocyte growth factor
Kif	Kinesin-like protein
KO	Knockout
KS	Knocksideways
LAMP1	Lysosome-associated membrane glycoprotein 1
LD	Lipid droplet
LECA	Latest eukaryotic common ancestor
M6P	Mannose-6-phosphate
MMP	Matrix metalloproteinase
Mon1	Vacuolar fusion protein MON1 homolog
MSD	Mean squared displacement
MT1-MMP	Membrane type MMP 1
mTOR	Mammalian target of rapamycin
MVB	Multivesicular body
MW	Molecular weight
Myo II	Myosin II
n.s.	Non-significant
NSF	N-ethylmaleimide-sensitive factor
Numb	Protein numb homolog
OCRL	Oculocerebrorenal syndrome of Lowe
ORP1L	Oxysterol-binding protein homolog1
PABP1	Polyadenylate-binding protein 1

PBS	Phosphate-buffered saline
PCR	Polymerase chain reaction
PDGF	Platelet-derived growth factor
PFA	Paraformaldehyde
PI3K	Phosphatidylinositol 3-kinase
PIKfyve	1-phosphatidylinositol 3-phosphate 5-kinase
PIP	Phosphatidylinositol phosphate
PIPK1	Phosphatidylinositol 4-phosphate 5-kinase 1
PM	Plasma membrane
PTB	Phosphotyrosine-binding
Rab	Ras-related protein
Rabex5	Rab5 GDP/GTP exchange factor
Rac	Ras-related C3 botulinum toxin substrate
RASA1	Ras GTPase-activating protein 1
RCP	Rab-coupling protein
RECK	Reversion-inducing cysteine-rich protein with Kazal motifs
REP	Rab escort protein
RILP	Rab-interacting lysosomal protein
RIPA	Radioimmunoprecipitation assay
RME-6	Receptor-mediated endocytosis protein 6
RNA	Ribonucleic acid
ROI	Region of interest
RS	Ribosomal protein S
RT	Room temperature
SEM	Standard error of the mean
SGSM	Small G protein signalling modulator
siRNA	Small interfering RNA
SNAP	Soluble NSF attachment protein
SNARE	SNAP receptor
SNX	Sorting nexin
STML2	Stomatin-like protein 2, mitochondrial
SWIP	Strumpellin and WASH-interacting protein
TACC3	Transforming acidic coiled-coil-containing protein 3

TBC1D5	TBC1 domain family member 5
TBS	Tris-buffered saline
TERA	Transitional endoplasmic reticulum ATPase
Tf	Transferrin
TfR	Transferrin receptor
TGN	trans-Golgi network
TIMP	Metalloproteinase inhibitor 1
TIP47	Tail-interacting protein of 47 kD
TPD	Tumor protein D
TRITC	Tetramethylrhodamine
UTR	Untranslated region
Vamp2	Vesicle-associated membrane protein 2
VDAC3	Voltage-dependent anion-selective channel protein 3
Vps	Vacuolar protein sorting-associated protein
WASH	WASP and Scar homologue
WASP	Wiskott-Aldrich syndrome protein
WB	Western blot
WT	Wild type
Y2H	Yeast two-hybrid

Declaration

This thesis is submitted to the University of Warwick in support of my application for the degree of Doctor of Philosophy. It has been written by myself and has not been submitted in any previous application for any degree. The work presented has been carried out by me, except for these experiments:

- CLEM experiments have been carried out by N.I. Clarke
- The mass spectrometry analysis identifying TPD54 and TPD52 as candidates for endocytic proteins having a mitotic moonlighting role has been published by Kaur et al., 2014

The appendix 1 contains a poster presented at the ASCB in December 2016 presenting my work. On this poster, N.I. Clarke did the CLEM experiment and B. Wilson, under the supervision of P.T. Caswell did the invasion experiments in A2780 cells.
The appendix 4 contains an article to which I have contributed. I have carried out the colocalisation experiments needed after revision presented in figures 3 and S4.

Summary

The expression of Tumor protein D52 (TPD52) family members is deregulated in many types of cancer. When overexpressed, it is suggested that they increase cell proliferation and migration/invasion as well as avoid apoptosis. Deregulation in the expression of the TPDs is therefore linked to poor prognosis. Little characterisation has been carried out to date, but it is known that the TPDs are found in association with components of the membrane trafficking pathway. The aim of this work is to uncover how the least studied member of the family, TPD54, affects cellular processes involved in carcinogenesis, such as cell migration and invasion. By using the knocksideways method, we have been able to map the cellular localisation of TPD54 and have identified association partners. These associations have been confirmed by immunoprecipitation and mass spectrometry analysis. Amongst these was the small GTPase Rab14. We have also found that TPD54 is involved in the trafficking of receptors containing a dileucine motif in their cytosolic tail, but not a tyrosine-based or NPXY motif. With the mapping of the localisation of TPD54, we hypothesise that TPD54 is on the recycling route following the Golgi apparatus, and in association with Rab14, regulates the trafficking of receptors containing a dileucine motif. Integrins are receptors controlling cell migration. They can be trafficked through the Golgi apparatus before being recycled back to the plasma membrane. This recycling route is not well characterised. We therefore hypothesise that TPD54 regulates this route with Rab14, and that this is the reason why TPD54 is important for cell migration, and that a defect in its function can cause cancer.

Chapter 1 – Introduction

1.1 Vesicle trafficking

1.1.1 Overview of vesicle trafficking

After their synthesis in the endoplasmic reticulum (ER), membrane proteins such as receptors, are translocated through the Golgi apparatus for post translational modification and then sent to the plasma membrane in vesicles. These vesicles will merge with the plasma membrane and the newly synthesised receptors will be ready for their first round of ligand binding. The types of ligands they will bind varies a lot, going from nutrients to growth factors and hormones. This is how mammalian cells are able to process signals sent by the environment and neighbouring cells. When a ligand is "caught", the receptor will be internalised and sent inside the cell. There, the ligand is released, and the receptor can be recycled by being transported back to the cell surface for more rounds of internalisation. However, ligand binding to a receptor is not a prerequisite for internalisation. Indeed, some receptors are internalised constitutively whether or not a ligand is bound.

Another way that the cell interacts with its environment is by remodelling it. Whether it is during embryo development or cancerous invasion, cells can remodel the extracellular matrix (ECM) by internalising these molecules and degrading them.

The trafficking of all these molecules is done by lipid vesicles transported by motors on the cytoskeleton. The vesicles are transported between a series of compartmentalised, membrane-formed organelles (**Figure 1.1**). There are a few different pathways that a newly internalised vesicle can take, and this route is dependent on the cargo inside the vesicle. The shortest one is the recycling pathway (orange arrows in **Figure 1.1**). The quickest way for a receptor to go back to the plasma membrane is to unload its ligand in the first

sorting hub, the sorting endosomes. Then, it can go back on the cell membrane through a short or long recycling pathway, leaving the tubular region of the sorting endosomes. A receptor can also go on the endolysosomal pathway, going through the late endosomes and leading to degradation in the endolysosomes (red arrows on **Figure 1.1**). Cargoes can be transported to the Golgi apparatus from the endosomes in a retrograde manner (**Figure 1.1**, blue arrows) and go back to the endosomes in an anterograde manner (**Figure 1.1**, green arrows). Finally, some molecules, like the ECM constituents collagen or fibronectin, are synthesised in the ER and secreted outside. These proteins take the biosynthetic pathway (purple arrows, **Figure 1.1**).

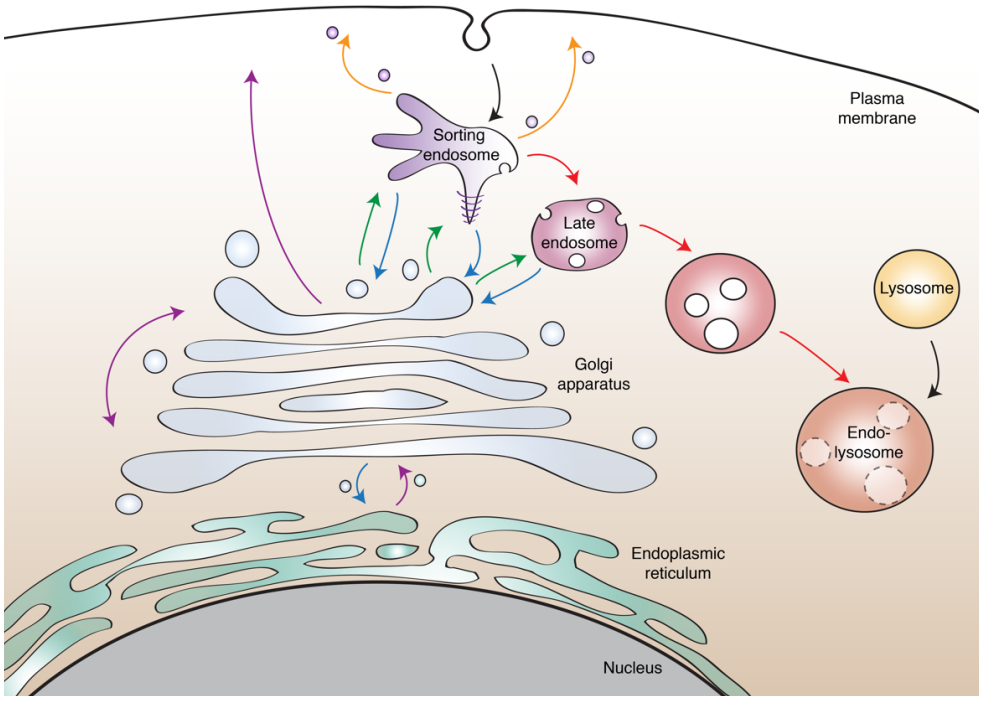

Figure 1.1: Pathways of vesicle trafficking. After invagination at the plasma membrane, a transport vesicle will go to the sorting endosomes. It has two different regions: an early endosomal region from which the fast recycling pathway starts and from which the maturation into late endosomes will happen, and a recycling endosomal region formed of tubules from which the slow-recycling pathway starts. The recycling pathways lead the cargoes from the endocytosed vesicles back to the plasma membrane (orange arrows). The late endosomes lead to the multivesicular body (MVB) and ultimately degradation with the lysosomes (red arrows). A route to the Golgi apparatus is possible (retrograde pathway, blue arrows) from either the late endosomes, the early part, or the recycling part of the sorting endosomes. An opposite route is also possible, going from the Golgi to these endosomes (anterograde pathway, green arrows). Finally, newly synthesised receptors go from the endoplasmic reticulum to the plasma membrane, passing and maturing through the Golgi apparatus (biosynthetic pathway, purple arrows).

This first section will describe the vesicle trafficking pathways and the main proteins acting on the different steps.

1.1.2 Endocytosis

Endocytosis is the process by which cells internalise extracellular material. It is needed for nutrient internalisation and can be hijacked by pathogens to enter the cell. It is also a way of keeping homeostasis in the lipid content of the plasma membrane (Doherty and McMahon, 2009). There are different types of endocytosis. Macropinocytosis forms large vesicles of a diameter of up to 5 µm (Swanson and Watts, 1995), which function in the uptake of fluids and nutrients, in an actin-dependent manner (Bloomfield and Kay, 2016).

Another type of endocytosis uses membrane invaginations coated with caveolin, the caveolae, for internalisation. In endothelia, for example, molecules go from one side of the endothelium to the other, by traversing the cells in caveolae (Cheng and Nichols, 2016).

The best studied type of endocytosis is clathrin-mediated endocytosis (CME). There, triskelia of clathrin molecules assemble in a coat around a vesicle containing the receptors to be internalised (Heuser and Kirchhausen, 1985; Pearse, 1976; Roth and Porter, 1964). CME involves a series of steps tightly regulated by many proteins. It is initiated by an enrichment of receptors. The adaptor protein complex AP2 binds the cytoplasmic tail of the receptor and recruits the clathrin coat. AP2 is the adaptor between the plasma membrane, the receptor (cargo) and the clathrin coat, since clathrin cannot bind the receptors directly (Collins et al., 2002). To be internalised, the receptor must have an endocytic motif on its cytosolic end. This will in turn be bound by an adaptor protein (Bonifacino and Traub, 2003). There are three main endocytic motifs: a dileucine motif ([D/E]XXXL[L/I/M], where X is any amino acid), a tyrosine-based motif (YXXΦ, where Φ is a bulky hydrophobic amino acid) and the [F/Y]XNPX[Y/F] motif. Dileucine and tyrosine motifs can both be bound by AP2. Dileucine motifs are bound by the α-σ2 subunits (Kelly et al., 2008)

whereas tyrosine motifs are bound by the μ2 subunit (Ohno et al., 1995). Although both motifs can bind AP2, they do not compete with each other as the σ and μ subunits are on opposite sides of the adaptor (Marks et al., 1996). The NPXY motif will be bound by the PTB (phosphotyrosine-binding) domain of alternative adaptors, like DAB2, ARH or Numb (Garcia et al., 2001; Mishra et al., 2002; Santolini et al., 2000).

The formation of the clathrin coat is followed by a deformation in the membrane, forming a clathrin-coated pit. BAR domain-containing proteins, such as SNX9, have affinity for curved membrane. SNX9 will bind AP2 and recruit the enzyme dynamin (Bendris and Schmid, 2017). Upon GTP hydrolysis, dynamin undergoes a conformational change and allow membrane fission at the neck of the pit (Sweitzer and Hinshaw, 1998). Once freed from the plasma membrane, the pit is called clathrin-coated vesicle (CCV). It will eventually lose its clathrin coat with the help of auxilin and Hsc70 and be transported inside the cell towards the early endosomes.

1.1.3 Rab GTPases

The Rab proteins are small GTPases of roughly 25 kDa that can be seen as master regulators of the trafficking pathways. Being GTPases, they cycle between a GTP-bound, active state, and a GDP-bound, inactive state. This cycling regulates the numerous steps of the trafficking pathway, from vesicle uncoating after invagination, to vesicle transport by motor proteins and vesicle fusion (Barr, 2013; Stenmark, 2009; Wandinger-Ness and Zerial, 2014; Zhen and Stenmark, 2015). The Rab GTPases are also responsible for endosome maturation (discussed below).

About 8000 Rab proteins have been identified so far throughout 247 genomes. In humans, 66 (isoforms included) can be found (Diekmann et al., 2011; Klopper et al., 2012). The great variety of Rab GTPases results from the fact that some are tissue specific, while each one of them is mainly associated with one organelle, assuring the correct trafficking to and from this organelle (**Table 1.1**). However, Rab protein localisation can overlap in the endosomal system

(Eathiraj et al., 2005), which can lead to formation of Rab-specific domains on one organelle (Sonnichsen et al., 2000).

Table 1.1: List of human Rab GTPases and their localisation.

Rab GTPase	Localisation/function
Rab1	ER to Golgi trafficking
Rab2	Golgi to ER trafficking
Rab3	Secretion, mainly in neurons
Rab4	Fast recycling, sorting endosomes to PM
Rab5	Endocytosis, sorting endosomes
Rab6	Golgi apparatus
Rab7	Late endosomes,
Rab8	Nucleus and PM, cilia
Rab9	Late endosome to Golgi apparatus
Rab10	GLUT4 exocytosis
Rab11	Slow recycling, sorting endosomes, perinuclear region
Rab12	Recycling, autophagosomes
Rab13	EGF endocytosis, tight junctions, recycling
Rab14	Phagosomes, GLUT4 exocytosis, endosomes
Rab15	Recycling
Rab17	Autophagosomes, recycling, filopodia, melanosomes
Rab18	Lipid droplets, ER
Rab19	Endosomes, Golgi apparatus
Rab20	Phagosomes, ER
Rab21	Endocytosis of integrins
Rab22	Sorting endosomes
Rab23	Cilia
Rab24	ER, late endosomes,
Rab25	Recycling of integrins, epithelial cells
Rab26	Lysosomes
Rab27	Melanosomes, secretion
Rab28	GLUT4 trafficking, nucleus
Rab29 (Rab7L1)	Endosomes to Golgi apparatus
Rab30	Golgi apparatus
Rab31	Golgi apparatus, endosomes
Rab32	Endosomes, lysosome-related Organelles, mitochondria
Rab33	ER, Golgi, autophagosomes
Rab34	Macropinosomes
Rab35	Fast recycling, endosomes
Rab36	Melanosomes
Rab37	Insulin exocytosis
Rab38	Endosomes, lysosome-related organelles

Rab39	Secretion, caspase-1 binding
Rab40	Filopodia
Rab41	ER to Golgi
Rab43	ER to Golgi

A genetic study has identified six supergroups amongst the Rab GTPases, classifying them according to their evolution from the last eukaryotic common ancestor (LECA) to humans (**Table 1.2**) (Klopper et al., 2012). This study allows us to understand similarities between certain members of the Rab GTPases large family.

Table 1.2: Regrouping of Rab GTPases present in vertebrates according to their evolution from the latest eukaryotic common ancestor (LECA) (adapted from Köpper et al., 2012).

	LECA	Vertebrata
Group I	Rab1	Rab1a
		Rab1b
		Rab35
		Rab33a
		Rab33b
		Rab19
		Rab43
		Rab30
	Rab8	Rab8a
		Rab8b
		Rab13
		Rab12
		Rab15
		Rab10
		Rab3a
		Rab3b
		Rab3c
		Rab3d
		Rab26
		Rab27
		Rab27a
		Rab27b
		Rab34
		Rab36
		Rab45
		Rab44a
		Rab44b
	Rab18	Rab18
		Rab40a
		Rab40aL
		Rab40c
		Rab40d
Group II	Rab5	Rab5a
		Rab5b
		Rab5c
		Rab17
	Rab21	Rab21

	Rab22	Rab22a
		Rab22b
	Rab24	Rab24
		Rab20
	RabX1	
Group III	Rab7	Rab7a
		Rab7b
		Rab9a
		Rab9b
	Rab23	Rab23
	Rab29	
	Rab32	Rab32
		Rab38
	Rab7L1	Rab7L1
Group IV	Rab2	Rab2a
		Rab2b
		Rab39a
		Rab39b
		Rab42
	Rab4	Rab4a
		Rab4b
	Rab11	Rab11a
		Rab11b
		Rab25
	Rab14	Rab14
Group V	Rab6	Rab6a
		Rab6b
		Rab6c
		Rab41
Group VI	Rab28	Rab28
	RabL4	RabL4

1.1.3.1 The Rab cycle

Rab GTPases cycle between an active and inactive state, and this cycle can be mainly described as such: a GDI (GDP dissociation inhibitor) escorts the Rab-GDP to the correct 'donor' membrane. A Rab GEF (guanine nucleotide exchange factor) will activate the Rab by exchanging GDP for GTP. Effectors (proteins that can bind Rab GTPases only in their GTP-bound state) can then bind the Rab proteins and allow them to regulate the pathway on which they are until the Rab proteins reach an 'acceptor' membrane. A GAP (GTPase activating protein) will inactivate the Rab GTPase by hydrolysing GTP into GDP. The GDI will be able to bind the Rab-GDP to recycle it back to the donor membrane, for another cycle (**Figure 1.2**) (Stenmark, 2009).

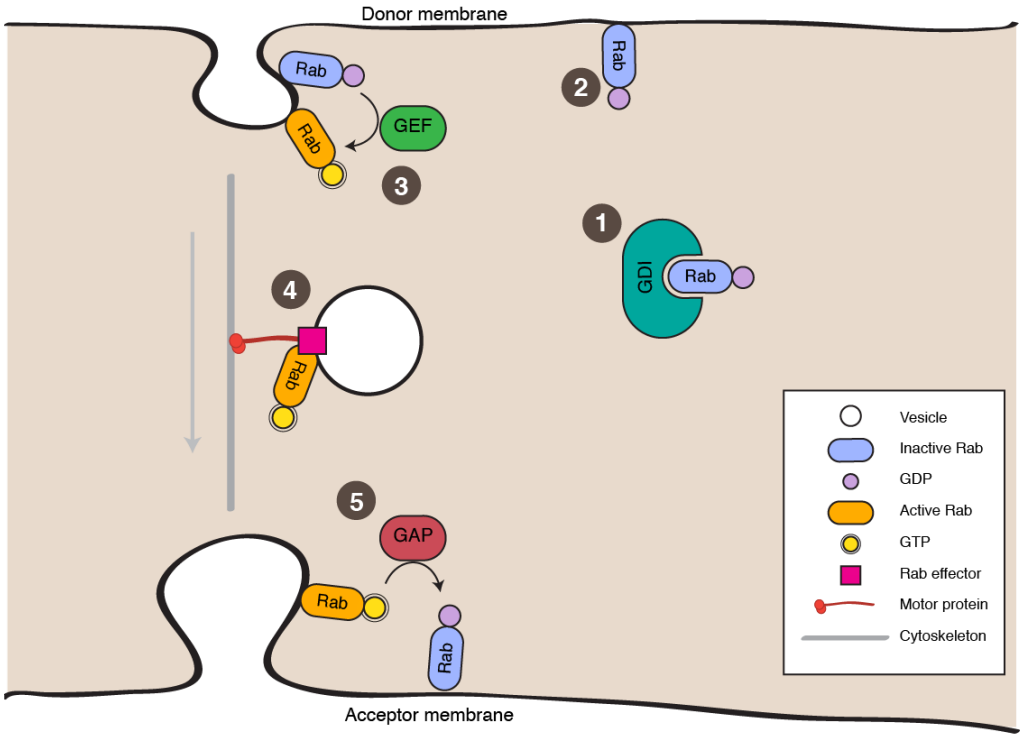

Figure 1.2: The Rab GTPase cycle. 1-2. A GDI escorts the Rab-GDP to the right initial donor membrane. 3. A GEF activates the Rab GTPase by changing the GDP for GTP. 4. The GTP-bound Rab can bind effectors and together regulate the trafficking pathway. 5. On the acceptor membrane, a GAP inactivates the Rab GTPase by hydrolysing GTP into GDP and the GDI can escort the Rab-GDP back for another cycle.

To be inserted into membranes, Rab GTPases needs prenylation (addition of a geranylgeranyl group) at its C-terminal, by a GGT (geranylgeranyl transferase) and a REP (Rab escort protein). The REP escorts the prenylated Rab to the right membrane (Leung et al., 2006). This geranylgeranyl group is hydrophobic, so when it is not hidden in membrane, the Rab GTPase needs to be chaperoned by the GDI, which hides the hydrophobic tail (Goody et al., 2005). The Rab's association with the GDI is how it can stay soluble (Ullrich et al., 1993). It is thought that the GDI-Rab complex can 'sample' many types of membranes, inserting and extracting the Rab from these membranes, until the association of the GTPase with a membrane is stabilised, generally by the presence of the Rab's specific GEF (Barr, 2013). By changing GTP for GDP, the GDI cannot extract the Rab anymore, and the effectors can bind the Rab and further stabilise it on the donor membrane (Blumer et al., 2013; Gerondopoulos et al., 2012; Pylypenko et al., 2006; Wu et al., 2010).

1.1.3.2 Rab GTPases in trafficking pathways

The Rab GTPases control the trafficking pathways via their binding with their multiple effectors while in GTP-bound state. These effectors have a broad range of functions: they can be phosphatases, kinases, motors, tethers, adaptors, membrane fusion regulators, etc. (Gillingham et al., 2014). To add another level of complexity, some effectors for one Rab can be GAPs or GEFs for other Rabs. For example, the Rab9 effectors SGSM1 and SGSM2 are GAPs for Rab32, Rab33 and Rab36 (Nottingham et al., 2011; Nottingham et al., 2012). By binding to the activated late endosomal Rab9, SGSM1 can inactivate the melanosome-related Rab32 and regulate their biogenesis (Ohbayashi et al., 2017). Another example is the HOPS complex. It is an early endosome-related Rab5 effector and a GEF for the late endosome-related Rab7. By binding to the activated Rab5, it can in turn activate Rab7, allowing the maturation of the early endosome in a late endosome (Rink et al., 2005).

As mentioned above, Rab GTPases are master regulators of the trafficking pathway via their association with different binding partners that will control every step of trafficking, from vesicle budding to vesicle fusion to the acceptor membrane.

Rab5-GDI complex has been shown to be required for clathrin-coated vesicle assembly *in vitro* (McLauchlan et al., 1998) . The same GTPase and its GEF RME-6 are important for uncoating of AP2 on newly budded endocytic vesicles. AAK1 is responsible for AP2 phosphorylation, which increases AP2 binding to $PI(4,5)P_2$ (Conner and Schmid, 2002). In an opposite way, RME-6 promotes dephosphorylation of AP2, making its binding to $PI(4,5)P_2$ unstable, which makes AP2 fall off the vesicle (Semerdjieva et al., 2008).

Once the vesicle is uncoated, it travels along the cytoskeleton towards its final destination. For shorter translocations, vesicles utilise the actin cytoskeleton. One of the motor protein 'walking' along actin is myosin V (Mehta et al., 1999). A few Rab GTPases (Rab3, Rab6, Rab8, Rab11, Rab14, Rab25, Rab27, Rab39) have been found to interact directly with myosin Va or Vb (Lapierre

et al., 2001; Lindsay et al., 2013; Nagashima et al., 2002) therefore making actin a molecule that many types of endosomes, melanosomes and secretion vesicles can use to reach their destination.

For longer trajectories, vesicles will rather use the microtubules. Dynein and the different members of the kinesin family are the motors used by the trafficking organelles moving along microtubules (Aniento et al., 1993; Bonifacino and Neefjes, 2017). Like for myosin V, many Rab GTPases can bind microtubule-associated motors. For example, Rab5 interacts with Kif16B to translocate early endosomes (Hoepfner et al., 2005; Nielsen et al., 1999). Rab4 has a role in the regulation of KifC2: when the GTP is hydrolysed, KifC2 motility is increased (Bananis et al., 2004). Rab7 is involved in the recruitment of dynein and is important for the transport of lysosomes, together with two effectors of Rab7's, RILP and ORP1L (Cantalupo et al., 2001; Johansson et al., 2007; Jordens et al., 2001).

Once the vesicle has reached its destination, Rab GTPases also regulate the fusion of the vesicle with the acceptor membrane. One good example for this is Rab5 and its effector EEA1 (early endosome antigen 1), resident of the sorting endosomes. It has been known for a while that EEA1 interacts with the SNARE syntaxin 6 or 13 (McBride et al., 1999; Simonsen et al., 1999; Simonsen et al., 1998), but it is only recently that Rab5-GTP has been shown to induce a conformational change in the long rod-shaped EEA1 that allow the tether to bring two vesicles together for subsequent fusion (Murray et al., 2016).

Since Rab GTPases affect so widely all parts of the trafficking pathway, it is to be expected that a deregulation in their expression can lead to generalised diseases like cancer. For example, high expression levels of Rab25 is a marker for breast and ovarian cancers (Cheng et al., 2004). It has been shown to be one of the few Rabs that can bind directly to the cytoplasmic tails of the extracellular matrix receptor integrins, specifically integrin $\alpha 5\beta 1$ (Caswell et al., 2007). By doing so, Rab25 regulates the recycling of the integrins and an overexpression of the protein is linked with increased invasion (Caswell et al.,

2007; Dozynkiewicz et al., 2012). In a similar manner, Rab21 also binds integrin β1 and control its endocytosis, therefore affecting cells attachment to their substrate and motility (Pellinen et al., 2006).

1.1.4 Endosomes

The classical view is that endosomes are distinct compartments, each having a defined set of proteins contributing to their function (Johannes and Popoff, 2008; Lieu and Gleeson, 2011; Pfeffer, 2009). However, it is becoming clear that such a precise segregation cannot be done. Endosomes are very dynamic organelles with different regions on one compartment, sorting receptors to different places, and losing proteins and gaining new ones while scission and maturation happen (**Figure 1.3**) (Bonifacino and Rojas, 2006; Huotari and Helenius, 2011; Johannes and Wunder, 2011; Progida and Bakke, 2016; Scott et al., 2014; Sonnichsen et al., 2000). Here, the traditional early endosomes and recycling endosomes will be called sorting endosomes (Hsu et al., 2012). It has been shown to have different microdomains characterised by either proteins (Sonnichsen et al., 2000) or lipids (Yoshida et al., 2017), further reinforcing the idea of sorting endosome rather than having separate early and recycling endosomes. The sorting endosome is the main hub for receptor sorting, since the internalised receptors can take one of the three available pathways from there: a recycling pathway to go back to the plasma membrane, a retrograde pathway to the trans-Golgi network (TGN) or a pathway leading to degradation in the endolysosomes.

1.1.4.1 Arrival in the endosome

The first region to be reached by internalised receptors is the early region of the sorting endosome, or early endosome. Its lipid composition is different than the plasma membrane (phosphatidylinositol 3-phosphate (PI(3)P) instead of $PI(4,5)P_2$, respectively). Rab5 and its effector Vps34, alongside the inositol 5-polyphosphatase OCRL1 (oculocerebrorenal syndrome of Lowe) are

responsible for the changes in lipid composition (Prosseda et al., 2017; Shin et al., 2005). Once the lipid composition is changed, Rab5 also recruits EEA1 (Simonsen et al., 1998) which binds one endosome's PI(3)P (Patki et al., 1997) on one end, and another endosome's Rab5 (Simonsen et al., 1998) on the other end. The binding of Rab5 induces a conformation change in EEA1 and instead of having a long, rod shape, EEA1 collapses to bring the two vesicles closer for fusion (Murray et al., 2016). EEA1 and Rab5 are therefore responsible for tethering incoming endocytic vesicles and preparing them for fusion with the endosome.

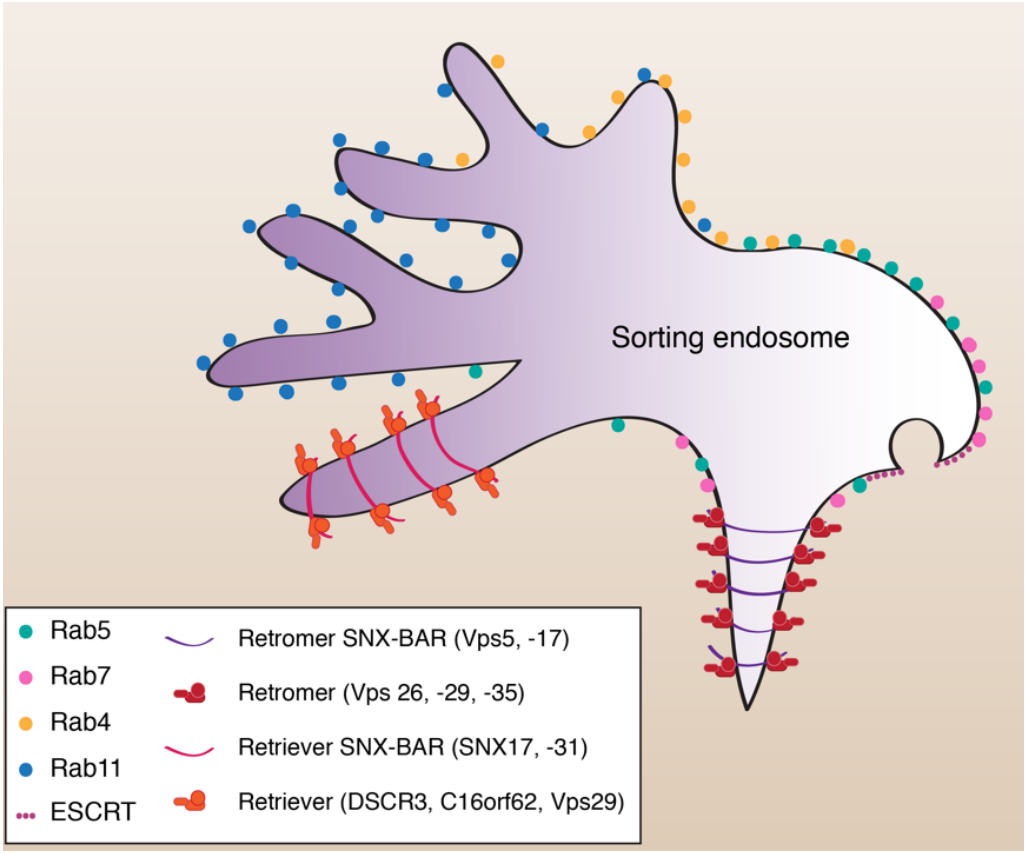

Figure 1.3: The sorting endosome. The sorting endosome is a sorting hub for receptors. They will be sorted through associations with different residents of the endosome. These proteins form domains that can be associated with the traditional view of early endosome (Rab5, Rab4), early endosome maturing towards becoming a late endosome (Rab5, Rab7, ESCRT), and recycling endosome (Rab4, Rab11). Alongside the recycling region of the sorting endosome, two complexes can also sort and recycle receptors either towards the Golgi apparatus or the plasma membrane (retromer and retriever).

As mentioned earlier, the sorting endosome is thought to have three regions, determined by the heterogeneity of the protein repartition. The part receiving the endocytic vesicle is the early endosome region. It is mainly characterised by the presence of Rab5 and EEA1, but also Rab4 and APPL1, although APPL1 colocalises only sparsely. Indeed, only about 30% of endosomes contain both EEA1 and APPL1 (Kalaidzidis et al., 2015). It is thought that these APPL1/EEA1-positive endosomes are sorting hubs where receptors are sorted for fast or slow recycling (Kalaidzidis et al., 2015).

CORVET (class C core vacuole/endosome tethering complex), is another protein complex associated with the early region of the endosomes. It binds Rab5 and facilitates tethering and fusion of vesicles to the endosomes (Balderhaar et al., 2013; Peplowska et al., 2007).

1.1.4.2 Endosomal recycling

Once in the sorting endosome, cargoes are "scanned" and sorted either for degradation or recycling. Example of protein having such a role are SNX17, which sends the ECM receptor integrins out or RCP, which sends the transferrin receptor (TfR) back to the surface (Bottcher et al., 2012; Peden et al., 2004). The fast recycling pathway is Rab4-dependent and sends receptors back to the plasma membrane either directly from the early endosomal region, or through the recycling endosomal region of the sorting endosomes (Vandersluijs et al., 1992; Wandinger-Ness and Zerial, 2014). This recycling endosomal part is characterised by the presence of Rab4, Rab11 and its tubular morphology. One of the main molecules used for studying receptor recycling is the transferrin receptor. It has been shown that the TfR is mainly colocalised with Rab5, 5 minutes post-internalisation, colocalised with Rab4 after 7 minutes, gradually losing its colocalisation with Rab5 after 7 minutes until 30 minutes, and colocalises with Rab11 on the slow recycling pathway after 30 minutes, to be completely returned to the plasma membrane after 60 minutes (Sonnichsen et al., 2000). This shows that internalisation is very quick

and that TfR can get returned to the plasma membrane via both recycling pathways (Ullrich et al., 1996).

1.1.4.3 Endolysosomal degradation

If a receptor needs to be downregulated after internalisation, it will be sent for degradation on the endolysosomal pathway and tagged with ubiquitin molecules. This is achieved by a series of endosome maturing steps starting in the sorting endosome. First, the so-called "Rab switch" needs to occur (Huotari and Helenius, 2011) (**Figure 1.4**). When Rab5-GDP arrives near an endosome, the GEF Rabex-5 activates Rab5 which can then bind to the endosome, and Rabaptin-5, a Rab5 effector, promotes Rabex-5 activity (Horiuchi et al., 1997; Lippe et al., 2001). The switch occurs when Ccz1 and Mon1 bind Rab5 and displace Rabex-5/Rabaptin-5. Rab5 will then return to its GDP-bound, inactive state. Then, Ccz1/Mon1 can move GDI from Rab7 which activates Rab7, and Rab7/Ccz1/Mon1 bind the maturing endosome's membrane (Kinchen and Ravichandran, 2010; Poteryaev et al., 2010; Wurmser et al., 2000). The newly acquired Rab7 and Ccz1 can in turn recruit HOPS, a Rab7 effector. The late endosomal Rab9 also plays a role in the maturation since it binds the Rab5 GAP SGSM3, making Rab9 a player in Rab5 inactivation (Gillingham et al., 2014; Kucera et al., 2016).

The lipids of the late endosomal membrane are mainly made of $PI(3,5)P_2$. PIKfyve is responsible for the lipid composition change (Odorizzi et al., 1998; Zolov et al., 2012). At the same time, the Hrs subunit of ESCRT-0 can bind the PI(3)P and the ubiquitin tags of the receptors in the sorting endosomes going to the degradative pathway. After binding of the other ESCRT complexes, the receptors will be invaginated within the endosome and this intralumenal vesicle (ILV) will be pinched off. This process is also used as a way to inactivate signalling receptors (Huotari and Helenius, 2011; Scott et al., 2014). The late endosomes mature gradually by losing "early" components and characteristics. Structurally, tubules are lost and ILVs are gained, SNARES necessary for fusion with other early endosomes are also lost,

as well as the ability to recycle receptors directly to the plasma membrane, and lysosomal proteins are transported from the Golgi apparatus to the late endosomes (Huotari and Helenius, 2011). The compartment acidity also changes, going from 6.2 to 5.5-5.0. The acidification is needed for the enzymatic activity of lysosomal proteins and the uncoupling of the receptors and their ligand (Scott et al., 2014). At this stage, the late endosome can be called multivesicular body (MVB). MVB will use microtubule motors to move towards the perinuclear region and ultimately fuse with lysosomes to form the degradative endolysosomes (Huotari and Helenius, 2011). There is at least one escape route from the late endosome, by returning to the Golgi apparatus in a Rab9 dependent manner (Barbero et al., 2002).

The cation-independent mannose-6-phosphate receptor (CIMPR) is one example of transmembrane protein able to escape the degradative route. It is needed to bring newly synthesised lysosomal enzymes to the lysosomes. These enzymes are tagged with mannose-6-phosphate in the Golgi, which bind CIMPR. CIMPR will then be sent to the endosomes in AP1- and GGA-dependent manner (Doray et al., 2002). CIMPR reaches the sorting endosome during the Rab switch and can therefore be colocalised with Rab5 and Rab7 (Kucera et al., 2016). Being on the endolysosomal pathway, CIMPR will eventually free its ligand in the acidic environment of the late endosomes and return to the Golgi apparatus in a Rab9-dependant way for another round of trafficking (Ganley et al., 2004; Riederer et al., 1994). TIP47, a putative Rab9 effector is also thought to be required for the retrograde trafficking of CIMPR (Carroll et al., 2001; Diaz and Pfeffer, 1998), although controversy exists on this matter, since another team has suggested that TIP47 does not bind to Rab9 and does not affect the recycling of CIMPR, and is indeed involved in lipid droplets metabolism (Bulankina et al., 2009).

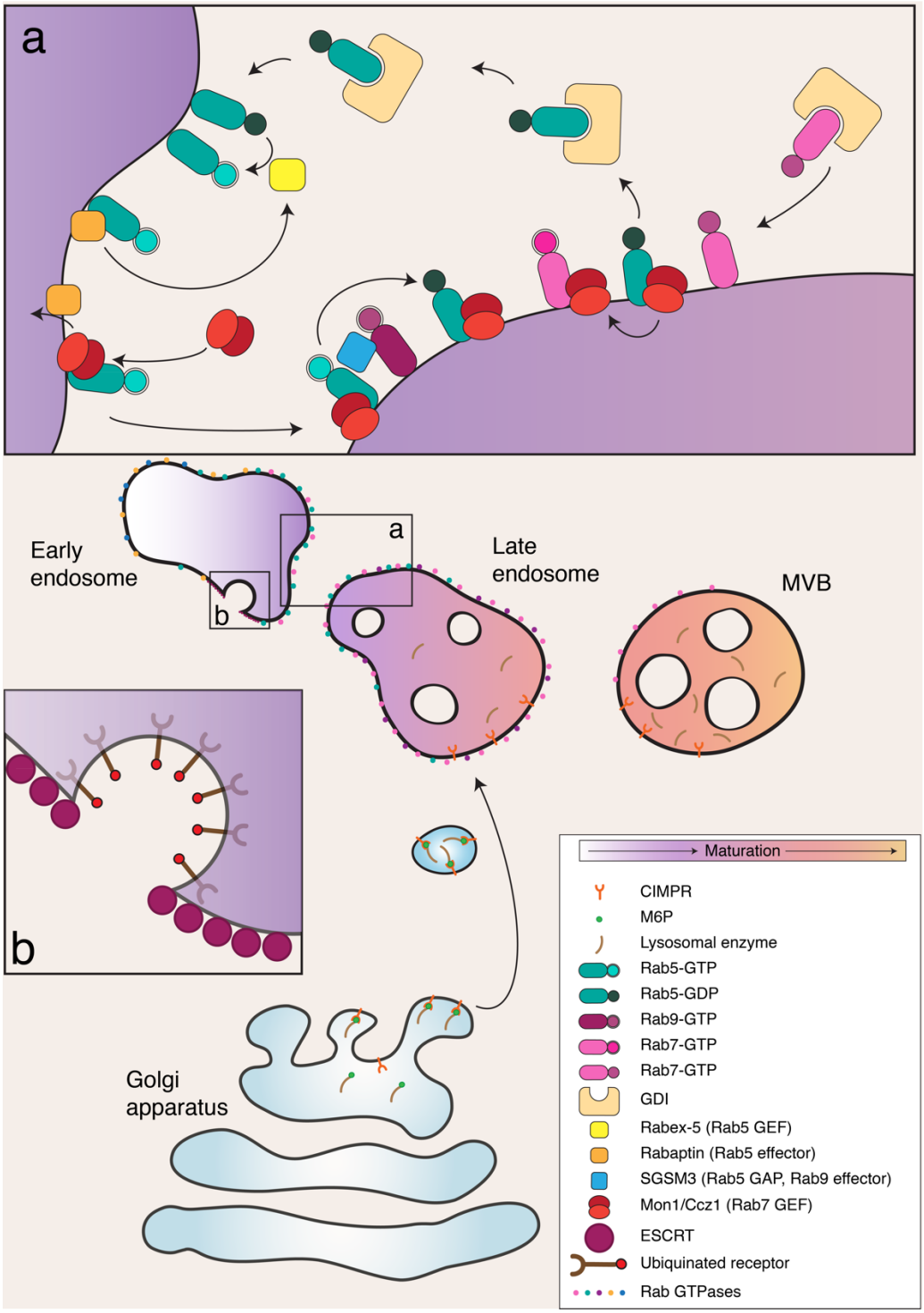

Figure 1.4: Endosome maturation. The early region of the sorting endosome will undergo maturation in order to become a late endosome, then a multivesicular body (MVB) that will eventually fuse with a lysosome for the degradation of ubiquitinated receptors. For an efficient degradation, the endolysosome needs lysosomal enzymes. After their synthesis, they are translocated to the Golgi apparatus where they will be tagged with mannose-6-phosphate. This tag will be recognised by transporters like CIMPR and the lysosomal enzymes will be transported to the endosomes. a) Zoom on the Rab switch. Rab5-GDP are transported to early endosomes with their chaperone, GDI. When Rab5-GDP is inserted into the membrane, Rab5-GDP becomes Rab5-GTP by the action of the GEF Rabex-5. The

effector Rabaptin in turns binds Rab5-GTP and positively regulates Rabex-5 to keep Rab5 activated. It takes the complex Mon1/Ccz1 to displace Rabaptin and stop this activation cycle. Then, the Rab9 effector SGSM3 inactivates Rab5-GTP with its GAP activity. Mon1/Ccz1 is a GEF for Rab7 and activates it, while Rab5-GDP is taken by GDI for another cycle. b) Zoom on ESCRT segregation of ubiquitinated receptors into intralumenal vesicles for degradation.

1.1.4.4 Retrograde transport from the sorting endosome

CIMPR does not only return to the Golgi apparatus via Rab9, but also from the sorting endosomes in a retromer-dependant manner (Arighi et al., 2004; Seaman, 2004). Retromer is a complex formed by a combination of sorting nexin 1 (SNX1) or SNX2 and SNX5, SNX6 or SNX32, along with Vps26, Vps29 and Vps35 (Horazdovsky et al., 1997; Rojas et al., 2007; Seaman et al., 1998; Wassmer et al., 2007). The membrane-bending ability of the SNXs create tubules on the endosomal membrane. Receptors accumulates in these tubules which will be recognised by the Vps proteins. The Vps proteins form a coat for the transport to the Golgi apparatus (Gallon and Cullen, 2015). Rab5 is needed for the presence of the SNX-Vps complex (Rojas et al., 2008) and Rab7 binds to Vps35, which will stay bound throughout the endosomal maturation (Rojas et al., 2008; Seaman et al., 2009; van Weering et al., 2012). Retromer is also needed for the completion of the maturation since Vps29 binds the Rab7 GAP TBC1D5 which inactivates Rab7 (Mukhopadhyay et al., 2007; Seaman et al., 2009). Although the retromer is generally involved in the endosome/TGN retrograde pathway, it has been shown to also be involved in transport of the β2-adrenergic receptor from endosomes to the plasma membrane in a SNX27- and Rab4-dependant manner (Temkin et al., 2011). The retromer-dependent trafficking of CIMPR needs the WASH complex (Gomez and Billadeau, 2009). WASH is made of five subunits (WASH1, strumpellin, SWIP, FAM21 and CCDC53) and is the main actin nucleating factor on endosomes (Derivery et al., 2009; Seaman et al., 2013). It colocalises with early endosomal markers like Rab5 and EEA1 (Duleh and Welch, 2010) or late endosomal/MVB marker like Rab7 and CD63 (Zech et al., 2011). It recruits the Arp2/3 complex, which in turn promotes actin

polymerisation. This is thought to create WASH-positive domains on the endosomes and therefore to organise actin around these domains in order to segregate proteins into them and arrange recycling routes out of the endosomes (Derivery et al., 2012; Puthenveedu et al., 2010).

Recently, a new protein complex, called retriever, involved in endosomal recycling has been identified (McNally et al., 2017). Much like the retromer, the retriever is a trimer. It is formed of DSCR3, C16orf62 and Vps29 and it interacts with SNX17. The retriever has been identified because SNX17 is involved in the recycling of β1 integrin from the endosomes in a retromer-independent manner (Steinberg et al., 2012).

Finally, there is some evidence for a retrograde pathway to the Golgi from the recycling endosomes, notably in a Rab11- and RCP-dependent manner (Jing et al., 2010). However, this pathway has yet to be defined, since recycling endosomes are poorly characterised on a molecular level (Johannes and Wunder, 2011).

1.2 Cell migration

Whether it is leucocytes chasing a bacterium, mesenchymal cells in an embryo or epithelial cells closing a wound, cellular migration is an important process utilised by many cell types in normal conditions. Although this process is highly controlled, deregulation in one of the many steps can occur and can lead to cancer and metastases. Indeed, an increased migratory ability is a hallmark of cancer (Paul et al., 2017).

1.2.1 Steps of cell migration

In order to start the migrating process, cells have to establish polarity. They need a leading edge and a trailing end. Although cells can be polarised spontaneously (Wedlich-Soldner and Li, 2003), polarity is generally established in response to chemotactic signals secreted by neighbouring cells and bound to the extracellular matrix (ECM). The main chemotactic molecules

are cytokines and growth factors like platelet-derived growth factor (PDGF), epidermal growth factors (EGF) and keratinocyte growth factors (KGF). These molecules will bind the receptors and initiate a signalling cascade inducing polarity (Majumdar et al., 2014; Maritzen et al., 2015). The plasma membrane composition also helps to establish polarity. PI3K is kept at the cell front and generates $PI(3,4,5)P_3$, which can amplify the response to chemotactic signals (Cain and Ridley, 2009; Funamoto et al., 2002; Iijima et al., 2002).

The morphology of a polarised cell changes whether the cell is migrating in a 2D or 3D environment. A cell migrating through tissues like a leucocyte through an endothelium will adopt an amoeboid or mesenchymal shape: elongated front for better insertion between other cells and rounded, deformable back (Friedl, 2004). The cell crawls forwards and, in the case of leucocytes, can move rapidly because of low interaction points with the ECM or other cells (Friedl et al., 1998). In the case of cells migrating on a 2D substrate, they will have an elongated tail and a lamellipodium at the leading edge. The lamellipodium is composed of a polymerising network of actin filaments. It is this polymerisation that pushes forward the plasma membrane for the cell to move (Keren and Shemesh, 2017). In both cases, cells migrating in 2D or 3D rely on actin protrusions in the plasma membrane for movement, except in the case of bleb migration, a type of migration used in 3D substrates. These cells use extensions in the anterior plasma membrane caused by hydrostatic pressure exerted by the actomyosin cortex (Mierke, 2015). Another variation of the bleb migration is the formation of lobopodia, small bleb formations on a cylindrical protrusion at the front of the cell (Petrie et al., 2012).

The actin polymerisation in the leading edge is the result of the signalling cascade initiated by the growth factor/chemokine binding to their receptors at the cell surface. The small GTPase Cdc42 is activated by this cascade. It is essential for maintenance of the cell polarity in most cell types (Heasman and Ridley, 2008; Nobes and Hall, 1999). It keeps the Golgi apparatus oriented in the direction of the movement and makes sure that the lamellipodium activity

stays at the cell front by recruiting the actin cytoskeleton at the front and activates another GTPase, Rac (Nobes and Hall, 1995). Rac is also activated by the binding of growth factors to their receptors. It activates the nucleation promoting factor (NPF) which in turn activates the actin nucleator Arp2/3. To keep Rac functioning at the lamellipodium, it is recycled in an Arf6-dependent manner to the cell front, ensuring furthermore the maintenance of polarity (Palamidessi et al., 2008). This recycling also creates a gradient of concentration of Rac at the front and another small GTPase, Rho is kept at the cell rear. Rho is responsible for the maintenance of cellular adhesions to the ECM (Nobes and Hall, 1999).

Once the protrusion is made, contraction of the actomyosin cortex will retract the tail and allow the cell to move. Rho, Rac and Ras (responsible for the turnover of the cellular adhesions (Nobes and Hall, 1999)) all play a role in this process. Non-muscle myosin II is activated by Rho at the front of the cell and induces contraction and tail retraction (Chrzanowska-Wodnicka and Burridge, 1996; Nalbant et al., 2009; Vicente-Manzanares et al., 2009). While the cell contracts and the tail retracts, the adhesions at the back need to be removed and replaced at the front. It is the adhesions at the front that allow force transmission through the actin stress fibres (Ridley et al., 2003). As well as controlling the turnover of adhesions, Ras is also required for the stress fibres turnover (Nobes and Hall, 1999).

When these migratory steps are deregulated, cells can become cancerous and induce metastases. Cellular adhesions are weaker or recycled more rapidly. Cell migration isn't growth factor-dependent anymore, and other chemotactic signals increase even more cell motility. There is also an increased release of proteases into the ECM in order to invade more efficiently (Hanahan and Weinberg, 2000; Porther and Barbieri, 2015a; Porther and Barbieri, 2015b). This shows that each and every step of cell migration needs to be tightly regulated in healthy individuals.

1.2.3 Cellular adhesion assembly

Cellular adhesions are the anchor points into the cell's environment. They are a direct link between the ECM components and the actin stress fibres. The main constituents of the ECM are collagen, elastin, fibronectin (FN), laminin, glycoproteins, proteoglycans and glycosaminoglycans (Keren and Shemesh, 2017). The ECM is secreted by the cells and serves as a physical scaffold for the cells to be embedded in. The ECM proteins are generally large. For example, FN is made of 2 subunits of about 250 kDa bound covalently together, and laminin is a trimer of between 400 and 800 kDa.

Adhesions are made of many different proteins, which are added while the adhesion is maturing until its turnover. Nascent adhesions are the first clusters to be made. They form in the lamellipodium and will either disassemble or mature (Alexandrova et al., 2008). It has been shown recently that, at least in fibroblasts, the addition of adhesion component is initiated by an increase in the plasma membrane tension following protrusion formation (Pontes et al., 2017). The next maturation stage is the focal complex. Its formation is myo II-dependent and is positioned at the border between the lamellipodium and the lamellum. Finally, the mature form is a focal adhesion (FA). They are at the end of actin bundles and measure between 2 and 10 μm (Valdembri and Serini, 2012).

The central constituent of the FAs are the integrins. These receptors for ECM components are made of a dimer of an α and β subunit. There are 18 different α integrins and 8 β integrins, for a total of 24 different heterodimers (Paul et al., 2015). Every cell type presents integrins, except for erythrocytes (De Franceschi et al., 2015). Integrin dimers exist in three conformations: inactive, primed and active (**Figure 1.5**). The ligand binds the active form, although it is also thought that the primed form can bind ligands (Adair et al., 2005). Integrins are activated from the inside by talin. It binds to the β subunit and induces a conformational change separating the two dimers and straightening them to allow ligands to bind with higher affinity (Iwamoto and Calderwood, 2015; Kim et al., 2003; Luo and Springer, 2006; Tadokoro et al., 2003;

Vinogradova et al., 2002). After talin, vinculin is recruited, then α-actinin, before this complex can be linked to the actin fibres (Parsons et al., 2010). Talin, α-actinin, vinculin and kindlin are responsible for the clustering of multiple integrin dimers and the growth of the adhesion (Ellis et al., 2014; Humphries et al., 2007; Roca-Cusachs et al., 2013; Ye et al., 2013). During the maturation process, paxillin is also recruited, which will in turn recruit other structural and signalling molecules (Brown and Turner, 2004) (**Figure 1.6**).

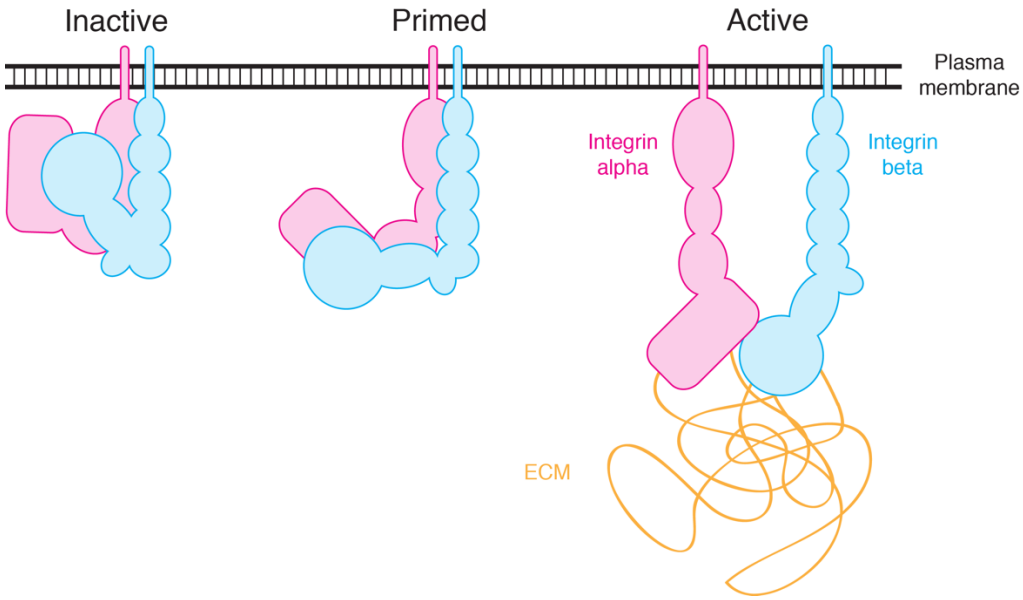

Figure 1.5: Structure of integrin dimer. The Three conformations available for an integrin dimer.

There are two other adhesion types, which are more specialised. Podosomes are ring-shaped adhesions present in fast moving cells and invadopodia are present in invasive cells. Generally, these adhesions are called podosomes in normal cells, while the term invadopodia is used for cancer cells. Invadopodia are the site of active ECM degradation by proteases, which allow cancer cells to invade more efficiently (Linder et al., 2011).

1.2.4 Cellular adhesion disassembly and integrin recycling

To allow the cell to move, adhesions need to be removed and their components have to be recycled. The inactive integrins, for example on the dorsal side of a migrating cells on a 2D substrate, also have to be internalised to be brought at a new adhesion site.

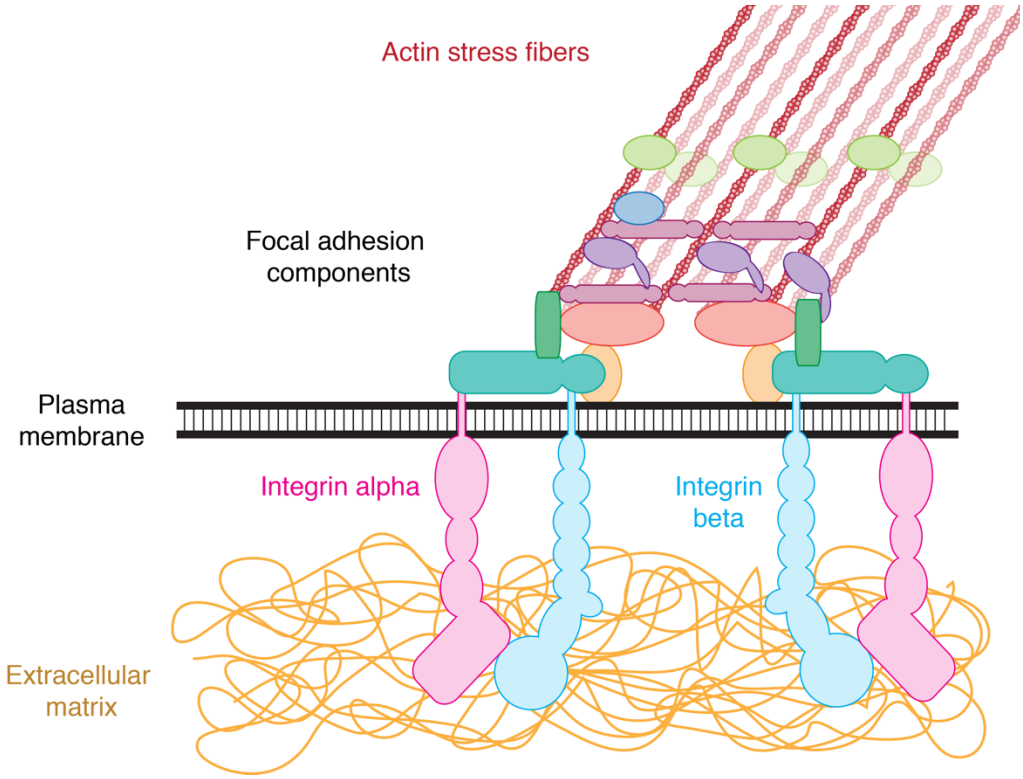

Figure 1.6: Sagittal plane of a focal adhesion. Integrins dimer formed of an α and β subunit binding the extracellular matrix. Inside the cell, the focal adhesion components (e.g. talin, vinculin, paxillin, α-actinin, focal adhesion kinase…) are the link between the integrins and the actin stress fibre.

On adhesion sites, the first step for the adhesion disassembly is matrix degradation by matrix metalloproteinases (MMPs). They will cleave, for example, FN bound to its main receptor, α5β1 integrins (Shi and Sottile, 2011). The adhesion will then be able to be recycled. MT1-MMP, a type of MMP, is brought to the plasma membrane in a Rab4- or Rab11-dependent pathway, if it comes from somewhere else on the plasma membrane, or in a Rab8-dependent manner from the Golgi apparatus (Bravo-Cordero et al., 2007). MMPs also arrive at the surface through filopodia, giving these

structures the ability to invade. Rab40b has been involved in this process (Jacob et al., 2013). Another step of disassembly is integrin and talin cleavage by calpain (Bate et al., 2012; Franco et al., 2004). Cleaved talin is important for adhesion turnover by allowing release of the focal adhesions components (Saxena et al., 2017). Microtubules have also been involved in the turnover of FAs. They make contact with the FAs with the tethers CLASP1 and CLASP2 (Stehbens et al., 2014). Microtubules deliver the endocytic machinery necessary for the internalisation of the integrins. Clathrin and the alternative adaptors ARH and Dab2 are needed for this (Ezratty et al., 2009; Ezratty et al., 2005; Kaverina et al., 1999). AP2 has also been shown to be important for the internalisation of adhesions. The kinase PIPK1β is recruited to the adhesions and generates $PI(4,5)P_2$ and allows AP2 to do the internalisation of integrin β1 (Chao et al., 2010). Different adaptor proteins can bind different types of integrins: Dab2 regulates α5β1 dimer internalisation in the mid region of the cell, while Numb regulate the endocytosis of the dimer on the leading edge (Teckchandani et al., 2012).

Although clathrin-mediated endocytosis clearly internalises integrins, this can also be done via clathrin-independent endocytosis. Caveolin-1 can internalise α5β1and αvβ3 integrins (Galvez et al., 2004; Shi and Sottile, 2008), and in cholestoreol-depleted cells, integrins can enter the cells via lipid rafts (Fabbri et al., 2005).

There are three models for the recycling of integrins, which all occur depending on the situation. The first and main model is the treadmill-like model in which integrins are removed from the back of the cell and placed at the front, allowing an efficient forward migration (Bretscher and Aguado-Velasco, 1998). In the second one, integrins are also recycled from the front of the cell allowing it to keep a pool of integrins available for fast migrating cells (Caswell et al., 2007; Laukaitis et al., 2001). Finally, in the third model, some integrins are trafficked from the front to the back in a Kif1C/microtubules-manner, allowing the adhesions in the tail to mature and

the tail to steer for a directional migration (Theisen et al., 2012). This is also the case in cancer cells, where integrins are first sent to the lysosomes. Instead of being degraded, the integrins are recycled back to the rear end in a CLIC3- and Rab25-dependant manner (Dozynkiewicz et al., 2012).

Integrin recycling is a well-studied but complex field of membrane traffic. Many different routes are taken by many different heterodimers, depending on the identity of these dimers, or their activation state (De Franceschi et al., 2015; Iwamoto and Calderwood, 2015; Paul et al., 2015; Rainero and Norman, 2013). Integrin recycling is efficient, the surface pool can be recycled within 30 minutes (Paul et al., 2015). This is the main fate for the integrins, only few of them are degraded. The half-time of the degradation process is approximately 12-24h (Lobert et al., 2010).

Both active and inactive integrins are internalised in a Rab5/Rab21-dependant manner (Arjonen et al., 2012; Pellinen et al., 2006). There is an endocytic motif (NPXY) on the cytosolic chain of integrin β1, which can be recognised by Numb and Dab2 (Nishimura and Kaibuchi, 2007). After entering the sorting endosomes, the integrin dimers will be recycled differently according to the situation. It has been found that active integrins can be sent to the lysosomes for degradation or back to the plasma membrane either in a direct way, via ACAP1-, RCP- and Rab11-dependant pathway or indirectly as mentioned earlier, in a Rab25- and CLIC3-dependant pathway (Arjonen et al., 2012; Caswell and Norman, 2008; Dozynkiewicz et al., 2012; Li et al., 2005; Powelka et al., 2004). Inactive integrins will rather be sent back to the plasma membrane either in a Rab25-dependant, local manner (Caswell et al., 2007) or via the short, Arf6- and Rab4-dependant recycling pathway (Arjonen et al., 2012). At least for the recycling of integrin β1, Ras GTPase-activating protein 1 (RASA1) displaces Rab21 to allow the integrin recycling (Mai et al., 2011).

The WASH complex has also been involved in the recycling of integrins. By recruiting the actin nucleator Arp2/3, integrin-containing vesicles are transported to recycling endosomes by actin-dependant motors. It has been shown that in the absence of WASH, integrin α5β1 is sent to the lysosomes

for degradation (Duleh and Welch, 2010; Zech et al., 2011). The NPXY motif present on the β subunit of the integrin dimer can also be bound by SNX17 which sends it back to the plasma membrane, in a retriever-dependant way (Bottcher et al., 2012; McNally et al., 2017; Steinberg et al., 2012). Finally, if the integrins are ligand-bound, they become ubiquitilated, which is recognised by the ESCRT machinery and the integrins will be invaginated into ILVs and send for degradation in the endolysosome (Lobert et al., 2010).

The recycling of integrins not only has a direct effect on migration by allowing new adhesions to be made, it also has an effect on the persistence of the migration. Indeed, there is a balance between two dimers. The recycling of α5β1 integrins allow cells to move rapidly in a random manner, whilst the recycling of αvβ3 integrins allow a more persistent migration (Danen et al., 2005; White et al., 2007). One type of recycling also inhibits the other, allowing the cell to either scan its environment or migrate in the same direction (White et al., 2007).

1.3 Tumor protein D52 (TPD52) family

The TPD52 family members are short proteins of about 200 amino acids. There are four members in humans, TPD52, TPD53, TPD54 and TPD55. The proteins are encoded by the genes TPD52, TPD52L1, TPD52L2 and TPD52L3, respectively. These genes are all on different chromosomes (8q21.13, 6q22.31, 20q13.33 and 9p24.1 respectively). While the first three are ubiquitously expressed, TPD55 is restricted to testis (Cao et al., 2006). All four members have a coiled-coil domain in the N-terminal region (**Figure 1.7**).

TPD52 is the most well studied member of the family, as well as being the first identified. It was cloned 20 years ago, from breast cancer cells (Byrne et al., 1995). TPD53 and TPD54 were then cloned shortly afterwards (Byrne et al., 1996; Byrne et al., 1998; Nourse et al., 1998) and TPD55 ten years later (Cao et al., 2006).

A plethora of articles have been written in the past 4 years, all stating that a deregulation of the level of the TPDs in different cancer cells cause abnormal migration, survival or proliferation. However, some of these articles (He et al., 2015; Wang et al., 2014b; Xu et al., 2015; Yang et al., 2015) present strikingly similar results, use erroneous controls or shRNAs for their target gene depletions (Byrne and Labbe, 2017), and the majority does not propose any mechanistic explanation for these alterations (Fujita and Kondo, 2015; Goto et al., 2014; He et al., 2015; Kumamoto et al., 2016; Li et al., 2017; Mukudai et al., 2013; Wang et al., 2014a; Wang et al., 2016; Yang et al., 2015; Yu et al., 2017; Zhao et al., 2017; Zhu et al., 2016). However, one thing that seems clear, is that the TPDs have some role in cell migration and/or invasion, on adhesion and on the cell cycle.

```
TPD52_ MDCREMDLYEDYQSPFDFDAGVNKSYLYLSPSGNSSPPGSPTLQKFGLLRTD-PVPEEGE 59
TPD53_ ----------------------------------------MEAQAQGLLETE-PLQGTDE 19
TPD54_ ---------------------------MDSAGQDINLNS---PNKGLLSDSMTDVPVDT 29
TPD55_ -------------------------------------------------MPHARTETSVGT 12
                                                          :         .

TPD52_ DVAATISATETLSEEEQEELRRELAKVEEEIQTLSQVLAAKEKHLAEIKRKLGINSLQEL 119
TPD53_ DAVASADFSSMLSEEEKEELKAELVQLEDEITTLRQVLSAKERHLVEIKQKLGMNLMNEL 79
TPD54_ GVAARTPAVEGLTEAEEEELRAELTKVEEEIVTLRQVLAAKERHCGELKRRLGLSTLGEL 89
TPD55_ YESHSTSELEDLTEPEQRELKTKLTKLEAEIVTLRHVLAAKERRCGELKRKLGLTALVGL 72
                . *:* *:.**: :*.::* ** ** :**:***::  *:*::**:. :  *

TPD52_ KQNIAKGWQDVTATSAYKK-------------------TSETLSQAGQKASAAFSSVGS 159
TPD53_ KQNFSKSWHDMQTTTAYKK-------------------THETLSHAGQKATAAFSNVGT 119
TPD54_ KQNLSRSWHDVQVSSAYVKTSEKLGEWNEKVTQSDLYKKTQETLSQAGQKTSAALSTVGS 149
TPD55_ RQNLSKSWLDVQVSNTYVK----------------------------QKTSAALSTMGT 103
       :**::::.* *: .:.:* *                            **::**:*.:*:

TPD52_ VITKKLED-------------VKNSPTFKSFEEKVE----NLKSKVGGTKPAGGDFGEVL 202
TPD53_ AISKKFGDMSYSIRHSISMPAMRNSPTFKSFEERVETTVTSLKTKVGGTNPNGGSFEEVL 179
TPD54_ AISRKLGD-------------MRNSATFKSFEDRVG----TIKSKVVGDRENGSDNLPSS 192
TPD55_ LICRKLGG-------------VKKSATFRSFEGLMG----TIKSKVSGGKRAWP------ 140
        * :*: .              :::* **:***  :     .:*:** * .

TPD52_ NSAANASATTTEPLPEKTQESL--- 224
TPD53_ SSTAHASAQSLAGGSRRTKEEELQC 204
TPD54_ AGSGDK--PLSDPAPF--------- 206
TPD55_ ------------------------
```

Figure 1.7: Alignment of the TPD52 family members. The four members of the family aligned according to their amino acid sequence. The coiled-coil domain is highlighted in yellow. TPD52 has a phosphoserine marked in red. "*" means conserved residue. "**:**" means strongly similar, "**.**" means weakly similar.

Early work on the TPDs have established their upregulation in cancer cells is caused by duplication and this leads to their tumorigenic effect (Balleine et al., 2000; Byrne et al., 1998; Lewis et al., 2007; Wilson et al., 2001). TPD53 has been shown to be expressed at the highest level at the G2/M transition (Boutros and Byrne, 2005) and phosphorylation of TPD52 on serine at position 176 is important for normal cytokinesis (Thomas et al., 2010a). This suggests that the TPDs might indeed be regulated by the cell cycle, especially that this serine is conserved in all 4 members of the family (**Figure 1.7**). It also has been shown that the PI3K/Akt pathway is activated when TPD52 is overexpressed in the human colon carcinoma cell line SW480 (Li et al., 2017). This pathway regulates signalling, from cytokines to growth factors. A deregulation is therefore likely to induce carcinogenesis (Spangle et al., 2017). Another pathway deregulated with a TPD52 overexpression is the NF-κB pathway. NF-κB controls transcription of cytokines increasing cell proliferation (Sun, 2017). It has been shown that TPD52 affects this pathway by binding NF-κB. This results in increased levels of TIMP and RECK RNA, which are two inhibitors of MMP-9 and MMP-2 (matrix metalloproteinase) (Dasari et al., 2017). MMPs are responsible for degradation of the ECM, allowing cells to invade (Hastie and Sherwood, 2016). An overexpression of TPD52 confers to the cells an increased ability to invade their surroundings. Finally, it has been shown that an overexpression of TPD52 decreases ATM-mediated DNA repair signalling (Chen et al., 2013). ATM (ataxia telangiectasia mutated) is a member of the PIKK family that phosphorylates proteins in response to DNA damage in order to induce DNA repair (Clouaire et al., 2017). The residues on TPD52 required for this role are aa 151-171 (Chen et al., 2013). This region is not conserved in TPD53 which has an insertion in this site, and not very conserved in TPD54 and TPD55, making this role likely to be unique to TPD52 (**Figure 1.7**).

Another role for TPD52 is its putative role in lipid droplet biogenesis. Lipid droplets (LDs) are contained by a phospholipid monolayer and act as fat reserve and storage for excess fatty acids (Chen et al., 2016). They are thought

to be formed in the ER and translocated to the Golgi apparatus before being released in the cytoplasm (Fujimoto and Parton, 2011; Wilfling et al., 2014). There was good evidence for investigating the role of TPD52 in lipid biogenesis. A screen made in obese vs lean mice showed that Tpd52 was upregulated up to 5-fold in obese mice (Nadler et al., 2000). In *C. elegans*, a depletion of TPD52 orthologue F13E6.1 is linked to decreased lipid storage (Ashrafi et al., 2003). In a yeast two-hybrid (Y2H) assay, TPD52 has been shown to bind perilipin-1, a protein associated with lipid droplets (Yamaguchi et al., 2006). Finally, proteomic studies say that TPD52 and TPD54 could interact with cholesterol in HeLa cells (Hulce et al., 2013) and are thought to be able to bind $PI(3,4,5)P_3$ (Catimel et al., 2009). It is only recently that the link between TPD52 and LDs has been directly investigated. It has been confirmed that TPD52 is present in the LDs fraction of human breast carcinoma cells MDA-MB-231. It also colocalises with the cis-Golgi marker GM130 and with Arl1, a GTPase involved in golgin recruitment and LDs formation (Kamili et al., 2015). It therefore seems that TPD52 might accompany LDs out of the Golgi apparatus.

The TPDs have also been linked to trafficking in other contexts. A Y2H assay has suggested that TPD52 can bind Rab5c. It has been confirmed with a GST-pulldown. The same Y2H result was found for TPD53, although the authors only mentioned the pulldown confirmation and didn't show the data in the article (Shahheydari et al., 2014). TPD52 could also be co-immunoprecipitated with ExoS a *Pseudomonas aeruginosa* toxin able to inhibit Rab5 functions (Simon and Barbieri, 2014; Zhang et al., 2007). TPD52 is also found in colocalisation with Rab27a and Lamp1 when phosphorylated in CHO cells (Thomas et al., 2010b). This phosphorylation is the same phosphorylation site found to be important for cytokinesis (Thomas et al., 2010a) and is known to be Ca^{2+}-dependent (Thomas et al., 2002). Ca^{2+}-dependent signal induces secretion of digestive enzymes in pancreatic acinar cells. In these cells, TPD52 is thought to regulate secretion. At resting state, TPD52 colocalises with TGN38 (rat orthologue of the trans-Golgi network

protein TGN46) and after stimulation of secretion, TPD52 is found under the apical plasma membrane and colocalises with early, late and recycling endosomes, regulating exocytosis of digestive enzymes (Messenger et al., 2013).

Finally, TPD53 has been shown *in vitro* to enhance the binding of synaptobrevin 2 and syntaxin 1, two SNAREs required for membrane fusion. The coiled-coil domain of TPD53 is required for this and it binds directly to synaptobrevin 2 (Proux-Gillardeaux et al., 2003). The coiled-coil domain is featured in each member of the TPD52 family (**Figure 1.7**). It might be possible that if TPD53 is a SNARE, the other members might also be.

What we need to focus on is the fact that TPD54 has not yet been well characterized, being the ubiquitously expressed member of the TPD52 family the least studied. It seems clear that it has a role in membrane trafficking since it might be able to bind lipids (Catimel et al., 2009; Hulce et al., 2013) and by sequence similarity to TPD52 and TPD53. TPD54 is also probably involved in regulation of cell migration and adhesion (Mukudai et al., 2013). The molecular mechanisms behind these roles are still elusive.

1.4 Aim of the thesis

We want to provide mechanistic insight into the role of TPD54 in membrane trafficking and cell migration, in order to finally explain why a deregulation in the expression level of the protein causes pathologies like cancer.

To do so, we will try to understand which type of membrane trafficking vesicle TPD54 is associated to and assess the consequences of depleting HeLa cells of TPD54, either by knockdown or knockout, as well as rapidly rerouting the protein for a more precise phenotype, less likely to be compensated by the cells.

We will also use similar tools to understand the role of TPD54 in cell migration in a 2D environment. We will try to link the potential role in cell

migration to its association to membrane trafficking components by investigating the role of TPD54 in the recycling of integrins.

Chapter 2 – Material and methods

2.1 Cell culture

2.1.1 Cell maintenance

HeLa cells (HPA/ECACC #93021013) were grown in Dulbecco Modified Eagle Medium (DMEM) (GIBCO 32430) supplemented with 1% antibiotics (100 U/ml penicillin, 100 µg/ml streptomycin) and 10% foetal bovine serum (FBS). RPE1 cells (HD-PAR-541 clone 7724) were grown in Ham's F12 Nutrient Mixture (Sigma, D6421) supplemented with 1% antibiotics (pen/strep), 10% FBS, 2.3 g/l sodium bicarbonate and 2 mM L-Glutamine. Both cell types were kept at 37°C with 5% CO_2 and the growth medium was changed every 3-4 days. HeLa cells were kept for a maximum of 30 passages and RPE1 cells for 20 passages.

2.1.2 siRNA transfection

Cells were plated on coverslips or in plates for a confluency of 50% on day 1 ($10x10^4$ cells/ml). On day 2, Lipofectamine 2000 (Thermo Fisher Scientific) was used to transfect the siRNAs according to the manufacturer's protocol. The oligonucleotides used are listed in table 2.1. If DNA was also transfected, the siRNA lipoplexes were left on the cells for ~6 h before plasmid transfection, otherwise, they were left until the next morning. Cells were processed 24-72h post-transfection. If two genes were knocked down, the total amount of oligonucleotides was doubled.

2.1.3 DNA transfection

Cells were plated on coverslips or in plates for a confluency of 50% on day 1 ($10x10^4$ cells/ml). On day 2, GeneJuice (EMD Millipore, 70967) was used to transfect plasmids according to the manufacturer's protocol. Medium was changed the next day and cells were processed 24-72 h post-transfection.

Table 2.1: Oligo sequences

Protein target	siRNA sequence (5′ – 3′)
TPD54, oligo 1	CUCACGUUUGUAGAUGAAA
TPD54, oligo 2	GUCCUACCUGUUACGCAAU
TPD54, oligo 3	CAUGUUAGCCCAUCAGAAU
Rab4a (Keil and Hatzfeld, 2014)	GAACGAUUCAGGUCCGUGA
Rab11a (Shafaq-Zadah et al., 2016)	GACGACGAGUACGACUACC
GL2 (luciferase, control)	CGTACGCGGAATACTTCGA

2.2 Molecular biology

2.2.1 Cloning: general protocol

The gene of interest was either first amplified by polymerase chain reaction (PCR) and then digested with restriction enzymes alongside the vector, or directly cut from a donor vector and pasted into an acceptor vector. In both case, the digested vector and insert were ligated with Quick ligase (NEB, M2200) and transformed in XL10 *E. coli*. Colonies were then tested by extracting their plasmidic DNA with GeneJET Plasmid Miniprep Kit (Thermo Sientific, K0503) and by digesting this DNA with the same restriction enzymes used for earlier digestion. The clones giving two bands of the right size were sent for sequencing to GATC Biotech UK. The clone giving the correct sequence was added to the Royle Lab plasmid collection.

2.2.2 Cloning: constructs made

Table 2.2: List of constructs cloned for this study

Construct name	Technique used for insert	Primers used
(PGK) GFP-TPD54 XV:79	Cut and paste	NA
pIRES-EGFP-TPD54	PCR	GL027 – GL028
GFP-MAL2	PCR	GL056 – GL057
GFP-Rab1a	PCR	GL050 – GL051
GFP-Rab2a	PCR	GL052 – GL053
GFP-Rab6	PCR	GL048 – GL049
GFP-Rab14	PCR	GL054 – GL055

Table 2.3: List of primers and their sequence

Primer identifier	Protein target	Sequence (5′ – 3′)	Annealing T (°C)
GL027	TPD54	GCGGCTAGCATGGACTCCGCCGGCC	52
GL028		GCGCTCGCGTTAGAAAGGTGCGGGATC	
GL048	Rab6	GCGAAGCTTAATGTCCACGGGCGGAG	50
GL049		GCGGGTACCTTAGCAGGAACAGCCTC	
GL050	Rab1a	GCGGAGCTCAATGTCCAGCATGAATCCC	52
GL051		GCGGGTACCTTAGCAGCAACCTCCACC	
GL052	Rab2a	GCGGAGCTCAATGGCGTACGCCTATCTC	52
GL053		GCGGGTACCTCAACAGCAGCCGCCC	
GL054	Rab14	GCGGTCGACaaATGGCAACTGCACCATACAAC	56
GL055		GCGGGTACCCTAGCAGCCACAGCCTTC	
GL056	Mal2	GCGAAGCTTAATGTCGGCCGGCGGAG	54
GL057		GCGGGTACCTTACGGTCGCCATCTTCG	

2.2.3 Plasmids used

Table 2.4: List of plasmids in this study

Construct	Database identifier	Insert	Vector	Restriction sites	Author/ Supplier
(CMV) GFP-TPD54	VIII:44	TPD54	pEGFP-C1	*Xho*I/*Mfe*I	Royle Lab
mCherry-TPD54	X:14	TPD54	pmCherry-C1	*Xho*I/*Mfe*I	Royle Lab
GFP-FKBP-TPD54	X:17	FKBP-TPD54	pEGFP-C1	*Xho*I/*Mfe*I	Royle Lab
mCherry-FKBP-TPD54	X:33	FKBP-TPD54	pmCherry-C1	*PspOM*I/ *BamH*1	Royle Lab
mCherry-FKBP-TPD52	X:32	FKBP-TPD52	pmCherry-C1	*PspOM*I/ *BamH*1	Royle Lab
FLAG-TPD54	VIII:45	TPD54	pFLAG-C1	*Xho*I/*Mfe*I	Royle Lab
pMito-mCherry (K70N)-FRB	XV:81	MitoTrap	pMito	–	Royle Lab
pMito-paGFP-FRB	VII:29	MitoTrap	pMito	*Age*I/*BsrG*I	Royle Lab
GFP-FKBP	IX:28	FKBP	pEGFP-C1	*Nhe*I/*Bgl*II	Royle Lab
CD8-8xA	VII:32	CD8-8xA	pIRES-Neo2	–	MS Robinson
CD8-YAAL	VII:33	CD8-YAAL	pIRES-Neo2	–	MS Robinson
CD8-EAAALL	VII:34	CD8-EAAALL	pIRES-Neo2	–	MS Robinson
CD8-FANPAY	VII:35	CD8-FANPAY	pIRES-Neo2	–	MS Robinson
CD8-CIMPR	VII:31	CD8-CIMPR	pIRES-Neo2	–	MS Robinson
GFP	I:02	–	pEGFP-C1	–	Royle Lab
pmNeonGreen-Rab4a	XIII:77	Rab4a	pmNeonGreen	*Xho*I/*BamH*I	Allele Biotech
GFP-Rab5	X:30	Rab5a	pEGFP-C3	*BsrG*I/*BamH*I	F Barr
GFP-Rab8	XI:16	Rab8a	pDEST53	–	M Nachury

GFP-Rab9	X:27	Rab9a	pEGFP-C3	–	F Barr
GFP-Rab11a	X:40	Rab11a	pEGFP-C2	–	P Caswell
GFP-Rab25	X:41	Rab25	pEGFP-C2	–	P Caswell
GFP-EEA1	XI:21	EEA1	pEGFP-C1	*Xho*I/*EcoR*V	S Corvera
LAMP1-GFP	XI:18	LAMP1	pEGFP-N3	*EcoR*I/*Sal*I	E Dell'Angelica
mCherry-OCRL1	VIII:16	OCRL1	pmCherry-C1	*Xho*I/*Xma*I	C Merrifield
GFP-Vamp2	I:64	Vamp2	pEGFP-C1	*Hind*III/*EcoR*I	Royle Lab
GFP-SNX5	IV:26	SNX5	pEGFP-C1	–	P Cullen
GFP-TACC3	VI:14	TACC3	pEGFP-C1	*Xma*I/*Xba*I	Royle Lab
CD8-FRB-mCherry (K70N)	XII:53	FRB	pMitoTrap	–	Royle Lab
Integrin-α5-GFP	XI:14	Integrin-α5	pEGFP-N3	*Kpn*I/*Kpn*I	R Horwitz
pmNeonGreen-TfR	XIII:81	TfR	pmNeonGreen	–	Allele Biotech

2.3 Biochemistry

2.3.1 Western blotting

Cell lysates were obtained by scraping the cells in 30-50 µl of RIPA buffer (10 mM HEPES pH 7.4, 150 mM NaCl, 0.1% SDS, 1% Triton-X100) on ice. The lysate was left on ice for 15 min, vortexed regularly, and then centrifuged at 14 000 rpm for 15 min at 4°C in an Eppendorf Centrifuge 5417R. The protein content in the supernatant was quantified with the Bradford method and an equal amount of protein was loaded with 5X Laemmli sample buffer (250 mM Tris-Cl pH 6.8, 10% SDS, 0.5% bromophenol blue, 50% glycerol, 25% β-mercaptoethanol) for a final concentration of 1X, in a 9x6 cm 4-15% acrylamide gel and ran at 100-150 V until the blue line is at the bottom of the gel. The proteins were then transferred to a nitrocellulose membrane using a semi-dry Trans-Blot Turbo (BioRad) at 2.5 A for 6 min. Total proteins were revealed with Ponceau stain and the membrane was then blocked for 1 h in 5% milk in TBS-T (20 mM Tris, 150 mM NaCl, 0.1% Tween 20, pH 7.6). The primary antibodies (see table 2.5 for specific dilution) were diluted in 2% milk in TBS-T and the membrane was incubated in this solution for the amount of time and at the temperature indicated in table 2.5. The membrane was then washed by incubation in TBS-T for 5 min, 3 times. The HRP-conjugated

secondary antibodies were diluted 1:10 000 in 2% milk in TBS-T and the membrane was incubated in the solution at room temperature for 1 h. The membrane was then dried with absorbant paper and secondary antibodies were detected by ECL. The membrane was put in a cassette and a radiological film captured the luminescence. The film was developed with a Xograph Compact X4 developer.

Table 2.5: Antibodies used for western blotting

Primary antibody target	Supplier	Working concentration
Rabbit anti-TPD54	Dundee Cell products	1:1000 (RT, 1h)
Rabbit anti-Rab4	Cell Signaling (2167)	1:1000 (4°C, O/N)
Rabbit anti-Rab11a	Abcam (ab65200)	1 µg/ml (1:1000) (4°C, O/N)
Mouse anti-clathrin heavy chain TD.1	hybridoma	1:1000 (RT, 1h)
Mouse anti-GFP clones 7.1 and 13.1	Sigma Roche (118144600010)	1:1000 (RT, 1h)
Mouse anti-α-tubulin DM1	Abcam (ab7291)	1: 10 000 (RT, 1h)

2.3.2 Integrin recycling assay

The ELISA plate (maxisorp 96 wells, Thermo Scientific) was prepared the day before the experiment by incubating the wells with 50 µl/well of 5 µg/ml of anti-integrin α5 antibodies (BD Biosciences, 555651) in 0.05 M Na_2CO_3 pH 9.6, overnight at 4°C. 20x10 cm dishes were needed per condition, and labelled as follows: 1: total, 2-4: blank, 5-8: internal pool, 9-12: 10 min recycling, 13-16: 20 min recycling, 17-20: 30 min recycling. RPE1 cells were serum starved (growth medium +antibiotics –serum) for 30 min at 37°C. Two washes were made with 5 ml of cold PBS and the surface receptors were labelled with 0.133 mg/ml of EZ-Link Sulfo-NHS-SS-Biotin (Thermo scientific, 21331) in PBS by gently rocking (7 see-saw movements/min) the cells at 4°C with 3 ml of the biotin solution for 30 min. The cells were washed twice with 5 ml of cold PBS on ice and 5 ml of warm growth medium serum-free was

added to plates 5-20, while plates 1-4 were left on ice. Plates 5-20 were incubated at 37°C for 30 min to allow internalisation of the receptors. Plates 5-20 were washed with 5 ml of cold PBS on ice.

The surface of the cells was reduced to remove non-internalised receptors by washing plates 2-20 once with 5 ml of cold reduction buffer (50 mM Tris pH 7.5, 102.5 mM NaCl, pH adjusted to 8.6) and then putting 3 ml of reduction buffer and 1 ml of reduction buffer containing mesna (sodium 2-mercaptoethane sulfonate) (390 mg of mesna was added to 26 ml of reduction buffer, mixed thoroughly and 39 µl of 10 N NaOH was added). The plates were rocked at 4°C for 20 min, while plate 1 was left on ice. The cells were washed twice with 5 ml of cold PBS. Plates 1-8 were left on ice with PBS while warm serum-free growth medium was added to plates 9-20. These plates were incubated at 37°C for 10, 20 or 30 min. Plates 2-20 were then reduced again for 20 min with the same method as described above. 1 ml of reduction buffer containing iodoacetamide (IAA, 442mg in 26 ml PBS) was added to the 4 ml of reduction buffer to quench the reduction reaction, and left for 10 min. This reduction step gets rid of the labelled recycled receptors, leaving labelled only the internal receptors in the cells.

At this point, the ELISA plate was blocked with 5% BSA in PBS-T at room temperature for ~1h. Plates 1-20 were washed twice with 5 ml of cold PBS on ice. Lysates were obtained by scraping the cells with a total of 100 µl/condition of lysis buffer (200 mM NaCl, 75 mM Tris pH 7.5, 15 mM NaF, 1.5 mM Na_3VO_4, 7.5 mM EDTA, 7.5 mM EGTA, 1.5% Triton-X100, 0.75% Igepal, protease inhibitors), passing the lysate through a 27G needle and centrifuging the lysate at 13 000 rpm for 15 min at 4°C. The ELISA plate was washed twice with PBS-T and 50 µl of lysate was put in each well. The plate was covered with parafilm and incubated at 4°C overnight.

The plate was then washed with PBS-T five times and 50 µl of 1 µg/ml streptavidin-HRP, 1% BSA in PBS-T was added to each well and left at 4°C for 1 h. Five more washes were performed with PBS-T and 50 µl of detection reagent (add 0.56 mg/ml of ortho-phenylenediamine dihydrochloride in

ELISA buffer (25.4 mM $NaHPO_4$, 12.3 mM citric acid, pH 5.4) mix thoroughly and add 0.003% H_2O_2) was added to the wells. The plate was incubated at room temperature in the dark and after 10-20 min, the plate was read at 450 nm with a Varioskan Flash (Thermo Scientific).

2.4 Imaging

2.4.1 Widefield microscopy

For widefield microscopy, a Nikon Eclipse Ti-U microscope was used with a CoolSNAP Photometrics Myo camera after illumination with a laser at 488, 568 or 633 nm, and using a 20X (0.50 NA) air, a 40X ELWD (0.60 NA) air, 60X (1.40 NA) oil or 100X (1.40 NA) oil objectives. If needed, the cells were kept at 37° C in a temperature-controlled chamber (OKOlab). Images were acquired with NIS Elements acquisition software. The pixel seize is as follow: 100X objective: 0.0453 µm, 60X objective: 0.07566 µm, 40X objective: 0.1135 µm, 20X objective: 0.22698 µm.

2.4.2 Confocal microscopy

For confocal microscopy, a spinning disk confocal system (Ultraview Vox, Perkin Elmer) with a 100X 1.4 NA oil objective on with a single Hamamatsu ORCA-R2 camera after excitation with a laser at 488, 561, and 640 nm, operated by Volocity 6.0 software (Perkin Elmer). The pixel size with the 100X objective is 0.06896µm.

2.4.3 Correlative Light Electron Microscopy (CLEM)

Nicholas I. Clarke carried out the CLEM experiment. HeLa cells expressing pMito-PAGFP-FRB (plasmid VII:29) and mCherry-FKBP-TPD54 (plasmid X:33) were imaged on gridded glass MatTek dishes (P35G-1.5-14-CGRD, Mat-Tek Corporation, Ashland, MA, USA) using widefield microscope with standard filter sets for visualization of mCherry. Light and epifluorescence micrographs were acquired with 20X air and 100X oil objectives, at 37°C. A 20X air

objective was used to record the photo-etched grid coordinate of the cell of interest with brightfield illumination. With a 100X oil objective, the same cell of interest was found and imaged. Rapamycin (200 nM) was added in media. Control cells had no rapamycin added. Once TPD54 had been rerouted to the mitochondria, cells were fixed in 3% glutaraldehyde and 0.5% PFA in 0.05 M phosphate buffer pH 7.4 for 1 h. Aldehydes were quenched in 50 mM glycine solution and thoroughly washed in dH_2O. Cells were post-fixed in 1% osmium tetroxide and 1.5% potassium ferrocyanide for 1 h and then in 1% tannic acid for 45 min to enhance membrane contrast. Cells were rinsed in 1% sodium sulphate then twice in dH_2O before being dehydrated in grade series ethanol and embedded in EPON resin (TAAB). The coverslip was removed from the polymerized resin and the grid was used to relocate the cell of interest. The block of resin containing the cell of interest was then trimmed with a glass knife and serial 70 nm ultrathin sections were taken using a diamond knife on an EM UC7 (Leica Microsystems) and collected on formvar coated hexagonal 100 mesh grids (EM resolutions). Sections were post-stained with Reynolds lead citrate for 5 mins. Electron micrographs were recorded using a JEOL 1400 TEM operating at 100 kV using iTEM software.

2.5 Cell biology

2.5.1 Knockout (KO) cell line generation using CRISPR-Cas9 method

1. Target sequence generation

Three different sequences were chosen in TPD52L2 exon 1 using the CRISPR design tool (tools.genome-engineering.org) developed by the Zhang Lab (Cong et al., 2013). The three sequences least likely to have an off-target somewhere else in the genome were chosen. The sequences of the primers generated with these oligonucleotides can be found in table 2.6. The primers were inserted in px459 vector with BbsI restriction enzyme. The plasmid generated are numbered XII:24 (target sequence 1), XII:25 (target sequence 2) and XII:26 (target sequence 3).

Table 2.6: CRISPR-Cas9 target sequences

Primer name	Primer sequence (5′ – 3′)
TPD54 target sequence 1 F (GL001)	caccgTCGCGGATTACGAAACGCCG
TPD54 target sequence 1 R (GL002)	aaacCGGCGTTTCGTAATCCGCGAc
TPD54 target sequence 2 F (GL003)	caccgTTTCGTAATCCGCGATGCGA
TPD54 target sequence 2 R (GL004)	aaacTCGCATCGCGGATTACGAAAc
TPD54 target sequence 3 F (GL005)	caccgACCGCTGTCGCGGGCGCTAT
TPD54 target sequence 3 R (GL006)	aaacATAGCGCCCGCGACAGCGGTc

2. Cell line generation

In a 6-well plate, low passage HeLa cells were seeded for 50% confluency on day 1. Plasmids XII:24, 25 and 26 and the empty vector (plasmid XI:44) were transfected with GeneJuice (EMD Millipore 70967) according to the manufacturer's protocol. After 24 h, transfected cells were selected with 1 µg/ml of puromycin. Once the control cells were dead, the remaining cells were seeded in 20 cm dishes (~100 cells/dish) and grown in growth medium until colonies were visible with the naked eye. Individual colonies were isolated with cloning rings and grown in 96-well plates. A total of 100 colonies were isolated. When the cells reached confluency, they were seeded in duplicate in 6-well plates, one for DNA extraction and one for protein extraction.

3. KO verification

A cell lysate was made for each clone by scraping cells in RIPA buffer (see section 2.3.1 for detailed protocol on how to make a cell extract). Proteins were loaded on a 12% polyacrylamide gel and the level of expression of TPD54 was assessed by Western Blot using rabbit anti-TPD54 antibody and mouse anti-CHC as loading control. The genomic DNA of the clones for

which TPD54 was not expressed was extracted with Qiagen's QIAampDNA Blood kit. TPD54 first exon and the three most likely off-target (Chr13:44259709, Chr1:82946499 and NELL1) were sequenced to check for mutations. The sequencing primers are listed in table 2.7. The potential off-targets were at least 100 bp downstream of the sequencing primers.

Table 2.7: Sequencing primers for the KO cell line

Primer name	Primer sequence (5' – 3')
TPD54 exon 1 F (GL0019)	ggttcgcccgcagtttc
TPD54 exon 1 R (GL0020)	gaacccaaactacgggag
NELL1 intron F (GL0021)	GGAAGCATGACTCTCTTTC
NELL 1 intron R (GL0022)	GGCCTTTTTCAGGAGATG
Chr13:44259709 F (GL0023)	CTGATACAGGGAAATCAG
Chr13:44259709 R (GL0024)	GTTTTGCCTCCTTGACAC
Chr1:82946499 F (GL0025)	GTATAGATCTTTCTCACTG
Chr1:82946499 R (GL0026)	CAATTCTCAGCAATATCTG

2.5.2 Mitotic progression

TPD54 KO HeLa cells were seeded in a 12-well plate transfected with H2B-mCherry (plasmid V:41) and pEGFP-C1 (plasmid I:02) or GFP-TPD54 (plasmid VIII:44). 48 h post-transfection, the cells were imaged in imaging medium with a 40X air objective on a widefield microscope. 20 fields were imaged per condition during 12 h, at a 3-min frame rate. The movies were imported in ImageJ and mitotic stages were assessed by the shape of the nucleus.

2.5.3 Immunofluorescence

Cells were fixed 24-48 h post transfection with 3% PFA, 4% sucrose in PBS for 15 min. Membranes were permeabilised with 0.5% Triton-X100 in PBS for 10 min and the cells were blocked with 5% goat serum, 3% BSA in PBS for 1 h. The cells were incubated with primary antibodies diluted in blocking solution (see table 2.8 for specific dilutions) for 1 h (50 µl solution per coverslip). If actin was stained, TRITC-phalloidin (Sigma, P1951) was added with the primary antibodies at a concentration of 2.5 µg/ml for 1 h. The cells

were then washed by incubating them 3 times with PBS for 5 min. The secondary antibodies conjugated with Alexa-Fluor (Invitrogen) were diluted 1:500 in blocking solution and left on the cells for 1 h. A final wash was done by 3 incubations of 5 min with PBS. Coverslips were then rinsed by being dipped in dH_2O and left to dry, cells up, for a few minutes. The coverslips were mounted on slides with mowiol, and once the mowiol is dry, put at 4°C in the dark.

Table 2.8: Antibodies used for immunofluorescence

Primary antibody name	Supplier	Working concentration
Mouse anti-CD8 (untagged)	Biorad (MCA1226GA)	10 µg/ml (1:100)
Rabbit anti-CIMPR (IFGR2)	Thermo Fisher (PA3-850)	1:500
Mouse anti EEA1 clone 14	BD Biosciences	1 µg/ml (1:250)
Rabbit anti-GM130	Sigma (G7295)	0.6 µm/ml (1:2000)
Rabbit anti-LAMP1 D2D11	Cell Signaling (9091)	1:200
Sheep anti-TGN46	AbD Serotec (AHP500G)	1.25 µg/ml (1:200)
Mouse anti-Vinculin	Sigma (V9264)	0.2 µg/ml (1:5000)
Mouse anti-VPS26 CL2287	Abcam (ab212530)	3.2 µg/ml (1:250)
Rat anti-Integrin β1 mAb13	P. Caswell Lab	10 µg/ml (1:100)

2.5.4 Immunoprecipitation (IP)

A cell lysate was prepared by scraping HeLa cells (2x10 cm dishes per condition) on ice in lysis buffer (10 mM Tris-Cl pH 7.5, 150 mM NaCl, 0.5 mM EDTA, 0.5% NP-40) (total of 500 µl buffer per condition). The lysate was passed through a 27G needle 3 times and left to rest on ice for 15 min while vortexed regularly. The lysates were then centrifuged at 14 000 rpm in an Eppendorf Centrifuge 5417R for 15 min at 4°C. The supernatant was quantified and an equal amount of proteins was put onto 10 µl of GFP-Trap beads (Chromotek, gta-20) washed with 500 µl of exchange buffer (10 mM Tris-Cl pH 7.5, 150 mM NaCl, 0.5 mM EDTA). The supernatant/beads mix was incubated at 4° C for 1 h while rotating. The beads were then centrifuged at 14 000 rpm for 1 min at 4°C. The supernatant was discarded and the beads were washed once with 500 µl of exchange buffer and a 1 min centrifugation at 4°C, then three times with 500 µl of wash buffer (10 mM Tris-Cl pH 7.5,

500 mM NaCl, 0.5 mM EDTA) and 1 min centrifugation at 4°C. The beads were resuspended in 15 µl of Leammli buffer and incubated at 95°C for 5 min before being loaded on a 4-15% acrylamide gel.

2.5.5 Mass spectrometry analysis

Three 10 cm dishes were seeded with HeLa cells for each condition. DNA was then transfected as follows: condition 1- pEGFP-C1 (plasmid I:02) and pIRES-CD8-YAAL (plasmid VII:33), condition2- pEGFP-C1 and pIRES-CD8-EAAALL (plasmid VII:34), condition 3- GFP-TPD54 (plasmid VIII:44) and pIRES-CD8-YAAL, condition 4- GFP-TPD54 and pIRES-CD8-EAAALL. GFP was immunoprecipitated with GFP-Trap beads as described in 2.4.4. The beads were then loaded on a 4-15% acrylamide gel and ran until the proteins have migrated in the gel for 1-2 cm. The lanes were cut with a clean razor blade and sent in a 1.5 ml tube to FingerPrints proteomics facility in Dundee, UK. This was done twice, giving 4 repeats of a GFP IP and 4 repeats of a GFP-TPD54 IP. The original idea was to verify is TPD54 can bind directly to the dileucine motif. No CD8 was found in the protein list after mass spectrometry, but the dataset obtained could still be used as TPD54 interactors. These interactors were classified according to the score and classified according of their degree of enrichment when compared to the GFP alone interactors, and according to whether or not their presence is significantly higher ($p<0.05$) in TPD54 samples vs GFP samples.

2.5.6 Transferrin uptake and recycling assay

HeLa cells were serum starved (DMEM +antibiotic –FBS) for 30-60 min at 37°C and incubated at 4°C for 30 min with 25 µg/ml of AlexaFluor 488-conjugated transferrin (Thermo Fisher Scientific, 11550756) (50 µl/coverslip). The coverslips were then dipped in dH_2O, placed in warm growth medium and incubated at 37°C for 5-75 min to allow internalisation and recycling.

Cells were then fixed and processed for immunofluorescence as described in section 2.4.3.

2.5.7 Knocksideways (KS)

1. Theory

KS is based on the dimerization of two protein domains after the addition of rapamycin. The normal target for rapamycin is the FKBP domain of FKBP12, a propyl isomerase. After binding, the rapamycin-FKBP complex then binds to the FRB (FKBP and rapamycin-binding) domain of mTOR. The technique relies on the fact that the FKBP and FRB domains can be fused to other proteins, allowing them to dimerise as well (Robinson et al., 2010). The idea here was to express a MitoTrap (mitochondria with the yeast outer membrane protein Tom70p fused to FRB and dark-mCherry) (Robinson et al., 2010) and TPD54 fused to a fluorescent tag and FKBP. By adding rapamycin, mCherry- or GFP-FKBP-TPD54 will be brought to the mitochondria, and anything that will bind to TPD54 will be brought as well (**Figure 2.1**).

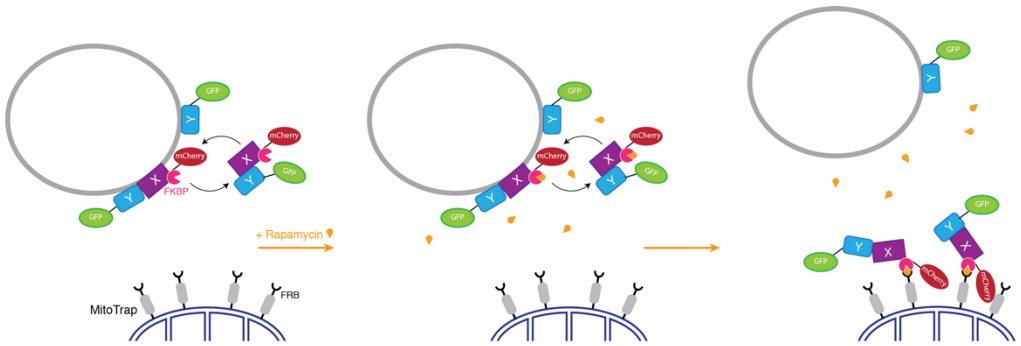

Figure 2.1: Knocksideways. Schematic representation of the knocksideways to test the potential association between protein X and Y. Protein X is fused to mCherry and FKBP, the mitochondria are tagged with a MitoTrap containing an FRB domain and protein Y is fused to GFP. Proteins X and Y could be on vesicles or in the cytosol. Knocksideways is induced by adding rapamycin, which will first bind FKBP, then the FKBP-rapamycin complex will dimerise will the FRB domain on the MitoTrap. Protein X will be rerouted to the mitochondria and if protein Y is associated with X, it will also be rerouted to the mitochondria.

2. Image acquisition

TPD54 siRNA treated HeLa or RPE1 cells were seeded in fluorodishes (World Precision Instruments) and transfected with dark-MitoTrap (pMito-mCherry (K70N)-FRB, plasmid XV:81), mCherry-FKBP-TPD54 (plasmid X:33) or GFP-FKBP-TPD54 (plasmid X:17) and a GFP-, mNeonGreen- or mCherry-tagged protein of interest. In the case of CD8-chimera co-KS, cells were surface labelled with AlexaFluor 647-conjugated anti-CD8 antibodies before KS. In imaging medium containing 100 nM MitoTracker Deep Red FM (Thermo Fisher scientific, M22426), cells were brought to the confocal microscope with a 60X oil objective or a 100X 1.4 NA oil objective. Cells of interest were imaged by either taking stills or movies of 12 frames/min, for 5 minutes. KS was induced by applying 200 nM rapamycin (Alfa Aesar) to the cells. In the case of movies, rapamycin was added 30 s after the start of the movie. The cells chosen were expressing low to medium amount of fusion proteins.

3. Quantification

Pre- and post-rapamycin confocal images of HeLa cells were analysed to assess the efficiency of co-rerouting of bait proteins. In ImageJ, 10 ROIs of 8x8 pixels (0.05 µm/px) were placed over mitochondria in the pre- and post-images and the mean grey value was measured in these ROIs for the bait and for the TPD54 channel. These 10 ROIs were then averaged and compared to the pixel intensity average of 10 other ROIs taken in the cytoplasm of the same channels. The ratio of the proteins on mitochondria versus in cytoplasm was measured for pre- and post-rapamycin images.

2.5.8 Timed KS

We wanted to know if the knocksideways of the CD8-chimera could be done as soon as the receptors enter the cell or if it needed to reach a certain compartment. Do to this, TPD54 siRNA treated HeLa cells were seeded on coverslips and transfected with dark-MitoTrap (plasmid XV:81), mCherry-FKBP-TPD54 (plasmid X:33) and one of the CD8-chimera (plasmids VII:31-

35). 24 h post-transfection, cells were labelled with 10 µg/ml AlexaFluor 488-conjugated anti-CD8 antibodies (AbD Serotec, MCA1226A488) at 4°C for 30 min (50 µl/coverslip). Cells were incubated at 37°C in warm growth medium for 5, 30, 60, 90 or 120 min. KS was then induced by adding 200 nM rapamycin at 37°C. After 5 min, cells were fixed with PFA as described in section 2.4.3 and mounted on slides with mowiol.

2.5.9 CD8-chimera tracking

1. Image acquisition

HeLa cells expressing a combination of CD8-chimera and trafficking markers were labelled with AlexaFluor 647-conjugated anti-CD8 antibodies (AbD Serotec MCA1226A647, 1:100) at 37°C and imaged immediately in the case of early trafficking markers or after up to 2 h for the late markers. Confocal microscope 10-min movies were taken at a frame rate of 12 images/min with a 100X 1.4 NA oil-immersion objective.

2. Colocalisation

Movies were imported in ImageJ and CD8-positive and membrane trafficking markers-positive particles were found with the ComDet v.0.3.5 plugin (particle size: 9px, SNR: 5). The output was fed in the Igor Pro code "ColocAnalysis" (https://github.com/quantixed/PaperCode/tree/master/Wood2017). The code calculates if the particles in the two channels overlap over time and compares the degree of colocalisation to the likelihood of that colocalisation to be due to chance (overlap of the particles in the two channels at random time points).

2.5.10 2D cell migration

1. Image acquisition

RPE1 cells were seeded on 10 µg/ml fibronectin- or 20 µg/ml laminin-coated LabTek dishes 24-72 h post transfection. Before bringing the cells under the

microscope, the growth medium was exchanged for imaging medium (Leibovitz L-15 (GIBCO, 21083-027), 10% FBS and 1% penicillin/streptomycin). Cells were imaged with a widefield microscope at 37°C. Movies were acquired for 12 h with a 20X air objective, using brightfield illumination, taking one frame every 10 min, 20 fields of view per condition, at minimum laser power. If cells were also expressing a fluorescent plasmid, the appropriate epifluorescence image was taken every 10th frame.

2. Image analysis

Up to 10 cells in the field of view at the start of the movie were tracked until they either left the field of view or entered mitosis. The cells were tracked using the Manual Tracking plugin in ImageJ. The tracks were then processed in Igor Pro with the "LoadMigration" code available at https://github.com/quantixed/CellMigration, which calculates the cumulative distance (μm) covered by the cells, the instantaneous velocity (μm/min) (cell speed at any given point of the movie), the frequency of this instantaneous velocity, the directionality ratio (d/D; where d is the shortest distance between point A and B, and D is the actual length of the path taken by the cell to go from A to B), the mean squared displacement (quantification of movement over time), the direction autocorrelation (which reflects the propensity of the cell for changing direction over time), the average speed of the cells for the whole movie (μm/min) and the variance in that speed (μm/min).

2.5.11 Cell shape analysis

Brightfield movies from the 2D migration experiments were used. A time frame was selected halfway through the movie and images from each condition were analysed. A USB-linked pen (Wacom) was used to draw an ROI on the periphery of the cells with the freehand selection tool. The area and the perimeter were measured and quantified using Igor Pro.

2.6 Figure preparation

Data were collected with Microsoft Excel or Igor Pro v.6.37 and graphs were made with Igor Pro. Immunofluorescence figures were prepared in ImageJ v.2.0.0-rc-43/1.51q. Nicholas I. Clarke prepared the electron micrographs. Figures were assembled in Adobe Illustrator CS5 v.15.0.0.

Chapter 3 – TPD54 is associated with membrane trafficking components

3.1 Introduction

Our interest in the TPDs comes from a proteomics study which compared clathrin coated structures (CCSs) in mitotic and interphase cells (Kaur et al., 2014). The aim of this study was to find endocytic proteins with a "mitotic moonlighting" role, a role in mitosis that is independent of their trafficking function (Royle, 2013). These proteins were likely to be enriched on CCSs during interphase and lost from CCSs during mitosis. The main finding of this study was that clathrin-mediated endocytosis is arrested in mitotic cells because of the unavailability of the actin cytoskeleton to perform its endocytic role since it is required for maintaining a mitotic cortex. It was therefore unsurprising to find in this proteomic screen many clathrin or actin interactors. However, it was also found that both TPD54 and TPD52 were among the top hits for candidate endocytic proteins having a mitotic role as well (**Figure 3.1**).

Very little is known about the TPDs but it is thought that they are associated with membrane trafficking components (Borner et al., 2006; Sathasivam et al., 2001). The potential role of TPDs in the cell cycle has also been highlighted (Boutros and Byrne, 2005; Thomas et al., 2010a). It then appears that the TPDs could be good candidates for being one of those trafficking proteins having a mitotic moonlighting role. In this chapter, we investigate this possibility with the best TPD candidate, TPD54.

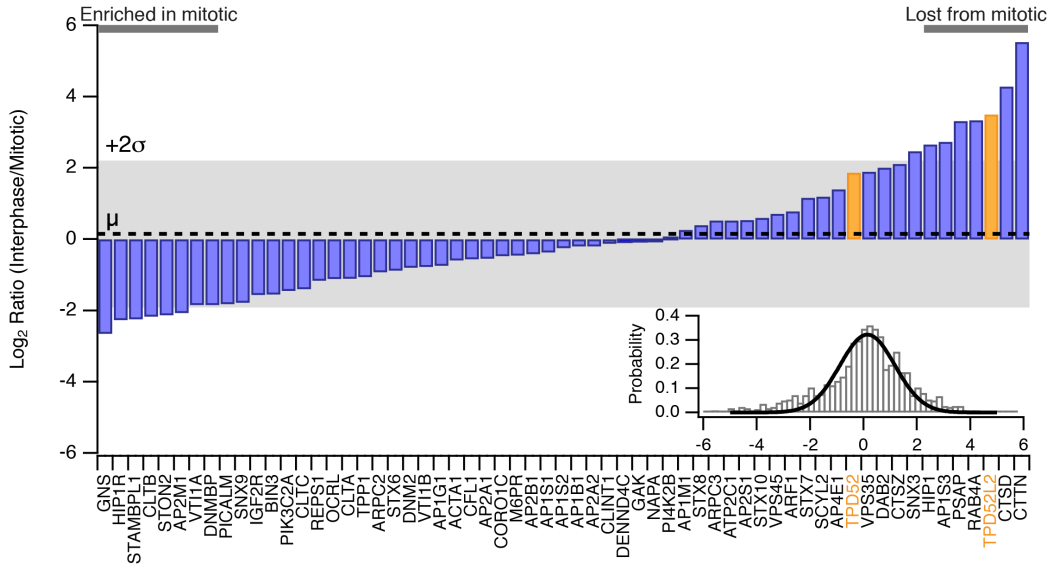

Figure 3.1: TPD54 and TPD52 are lost from mitotic CCSs (adapted from Kaur et al., 2014). Ratio of enrichment of proteins found in a mass spectrometry analysis of CCSs isolated from interphase or mitotic HeLa cells. TPD52 and TPD54 are highlighted in orange. The dotted line represents the mean abundance and the grey area is ±2 standard deviations. Inset: Relative abundance of the proteins found at a specific enrichment ratio, with a Gaussian function fitted to the data.

3.2 TPD54 is tightly associated with membrane trafficking vesicles

The role of TPD54 in membrane trafficking is still unclear, despite the fact that the protein was identified more than 20 years ago (Byrne et al., 1995). In order to better understand the cellular localisation of TPD54, the knocksideways (KS) technique was used. We have used it as "an in-cell immunoprecipitation": we transfect TPD54, use it as a bait and co-transfect other proteins to use them as pray. A protein being co-knocked sideways with TPD54 is associated with the latter, both acting on the same pathway.

To determine where on the trafficking pathway TPD54 is, Rab proteins were used as pray. The well-characterised Rab4, 5, 7, 9 and 11 have been chosen in this assay. They are markers of the early endosomes and fast recycling pathway, the early endosomes, the late endosomes, the late endosome-Golgi apparatus pathway, and the recycling endosomes, respectively (Zerial and McBride, 2001).

As shown in figure 3.2, before adding rapamycin, TPD54 is mainly cytosolic and sometimes vesicular, the GFP control is diffuse and the Rab GTPases are vesicular. After rapamycin was added, mCherry-KFBP-TPD54 covered the mitochondria. GFP-Rab4 and GFP-Rab11 partially follow TPD54, whereas the localisation of GFP, GFP-Rab5, GFP-Rab7 and GFP-Rab9 is unaltered. This suggests that TPD54 is binding to Rab4 and Rab11. Although, it could also mean that we capture whole vesicles and that we pick Rab4 and Rab11 because they are on the same vesicle or finally, that they are on the same vesicle and bind together.

To test this, we looked at rerouted cells with correlative light electron microscopy (CLEM) (**Figure 3.3**). First, cells expressing the MitoTrap and GFP-FKBP-TPD54 were imaged on a gridded dish and then knocksideways was induced by adding rapamycin. The cells were fixed and processed for electron microscopy (**figure 3.3A**). The same cell was found to make sure that the imaged cell was knocked sideways. As seen in figure 3.3B, in rapamycin-treated cells, the mitochondria are studded with small homogenous and regular vesicles of about 25 nm. This was only visible for cells expressing GFP-FKBP-TPD54, suggesting that when we knock TPD54 sideways, we bring entire transport vesicles rather than bringing only TPD54 and its binding partners (**Figure 3.3C**).

Another membrane trafficking-associated binding partner of the TPDs is MAL2 (myelin and lymphocyte 2). MAL2 is a membrane-bound protein, having a role in transcytosis (de Marco et al., 2006) and is mainly expressed in polarized epithelial cells and hepatocytes. It has been found to bind the TPDs in a yeast two-hybrid assay and it has further been confirmed by immunoprecipitation that TPD52 and MAL2 are binding partners (Wilson et al., 2001) and are linked to poor prognosis when both are overexpressed in either ovarian carcinoma (Byrne et al., 2010) or colorectal cancer (Li et al., 2017). We wanted to know if i) the knocksideways technique was reliable for detecting binding partners and ii) if TPD54 was indeed a binding partner of

MAL2. As seen in figure 3.4, we could confirm the association between MAL2 and TPD52, as previously found by Wilson and colleagues (2001), but unlike

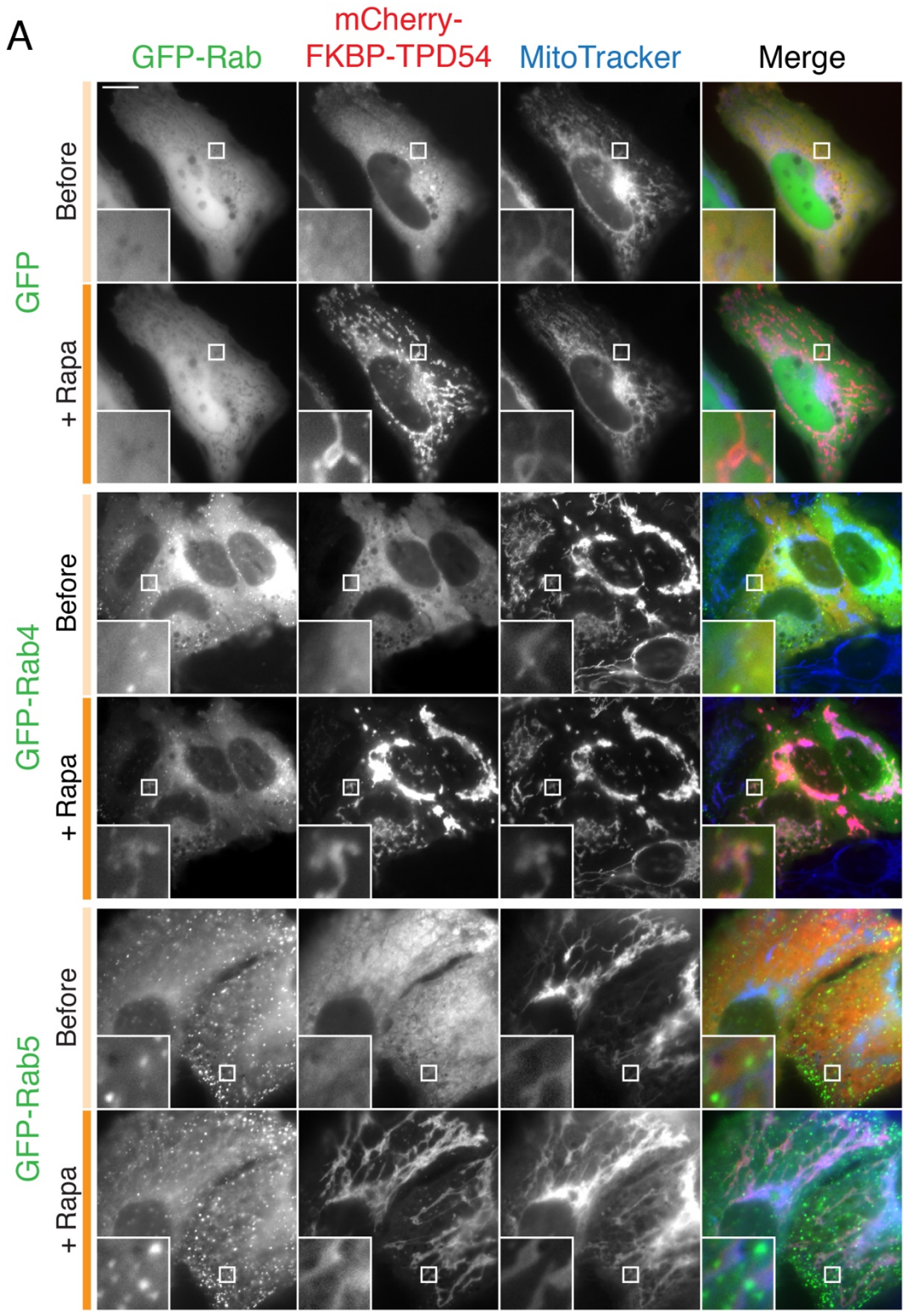

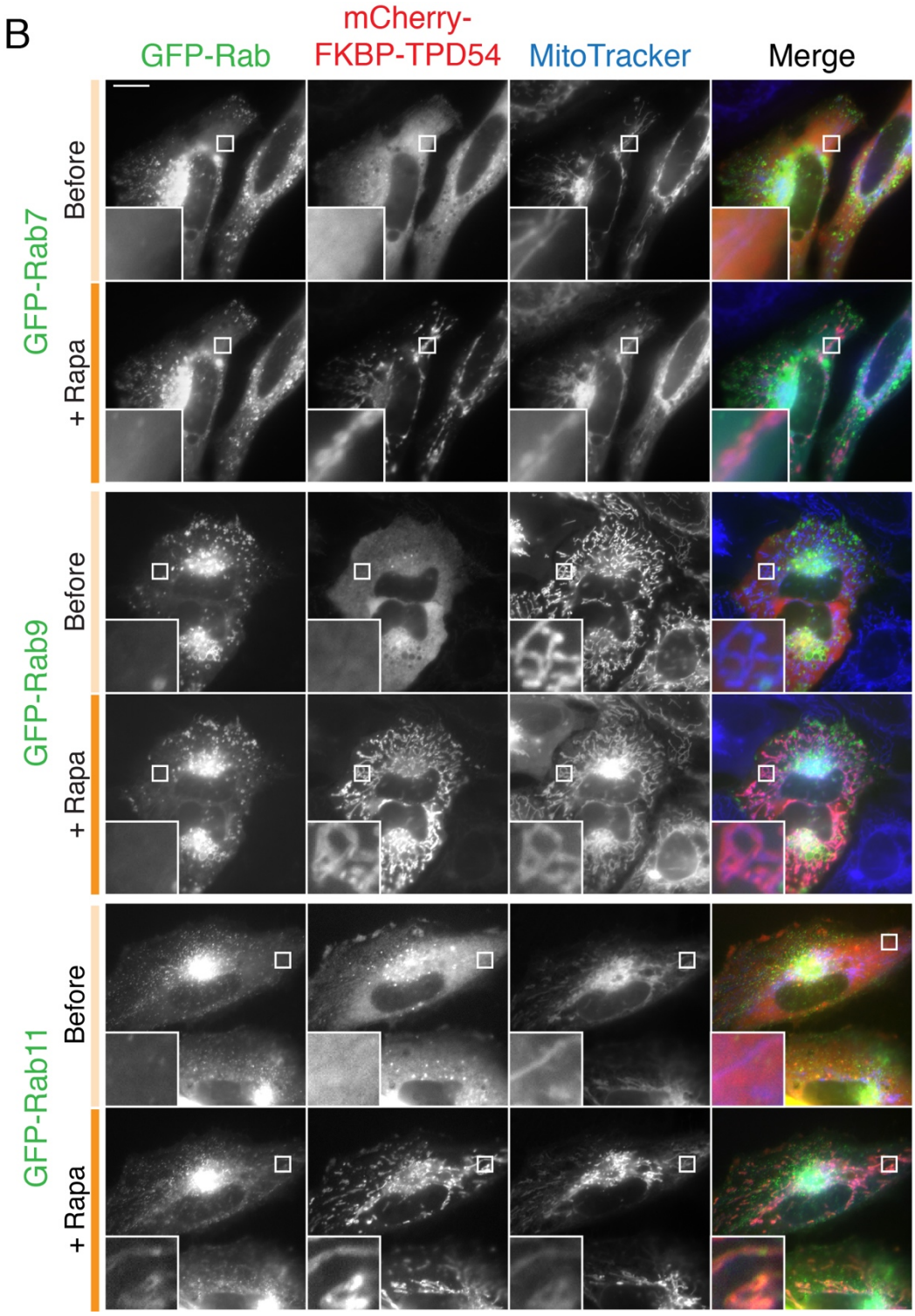

Figure 3.2: Knocksideways of TPD54 reroutes Rab4 and Rab11 to the mitochondria specifically. Representative confocal micrographs showing the effect of mCherry-FKBP-TPD54 knocksideways upon either A) GFP, GFP-Rab4, GFP-Rab5, B) GFP-Rab7, GFP-Rab9 or GFP-Rab11 in HeLa cells also expressing dark-MitoTrap. KS was induced by adding 200 nM rapamycin to the cells (dark orange bars). Mitochondria are labelled with far-red MitoTracker. Scale bar: 10 μm. Inset: 5X zoom.

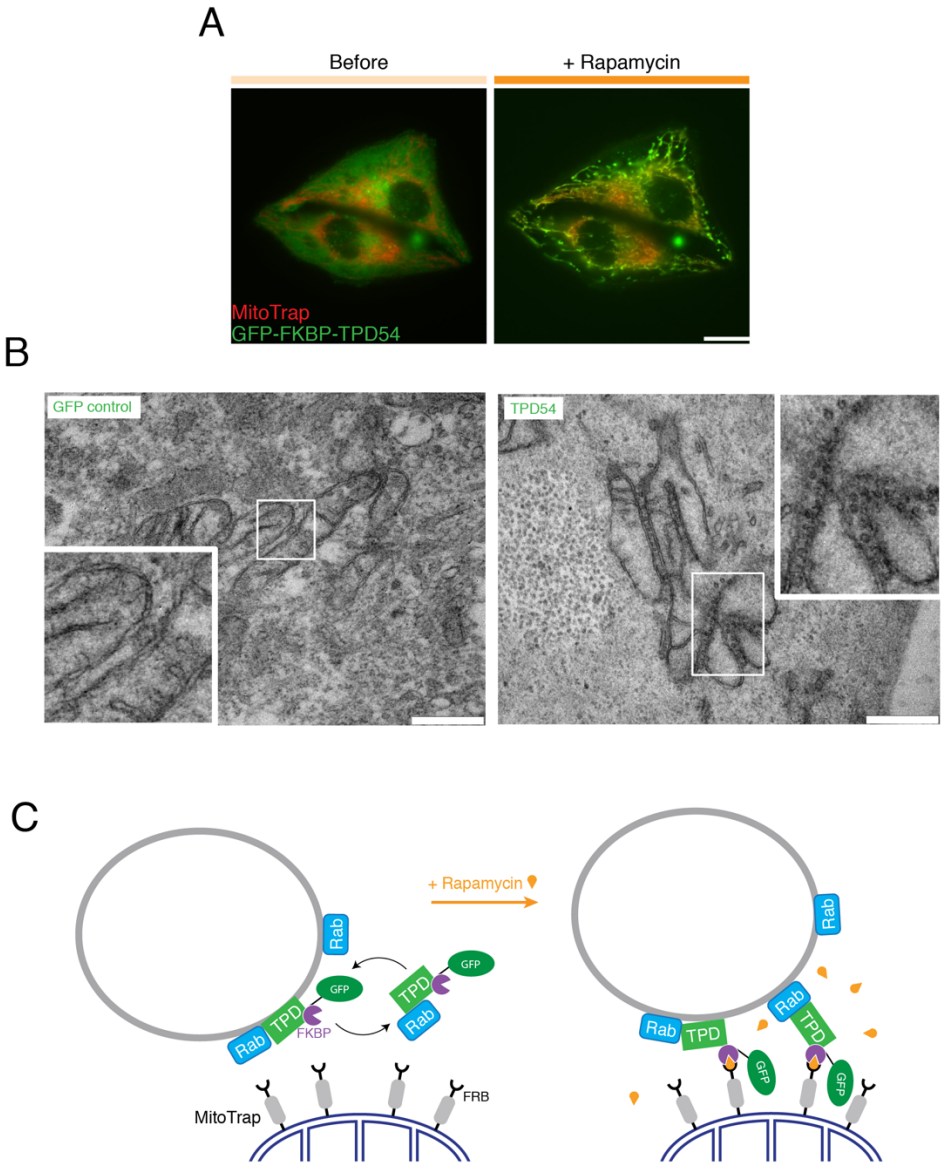

Figure 3.3: TPD54 knocksideways reroutes vesicles to mitochondria. A) HeLa cells expressing GFP-FKBP-TPD54 and MitoTrap were treated with rapamycin on gridded dishes allowing the same cells to be imaged with electron microscopy. B) Electron micrographs of mitochondria in cells exposed to rapamycin and expressing GFP-FKBP or GFP-FKBP-TPD54. Scale bar: 500 nm. C) Schematic representation of what happens to TPD54-positive vesicles after a knocksideways.

their yeast two-hybrid assay results, our knocksideways experiment suggests no interaction between TPD54 and MAL2. Taken together, our data show that the knocksideways is a good technique to assess protein-protein interactions. With it, we have found that TPD54 is associated with Rab4- and Rab11-positive vesicles, and that TPD52 but not TPD54 is an interactor of MAL2.

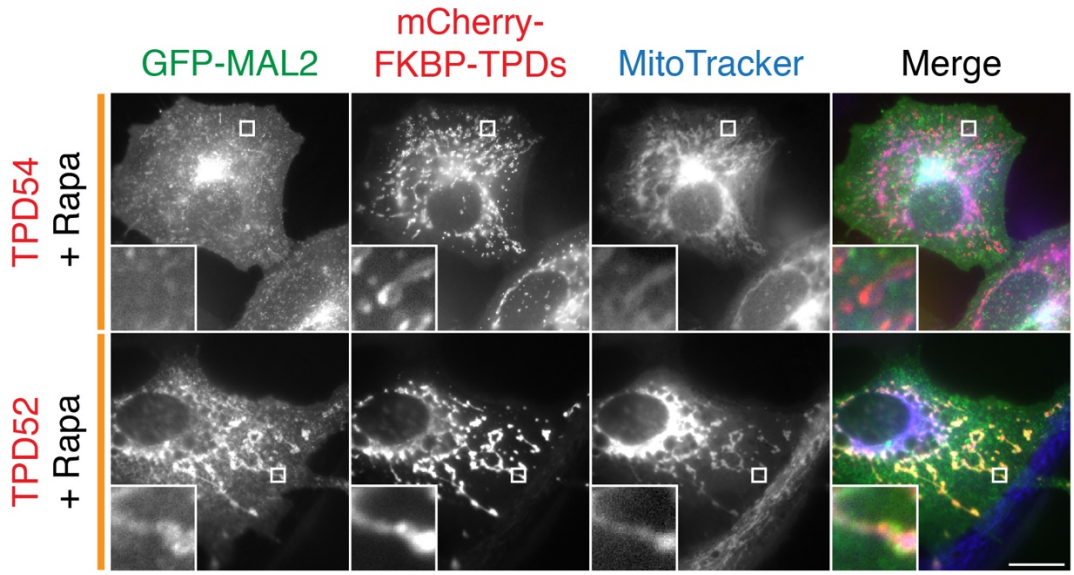

Figure 3.4: TPD52 but not TPD54 is associated to MAL2. Representative widefield micrograph showing the effect of the knocksideways of mCherry-FKBP-TPD54/52 on GFP-MAL2. KS was induced by adding 200 nM rapamycin to the cells. Mitochondria are labelled with far-red MitoTracker. Scale bar: 10 µm. Inset: 7x zoom.

3.3 Generation of a TPD54 KO cell line

To gain insight into the cellular function of TPD54, a knockout (KO) cell line was generated using the CRISPR-Cas9 system (Cong et al., 2013). Briefly, oligonucleotides were designed to target exon 1 of TPD54, which is common to all TPD54 isoforms. These 'target sequences' will position the nuclease Cas9 within exon 1 and induce a double strand break which might then be repaired with an insertion or a deletion (indel) likely to cause a reading frameshift. Using this technique, two HeLa TPD54KO clones (clone 2.2 and 2.4) were generated with the target sequence no.2 (see section 2.4.1) showing no expression for clone 2.4 and barely any for clone 2.2 (**Figure 3.5A**), since the genomic DNA sequence of both of these clones exhibited no start codon (**Figure 3.5B**).

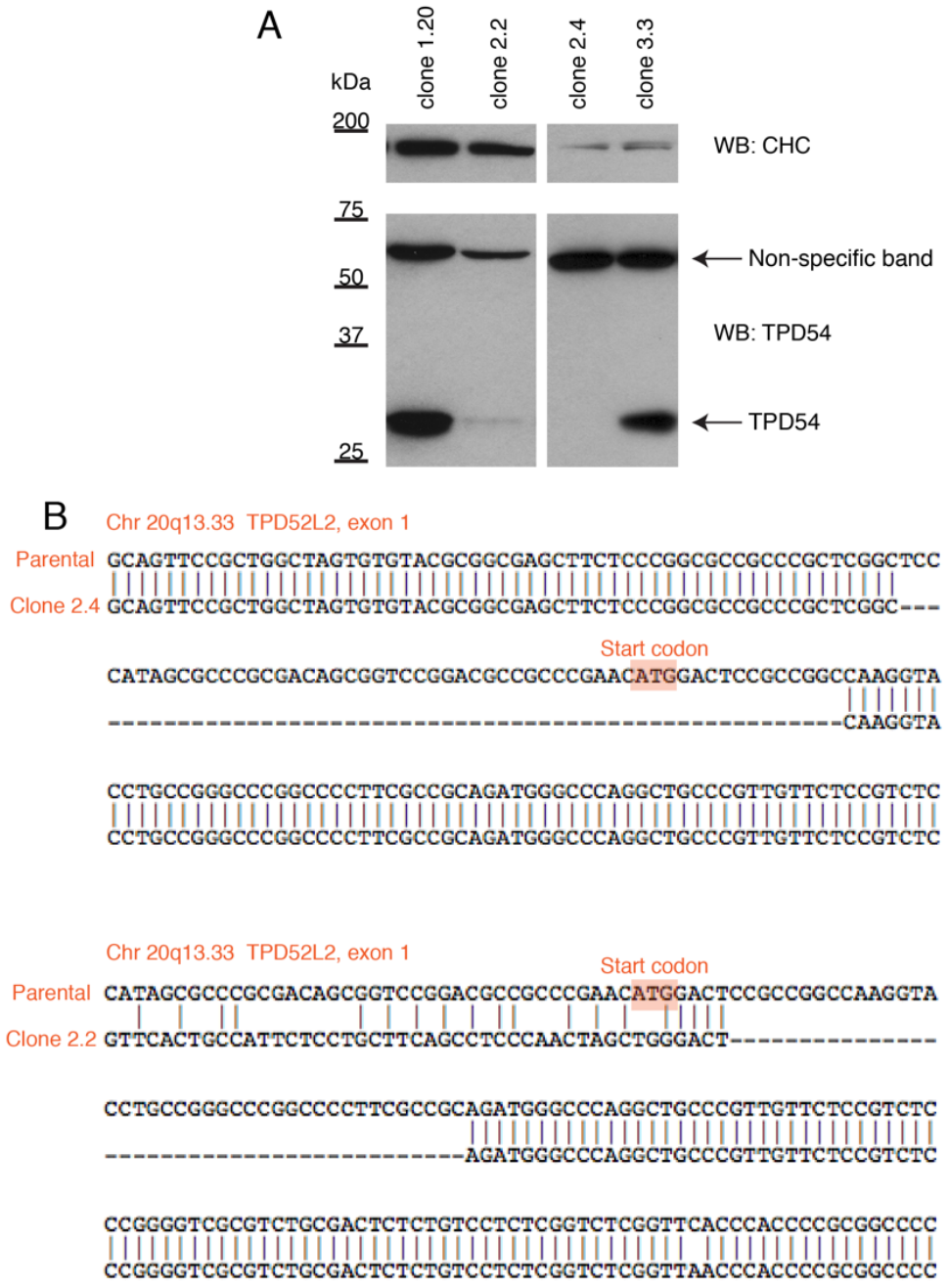

Figure 3.5: TPD54 knockout cell lines. A) Western blot showing two clones still expressing TPD54 (clones 1.20 and 3.3) and two clones expressing no TPD54 (clones 2.2 and 2.4). Clathrin heavy chain (CHC) is used as a loading control. B) Sequencing of TPD52L2 exon 1 of clones 2.4 and 2.2. Clone 2.4 exhibits no start codon, while clone 2.2 has a mutation at the start codon, making it impossible for the protein to be expressed.

One of the pitfalls of using this technique for knocking out genes is the possibility of having off-target effects by introducing indels at other sites (Komor et al., 2017). The three most likely off-target regions were also

sequenced and showed no difference when compared to parental genomic DNA.

Since TPD54 has an apparent a role in membrane trafficking, a few organelles were stained in clone 2.4 in order to detect a defect. Early endosomes (Rab5), late endosomes (Rab7) and the Golgi apparatus (TGN46) were stained. No problem was detected in early or late endosomes (data not shown), but the majority of TPD54 KO cells exhibited a fragmented Golgi phenotype (**Figure 3.6A**). In control cells the Golgi (TGN46) was focused, but in KO cells, the Golgi is vesicular, suggesting unstable cisternae. This phenotype was quantified by calculating the ratio of the area of the Golgi dispersal over the area of the cell, meaning that a value near 1 reflects a very fragmented Golgi (**Figure 3.6B**). The phenotype could be rescued by the transient expression of FLAG-TPD54. FLAG-TACC3, a protein bearing a coiled-coil domain like TPD54, was used as a control to show the specificity of the rescue. The effect of an overexpression of TPD54 or TACC3 was also assessed and showed no significant difference with control cells. Finally, both TPD54 KO clones showed a similar Golgi phenotype (**Figure 3.6C**), suggesting that this phenotype isn't specific to one clone and re-enforcing the hypothesis that this fragmented Golgi phenotype is due to the loss of TPD54 and not the result of CRISPR-Cas9 or an off-target effect.

Another pitfall of working with KO cells is the possibility for these cells to adapt to the lack of the protein targeted. After a while, the Golgi apparatus of both clones became more similar to the parental cells until no significant difference remained. TGN46 antibodies and TPD54 KO clone aliquots were changed, and the phenotype was still lost, making it plausible that the cells adapted to loss of TPD54.

In order to check if the same phenotype could be studied with RNA interference, HeLa cells were transfected with siRNA targeting TPD54 3′ UTR

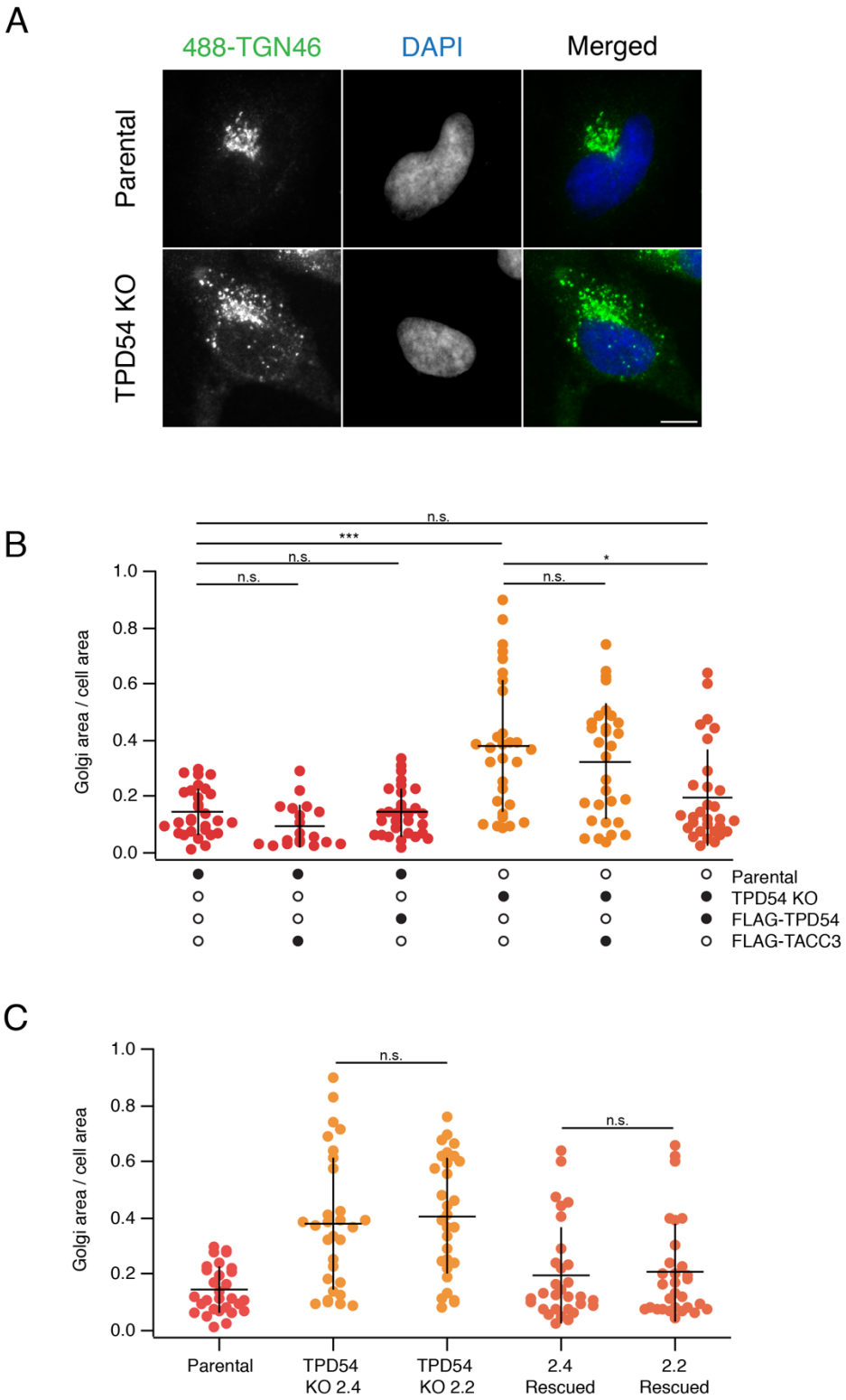

Figure 3.6: TPD54 KO cells show Golgi apparatus cisternae instability. A) Representative widefield micrograph showing the trans Golgi network marker TGN46. Scale bar: 10 µm. B) Quantification of the dispersal of the Golgi apparatus in parental cells or TPD54 KO cells expressing either the control construct FLAG-TACC3, FLAG-TPD54 or no plasmid. n=3. C) Comparison between TPD54 KO clones 2.4 and 2.2. n=3. Dots are single cells and bars are mean and standard deviation. p values from Tukey post-hoc comparison. *<0.05, ***<0.001.

(**Figure 3.7**). The expression is reduced by more than 50 % after only 24 h and was almost undetectable after 48 h (**Figure 3.7A**). No significant difference was found between the Golgi dispersal of siGL2 transfected cells and siTPD54 transfected cells (48 h). Also, cells receiving the siRNA transfection mix and the DNA transfection exhibited a tight Golgi phenotype (dispersal index around 0.1). Taken together, the data suggests that TPD54 might have a role in Golgi cisternae stability although this could not be repeated in knockdown conditions.

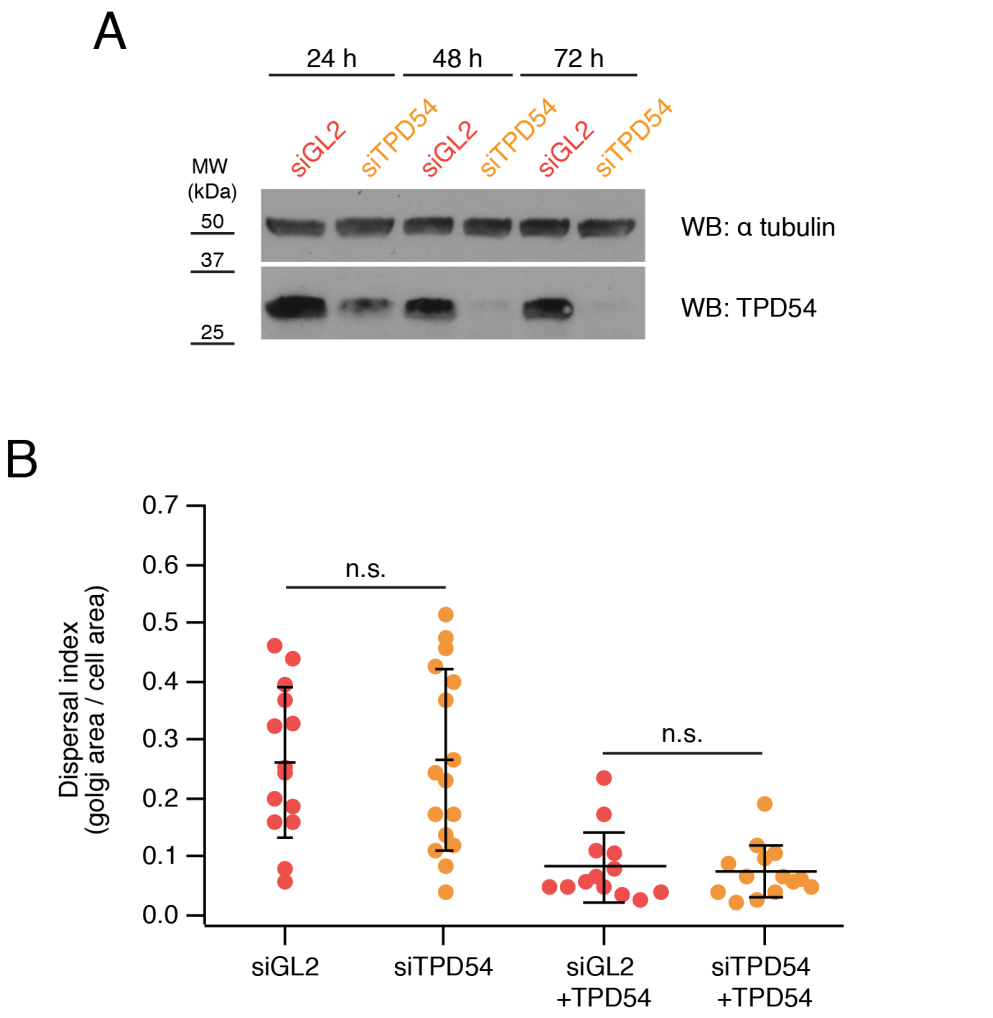

Figure 3.7: RNA interference TPD54 does not destabilise the Golgi apparatus. A) Western blot showing the depletion of TPD54 using siRNA. α tubulin is used as a loading control. B) Quantification of the Golgi fragmentation in siRNA treated HeLa cells for 48 h. n=1. p values from Tukey post-hoc comparison. Dots are single cells and bars are mean and standard deviation.

3.4 TPD54 KO cells do not show a mitotic defect

TPD54 most probably has a role in membrane trafficking (**Figures 3.2 and 3.3**) (Borner et al., 2006; Proux-Gillardeaux et al., 2003) and is a good candidate for also having a role in mitosis (**Figure 3.1**) (Kaur et al., 2014). We then wanted to know if TPD54 might have a mitotic moonlighting role. Before the loss of the Golgi phenotype, a mitotic progression experiment was conducted with the TPD54 KO cell line clone 2.4 (**Figure 3.8**). The mitotic stage was assessed by expressing the DNA marker H2B-mCherry. The time required to go through each mitotic phase was estimated and no difference was found between parental HeLa cells and TPD54 KO cells. Overexpression of GFP-TPD54 had no impact on the progression through mitosis. Taken together, the data suggests that a lack of TPD54 does not impair the normal progression of mitosis.

3.5 Discussion

The first aim of the project was to determine whether or not TPD54 is a membrane trafficking protein with a mitotic moonlighting role. TPD54 is indeed associated with membrane trafficking components since Rab4 and Rab11 positive vesicles can be rerouted to the mitochondria after a TPD54 knocksideways (**Figures 3.2 and 3.3**). It is possible to note that the rerouting of TPD54 to the mitochondria is more efficient then the rerouting of Rab4 and Rab11. This could be due to either a higher expression of Rab4 and 11 than TPD54, or that the hypothetical binding to these Rab GTPases is only transient. Also, the vesicles seen on the electron micrographs look particularly regular. It is then unlikely that recycling endosomes are rerouted since they exhibit a tubular shape (Ullrich et al., 1996) that would have been seen by EM. It is therefore more likely that TPD54 is associated with transport vesicles, probably on the recycling pathway since members of both the fast (Rab4) and the slow (Rab11) recycling pathway (Stenmark, 2009) are rerouted with

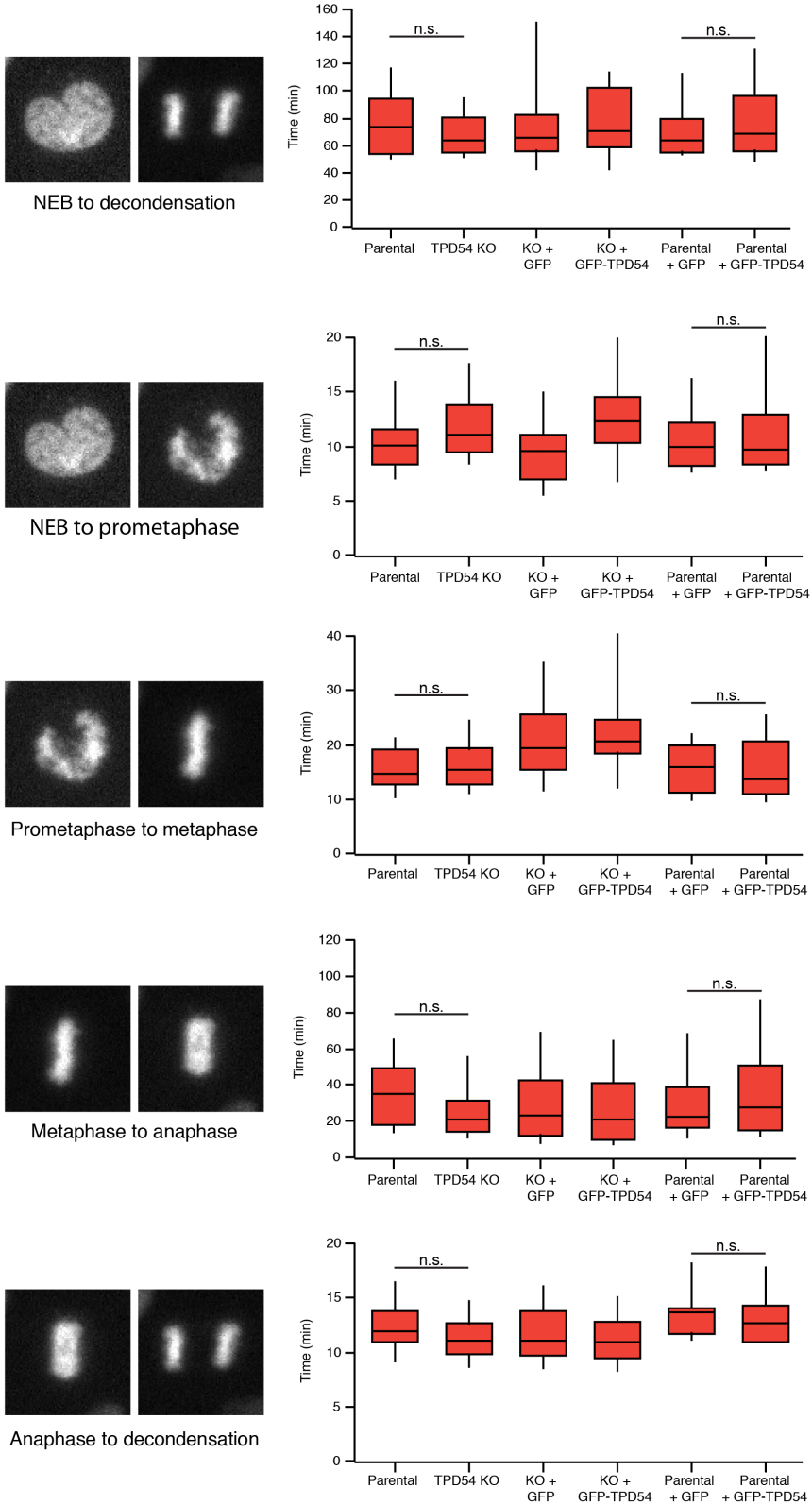

Figure 3.8: TPD54 KO cells can go through mitosis at a normal pace. Boxplot showing the rate at which TPD54 KO HeLa cells clone 2.4 go through each mitotic stage (NEB: nuclear envelope breakdown). n=3. Box represents the higher and lower quartile, bar is the median value, and the whiskers show 10th and 90th percentile. On the left: representative widefield micrograph of nuclei marked by expressing H2B-mCherry. p value: Tukey post-hoc comparison.

TPD54. We have also been able to confirm an interaction between MAL2 and TPD52 but not TPD54 (**Figure 3.4**), unlike previously found (Wilson et al., 2001).

This is probably due to the fact that yeast two-hybrid assays can result in false-positives (Rao et al., 2014) and that only TPD52 binding to MAL2 was confirmed by immunoprecipitation. We are therefore confident that knocksideways is an effective technique for the detection of protein associations, however the technique is inadequate to confirm protein-protein binding.

A fragmented Golgi phenotype was also quantified and rescued with a TPD54 KO HeLa cell line (**Figure 3.6**), but this phenotype disappeared over time and could not be repeated with RNA interference, even though the depletion was almost complete after 48 h (**Figure 3.7**). This is puzzling given the fact that the fragmented phenotype could be rescued and was observed in two different KO cell lines.

Finally, in the same KO cell line, no detectable defect in mitotic progression was found (**Figure 3.8**), suggesting that if TPD54 has a role in mitosis, this role is subtle or that TPD54 affects the ability of the mitotic checkpoints to detect a problem that TPD54 would cause. It is also impossible at the moment to rule out a role for TPD54 in mitosis, since the experiment would need to be done with RNA interference: it seems that the use of CRISPR-Cas9 technique for knocking out TPD54 was not effective at keeping the early phenotypes observed. RNA interference is therefore a better solution for depleting the protein, since it can be done quickly (more than 50 % depletion after 24 h (**Figure 3.7**) and the cells are less likely to adapt within this window of opportunity.

We have so far been unsuccessful at finding a mitotic moonlighting role for TPD54. However, we have established that the protein is probably involved

the trafficking of vesicles on the recycling pathways. We also have an efficient way of depleting the protein (KD) or moving it quickly from its normal location (KS) and as such, probably inactivating it. We will therefore next investigate the cellular roles of TPD54 using these tools.

Chapter 4 – TPD54 is required for normal cell migration

4.1 Introduction

In the past few years, many clinical articles have been published, suggesting that TPDs either increase (He et al., 2015; Xu et al., 2015; Yang et al., 2015; Yu et al., 2017; Zhao et al., 2017) or decrease (Kato et al., 2017; Mukudai et al., 2013) cellular migration, invasion or proliferation. These studies all used cancer cell lines, and alterations in the processes mentioned are hallmarks of cancer. Although the authors come to different conclusions, TPD54 does appear to have a role in cell motility. Exactly what this role is and the mechanism behind it is still unclear.

We have shown so far that TPD54 is associated with the recycling Rab GTPases Rab4 and Rab11. One key step in cell migration and invasion is the trafficking of the integrins (Caswell and Norman, 2006), and two of the pathways the integrins are trafficked on are the Rab4 and Rab11-mediated recycling pathways (Roberts et al., 2001; Roberts et al., 2004; Woods et al., 2004). Since TPD54 has a potential a role in cell migration and invasion, and because we found that it is associated with proteins important for cell motility, we decided to investigate the function of TPD54 in cell migration.

4.2 TPD54 is required for 2D cell migration

To look at the role of TPD54 in cell migration, a 2D migration assay was performed with cells depleted of TPD54 plated on dishes coated with the ECM protein, fibronectin. Movies of RPE1 cells migrating freely were recorded over 12 hours and the cells were tracked until they reached mitosis or exited the field of view (**Figure 4.1**). Three different siRNAs targeting the 3′ UTR of TPD54 were assessed individually, and all resulted in a significant decrease in migration speed (**Figure 4.1A**). This indicates that the migration phenotype described is unlikely to be due to an off-target effect of a given siRNA.

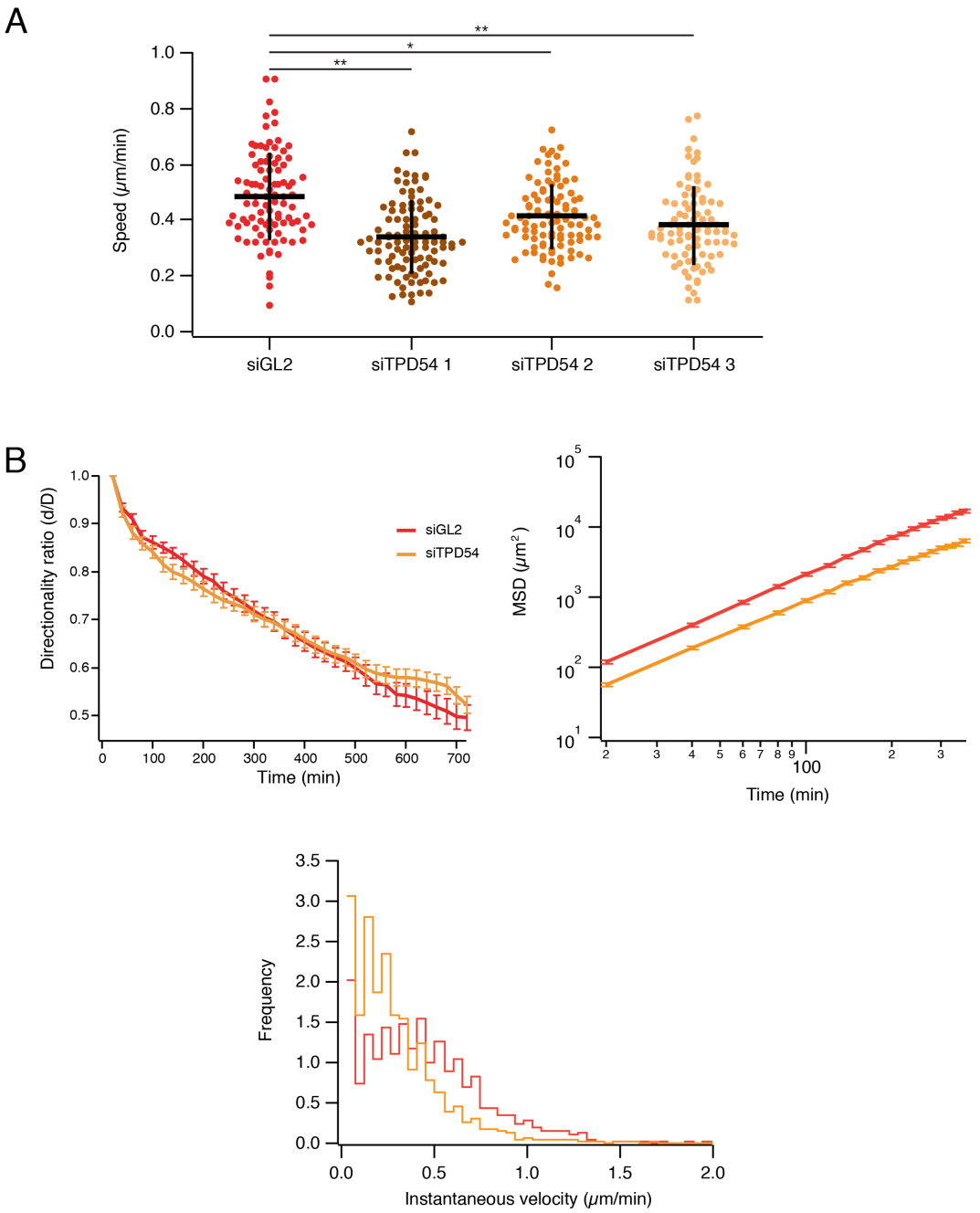

Figure 4.1: TPD54 depletion in RPE1 cells decreases 2D migration speed. A) 2D migration of RPE1 cells seeded on fibronectin and transfected with control or three different TPD54 siRNA. n=1. Dots are individual cells, horizontal bar is mean value and vertical bars are standard deviation. p values from Tukey post-hoc comparison. * <0.05, **<0.01. B) Directionality ratio, mean squared displacement and histogram of instantaneous velocity of RPE1 cells seeded on fibronectin and transfected with either control siRNA or TPD54 siRNA 2. n=3. Mean + SEM is shown.

Single cell tracking revealed a number of statistics on cell motility. Analysis showed that only the migration speed is impaired in TPD54 depleted RPE1 cells. The directionality ratio is not different (**Figure 4.1B**) meaning that the TPD54 KD cells do not make more or less turns than the control cells. Also, the instantaneous velocity is functions of migration speed; it is then expected that control cells have faster bursts of speed than the TPD54 depleted cells. Finally, the slope of the MSD is not different between control and KD cells, meaning the cells explore their environment in a similar manner. The only difference is the error in the measurement (intercept) is higher in control cells, probably because of greater migratory speed (**Figure 4.1B**). Since all three siRNAs against TPD54 resulted in a similar migration phenotype, we continue the experiments with the siRNA siTPD54 2, since it is efficient in HeLa (**Chapter 3 Figure 3.7**) and in RPE1 (**Figure 4.2A**).

The ECM on which the cells migrate is composed of many types of proteins (Randles et al., 2017), and very motile or static cells utilise different molecules for attachment. Epithelial cells, which are more static, rely on integrin α6β1 to anchor themselves to laminin and on integrins in hemidesmosomes to stabilise the epithelium. More motile cells depend mainly on integrin α5β1 and α2β1 for anchoring to fibronectin (Huttenlocher and Horwitz, 2011; Rainero and Norman, 2013). We therefore wanted to see if the role of TPD54 was dependant on one type of ECM component or if its effect was more generalised. To do so, RPE1 cells were seeded in dishes coated with laminin or fibronectin, or no ECM protein and allowed to migrate. Figure 4.2 B-C shows that TPD54 depletion affects RPE1 cell migration speed only when migrating on laminin or fibronectin.

Next, we wanted to make sure that the migration speed phenotype was due to the loss of TPD54. To do so, we tried to rescue migration speed by re-expression of TPD54 in TPD54-depleted cells seeded in dishes coated with fibronectin.

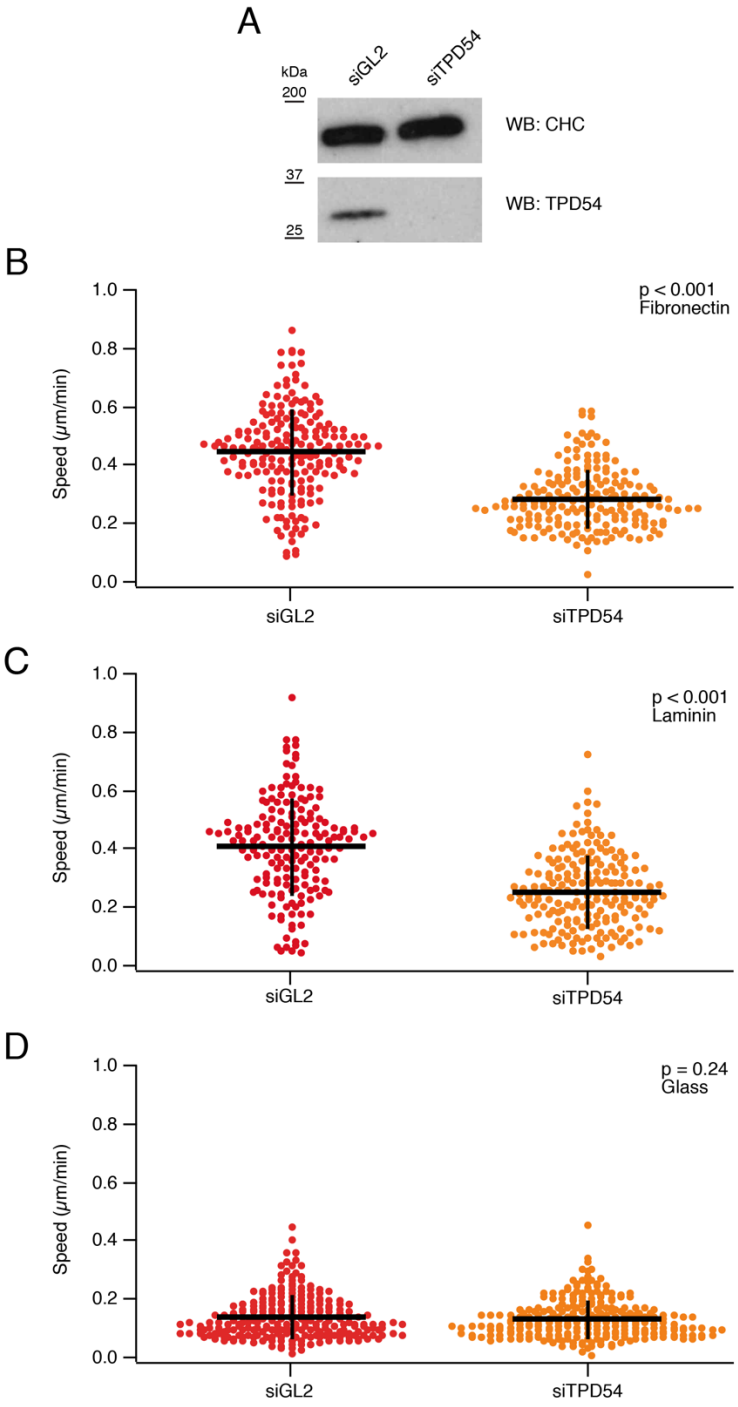

Figure 4.2: TPD54 knockdown affects migration speed of RPE1 cells on different substrates. A) Western blot showing the expression level of TPD54 48 h post transfection of siRNA 2 for the migration experiments. Clathrin heavy chain is used as a loading control. B-D) Migration speed of RPE1 cells plated in dishes coated with (B)fibronectin, (C) laminin or (D) uncoated, and transfected with control or TPD54-targeting siRNAs. n=3 for each experiement. p values from Student t-test. Dots represent single cells. Bars: mean and standard deviation.

As seen in figure 4.3, GFP-TPD54 under a CMV promoter did not rescue migration speed (**Figure 4.3A**). Also, cells transfected with a plasmid after being exposed to siRNA transfection mix (GFP+ and GFP-TPD54+) migrate

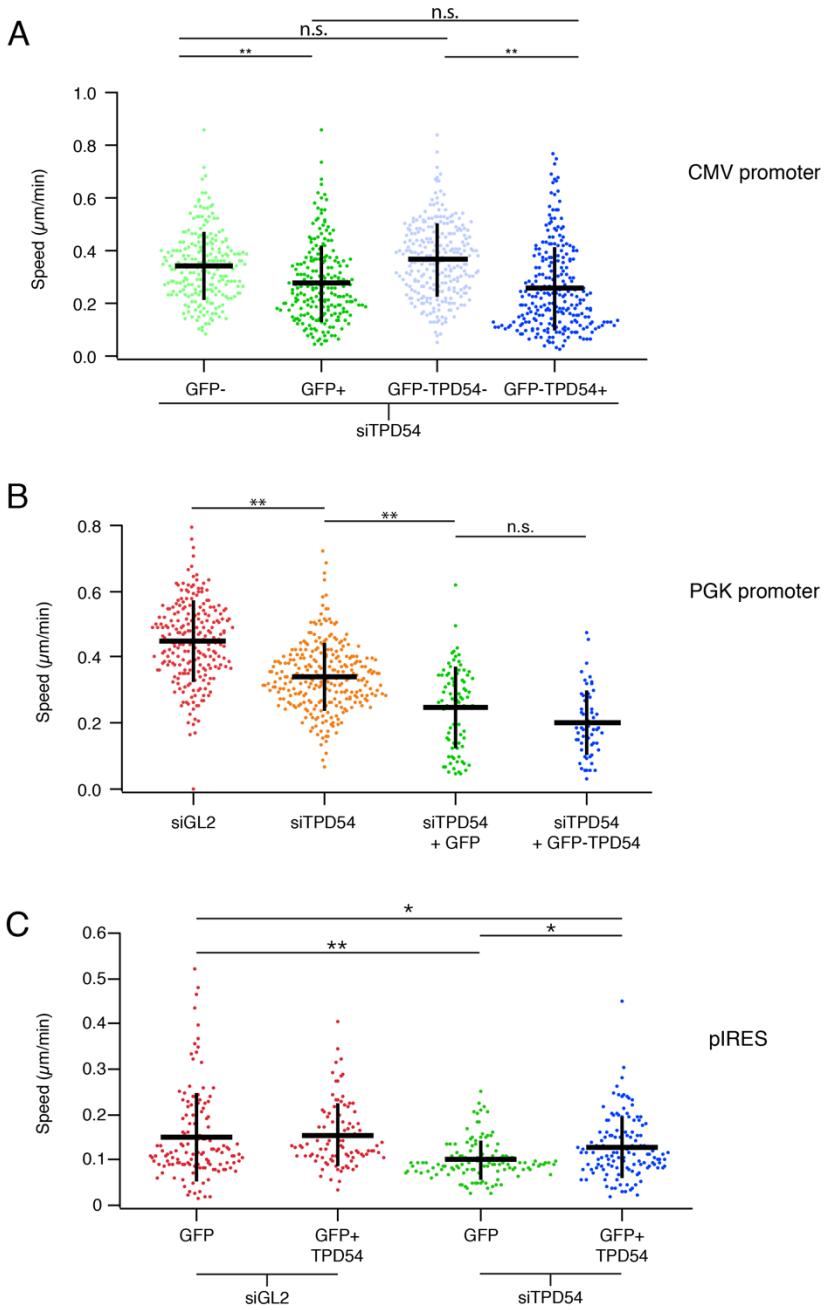

Figure 4.3: Migration speed can be rescued by pIRES-EGFP-TPD54. In RPE1 cells seeded on dishes coated with fibronectin, migration speed is not rescued by the expression of GFP-TPD54 either under a CMV (A) or a PGK (B) promoter. The phenotype could be rescued by an untagged version of TPD54 (C, normalised speed) expressed in a pIRES-EGFP vector. n=3 for each experiment. p values from Tukey post-hoc comparison. * <0.05, **<0.01. Dots are single cells and bars are average and standard deviation.

significantly slower than cells treated with siRNA but not transfected with a plasmid (GFP– and GFP-TPD54–). We hypothesized that since the CMV promoter drives high expression, reducing the level of re-expression of TPD54 might rescue the phenotype. We then expressed GFP-TPD54 from a PGK promoter in TPD54 depleted cells seeded in dishes coated with fibronectin (**Figure 4.3B**). Cells transfected with a plasmid showed again a significantly lower migration speed when compared to TPD54 KD cells, indicating that the level of expression is not responsible for the decrease in migration speed. We next wanted to test if expressing a tagged version of TPD54 was preventing us from rescuing the migration phenotype. TPD54 and GFP were expressed in cells seeded in dishes coated with fibronectin with a bicistronic pIRES-EGFP vector, allowing us to express an untagged TPD54 and a transfection reporter (GFP) in the same cells (**Figure 4.3C**). Three repeats were done, each one having a different average migration speed but all showing a rescue. Taken together, these data show that TPD54 has a role in cell migration and that this role is specific, since three different siRNAs cause a similar phenotype and that this phenotype can be rescued by re-expressing TPD54.

We finally wanted to check if we could induce a slower migration speed in RPE1 cells seeded in dishes coated with fibronectin by rapidly inactivating TPD54 by knocking it sideways. As seen in figure 4.4, we have been unable to affect migration speed by knocking TPD54 sideways, suggesting a longer depletion is required to affect migration.

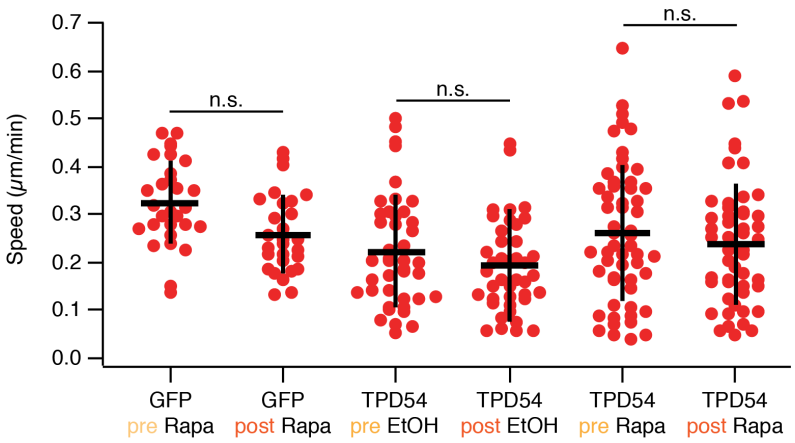

Figure 4.4: Knocksideways of TPD54 has no effect on RPE1 migration speed on fibronectin. TPD54-depleted cells expressing either GFP-FKBP or GFP-KFBP-TPD54 were treated with either rapamycin or ethanol (vehicle) and migration speed was measured. p values from Tukey post-hoc comparison. Dots are single cells and bars are average and standard deviation. Pre-rapamycin were recorded for 2 hours and post-rapamycin movies for ten hours. n=3.

4.3 The role of TPD54 in migration is independent of Rab4 and Rab11

It has been shown that cell migration requires Rab4 and Rab11 recycling pathways (Caswell and Norman, 2006), and we have demonstrated so far that TPD54 is associated with Rab4 and Rab11 (section 3.2) and is required for 2D cell migration. The next question to answer is then whether or not TPD54 is on the same pathway as Rab4 and/or Rab11 and if so, is this the mechanism behind the role of TPD54 in cell migration? We would expect that if TPD54 is on the same pathway as Rab4 or Rab11, depleting both TPD54 and Rab4/11 would not create a greater phenotype than the depletion of either one. Similarly, if TPD54 is on another pathway important for migration, a depletion of TPD54 and Rab4/11 would create a worse phenotype than the depletion of only one. To assess this, we depleted Rab4 or Rab11 in RPE1 cells seeded on fibronectin and compared the migration speed of these cells with cells depleted of TPD54 (**Figure 4.5**). The cells were treated with siRNAs for 48 h with a combination of siGL2, siRab4, siRab11 and siTPD54 which all gave a good depletion (**Figure 4.5A**). To our surprise, we found that depletion of either Rab4 (**Figure 4.5B**) or Rab11 (**Figure 4.5C**)

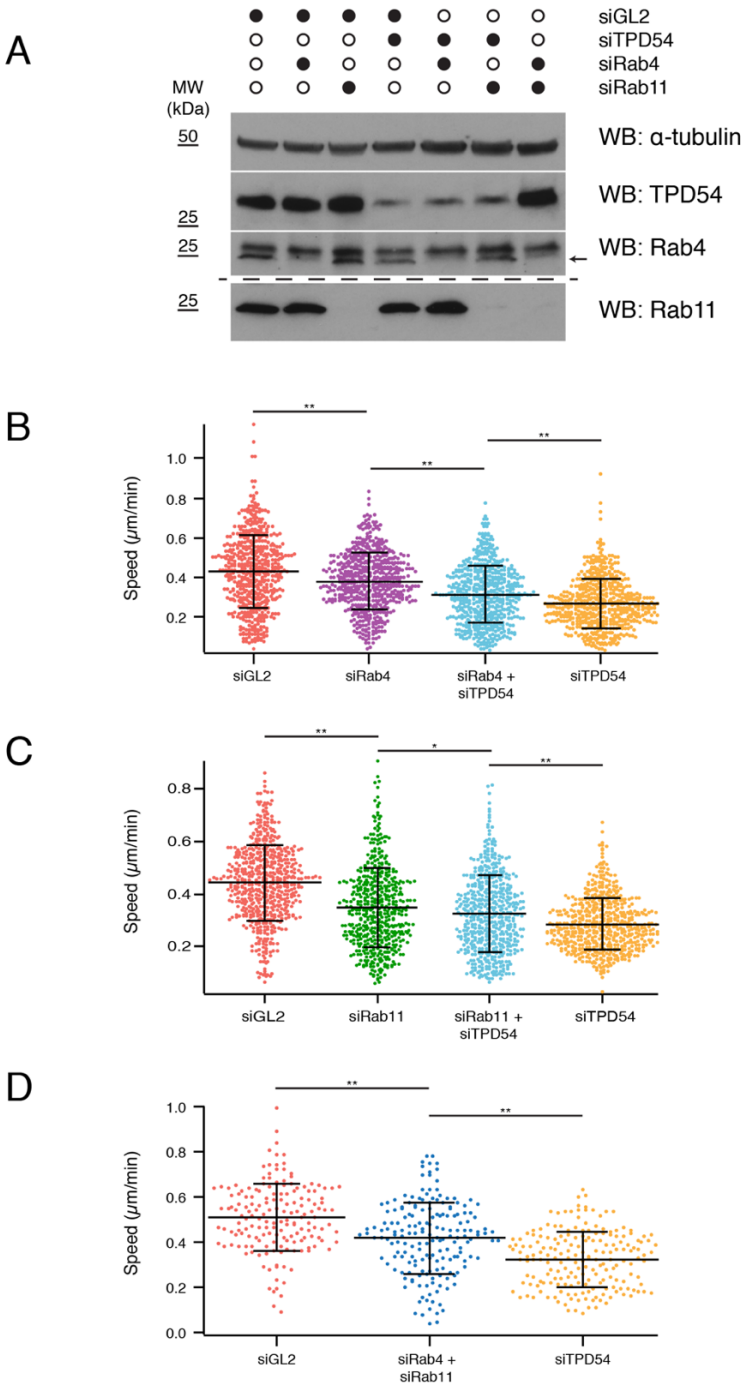

Figure 4.5: Knockdown of Rab4 and/or Rab11 didn't affect migration speed as much as TPD54 KD. A) Western blot showing the levels of tubulin (loading control), TPD54, Rab4 and Rab11 after 48 h of KD. Rab11 blot was done on another experiment, in which the level of tubulin was checked to make sure the conditions were the same as the experiment shown above. Migration speed of RPE1 cells treated with control, TPD54 or Rab4 (B), Rab11 (C) or Rab4/11 dKD. p value from Tukey post-hoc comparison. Dots are single cells and bars are average and standard deviation. n=3 for each experiment.

did not affect migration speed as much as depletion of TPD54 did. We then thought that by depleting both TPD54 and the Rab GTPases, we might affect migration speed at least as much as a depletion of TPD54, which was not the case. Indeed, a combination of Rab4/TPD54 (double knockdown or dKD), or Rab11/TPD54 didn't have a greater phenotype than depletion of TPD54 alone. It was possible that impairing one recycling pathway (slow or fast) results in the other one being upregulated and that there was compensation. We therefore depleted both Rab4 and Rab11 and compared the migration speed of these cells with TPD54-depleted cells. As shown in figure 4.5D, a TPD54 KD affects RPE1 cells migration speed more than a Rab4/11 double KD, suggesting that TPD54 could be on Rab4- and/or Rab11 pathways, potentially upstream of the GTPases during cell migration, since the phenotype is greater than the Rab4/11 dKD phenotype. The severity of this TPD54 KD phenotype highlights the importance of TPD54 in cell motility.

Although no worsening of migration speed was detected during these experiments, we noticed that the cell shape was affected by either a Rab11 or a TPD54 depletion (**Figure 4.6**). Control RPE1 cells migrating on fibronectin displayed an archetypal shape: quite compact, with a clear tail at the rear end and a lamellipodium at the leading edge (**Figure 4.6A**). Rab4-depleted cells did not display a real difference when compared to control cells. Rab11 KD cells were very long, with a disproportionate tail that tended to get 'stuck' behind the cell, the cell cannot retract its tail (**Figure 4.6A**). As for TPD54 KD cells, they were flattened and appeared much larger than control cells, making many protrusions with no clear leading edge (**Figure 4.6A**). Rab4 did not have a much different phenotype than control cells. To examine these shapes in more detail, we quantified the cell footprint area and compared our different conditions (**Figure 4.6B-C**). This quantification further re-enforced the hypothesis that TPD54 might not act on Rab4 or Rab11 pathways, since neither cell shape nor migration speed of TPD54 depleted cells is phenocopied by a depletion of Rab4 or Rab11.

Finally, we wanted to see if we could mimic the TPD54 KD cell size by rapidly removing TPD54 from its normal localisation with a knocksideways of TPD54

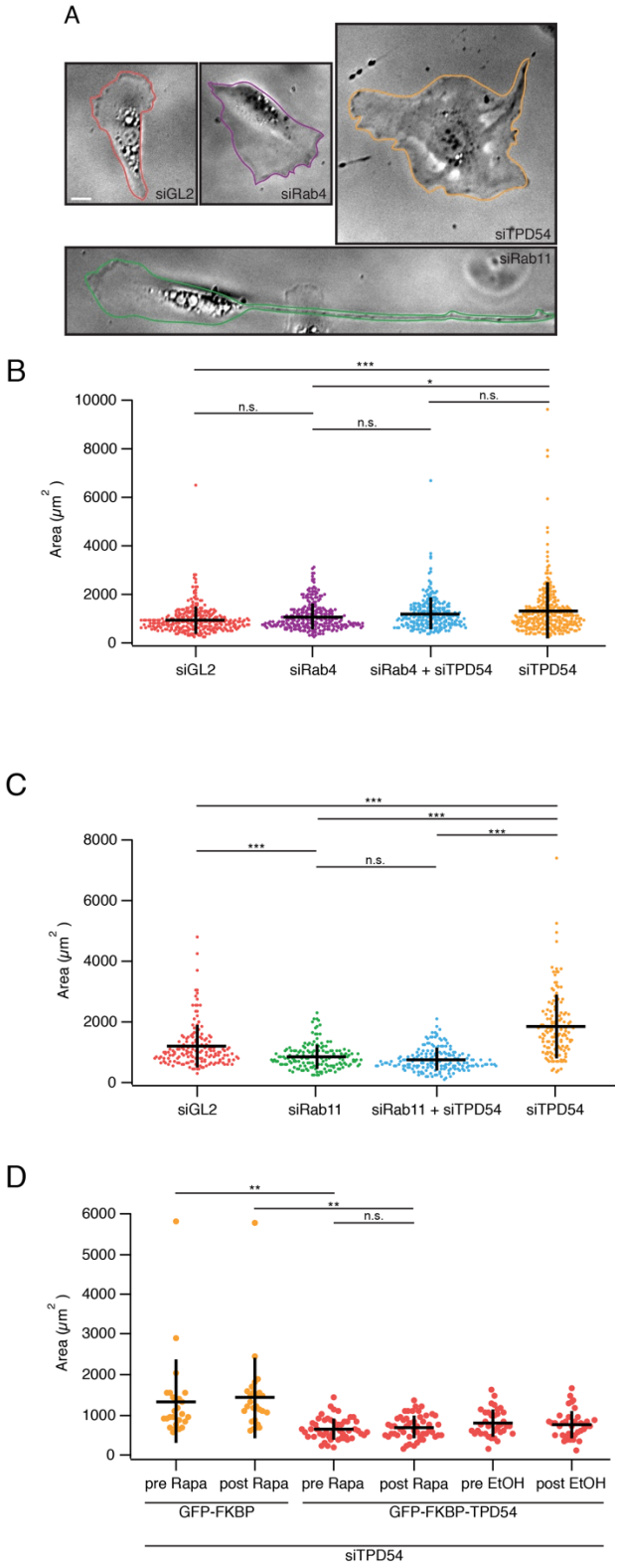

Figure 4.6: TPD54-depleted RPE1 cells have a larger footprint. A) Representative micrographs of cells in the different conditions freely migrating on fibronectin-coated

dishes. B-C) Cell area comparison between control, Rab4/11 KD, TPD54 KD or TPD54/Rab dKD. D) Effect of a GFP-FKBP(-TPD54) knocksideways on RPE1 cells area. p values from Tukey post-hoc comparison. n=3 for each experiment.

(**Figure 4.6D**). We have been able to see that TPD54-depleted cells have a bigger footprint than TPD54-depleted cells re-expressing GFP-FKBP-TPD54 (we could rescue the cell footprint area). However, taking away TPD54 quickly had no effect on cell size.

Taken together, the data suggest that since depletion of Rab4 and/or Rab11 doesn't phenocopy depletion of TPD54, the latter might have a role in 2D cell migration that is independent of its putative association with Rab4 or Rab11. It remains possible that TPD54 has a role in cell motility which is independent of membrane traffic (and that this could be in addition to a trafficking-specific role in migration). However, we propose the idea that the role of TPD54 in trafficking underlies the migration phenotype.

4.4 TPD54 has a role in the recycling of integrins

One of the key steps enabling cell migration is the trafficking of integrins, allowing assembly and disassembly of cellular adhesions. As mentioned in section 4.1, Rab4 and Rab11 are not the only recycling routes that integrins can be trafficked on (De Franceschi et al., 2015). Another important route is the Rab25-dependant pathway, either salvaging ligand-bound integrins from the lysosomal pathway (Dozynkiewicz et al., 2012) or keeping a pool of integrins at the cell front for a more efficient invasion (Caswell et al., 2007). Since it doesn't seem like TPD54 is entirely on Rab4 or Rab11 pathway but still have an important role in cell migration we wanted to investigate the possibility of an association with Rab25. To do so, we used to co-knocksideways approach to test if Rab25-positive vesicles could also be rerouted by a TPD54 knocksideways. As shown in figure 4.7, Rab25 colocalises with TPD54 on the mitochondria after the addition of rapamycin, suggesting an association between TPD54 and Rab25-recycling pathway too. Given the role of TPD54 in migration and its association with the recycling pathways, we next wanted to test directly this hypothesis by assessing the

requirement for TPD54 in the recycling of the integrins. Briefly, in RPE1 cells, surface receptors were labelled with biotin and allowed to be internalised. Biotin on receptors that stayed at the surface was removed and internalised receptors allowed to be recycled for 10, 20 or 30 minutes. Biotin on the recycled receptors was removed from the cell surface and the internal content of the cell was quantified, measuring the recycling efficiency (**Figure 4.8A**). Figure 4.8B shows that TPD54 has a role in the recycling of integrin α5 since its depletion causes a significant decrease in the cells ability to recycle the receptors.

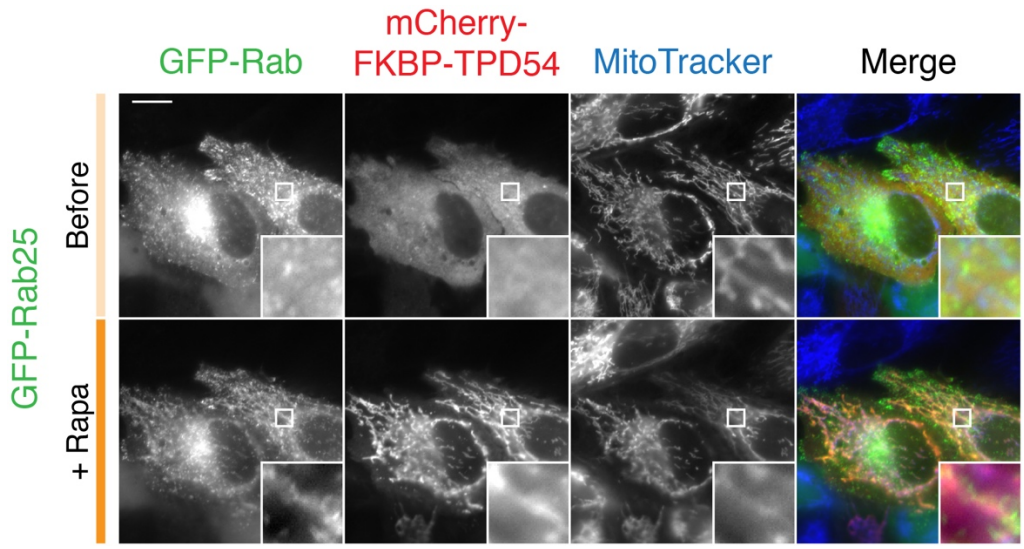

Figure 4.7: Rab25 is rerouted to the mitochondria with a mCherry-FKBP-TPD54 knocksideways. HeLa cells expressing GFP-Rab25, mCherry-FKBP-TPD54 and dark MitoTrap were treated with 200 μM rapamycin. Inset: 5X zoom. Scale bar: 10 μm.

If TPD54 is important for integrin traffic, we would be able to see colocalisation of TPD54 and integrin α5 in live cells. We used widefield microscopy and co-expressed integrin α5-GFP and mCherry-TPD54 to test this. We have been able to see both proteins on the same structure, being trafficked together over time (**Figure 4.9**). This is more evidence that TPD54 has a role in the trafficking of integrins, and that this might be the underlying role of the protein in cell motility.

We also wanted to know if integrins were present on the vesicles removed during knocksideways. We have tested a conformation-independent integrin

α5 and a conformation-dependant integrin β1, because different routes can be taken by the integrins depending on their conformation state (Arjonen et al., 2012) . In figure 4.10, we show that this could not be done, either with integrin α5-GFP or an antibody recognising the inactive form of integrin β1, mAb13.

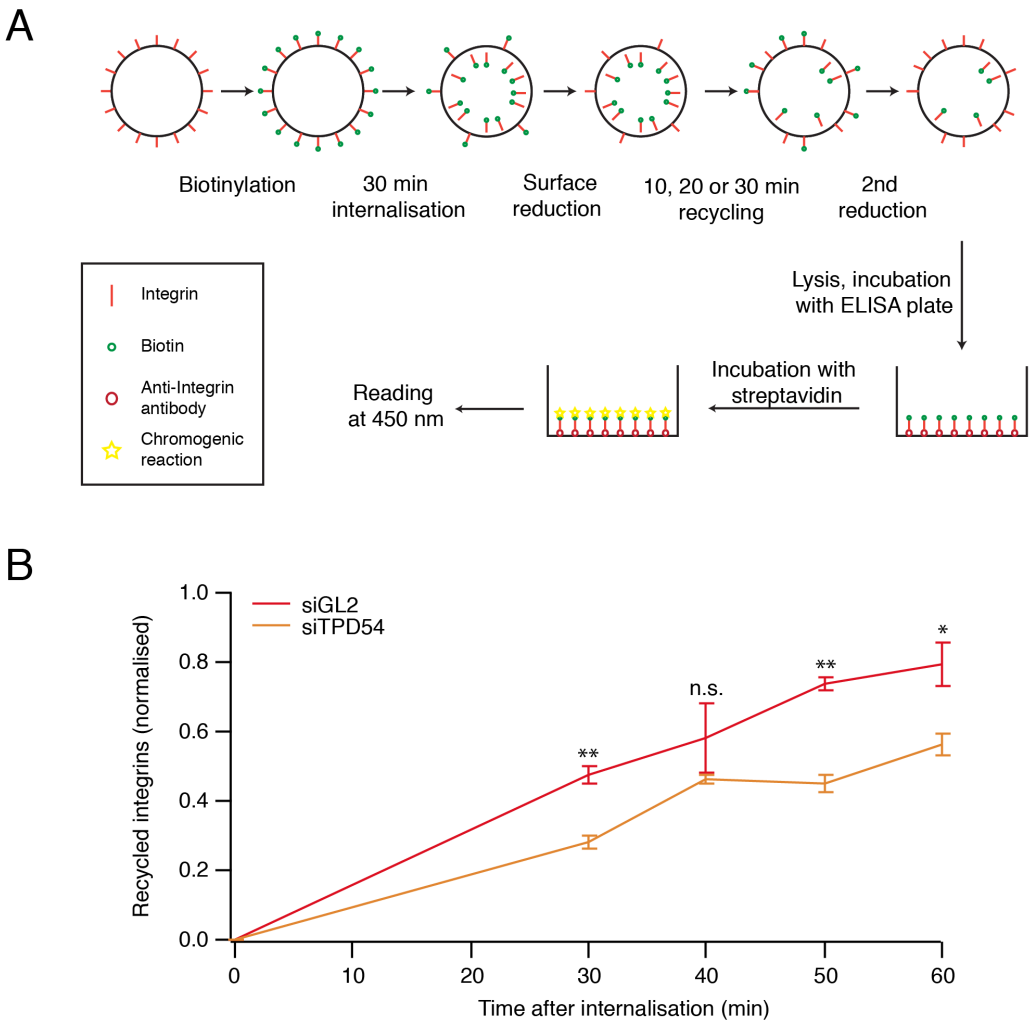

Figure 4.8: Integrin recycling is impaired in TPD54 depleted cells. A) Schematic diagram of the recycling assay. B) RPE1 cells were transfected with control of TPD54 targeting siRNAs for 48 h. Graph showing the amount of recycled integrin α5 as a function of time. Three independent experiments were averaged. Bars show standard deviation. p values from Student t-test. * <0.05, **<0.01.

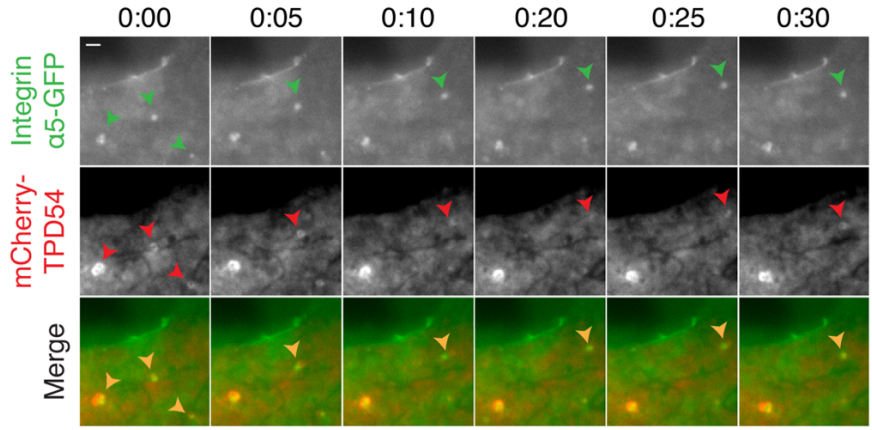

Figure 4.9: mCherry-TPD54 and integrin α5-GFP are trafficked together. Time course showing that both proteins can be found on the same vesicles in HeLa cells. Arrows indicate colocalisation. Scale bar: 1μm.

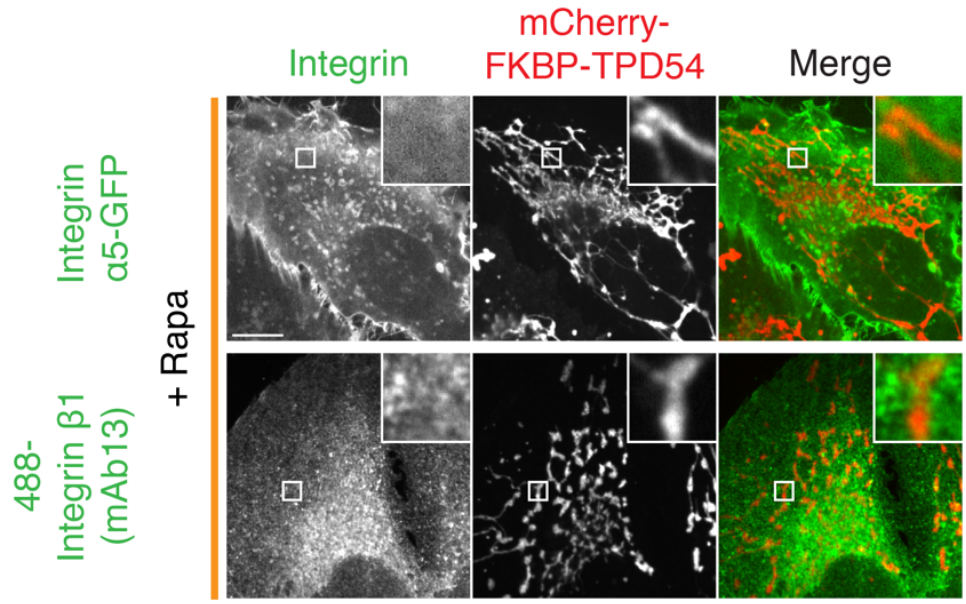

Figure 4.10: Knocksideways of TPD54 does not reroute integrin α5β1. TPD54-depleted HeLa cells were transfected with dark MitoTrap, mCherry-FKBP-TPD54 and integrin α5-GFP (upper panel) and treated with 200 μM rapamycin for 20 min before fixation and staining with mAb13 (lower panel). Scale bar: 10 μm, inset: 5X zoom.

The trafficking of integrins results in the cell's ability to remove old focal adhesions and form new ones, allowing them to move. TPD54 is important for cell migration and for the recycling of integrins. We next wanted to know whether or not focal adhesions are altered in TPD54 depleted cells. An

immunofluorescence of vinculin was performed on control or TPD54-depleted RPE1 cells (**Figure 4.11**). Micrographs were acquired and analysed with an automated workflow. The cells area and the size of focal adhesions were measured in an unbiased manner (**Figure 4.11A**). With this technique, we have found no significance difference in the density of bigger focal adhesion (>500 μm/μm^2) (**Figure 4.11B**), of smaller focal adhesions (>100 μm/μm^2) (**Figure 4.11C**) or in the total density of focal adhesions (**Figure 4.11D**).

4.5 Discussion

In this chapter, we saw that TPD54 is important for 2D cell migration, on either fibronectin or laminin. This suggests that the effect of TPD54 on migration is not limited to very motile cells, like cancer cells, which is the model that has been favoured so far for assessing the role of TPDs in cell migration (Mukudai et al., 2013; Yu et al., 2017). We have also shown that TPD54 does not affect directionality. The cells are not more or less likely to change direction while migrating. Studies have suggested that migration persistence can be affected by Rab11 or Rab6 (Shafaq-Zadah et al., 2016; Theisen et al., 2012; White et al., 2007). The fact that TPD54 KD cells have similar directionality ratio as control cells suggests that TPD54 depletion doesn't impair these pathways. The migration speed phenotype can be rescued by an untagged TPD54. We have so far been unable to rescue the phenotype with GFP-TPD54, suggesting that this tag might alter the protein's integrity or its role in migration.

During a knocksideways, the rerouted protein is sequestered to the mitochondria and unavailable for its normal role, and defects can become apparent on a short time scale. In a study conducted by Cheeseman et al. in 2013, a knocksideways of TACC3, an essential protein for mitotic spindle stability, caused a delay in different stages of mitosis within minutes after

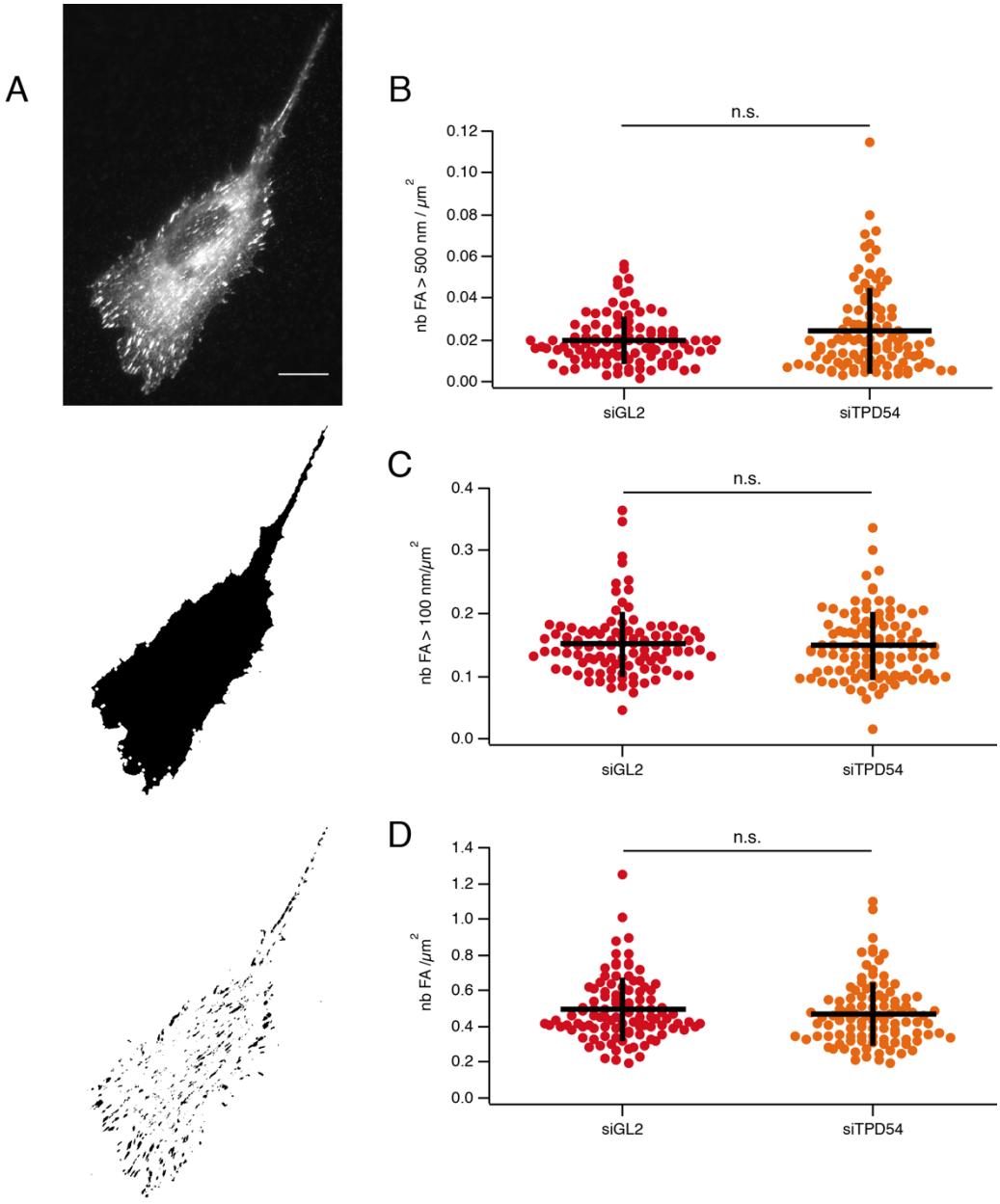

Figure 4.11: Depletion of TPD54 doesn't cause an alteration in focal adhesion number. A) Representative micrograph of an RPE1 cell stained with anti-vinculin antibody (top panel) and the mask generated by our automated workflow for Igor Pro for the analysis of focal adhesion number: the cell footprint (middle panel) and the focal adhesions (lower panel). Scale bar: 10 µm. B-D) Density of focal adhesions according to their size. p value from Student t-test. Dots are single cells and bars are average and standard deviation. n=3.

rerouting (Cheeseman et al., 2013). We would then expect a knocksideways of TPD54 to impair migration of cell size within a few hours. Although to our surprise, rerouting TPD54 to the mitochondria has had no effect on migration speed.

As seen by immunofluorescence, barely any TPD54 is left in the cytosol (**Figures 4.7 and 4.10**) after knocksideways. Therefore, the reason why we detected no effect on migration cannot be explained by enough proteins left free. This is also re-enforced by the fact that a slower migration speed can be observed after only 24 h of treatment with TPD54 siRNA (data not shown), which leaves some proteins in the cell (**Chapter 3, Figure 3.7**). The reason why a knocksideways has no effect on migration could be due to an experimental time course that is not long enough. In this experiment, rapamycin was added to the cells after two hours and cells were recorded for ten more hours. We might have seen a decrease in migration speed after a longer time. This could be tested, although it would have to be kept in mind that the dissociation $t_{1/2}$ of rapamycin and FKBP is 17.5 h (Hosoi et al., 1999). The longer we record, the less dimerization we have. Another reason why no change in speed was recorded might be that, on whichever pathway TPD54 is acting, interfering with one might upregulated another. We can also imagine that if TPD54 is indeed on Rab4-, Rab11-, or Rab25-dependent pathways, there might also be some Rab-positive but TPD54-negative vesicles left, and that these vesicles are able to carry on their migration role. Indeed, as seen in figure 4.7, the amount of GFP-Rab25 rerouted to the mitochondria is minor when compared to the amount of mCherry-FKBP-TPD54. We could also be facing a case where the role of TPD54 in migration is independent from its role in membrane trafficking. This is however unlikely, because TPD54 can be seen on the same vesicles as integrins, and it is required for integrin trafficking.

For the cell to move, the integrins linking the cell to the ECM must be trafficked. We found that a depletion of TPD54 causes a greater effect on 2D migration than a depletion of Rab4- or Rab11-dependant recycling pathways.

This could be due to the fact that integrins can take multiple different routes to go back to the surface once internalised, whether they are at the cell front or the tail, whether the integrins are in an active or inactive conformation, or depending on the identity of the integrins forming the dimer (De Franceschi et al., 2015). This indicates that the role of TPD54 in 2D cell migration might come from its association with another pathway.

The fact that we rerouted Rab25 alongside TPD54 suggests that the protein also have a role in invasion. We have been able to collaborate with Dr. P.T. Caswell. His team has used breast cancer cell line A2780 stably expressing GFP-Rab25. They found that invasion efficiency on a 3D cell-derived matrix is significantly decreased in TPD54 depleted cells (Larocque et al., 2016) (see poster in appendix 1).

To check if we indeed affect the recycling of the integrins, we have done an assay that did show a defect in recycling which was similar to published defects observed for a CLIC3- (Dozynkiewicz et al., 2012) or a GGA3-depletion (Ratcliffe et al., 2016), re-enforcing the hypothesis that TPD54 affects migration by having a role in integrin recycling, even though knocksideways of TPD54 could not reroute integrins. There might not be enough integrins in the rerouted vesicles to be detected by immunofluorescence. However, we have not had a migration phenotype with knocksideways either. It therefore appears that knocksideways might not be the right technique for assessing the role of TPD54 in migration.

Finally, we have not been able to see an effect on the size or number of focal adhesions so far, but we would probably need to look at the dynamics of this process. We can hypothesise that the number of adhesion doesn't change but the assembly or disassembly efficiency might be impaired. Movies of migrating cells expressing a focal adhesion marker would give us more insight on this.

To conclude, we have found that TPD54 is required for 2D cell migration on either fibronectin or laminin and also in the recycling of integrins, probably via its association with Rab25. We also hypothesise that this role in integrin

trafficking is independent of the Rab4- and Rab11-dependent recycling pathway, despite an association with these vesicles.

Chapter 5 – TPD54 is required for recycling of dileucine motif-containing receptors

5.1 Introduction

TPD54 is associated with transport vesicles, probably on a pathway before or after the recycling endosomes, since the protein reroutes vesicles containing Rab4, Rab11 or Rab25 to the mitochondria after a knocksideways. Furthermore, the TPD52 family has been reported to be associated with membrane trafficking components like clathrin (Borner et al., 2006) and SNARES (Proux-Gillardeaux et al., 2003), and involved in secretion (Messenger et al., 2013) of polarized cells endosomes (Sathasivam et al., 2001), suggesting a role for TPD54 in trafficking. However, the rerouting of the Rab GTPases was partial, arguing that the association is not exclusive. We also don't know what cargo the TPD54-positive vesicles contain.

We hypothesised in the previous chapter that TPD54 is involved in the recycling of the integrins and we have shown that a depletion of TPD54 in RPE1 cells results in a defect in integrin α5 trafficking. Both proteins can also be imaged on the same vesicle, but we were surprised by the fact that we could not reroute integrin α5 or β1 with a TPD54 knocksideways even though we could affect their recycling by TPD54 RNAi.

In this chapter, we aim to determine which cargo is in TPD54-positive vesicles and what pathway it acts on. This will help us uncover the role of TPD54 in membrane trafficking.

5.2 TPD54 is associated with the dileucine motif

What cargo do TPD54-positive vesicles contain? Rab4, Rab11 and Rab25 are all recycling-associated GTPases. One of the well characterised proteins going through the recycling pathways is the transferrin receptor (TfR)

(Sonnichsen et al., 2000; Vandersluijs et al., 1992). TfR binds to iron-bound transferrin (Tf) at the cell surface and gets internalised. When the complex reaches the lower pH of the early endosomes, iron ions are released and the TfR-Tf complex returns to the cell surface and dissociates (Hsu et al., 2012). Is TPD54 involved in the recycling of TfR, and if so, would we be able to co-reroute it with TPD54 knocksideways? To investigate this, HeLa cells were treated with control or TPD54-targeting siRNA for 48 h. Cells were then incubated with AlexaFluor-488 labelled transferrin (Tf) and internalisation and recycling were allowed. Figure 5.1 shows that depletion of TPD54 does not affect Tf uptake (0-15 min after internalisation), but has a significant effect on its recycling.

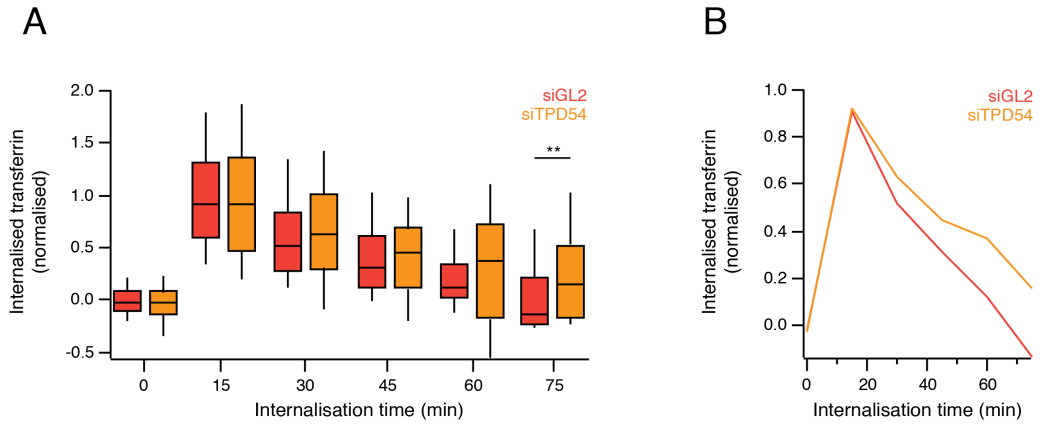

Figure 5.1: Depletion of TPD54 significantly affects the recycling of Tf. A) Boxplot showing the uptake and recycling of Tf in control and TPD54-depleted HeLa cells. Boxes show lower and upper quartile, bar is median value and whiskers show 10th and 90th percentile. p value from Student T-test. **<0.01. B) Graph showing the median value of internalised Tf in control and TPD54 depleted HeLa cells as a function of time. n=3.

To see if the TfR could be co-rerouted by TPD54 knocksideways, HeLa cells were treated with TPD54 siRNA and transfected with dark MitoTrap, mCherry-FKBP-TPD54 and mNeonGreen-TfR. The cells were treated with rapamycin for 20 minutes and fixed. As seen in figure 5.2, like integrins, the TfR does not go to the mitochondria with TPD54 knocksideways.

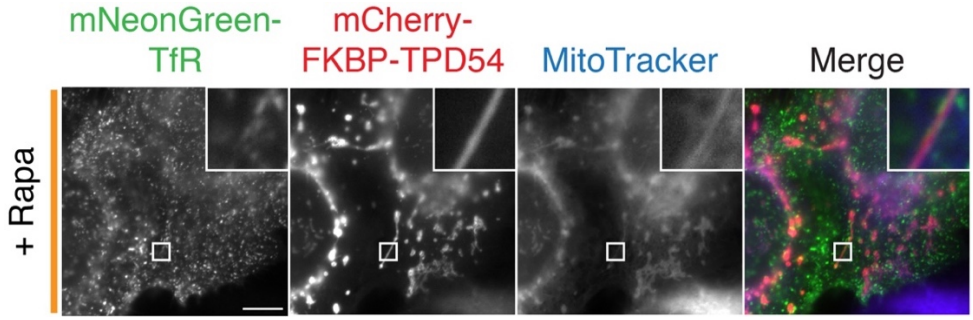

Figure 5.2: TfR is not co-rerouted with a TPD54 KS. Representative micrograph of knocksideways of TPD54. TPD54-depleted HeLa cells were transfected with mNeonGreen-TfR, mCherry-TPD54 and dark MitoTrap, treated with 200 nM rapamycin for 20 min and fixed. Mitochondria were stained with far-red MitoTracker. Scale bar: 10 µm, inset: 5X zoom.

We now have two different transmembrane proteins, for which recycling is well characterised, that do not reroute with TPD54 and yet, a depletion of the protein affects their recycling. The question is then: what cargo can be rerouted with TPD54 knocksideways?

To answer this question, we used prototypical cargoes, the CD8-chimeras developed by Kozik et al. With no engineered tail, CD8 stays at the surface and isn't internalised. The chimeras contain one of the three most common endocytic motifs. CD8-YAAL contains the YXXΦ motif, where Φ is a bulky hydrophobic amino acid and X is any amino acid. CD8-EAAALL contains the [D/E]XXXL[L/I] motif and CD8-FANPAY contains the FXNPXY motif. There is also a negative control, CD8-8xA with is a tail of eight alanines (the construction base for the three other motifs), and CD8-CIMPR containing the tail of cation-independent mannose-6-phosphate receptor (CIMPR) which has multiple motifs (**Figure 5.3**) (Kozik et al., 2010). The three endocytic motifs are internalised normally, and CD8-CIMPR goes to the cell surface but is mainly trafficked between the TGN and the endosomes (Fielding and Royle, 2013; Kozik et al., 2010).

CD8 WT	KRLKRRRVCKCPRPVVKSGDKPSLSARYV*
CD8-CIMPR	KRLKYKKERREMVMSRLTNCCRRSANVSYKYSKVNKEEEA
	DENETEWLMEEIQPPAPRPGKEGQENGHVAAKSVRAADTL
	SALHGDEQDSEDEVLTLPEVKVRPPGRAPGAEGGPPLRPL
	PRKAPPPLRADDRVGLVRGEPARRGRPRAAATPISTFHDD
	SDEDLLHV*
CD8-8XA	KRLKRRRIPAAAAAAAAV*
CD8-YAAL	KRLKRRRIPAAYAALAAV*
CD8-EAAALL	KRLKRRRIPAEAAALLAV*
CD8-FANPAY	KRLKRRRIPAFANPAYAV*

Kozik et al., 2010

Figure 5.3: Sequence of the CD8-chimeras. Different endocytic motifs have been added to the CD8 receptor by Kozik and colleagues. The motifs have been added after the transmembrane domain of CD8, to the C-terminus cytoplasmic end of the protein. Known endocytic motifs are coloured.

To see whether or not a receptor containing one of the three main endocytic motifs could be rerouted with TPD54, TPD54-depleted HeLa cells were transfected with dark MitoTrap, mCherry-FKBP-TPD54 and one of the CD8-chimeras. Cells were either fixed and stained before treatment or treated with 200 nM rapamycin for 20 minutes, fixed and stained with a AlexaFluor488-CD8 antibody. We are therefore looking at total receptor and changes in its steady-state distribution. Figure 5.4A and B shows that only CD8-EAAALL and CD8-CIMPR (which also contains a dileucine motif) were rerouted to the mitochondria alongside TPD54, suggesting that only receptors containing the dileucine motif are associated with TPD54, and not receptors with the tyrosine-based or FXNPXY motifs. To verify that our result was not simply specific to designer cargoes, we testes the ability of the endogenous, dileucine motif-containing protein CIMPR, to be rerouted alongside TPD54 with a knocksideways and found both on mitochondria (**Figure 5.4C**). This suggested a real association between TPD54 and dileucine motif.

TPD54 can reroute a cargo containing a dileucine motif, but not a tyrosine-based motif. Since both are recognised by the same set of adaptor proteins and have the same sorting functions (Bonifacino and Traub, 2003), we wanted to see if we could track CD8-YAAL and CD8-EAAALL to perhaps, a TPD54 specific compartment, where the cargoes bearing these motifs could diverge. To do so, we transfected cells with either CD8-YAAL or CD8-EAAALL and markers of the trafficking pathways. On the confocal microscope, cells were

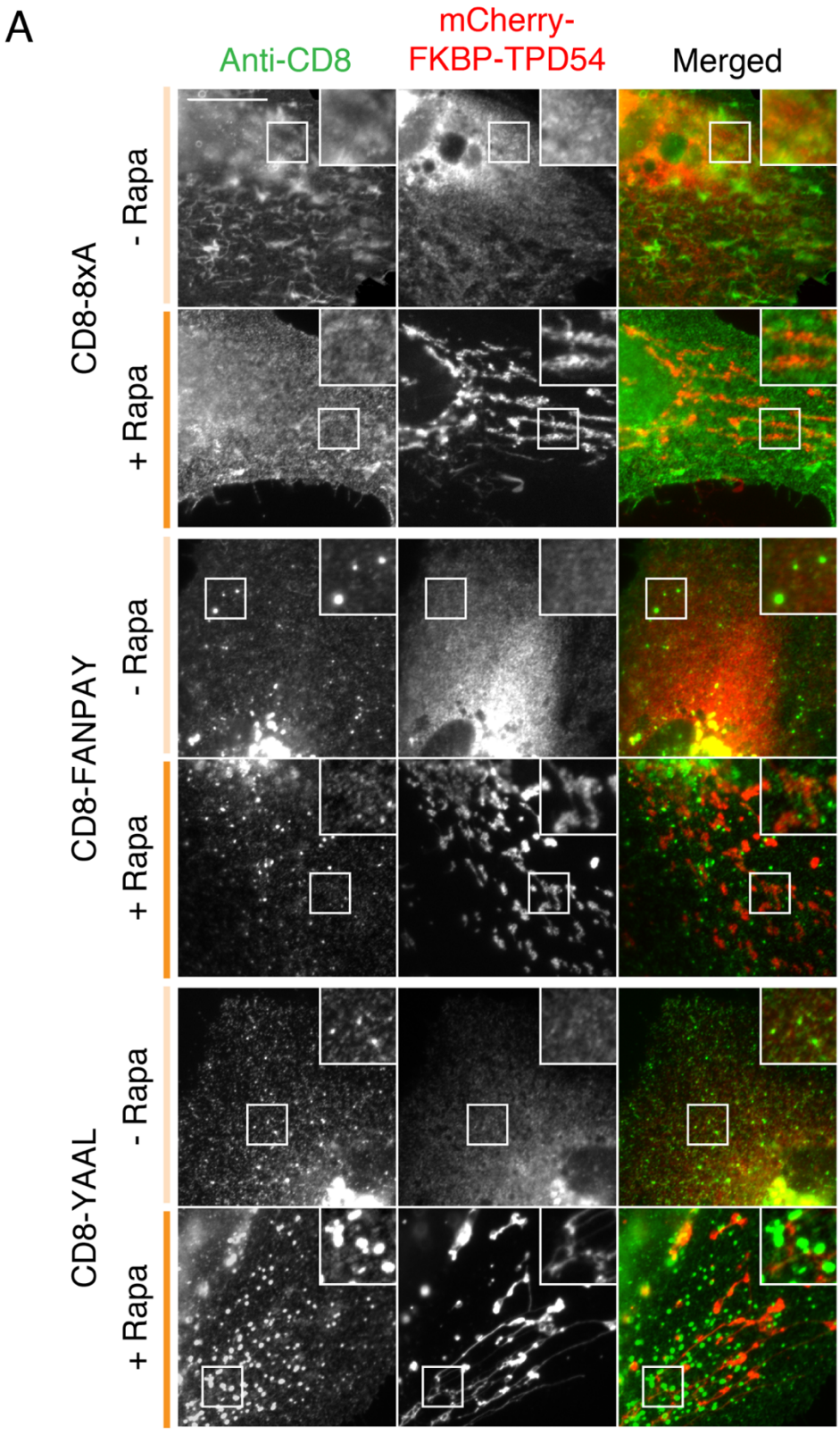
A
Anti-CD8
mCherry-
FKBP-TPD54
Merged
CD8-8xA
- Rapa
+ Rapa
CD8-FANPAY
- Rapa
+ Rapa
CD8-YAAL
- Rapa
+ Rapa

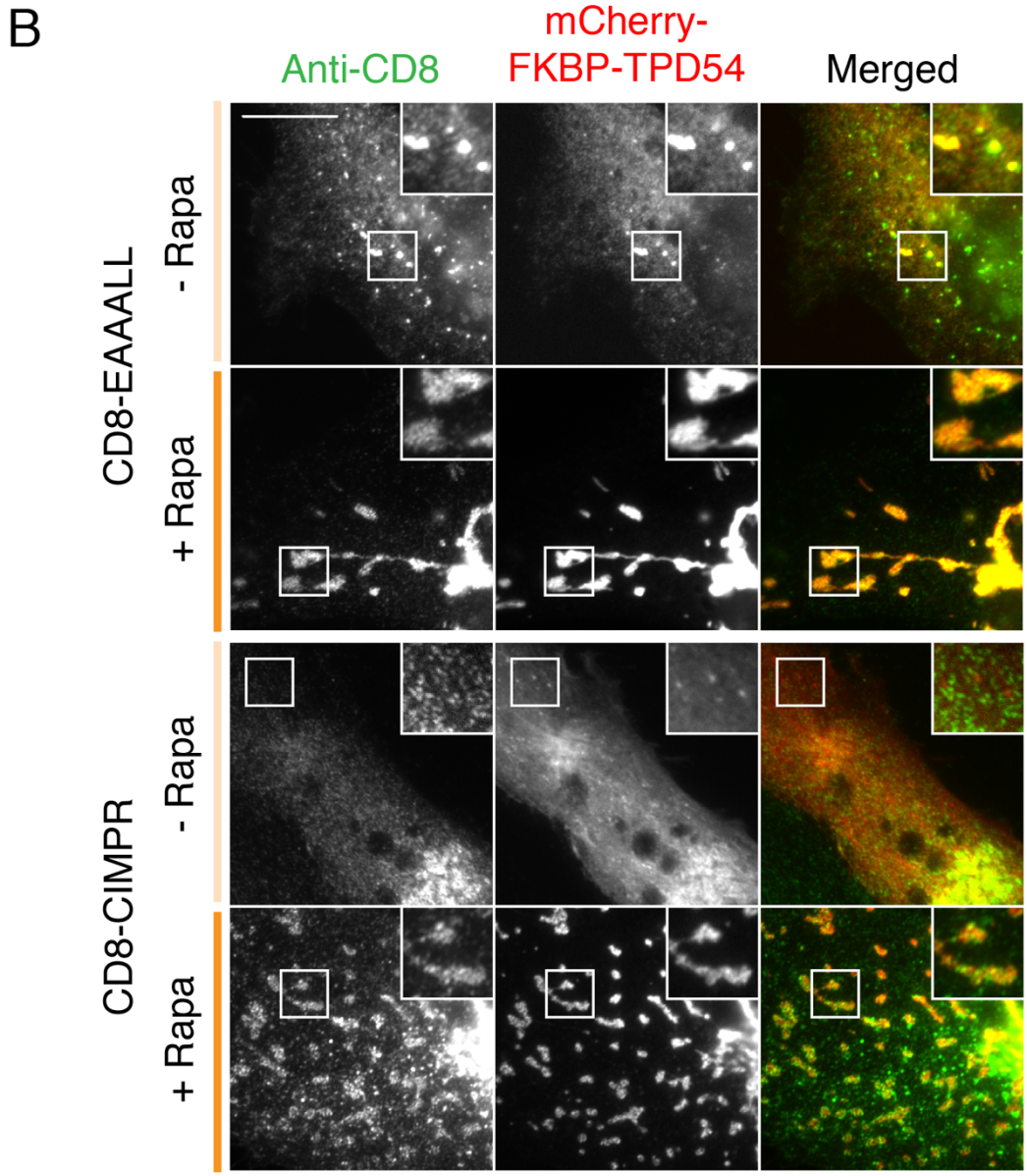
B
Anti-CD8
mCherry-
FKBP-TPD54
Merged
CD8-EAAALL
- Rapa
+ Rapa
CD8-CIMPR
- Rapa
+ Rapa

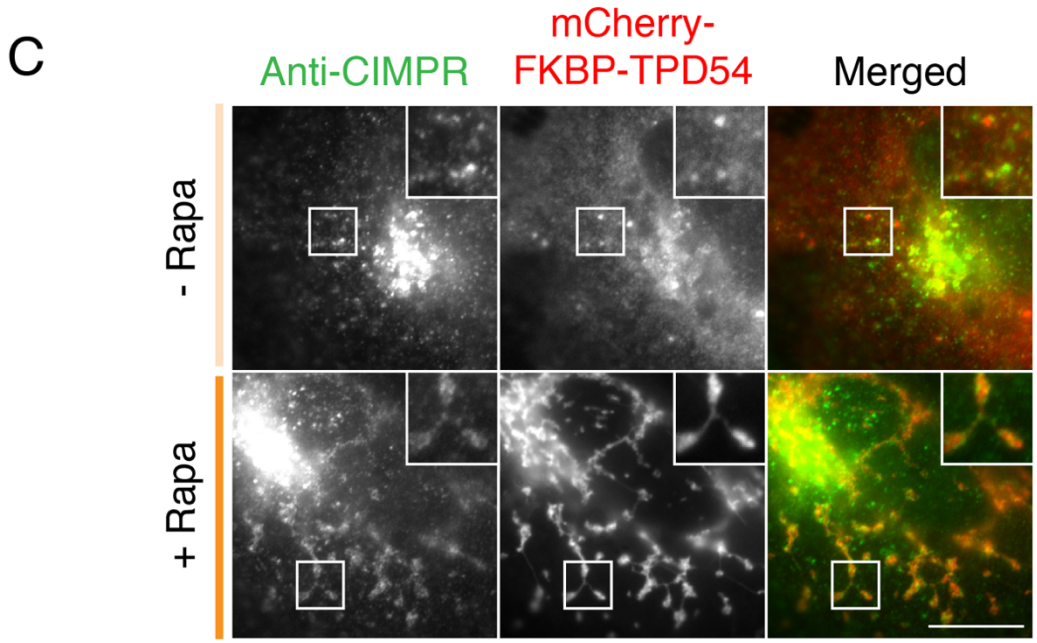

Figure 5.4: Knocksideways shows that TPD54 is associated with dileucine motif exclusively. Representative widefield micrographs of TPD54-depleted cells transfected with dark Mitotrap, mCherry-FKBP-TPD54 and CD8-8A, CD8-FANPAY and CD8-YAAL (A) or CD8-EAAALL and CD8-CIMPR (B). TPD54 is rerouted by adding 200 nM rapamycin to the cells (dark orange bar). C) Knocksideways of TPD54 in TPD54 KD cells expressing mCherry-FKBP-TPD54 and dark MitoTrap, fixed and stained with AlexaFluor488-conjugated anti-CIMPR antibody. Scale bar: 10 µm, inset: 2X zoom.

live-labelled with AlexaFluor-647-conjugated anti-CD8 antibodies and imaged for up to two hours depending on the trafficking marker. As seen in figure 5.5, CD8-YAAL and CD8-EAAALL both colocalised with markers of TGN-late endosomes and Golgi-endoplasmic reticulum respectively, Rab9 and Rab2 (**Figure 5.5A**) early endosomes Rab5 and EEA1 (**Figure 5.5B**), with markers of recycling pathways Rab4 and Rab11 (**Figure 5.5C**), markers of late endosomes and lysosomes respectively Rab7 and LAMP1 (**Figure 5.5D**) but not the intra-golgi Rab6 (**Figure 5.5E**). This argues against the hypothesis that dileucine motif-containing receptors are trafficked differently than tyrosine-base motif-containing receptors. However, we could also have missed a compartment on which TPD54 could be, since our colocalisation assay was partial, utilising only the best described markers.

We also wanted to have a quantitative estimate of the colocalisation between these receptors and the trafficking markers. To do so, we tracked the CD8-positive and marker-positive spots in our movies with an automated work-

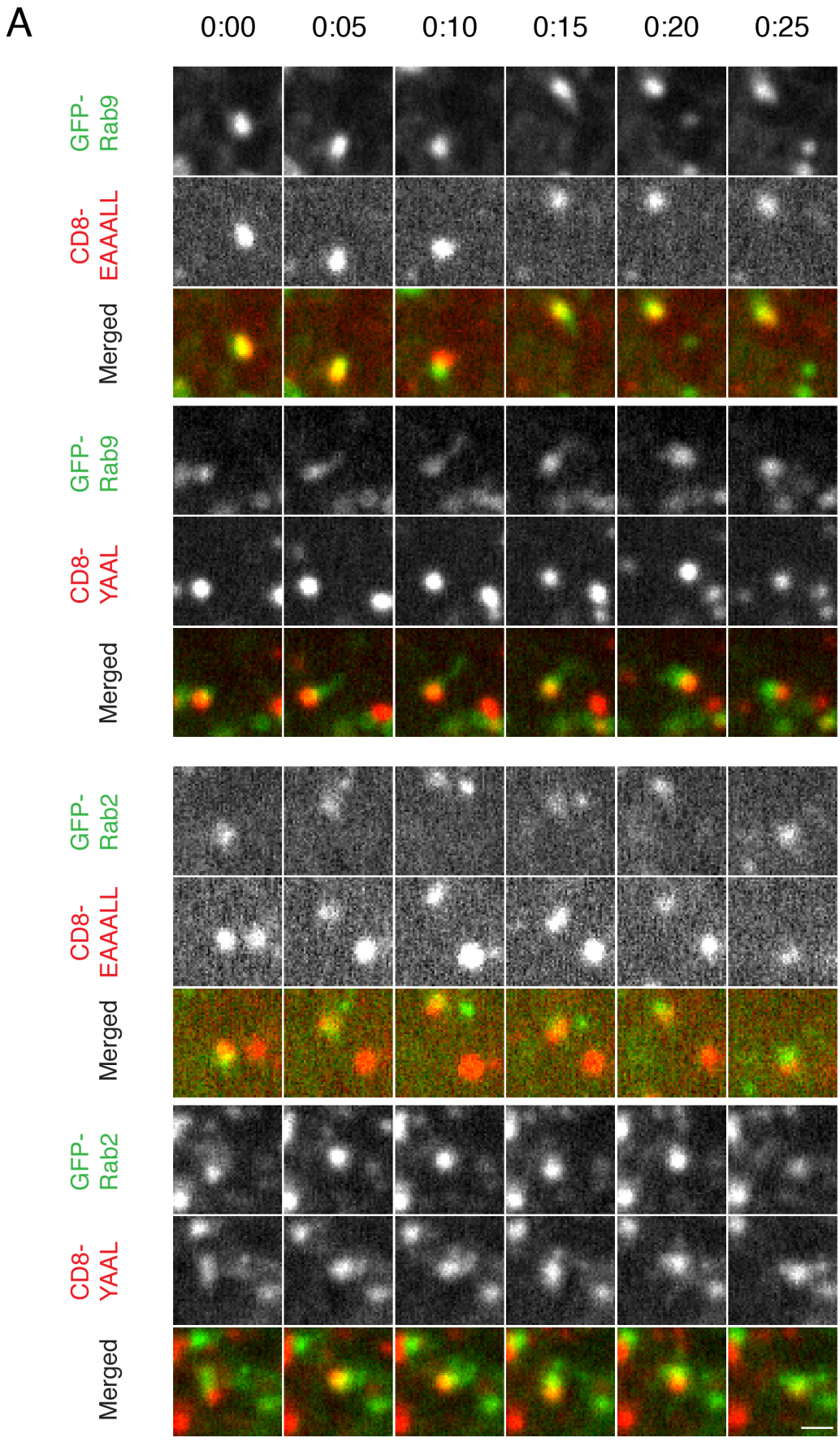
A
0:00
0:05
0:10
0:15
0:20
0:25
GFP-Rab9
CD8-EAAALL
Merged
GFP-Rab9
CD8-YAAL
Merged
GFP-Rab2
CD8-EAAALL
Merged
GFP-Rab2
CD8-YAAL
Merged

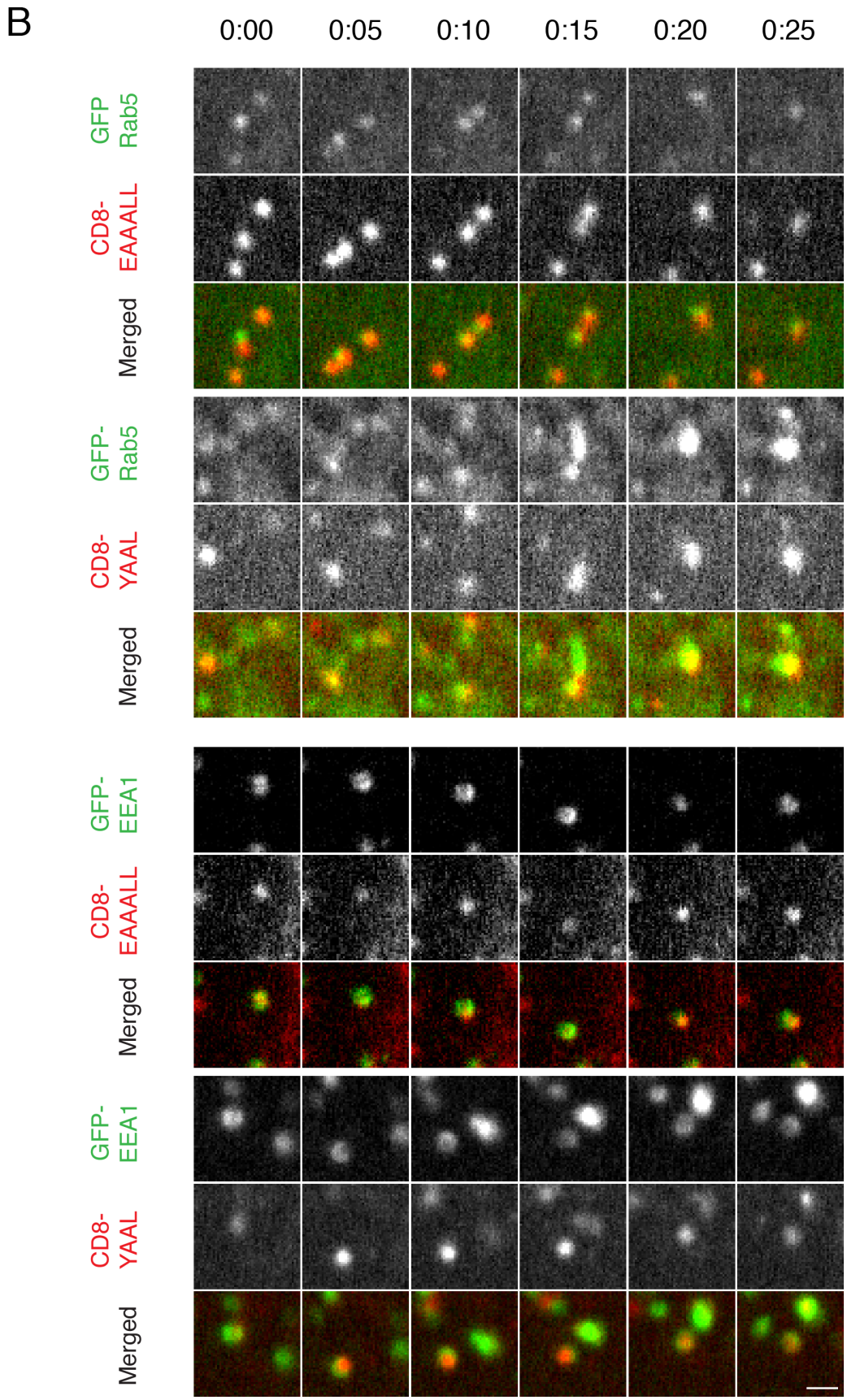
B
0:00
0:05
0:10
0:15
0:20
0:25
GFP Rab5
CD8-EAAALL
Merged
GFP-Rab5
CD8-YAAL
Merged
GFP-EEA1
CD8-EAAALL
Merged
GFP-EEA1
CD8-YAAL
Merged

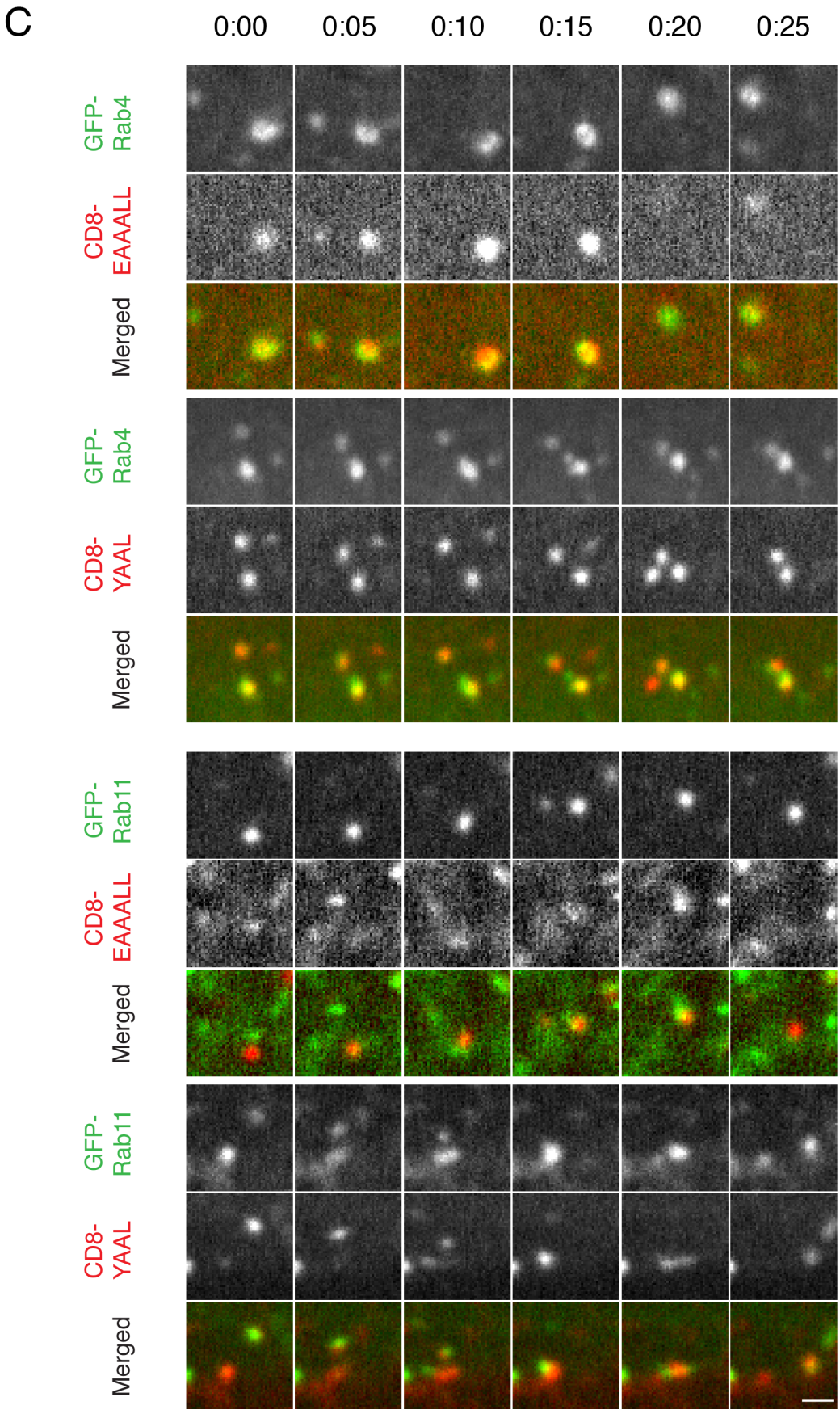
C
0:00
0:05
0:10
0:15
0:20
0:25
GFP-Rab4
CD8-EAAALL
Merged
GFP-Rab4
CD8-YAAL
Merged
GFP-Rab11
CD8-EAAALL
Merged
GFP-Rab11
CD8-YAAL
Merged

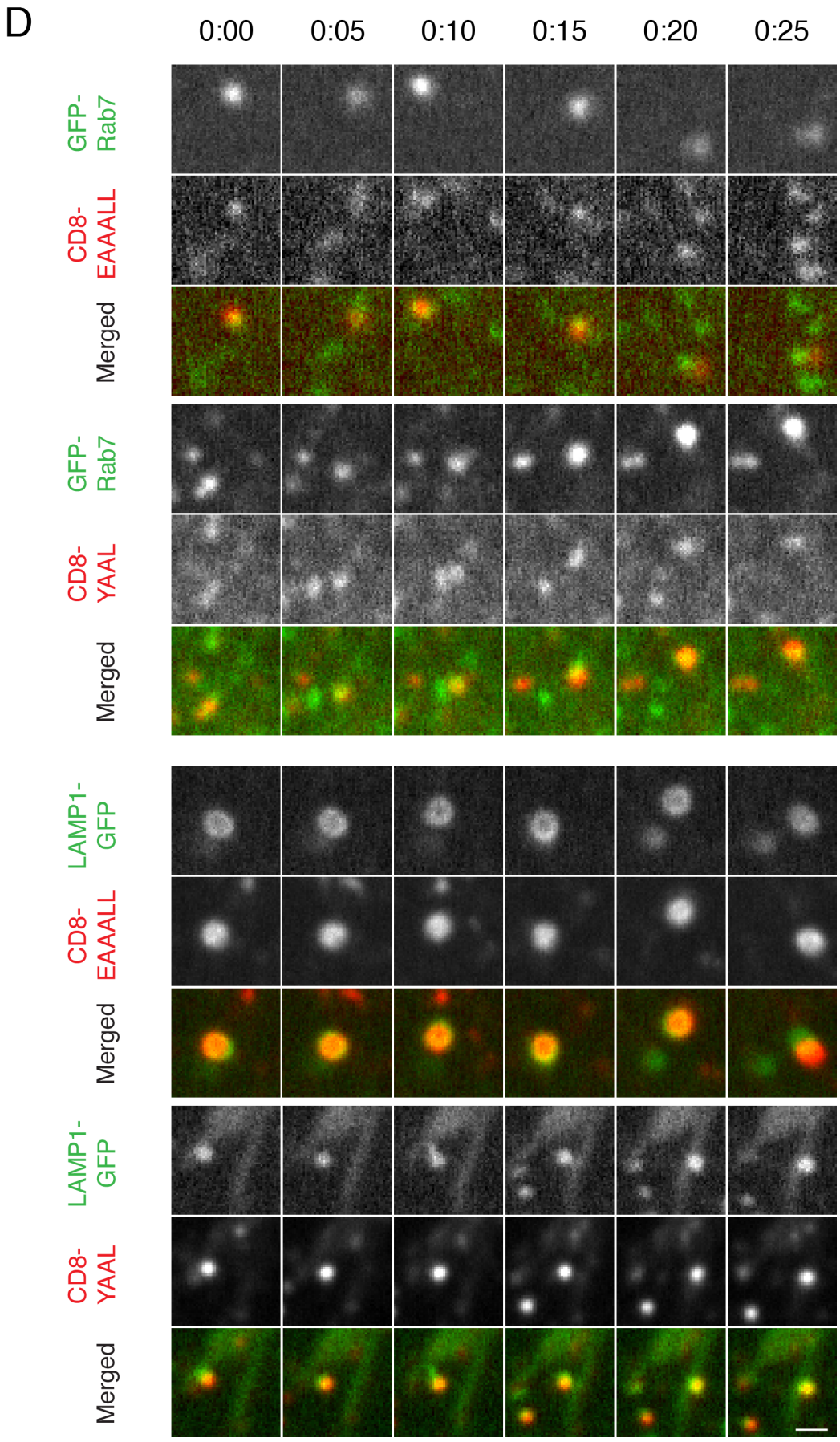
D
0:00
0:05
0:10
0:15
0:20
0:25
GFP-Rab7
CD8-EAAALL
Merged
GFP-Rab7
CD8-YAAL
Merged
LAMP1-GFP
CD8-EAAALL
Merged
LAMP1-GFP
CD8-YAAL
Merged

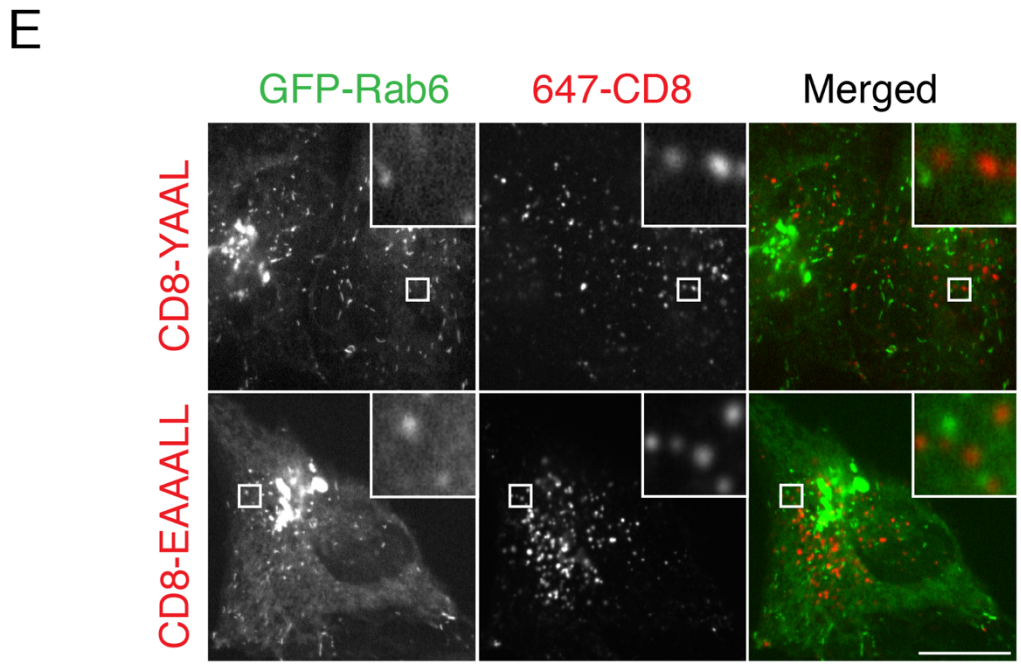

Figure 5.5: CD8-YAAL and CD8-EAAALL both colocalise with Rab5, EEA1, Rab4, Rab11, Rab7, LAMP1, Rab9 and Rab2 but not Rab6. HeLa cells were transfected with either CD8-YAAL or CD8-EAAALL, a GFP- or mNeonGreen-tagged marker of trafficking and live-labelled with AlexaFluor-647-conjugated anti-CD8 antibodies. Cells were imaged on confocal microscope up to two hours post-labelling. A) Colocalisation with Rab9 and Rab2, B) with Rab5 and EEA1, C) with Rab4 and Rab11, D) with Rab7 and LAMP1 and E) with Rab6. Scale bar in A = 10 µm, inset: 5X zoom. Scale bar in B-E: 1 µm.

flow using the ImageJ plugin ComDet and Igor Pro code to analyse the colocalisation between the spots detected (**Figure 5.6**). We compared colocalisation of spots with the likelihood of two spots being randomly at the same place. With this method, we have been able to confirm objectively the imaging data stating that CD8-YAAL and CD8-EAAALL are trafficked through the tested organelles.

We next wanted to know how TPD54 recognises the dileucine motif. Is the protein binding to it directly, or are they in the same vesicle when TPD54 is rerouted to the mitochondria? A way to test whether or not TPD54 binds directly and immediately to dileucine motif, is by trying to "catch" it with a knocksideways at a certain time point after the motif's internalisation. To do so, we transfected TPD54-depleted cells with dark MitoTrap, mCherry-FKBP-TPD54 and CD8-EAAALL or CD8-CIMPR, surface-labelled the cells with AlexaFluor488-conjugated anti-CD8 antibodies, and allowed internalisation

of CD8 for 5, 30, 60, 90 or 120 minutes before inducing knocksideways (**Figure 5.7**). As figure 5.7A shows, we can only co-reroute CD8-EAAALL with TPD54 knocksideways after at more than 60 minutes. As for CD8-CIMPR, it can be co-rerouted after 30 minutes (**Figure 5.7B**). This argues against the fact that TPD54 can bind directly to the dileucine motif, because it would have been expected that if this were the case, we would have been able to reroute it as soon as it is internalised.

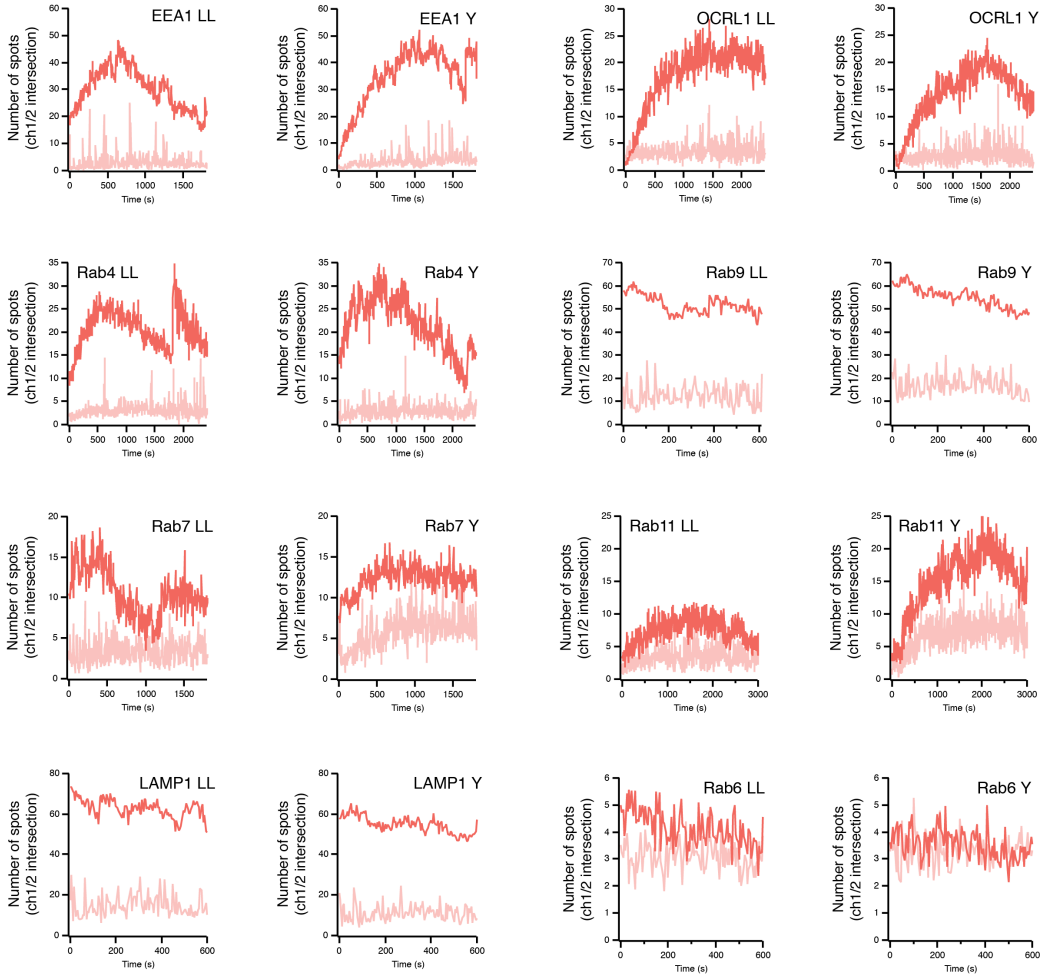

Figure 5.6: Quantification of CD8-YAAL or CD8-EAAALL colocalisation with trafficking markers. Number of trafficking marker-positive spots colocalising with CD8-YAAL (Y) or CD8-EAAALL (LL)-positive spots as a function of time after the start of the recording. Dark trace: colocalisation. Pale trace: colocalisation that would only be due to chance. EEA1 LL: n=3. EEA1 Y: n=3. OCRL1 LL: n=3. OCRL1 Y: n=1. Rab4 LL: n=2. Rab4 Y: n=1. Rab6 LL: n=4. Rab6 Y: n= 4. Rab7 LL: n=1. Rab7 Y: n=1. Rab9 LL: n=3. Rab9 Y: n=2. Rab11 LL: n=2. Rab11 Y: n=2. LAMP1 LL: n=2. LAMP1 Y: n=2.

One of the main differences between the dileucine motif and the tyrosine-based motif is their recognition by AP2. Since it appears that CD8-YAAL and

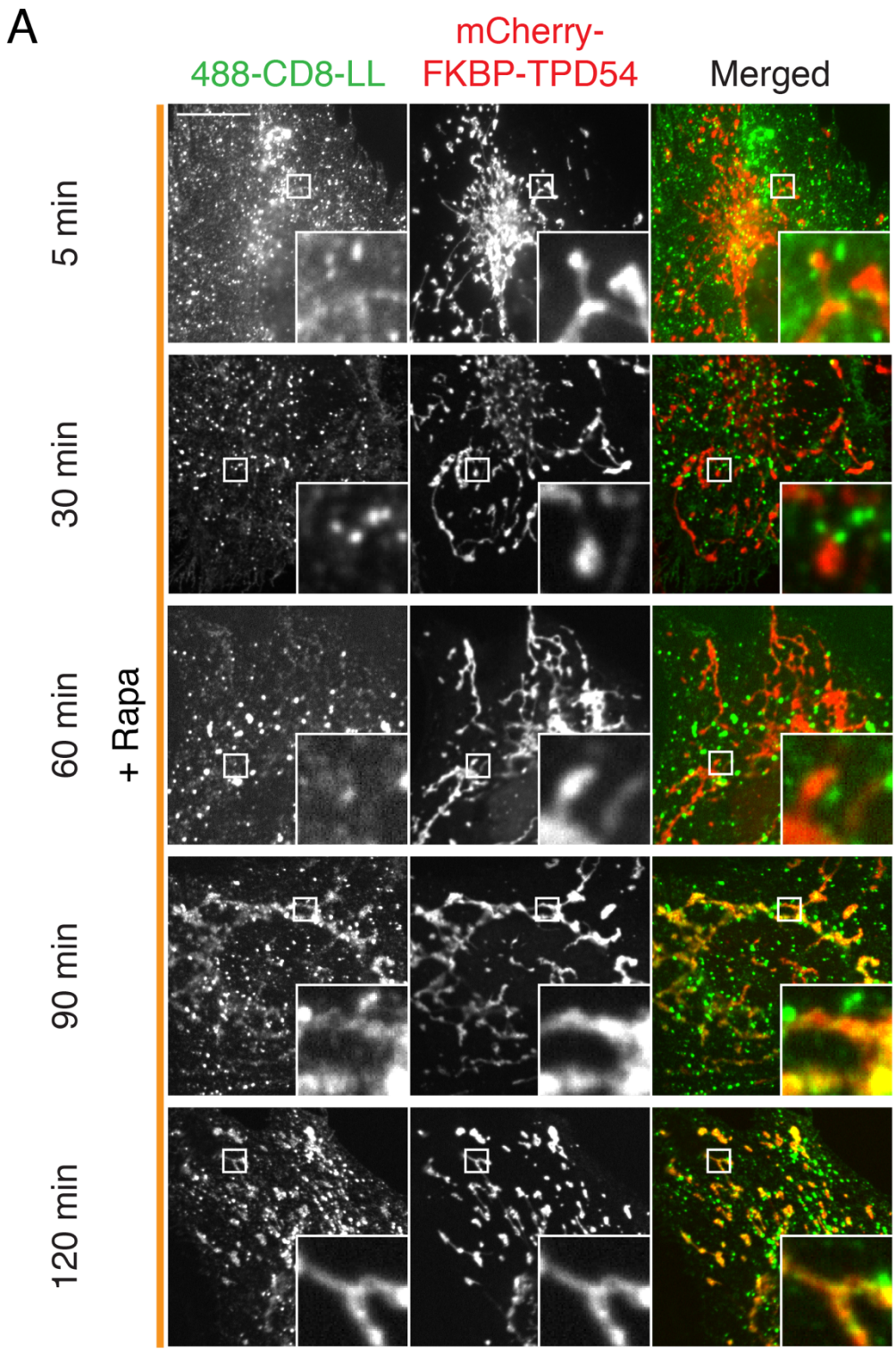

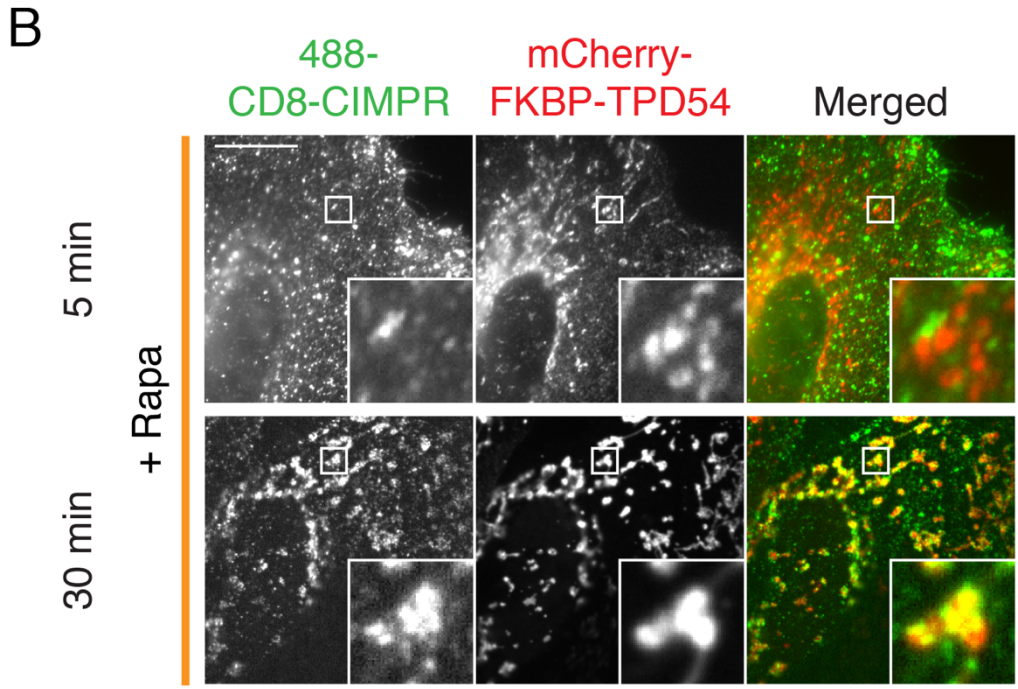

Figure 5.7: CD8-EAAALL can only be rerouted with TPD54 after more than 60 minutes, and CD8-CIMPR after more than 30 minutes. Representative widefield micrographs showing the colocalisation of CD8-EAAALL (A) or CD8-CIMPR (B) with mCherry-FKBP-TPD54 after addition of 200 nM rapamycin. 20 minutes post-rapamycin, HeLa cells were fixed and stained with AlexFluor488-anti-CD8. Scale bar: 10 µm. Inset: 5X zoom.

CD8-EAAALL are trafficked through the same compartment, but that TPD54 is only associated with dileucine motif, could the TPDs be another mechanism to sort separately the two motifs? It is known that TPD54, TPD53 and TPD52 can bind to each other via their coiled-coil domain (Byrne et al., 1998; Sathasivam et al., 2001). A tempting hypothesis is that the TPDs might be subunits of a protein complex, perhaps involved in protein sorting. We therefore wanted to know if TPD54 only can reroute the dileucine motif, and that the other TPDs might bind another motif. To do so, we did the same co-knocksideways experiment that we did to determine which CD8-chimera TPD54 binds. TPD52-depleted HeLa cells were transfected with dark MitoTrap, mCherry-FKBP-TPD52 and the CD8-chimeras. TPD52 was knocked sideways, fixed and stained with an anti-CD8 antibody (**Figure 5.8**). The figure shows that like TPD54, TPD52 is only associated to the dileucine motif, arguing against the hypothesis.

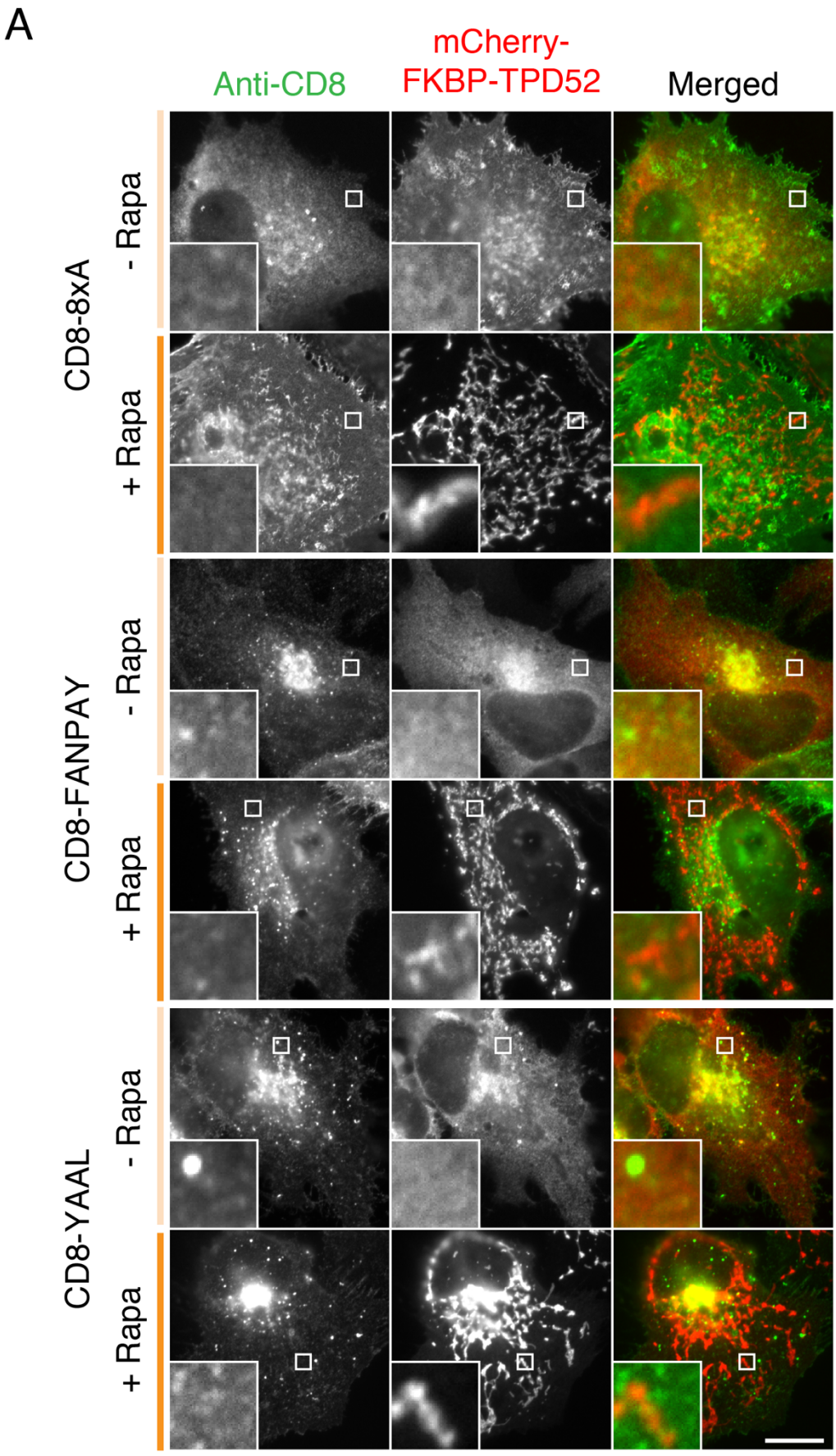
A
Anti-CD8
mCherry-
FKBP-TPD52
Merged
CD8-8xA
- Rapa
+ Rapa
CD8-FANPAY
- Rapa
+ Rapa
CD8-YAAL
- Rapa
+ Rapa

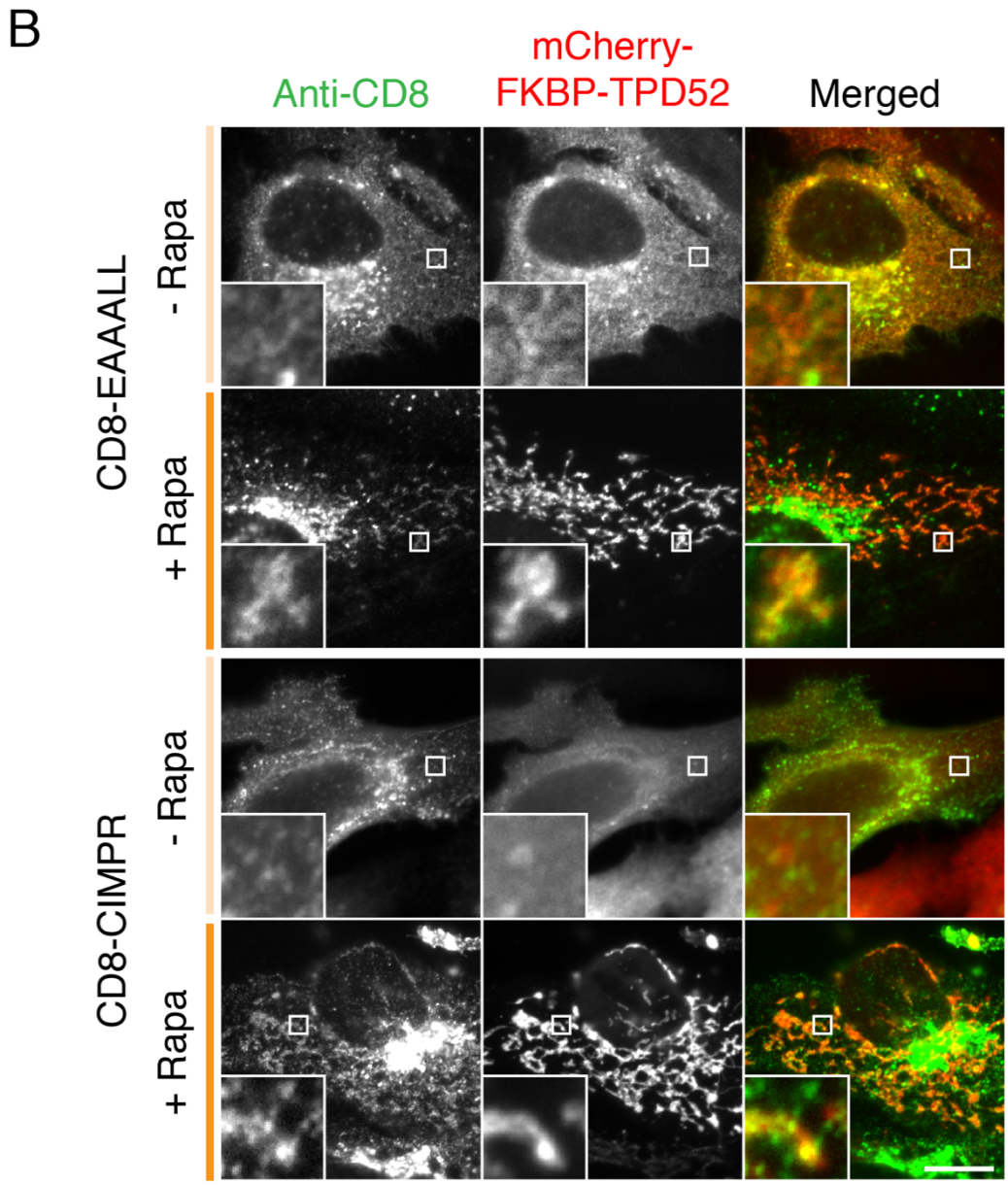

Figure 5.8: TPD52 knocksideways co-reroutes dileucine motif-containing receptors but not tyrosine based- or FXNPXY-containing receptors. Representative widefield micrographs showing that TPD52 does not co-reroutes CD8-8xA, CD8-FANPAY or CD8-YAAL (A) but does reroute CD8-EAAALL and CD8-CIMPR (B) to the mitochondria. TPD52-depleted HeLa cells were transfected with dark MitoTrap, mCherry-FKBP-TPD52 and one of the CD8-chimeras. Knocksideways was induced by adding 200 nM rapamycin (dark orange bars) to the cells. Scale bar: 10 μm, inset: 7X zoom.

Taken together, the data confirm that TPD54 has a role in membrane trafficking. It is needed for normal recycling of TfR and is associated with receptors containing dileucine motifs (CD8-EAAALL, CIMPR) but not FXNPXY or tyrosine-based motifs.

5.3 TPD54 is strongly associated with Rab14

It seems that the tyrosine and dileucine motifs are generally going to the same compartments and that TPD54 doesn't bind them directly. How and where does TPD54 becomes associated with dileucine motif? Are we missing the sorting compartment on which TPD54 is? So far, we have seen that TPD54 is mostly cytosolic when overexpressed, with sometimes a vesicular location, potentially around the Golgi apparatus (**Chapter 3, Figure 3.2, and Figure 5.4**). However, we don't clearly know where the TPD54-positive vesicles that we reroute to the mitochondria come from. To have a more precise idea on the protein's location, we performed a co-knocksideways experiment with dark MitoTrap, mCherry-FKBP-TPD54 and GFP-tagged markers of membrane trafficking organelles (**Figure 5.9**). Figure 5.9A shows the markers that did reroute with TPD54, the v-SNARE VAMP2 and the trans Golgi network resident TGN46. This suggests that TPD54 is indeed located near the trans Golgi network, potentially on transport vesicles. Figure 5.9B shows the markers that didn't reroute alongside TPD54. Indeed, the early endosomal EEA1, the cis Golgi network GM130, the early endosomal-retromer component SNX5, another retromer component Vps26, the lysosomal LAMP1 and the more widely distributed OCRL1 do not follow TPD54 to the mitochondria. This suggests that TPD54 is on transport vesicles somewhere between the recycling endosomes and the Golgi apparatus since VAMP2, Rab11, Rab4 and TGN46 could be co-rerouted with TPD54.

We now have marked a wide range of pathways in order to better understand where TPD54 exactly is inside the cell. We also know that TPD54 can somehow be associated with CD8-EAAALL or CD8-CIMPR, but not CD8-FANPAY or CD8-YAAL. We have tried to discriminate CD8-EAAALL and CD8-YAAL on the basis of their sorting, but we have seen so far that both go to the same compartments. We also know that it is unlikely that TPD54 binds to the dileucine motif directly. This all suggests that the motif needs to be in a

specific TPD54-positive compartment that we have so far missed with our tracking and co-KS assays. We therefore wanted to try to have a better understanding of the localisation of TPD54 by knowing more about its binding partners. To do so, we performed a GFP-IP in HeLa cells expressing either GFP or GFP-TPD54 and CD8-EAAALL or CD8-YAAL and analysed the proteins by mass spectrometry. Although the original idea was to confirm that we indeed couldn't see an interaction between dileucine motif and TPD54, the dataset generated allowed us to know more about the binding partners of TPD54 (see appendix 2 for complete list of interactors).

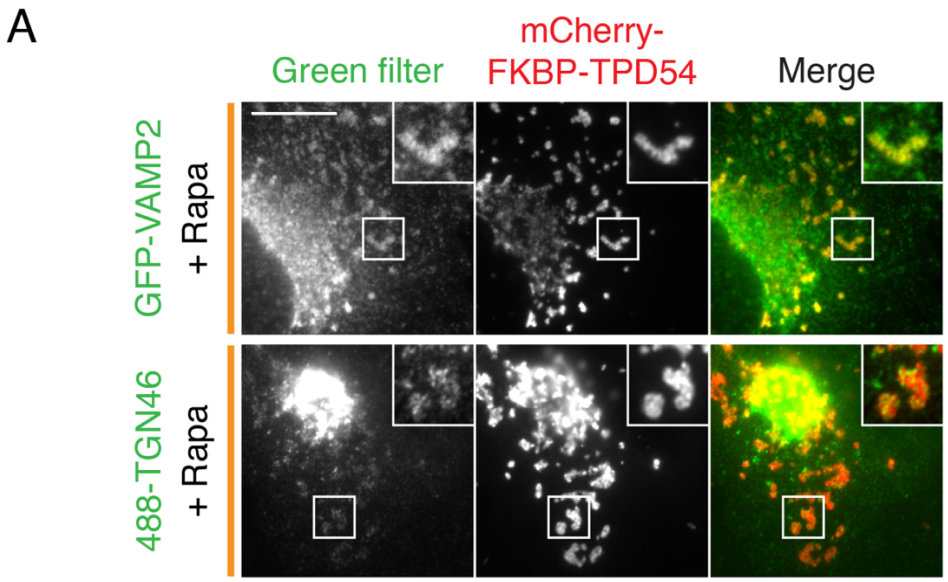

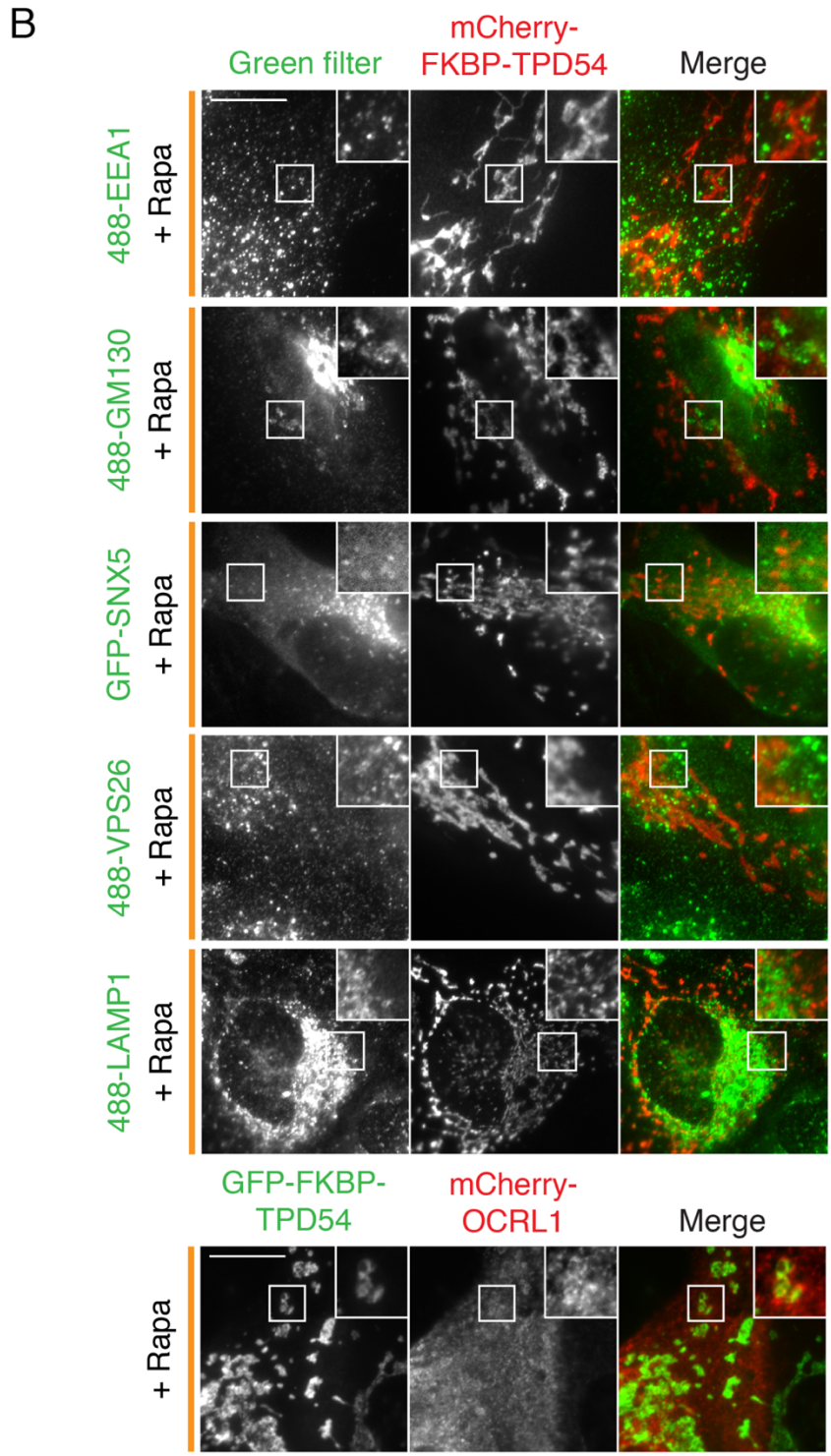

Figure 5.9: Knocksideways of TPD54 co-reroutes TGN46 and VAMP2 exclusively. Representative widefield micrographs of TPD54 knocksideways on TGN46 and VAMP2 (A) or EEA1, SNX5, VPS26, LAMP1 or OCRL1 (B). TPD54-depleted cells were transfected with either GFP-FKBP-TPD54 or mCherry-FKBP-TPD54, dark MitoTrap and a fluorescently tagged marker of the trafficking pathways, in the case of VAMP2, OCRL1 and SNX5. For the other the protein of interest was stained with AlexaFluor 488-conjugated antibody. Knocksideways was induced by adding 200 nM rapamycin to the cells. Scale bar: 10 µm, inset: 2X zoom.

Figure 5.10 highlights the most interesting hits of this analysis. TPD54 interactors are classified according to the significance of the presence difference between the GFP and GFP-TPD54 samples, and according to the degree of enrichment in the GFP-TPD54 samples. Out of many interesting hits, we found proteins involved in membrane trafficking (Rab5c, Rab7, Rab2a, etc) or in cell migration (integrin β1, desmoglein-2). We also found TPD53 and TPD52, suggesting that the trio of TPDs might indeed be a complex. The protein that mainly caught our attention was the GTPase Rab14. Rab14 has been involved in cell migration (Linford et al., 2012), in the transport from the Golgi apparatus to the endosomes (Junutula et al., 2004) and in the transport of the dileucine motif-containing protein GLUT4 (Brewer et al., 2016), therefore making it the perfect candidate marker for the cellular localisation of TPD54.

We next wanted to assess the association of TPD54 with Rab14 in our co-knocksideways assay. We also added more Rabs to the assay, to give a wider picture of the role of TPD54 in Rab GTPases binding. We therefore tried a co-knocksideways with GFP-Rab1a (ER to cis Golgi), Rab2a (cis-Golgi to ER), Rab6 (intra-Golgi and endosomes to Golgi), Rab8a (polarised trafficking and protrusion formation) or Rab14 in TPD54-depleted HeLa cells (**Figure 5.11**). We found that Rab1a, Rab2a and Rab14 are co-rerouted to mitochondria alongside TPD54 (**Figure 5.11A**) but that Rab6 and Rab8a are not (**Figure 5.11B**). It is also possible to notice that before adding rapamycin, TPD54 vesicles colocalise strongly with Rab14 vesicles (**Figure 5.11B)**, making an interaction between Rab14 and TPD54 even more likely. This further involves TPD54 at the Golgi apparatus and confirms the interactions found by mass spectrometry.

We now have a few Rab GTPases that associate with TPD54: Rab1a, Rab2a, Rab4a, Rab11a, Rab14 and Rab25. We wanted to quantify the knocksideways level to see if we could determine if rerouting was more efficient with certain Rab GTPases. To do so, we compared confocal micrographs for the mitochondrial recruitment of the GTPases with the intensity of the Rab

GTPases left in the cytosol. Figure 5.12 shows that according to the quantification, Rab1a, Rab11a, Rab14 and Rab25 are rerouted to the mitochondria. The recruitment to the mitochondria of Rab1a, Rab11a, Rab14

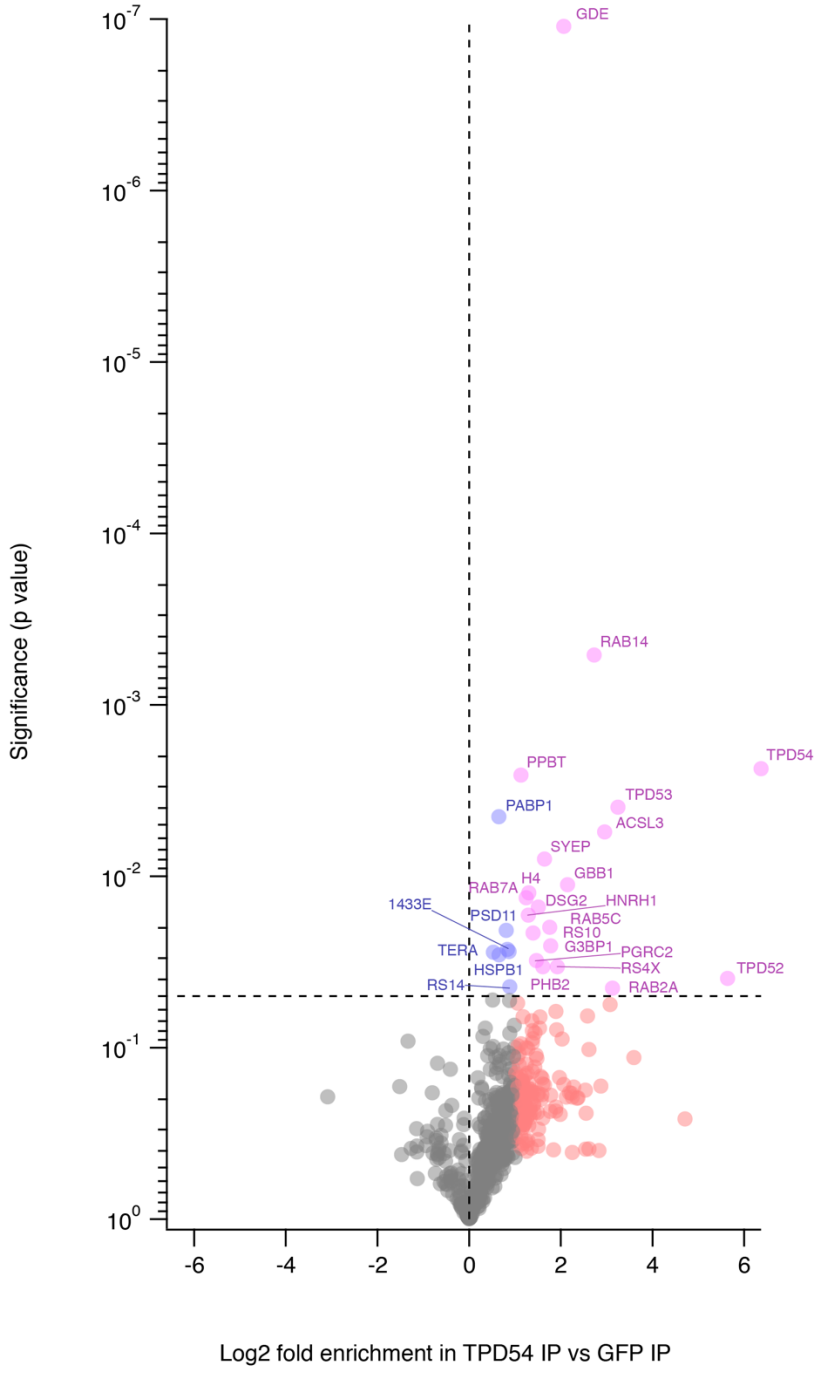

Figure 5.10: Mass spectrometry analysis of TPD54 interactors. Volcano plot showing TPD54 interactors according to the significance of their presence in TPD54 samples compared to GFP samples and their enrichment in TPD54 samples. Black spots: not significant and enriched in GFP samples. Red: not significant but enriched more than two fold in TPD54 samples. Violet: significant and less than two fold enriched in TPD54 samples. Pink: significant and more than two fold enriched in TPD54 samples. n=4.

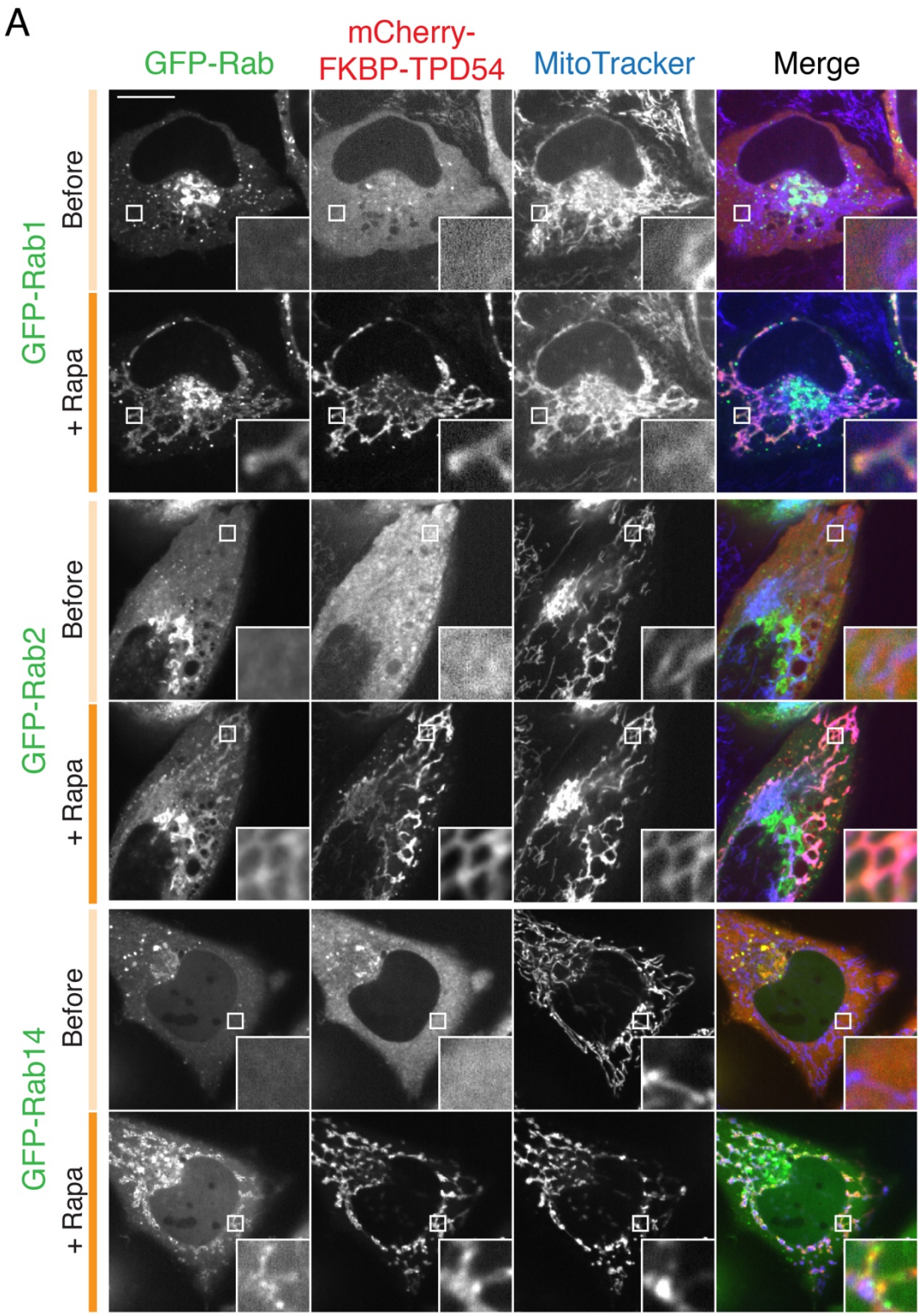
A
GFP-Rab
mCherry-
FKBP-TPD54
MitoTracker
Merge
GFP-Rab1
Before
+ Rapa
GFP-Rab2
Before
+ Rapa
GFP-Rab14
Before
+ Rapa

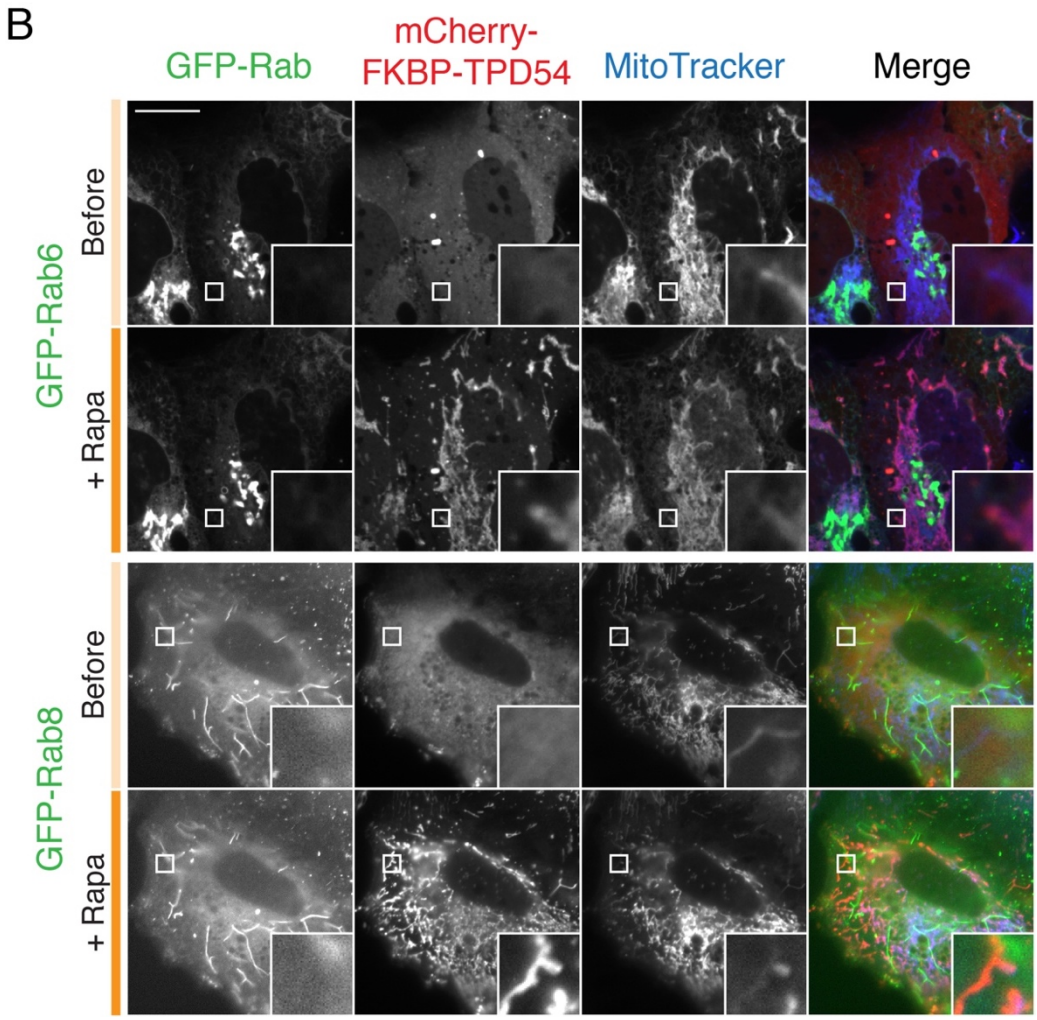

Figure 5.11: Knocksideways of TPD54 reroutes Rab1a, Rab2a, Rab14 but not Rab6 or Rab8a to the mitochondria. Representative confocal micrographs of TPD54-depleted HeLa cells expressing dark MitoTrap, mCherry-FKBP-TPD54 and either GFP-Rab1a, GFP-Rab2a, GFP-Rab14 (A), GFP-Rab6 or GFP-Rab8a (B). Mitochondria are stained with MitoTracker. Kkocksideways was induced by adding 200 nM rapamycin to the cells (dark orange band). Scale bar: 10 µm. Inset: 7X zoom.

and Rab25 are the most dramatic in every cell imaged. It also shows that only Rab1a, Rab11a, Rab14 and Rab25 are significantly more present on the mitochondria than in the cytosol, suggesting that only these GTPases are truly rerouted with TPD54, therefore are associated to it.

These knocksideways experiments have also allowed us to localise TPD54 at steady state. Indeed, by looking at colocalisation with the different Rab GTPases before any rapamycin treatment (**Figure 5.13**), we have been able to notice that some colocalisation can be seen with all Rabs but Rab6 and Rab8,

the most striking one being with Rab14, further reinforcing our hypothesis of direct and functional interaction.

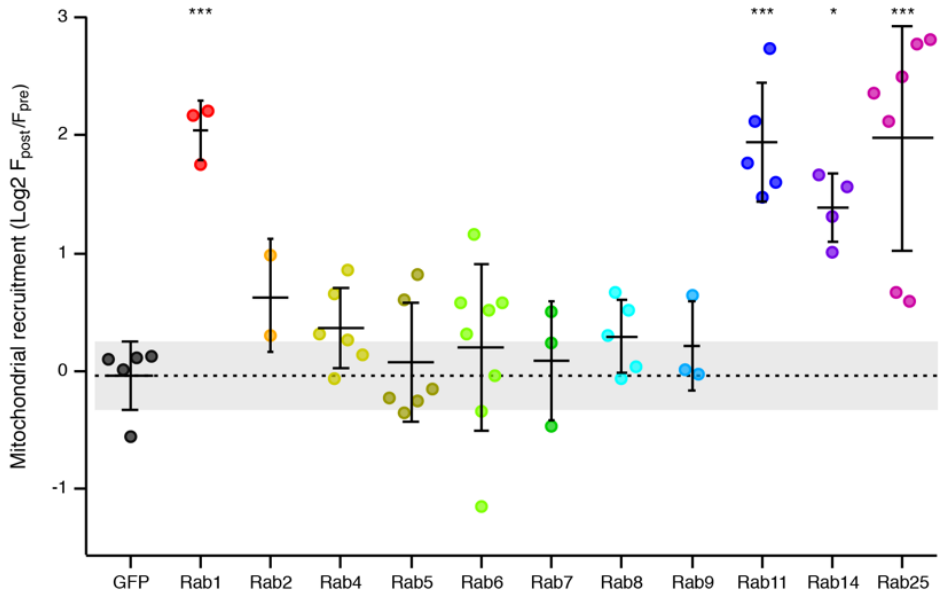

Figure 5.12: Knocksideways quantification. Log2 transformed ratios of post- over pre-rapamycin Rab GTPases or GFP mitochondrial recruitment. n=1. Bars: mean and standard deviation. Doted line: GFP mean. Shaded area: GFP standard deviation. p values from Tukey post-hoc comparison. *<0.05, ***<0.001.

5.4 Discussion

In this chapter, we were able to confirm that TPD54 is involved in membrane trafficking by its association with CD8-EAAALL trafficking vesicles and by uncovering three new associations with Rab14, Rab1a and potentially Rab2a. We now have a few Rab GTPases associated with TPD54, and if we combine the other associations found with the knocksideways technique, we can have a good idea of the cellular localisation of TPD54 (**Figure 5.14**).

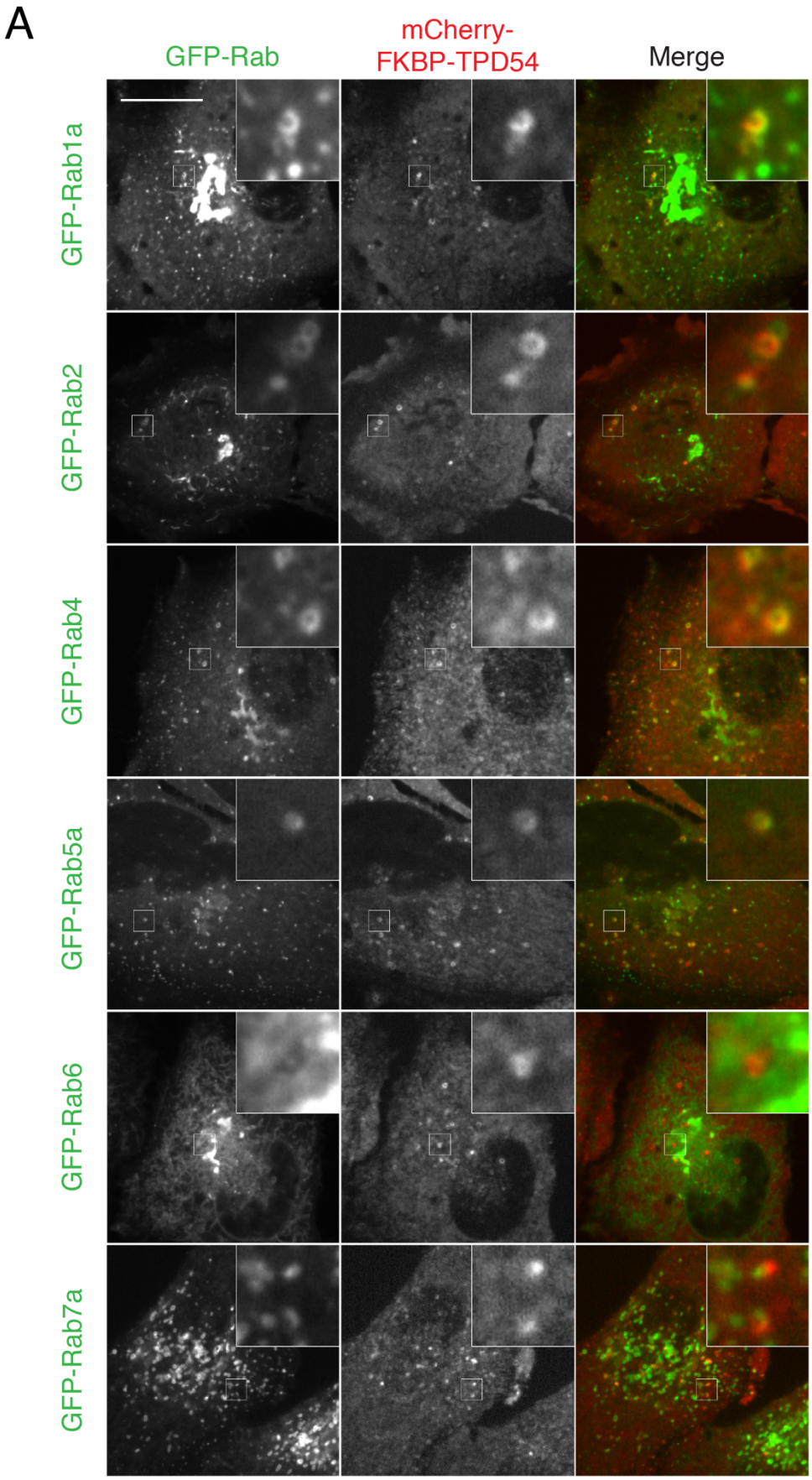
A
GFP-Rab
mCherry-
FKBP-TPD54
Merge
GFP-Rab1a
GFP-Rab2
GFP-Rab4
GFP-Rab5a
GFP-Rab6
GFP-Rab7a

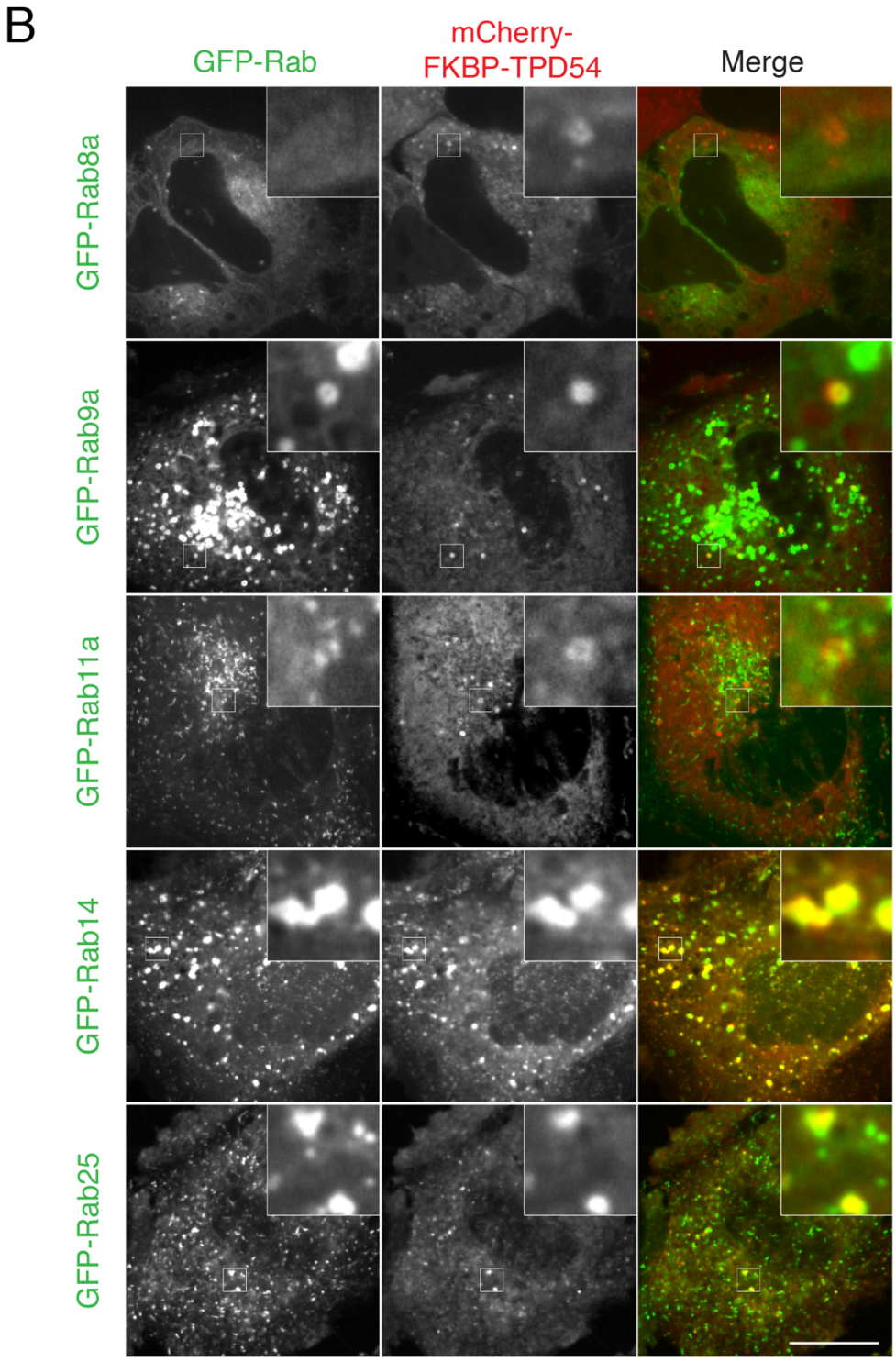

Figure 5.13 Colocalisation of TPD54 and Rab GTPases. Representative confocal micrographs showing the colocalisation of mCherry-FKBP-TPD54 and GFP-Rab1a, 2, 4, 5a, 6, 7, 8, 9, 11, 14 and 25 in HeLa cells at steady-state. Scale bar: 10 µm. Inset: 5X zoom.

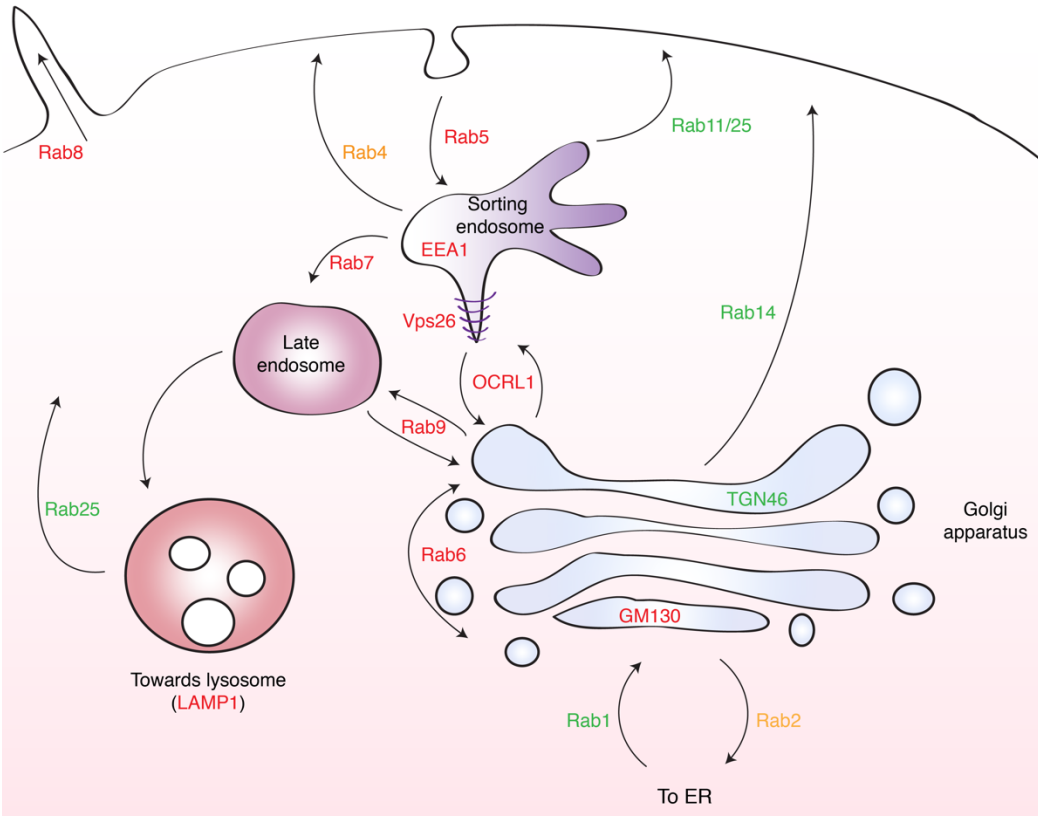

Figure 5.14: Where is TPD54? Cartoon of the membrane trafficking pathways with the markers tested for their association with TPD54. Markers highlighted in red did not co-reroute, and in markers in green rerouted. Markers in orange gave mixed results. Arrows indicate sense of traffic.

We also showed that TPD54 has a role in the recycling of the transferrin receptor, but not its internalisation. However, as for integrin α5 and β1, TfR could not be seen at the mitochondria with TPD54 after a knocksideways. This could mean that TPD54-positive vesicles do not contain enough of these two types of cargo to be seen by knocksideways. This would also explain why we can see some colocalisation with Rab5, Rab7 and Rab9 at steady-state. We can see both proteins on some structures, but not enough to perceive with the KS. It could also be TPD54-positive vesicles are an artefact of the technique, that vesicles are formed artificially and that they contain only membrane residents but no cargo. However, this is not the case because we have been able to reroute two types of cargoes: the CD8-chimeras containing a dileucine motif (EAAALL and CIMPR) and CIMPR itself which has to be

trafficked from the Golgi apparatus to the endosomes and back again (Arighi et al., 2004; Meyer et al., 2000; Puertollano et al., 2001).

We also tried to distinguish CD8-YAAL from CD8-EAAALL in order to understand how TPD54 can only be associated with one but not the other. We hypothesised that TPD54 might bind directly to the dileucine motif. Using two different ways of detection, we are now confident that this is not the case. We tried to co-immunoprecipitate either mCherry-CD8-EAAALL or mCherry-CD8-YAAL with GFP-TPD54. We have detected bands corresponding to mCherry-CD8 in both cases, although because the same band was also detected when co-immunoprecipitating mCherry-CD8-EAAALL with GFP only, we concluded that mCherry binds the GFP-Trap used to do the immunoprecipitation. This has later been confirmed (data not shown). Another argument in favour of this was the substantial increase of signal in our positive control, GFP-FKBP-TPD54 + rapamycin + mCherry-FRB-CD8.

The other way of confirming this negative result was to send the immunoprecipitations for mass spectrometry analysis. In the list of many interactors for TPD54, no CD8 peptide was found, arguing against the hypothesis that TPD54 recognise directly the dileucine motif by binding to it.

The other experiment we used to confirm this hypothesis is the 'timed' knocksideways. We wanted to know if we could co-reroute CD8-EAAALL to the mitochondria with TPD54 as soon as the receptor is internalised, or if it needed to be transported to a certain compartment before it associates with TPD54. We found that the latter is true. TPD54 is only associated with dileucine motifs after more than 60 minutes post-internalisation, in the case of CD8-EAAALL. This not only suggests that in order to be associated with TPD54, CD8-EAAALL needs to be in the right compartment but also that this TPD54-positive compartment is likely to be on the Golgi anterograde pathway. Furin, a molecule that is trafficked on the retrograde pathway, takes about 45 minutes to reach the trans Golgi network from the plasma membrane and through late endosomes in a Rab9-dependent manner (Chia et al., 2013;

Mallet and Maxfield, 1999). CD8-EAAALL colocalises with the late endosomal Rab7a, Rab9a but is also recycled to the plasma membrane. This suggests that it is internalised, goes to the late endosomes, and then back to the plasma membrane, most probably through the Golgi apparatus. The fact that we see an association with TPD54 after more than 60 minutes suggests that TPD54 is on this Golgi recycling pathway.

We haven't been able so far, to dissociate CD8-YAAL and CD8-EAAALL. We have quantified their colocalisation with different trafficking markers such as the endosomal OCRL1, the early endosomal EEA1, the late endosomal Rab7a, the lysosomal LAMP1 and the recycling endosomes-associated Rab4a and Rab11a. Both CD8 receptors appeared to localise with them all to a similar extent. This then suggests that the compartment that could differentially sort the two motifs, on which TPD54 probably is, has not been identified yet.

The localisation of TPD54 has also been examined more closely (**Figure 5.14**). According to our co-knocksideways experiments, TPD54 is likely to be on transport vesicles (VAMP2) located on an anterograde, post-Golgi pathway (Rab14, TGN46), potentially going through the recycling endosomes (Rab11a/Rab25). The fact that Rab1a, and potentially Rab2a, can be co-rerouted with TPD54 is puzzling. We haven't seen rerouting of GM130 (marker of cis-Golgi network), but have seen rerouting of TGN46 (marker of trans-Golgi network). This was found by staining for endogenous proteins with antibodies, rather than overexpression. We did overexpress Rab1a and Rab2a, therefore we might only be seeing an association because of a protein excess. Another way of looking at the association between TPD54 and the different Rab GTPases, would be that instead of being on a fixed organelle, TPD54 might recognise one or more Rab GTPases through a conserved motif on them. There might be one main Rab, probably Rab14, given the mass spectrometry analysis, and TPD54 binds to a similar sequence on others. Rab2a, Rab4a, Rab11a (and Rab25) and Rab14 are all members of a same Rab sub-family, meaning that they are more likely to be similar, having

evolved together (Klopper et al., 2012). This similarity might be the reason why we can co-reroute them all at least partially, with TPD54.

This rises the validity of our knocksideways quantification. We have been able to see in chapter 3 that TPD54 is associated with Rab4a. In the same way, figure 5.11A clearly shows that Rab2a is associated with TPD54 as well. However, these two Rab GTPases failed to pass the significance test in our quantification. This could again be due to overexpression. The association is perhaps only triggered by an excess of Rab4 or Rab2 and since they share similarities with Rab11a, Rab25 and Rab14, TPD54's binding sequence could be mildly conserved.

Finally, we have also been able to acquire a list of interactors for TPD54. Besides Rab14, TPD53 and TPD52 caught our attention. This confirms that the TPDs are indeed able to bind to each other, but also that the TPDs are likely to be part of a complex constitutively. This experiment also confirms that, at least for its role in membrane trafficking, GFP-TPD54 is functional. We have been able to co-immunoprecipitate known interactors and new ones fitting well in what we already know about its biology. Amongst these new interactors are proteins involved in cell motility (desmoglein-2, integrin β1) and trafficking (TPDs, Rab14, Rab5c, Rab2a, Rab7a, TERA), but also a few nucleic acids-associated proteins (H4, RS14, RS4X, HNRH1, SYEP, RS10), which are likely to be contamination.

Integrin β1 was interesting, because although we haven't been able to knock it sideways, this shows that TPD54 is likely to be binding it and argues in favour that the role of TPD54 in cell migration is indeed through its trafficking role and the recycling of integrins.

Desmogleins are the main components for desmosomes, together with desmocollins. Desmososmes are important for maintenance of the integrity of an epithelium, by linking intermediate filaments of one cell to the filaments of a neighbouring cell. The disassembly/reassembly of desmoglein polymers is therefore important for the cells ability to migrate, after a rupture of the epithelium, for example (Cadwell et al., 2016). Internalisation of desmogleins

is done in a Kif5B- and microtubules-dependent manner (Nekrasova et al., 2013) and in a clathrin-independent way (Delva et al., 2008). TPD54, and potentially Rab14 could therefore be a mechanism to bring newly synthesized desmoglein-2 molecules to the surface, into desmosomes.

ACSL3 (long-chain acyl-CoA synthetase 3) is mainly known for its role in lipid metabolism and lipid droplets (Poppelreuther et al., 2012), like TPD53 and TPD52 (Kamili et al., 2015). It has also been shown to be important for Golgi export to the plasma membrane of the tyrosine kinase Lyn (Obata et al., 2010). TPD54 could therefore, alongside TPD52 and TPD53, have a role in lipid droplet metabolism, and participate in the transport of the kinase Lyn through the Golgi apparatus.

The interactor with the highest level of significance is GDE (glycogen debranching enzyme). Linking TPD54 with GDE is a bit challenging, nothing has been found so far about TPD54 being involved in glycogen metabolism. However, glycogen is a form of glucose storage in liver cells and muscles. The additional glucose will be glycolysed to form lipids, and these lipids can be translocated to the mitochondria by proteins of the ACSL family, including ACSL3 (Sahini and Borlak, 2014).

Our knocksideways experiments showed that Rab5a cannot be rerouted with TPD54, but the mass spectrometry analysis revealed that there might be a binding between Rab5c and TPD54. Although Rab5a, b and c are expressed in all tissues (Gurkan et al., 2005), the three isoforms have been shown to have different functions, rather than being redundant. For example, Rab5a is involved in internalisation of EGFR, and depletion of Rab5c has no effect on the trafficking of this receptor (Chen et al., 2009). It has also been shown that Rab5c, but not Rab5a or Rab5b, is associated with the activation of Rac1 and promotes cell motility (Chen et al., 2014). It would therefore be possible that Rab5c, but not Rab5a is associated with TPD54. It is also worth noting that TPD52 has been shown to bind Rab5c in a yeast two-hybrid screening (Shahheydari et al., 2014).

On the other hand, having Rab7a in our analysis is surprising. We couldn't reroute it to the mitochondria with TPD54. However, it was the same situation for integrin β1. This might suggest that the knocksideways technique might give false-negatives.

In this chapter, we have been able to show that TPD54 is indeed involved in membrane trafficking. It is associated with Rab1, 11, 14 and 25, and receptors containing a dileucine motif (CD8-EAAALL, CD8-CIMPR, CIMPR) but not a NPXY or a tyrosine-based motif. We have also been able to identify many TPD54 interactors, such as Rab14, Rab2a and Rab5c confirming its role in membrane trafficking and such as desmoglein-2 and integrin β1, confirming its role in cell motility.

Chapter 6 – General discussion

The aim of this thesis was to provide mechanistic insights into the role of the Tumor protein D52 family member TPD54, in two fundamental cellular processes, cell migration and membrane traffic. By doing so, we would be able to understand why a gene duplication of TPD54 in cancer is likely to lead to a poor prognosis.

In the Introduction I described how TPD54 probably has a role in membrane trafficking since the Tumor protein D52 family members are found with CCSs, can act as a SNARE (at least *in vitro*), and is required for the secretion of digestive enzymes (Kaur et al., 2014; Messenger et al., 2013; Proux-Gillardeaux et al., 2003). The fact that the sequence of the TPD52 family members is similar and that TPD52, 53 and 54 can interact with each other, we had good reason to believe that TPD54 might indeed have a role in membrane traffic (Sathasivam et al., 2001).

It was also clear that since one of the main effects of overexpression of the TPDs in cancer is altered migration/adhesion/invasion, TPD54 must also have a role in these processes (Ito et al., 2017; Mukudai et al., 2013).

We have found using the knocksideways technique that TPD54 is strongly associated with small vesicles and that these vesicles contain recycling Rab GTPases (Rab4, Rab11 and Rab25), as well as other Rabs in the supergroup (Rab14 and Rab2) and Rab1 (summarized in **Table 6.1**). These associations were also seen by co-IP and mass spectrometry (Rab2, Rab14) and a BioID experiment (Rab11, Rab25) conducted in the laboratory of our collaborator Dr P. Caswell (Manchester). We also saw by mass spectrometry that Rab7 might be an interactor of TPD54, although this was not observed by KS. We also found Rab5c as a potential interactor by MS, however we only assessed Rab5a using KS. Rab5c is different enough from Rab5a for these two proteins

not to be redundant (Chen et al., 2009; Chen et al., 2014). It will be worth investigating Rab5c by KS in the future.

Table 6.1 Summary of the Rab GTPases associations with TPD54. Y: yes, N: no, NA: not available

Protein	Steady-state colocalisation	Knocksideways	IP/MS	BioID
Rab1a	Y	Y	N	NA
Rab2a	Y	N?	Y	NA
Rab4a	Y	N	N	N
Rab5a	Y	N	N	NA
Rab5c	NA	NA	Y	NA
Rab6	N	N	N	NA
Rab7a	Y	N	Y	NA
Rab8a	N	N	N	NA
Rab9a	Y	N	N	NA
Rab11a	Y	Y	N	Y
Rab14	Y	Y	Y	NA
Rab25	Y	Y	NA	Y

The discrepancies we see between the Rab GTPases associated with TPD54 by co-IP/MS and by KS might be explained the fact that not every Rab is expressed in HeLa cells, the model used for the mass spectrometry assay. Also, in the KS experiment, we overexpressed TPD54 and the Rab GTPases. The abnormally high amount of proteins might force interactions. However, these hypotheses do not explain why we saw an association with Rab7a by mass spectrometry and not by KS. An explanation for this could be that the vesicles we reroute to the mitochondria with a KS are only the very small vesicles and that Rab7-positive late endosomes are too big to be rerouted. However, there has been an example where a group was able to reroute large parts of the Golgi apparatus to the mitochondria using KS (Dunlop et al., 2017). We have also seen colocalisation of all the Rabs (except Rab6 and Rab8) with TPD54. This will however need to be quantified more closely with the particle analysis ComDet plugin, to see the extent of the colocalisation.

We think it is unlikely that if TPD54 binds to Rab GTPases, it binds such a large number and a large variety of them. First, these Rabs are all scattered in

the membrane trafficking pathway, from the ER to the plasma membrane. Second, they are evolutionarily distant in the Rab GTPases tree (Rab1 and Rab5 being quite distant, as well as Rab4 and Rab7) (**Figure 6.1**) (Klopper et al., 2012). Few proteins are able to bind such a wide diversity of Rabs. The GDIs chaperone them from the acceptor membrane to the donor membrane are example of proteins having this ability, although there are only two known GDI in humans, GDI1 and GDI2 (Goody et al., 2017; Pfeffer, 2017), meaning that this is not a role that many different types of proteins can have. Also, it would be expected that if TPD54 is a new GDI-like protein, we would not see it reroute vesicles to the mitochondria, since the complex GDI-Rab is cytosolic (Wandinger-Ness and Zerial, 2014). Another hypothesis is that TPD54 binds one main Rab (maybe Rab14, given the intensity of Rab14 in the mass spectrometry experiment), and that it binds also other similar Rabs (2, 4, 11, 25) more weakly. If this is the case, the Rabs from other supergroups are false-positives due to overexpression or suboptimal washes during the immunoprecipitation leading to the mass spectrometry analysis. The Rab5c interaction argues against this. Rab5c has also been found to interact with TPD52 by another group (Shahheydari et al., 2014), which argues that this interaction is likely to be real.

We think the main Rab GTPase interacting with TPD54 might be the post Golgi Rab14 (Junutula et al., 2004). Not only was it a strong hit in the mass spectrometry experiment, but Rab14 is also on the pathway that agrees the most with our other experiments. We have concluded that TPD54 is somewhere between the trans-Golgi network and the endosomes, since we could reroute TGN46, but not GM130, and Rab11/25 with a KS. Also, the CD8-chimera containing a dileucine motif was only rerouted with TPD54 after more than 60 minutes post-internalisation, which agrees with the idea that TPD54 is on the post-Golgi recycling pathway. If TPD54 were simply on the recycling route, the dileucine motif, and probably TfR, would have been rerouted with TPD54, at some point between 30 and 60 minutes port-internalisation.

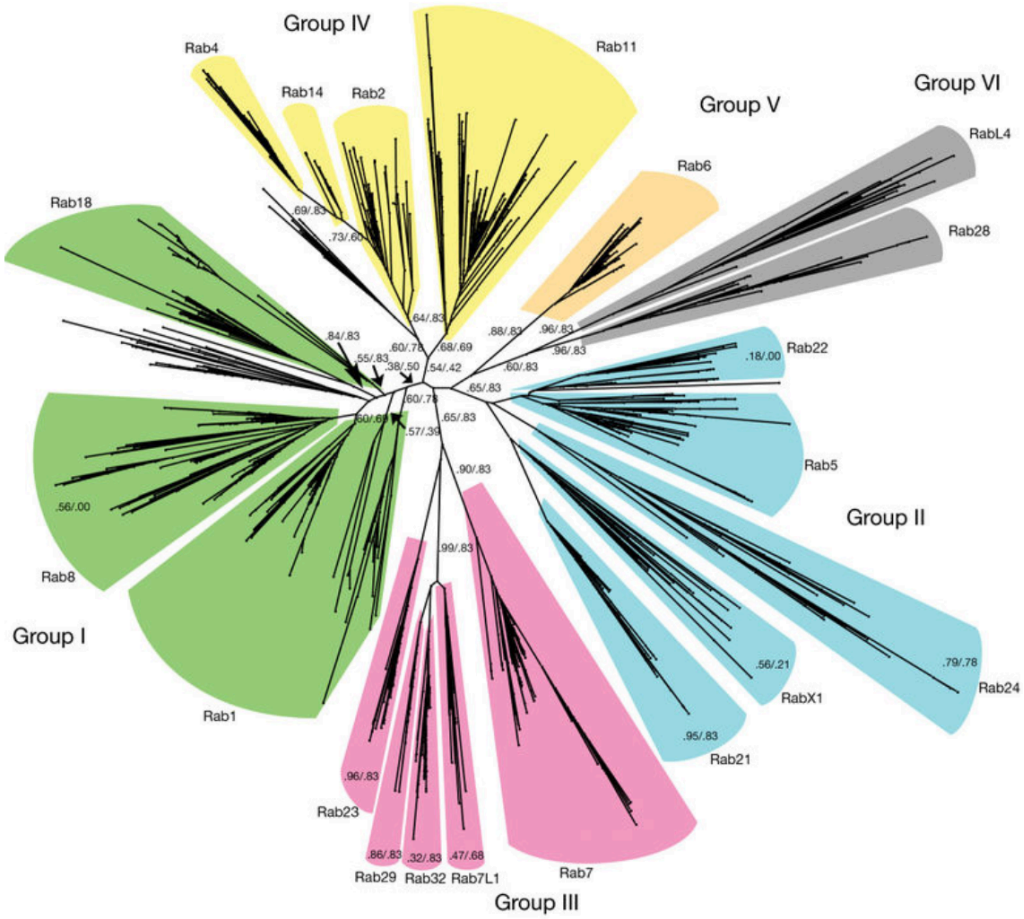

Figure 6.1: Phylogenetic tree of the Rab GTPases subfamilies, from Klopper et al., 2012. Each Rabs inside a group have evolved more closely and therefore are more likely to have similar features and sequence. Rab25, which was also called Rab11c, is in the Rab11 branch.

We therefore hypothesise that TPD54 is on the Rab14-positive vesicles regulating the recycling of receptors with a dileucine motif to the plasma membrane after the Golgi apparatus. We don't know yet the precise role of TPD54 with the Rab GTPases. We think TPD54 might be an effector because of the size of the vesicles we reroute with a KS. We can imagine that if TPD54 were a GDI, as mentioned earlier, no vesicle would be rerouted. Similarly, if TPD54 were a GEF, we would capture bigger vesicles, such as Golgi fragments, and that if TPD54 were a GAP, we would also capture bigger endosomal vesicles, or tubular vesicles from the recycling endosome. Instead, we have small and regular vesicles, such as transport vesicles. TPD54 might

therefore be an effector regulating the translocation of transport vesicles. To confirm this hypothesis, we would need to do a better quantification of the size and shape of these vesicles seen by electron microscopy, as well as verifying the affinity of TPD54 for a GDP- or GTP-bound Rab GTPase. Proux-Gillardeaux et al. have shown that TPD53 might be a SNARE, we can therefore hypothesize that TPD54 is an affeector by being a SNARE as well. We could test this by monitoring fusion of TPD54-positive liposomes *in vitro*.

If TPD54 is indeed on the post-Golgi recycling pathway, this might explain why depletion of TPD54 slows migration and impairs invasion. Integrins are known to transit through the Golgi apparatus, but the way out to the plasma membrane after this is still unclear. We hypothesise that Rab14 and TPD54 regulate this pathway, since we monitored a defect in integrin recycling, and found an interaction between TPD54 and integrin β1 by mass spectrometry. To confirm this hypothesis, we will assess the anterograde transport of GFP-tagged VSVG (vesicular stomatitis virus G) particle. This will allow us to see if the particle is trafficked normally from the ER to the Golgi, and from the Golgi to the PM, in TPD54 KD cells. To assess transport on the retrograde pathway, we will use Shiga toxin, since it traffics from the PM to endosomes, endosomes to Golgi in a retromer-dependant manner, and Golgi to ER (Johannes and Roemer, 2010).

In the future, we will need to understand the structure of TPD54 and the role of its interaction with TPD52 and TPD53. We have been able to confirm that TPD54 interacts with the two others, and we can hypothesise that the three main TPDs are perhaps part of a complex. Predicted models of the structure of TPD54 are available (see appendix 3), but a crystal structure would be very revealing. This would also allow us to better explore the sequence of TPD54 in order to make mutants inhibiting the functions of the protein.

This study has definitely allowed us to better understand the function of TPD54, by having more mechanistic insights into its cellular roles, and how this promotes cancer and lead to a poor prognosis.

References

Adair, B.D., J.P. Xiong, C. Maddock, S.L. Goodman, M.A. Arnaout, and M. Yeager. 2005. Three-dimensional EM structure of the ectodomain of integrin alpha V beta 3 in a complex with fibronectin. *Journal of Cell Biology*. 168:1109-1118.

Alexandrova, A.Y., K. Arnold, S. Schaub, J.M. Vasiliev, J.J. Meister, A.D. Bershadsky, and A.B. Verkhovsky. 2008. Comparative Dynamics of Retrograde Actin Flow and Focal Adhesions: Formation of Nascent Adhesions Triggers Transition from Fast to Slow Flow. *Plos One*. 3.

Aniento, F., N. Emans, G. Griffiths, and J. Gruenberg. 1993. CYTOPLASMIC DYNEIN-DEPENDENT VESICULAR TRANSPORT FROM EARLY TO LATE ENDOSOMES. *Journal of Cell Biology*. 123:1373-1387.

Arighi, C.N., L.M. Hartnell, R.C. Aguilar, C.R. Haft, and J.S. Bonifacino. 2004. Role of the mammalian retromer in sorting of the cation-independent mannose 6-phosphate receptor. *Journal of Cell Biology*. 165:123-133.

Arjonen, A., J. Alanko, S. Veltel, and J. Ivaska. 2012. Distinct Recycling of Active and Inactive ss 1 Integrins. *Traffic*. 13:610-625.

Ashrafi, K., F.Y. Chang, J.L. Watts, A.G. Fraser, R.S. Kamath, J. Ahringer, and G. Ruvkun. 2003. Genome-wide RNAi analysis of Caenorhabditis elegans fat regulatory genes. *Nature*. 421:268-272.

Balderhaar, H.J.K., J. Lachmann, E. Yavavli, C. Broecker, A. Luerick, and C. Ungermann. 2013. The CORVET complex promotes tethering and fusion of Rab5/Vps21-positive membranes. *Proceedings of the National Academy of Sciences of the United States of America*. 110:3823-3828.

Balleine, R.L., M.S. Fejzo, P. Sathasivam, P. Basset, C.L. Clarke, and J.A. Byrne. 2000. The hD52 (TPD52) gene is a candidate target gene for events resulting in increased 8q21 copy number in human breast carcinoma. *Genes Chromosomes & Cancer*. 29:48-57.

Bananis, E., S. Nath, K. Gordon, P. Satir, R.J. Stockert, J.W. Murray, and A.W. Wolkoff. 2004. Microtubule-dependent movement of late endocytic vesicles in vitro: Requirements for dynein and kinesin. *Molecular Biology of the Cell*. 15:3688-3697.

Barbero, P., L. Bittova, and S.R. Pfeffer. 2002. Visualization of Rab9-mediated vesicle transport from endosomes to the trans-Golgi in living cells. *Journal of Cell Biology*. 156:511-518.

Barr, F.A. 2013. Rab GTPases and membrane identity: Causal or inconsequential? *Journal of Cell Biology*. 202:191-199.

Bate, N., A.R. Gingras, A. Bachir, R. Horwitz, F. Ye, B. Patel, B.T. Goult, and D.R. Critchley. 2012. Talin Contains A C-Terminal Calpain2 Cleavage Site Important In Focal Adhesion Dynamics. *Plos One*. 7.

Bendris, N., and S.L. Schmid. 2017. Endocytosis, Metastasis and Beyond: Multiple Facets of SNX9. *Trends in Cell Biology*. 27:189-200.

Bloomfield, G., and R.R. Kay. 2016. Uses and abuses of macropinocytosis. *Journal of Cell Science*. 129:2697-2705.

Blumer, J., J. Rey, L. Dehmelt, T. Mazel, Y.W. Wu, P. Bastiaens, R.S. Goody, and A. Itzen. 2013. RabGEFs are a major determinant for specific Rab membrane targeting. *Journal of Cell Biology*. 200:287-300.

Bonifacino, J.S., and J. Neefjes. 2017. Moving and positioning the endolysosomal system. *Current Opinion in Cell Biology*. 47:1-8.

Bonifacino, J.S., and R. Rojas. 2006. Retrograde transport from endosomes to the trans-Golgi network. *Nature Reviews Molecular Cell Biology*. 7:568-579.

Bonifacino, J.S., and L.M. Traub. 2003. Signals for sorting of transmembrane proteins to endosomes and lysosomes. *Annual Review of Biochemistry*. 72:395-447.

Borner, G.H.H., M. Harbour, S. Hester, K.S. Lilley, and M.S. Robinson. 2006. Comparative proteomics of clathrin-coated vesicles. *Journal of Cell Biology*. 175:571-578.

Bottcher, R.T., C. Stremmel, A. Meves, H. Meyer, M. Widmaier, H.Y. Tseng, and R. Fassler. 2012. Sorting nexin 17 prevents lysosomal degradation of beta(1) integrins by binding to the beta(1)-integrin tail. *Nature Cell Biology*. 14:584-+.

Boutros, R., and J.A. Byrne. 2005. D53 (TPD52L1) is a cell cycle-regulated protein maximally expressed at the G2-M transition in breast cancer cells. *Experimental Cell Research*. 310:152-165.

Bravo-Cordero, J.J., R. Marrero-Diaz, D. Megias, L. Genis, A. Garcia-Grande, M.A. Garcia, A.G. Arroyo, and M.C. Montoya. 2007. MT1-MMP proinvasive activity is regulated by a novel Rab8-dependent exocytic pathway. *Embo Journal*. 26:1499-1510.

Bretscher, M.S., and C. Aguado-Velasco. 1998. Membrane traffic during cell locomotion. *Current Opinion in Cell Biology*. 10:537-541.

Brewer, P.D., E.N. Habtemichael, I. Romenskaia, A.C.F. Coster, and C.C. Mastick. 2016. Rab14 limits the sorting of Glut4 from endosomes into insulin-sensitive regulated secretory compartments in adipocytes. *Biochemical Journal*. 473:1315-1327.

Brown, M.C., and C.E. Turner. 2004. Paxillin: Adapting to change. *Physiological Reviews*. 84:1315-1339.

Bulankina, A.V., A. Deggerich, D. Wenzel, K. Mutenda, J.G. Wittmann, M.G. Rudolph, K.N.J. Burger, and S. Hoening. 2009. TIP47 functions in the biogenesis of lipid droplets. *Journal of Cell Biology*. 185:641-655.

Byrne, J.A., and C. Labbe. 2017. Striking similarities between publications from China describing single gene knockdown experiments in human cancer cell lines. *Scientometrics*. 110:1471-1493.

Byrne, J.A., S. Maleki, J.R. Hardy, B.S. Gloss, R. Murali, J.P. Scurry, S. Fanayan, C. Emmanuel, N.F. Hacker, R.L. Sutherland, A. deFazio, and P.M. O'Brien. 2010. MAL2 and tumor protein D52 (TPD52) are

frequently overexpressed in ovarian carcinoma, but differentially associated with histological subtype and patient outcome. *Bmc Cancer*. 10.

Byrne, J.A., M.G. Mattei, and P. Basset. 1996. Definition of the tumor protein D52 (TPD52) gene family through cloning of D52 homologues in human (hD53) and mouse (mD52). *Genomics*. 35:523-532.

Byrne, J.A., C.R. Nourse, P. Basset, and P. Gunning. 1998. Identification of homo- and heteromeric interactions between members of the breast carcinoma-associated D52 protein family using the yeast two-hybrid system. *Oncogene*. 16:873-881.

Byrne, J.A., C. Tomasetto, J.M. Garnier, N. Rouyer, M.G. Mattei, J.P. Bellocq, M.C. Rio, and P. Basset. 1995. A SCREENING METHOD TO IDENTIFY GENES COMMONLY OVEREXPRESSED IN CARCINOMAS AND THE IDENTIFICATION OF A NOVEL COMPLEMENTARY-DNA SEQUENCE. *Cancer Research*. 55:2896-2903.

Cadwell, C.M., W.J. Su, and A.P. Kowalczyk. 2016. Cadherin tales: Regulation of cadherin function by endocytic membrane trafficking. *Traffic*. 17:1262-1271.

Cain, R.J., and A.J. Ridley. 2009. Phosphoinositide 3-kinases in cell migration. *Biology of the Cell*. 101:13-29.

Cantalupo, G., P. Alifano, V. Roberti, C.B. Bruni, and C. Bucci. 2001. Rab-interacting lysosomal protein (RILP): the Rab7 effector required for transport to lysosomes. *Embo Journal*. 20:683-693.

Cao, Q.H., J. Chen, L. Zhu, Y. Liu, Z. Zhou, J. Sha, S. Wang, and J. Li. 2006. A testis-specific and testis developmentally regulated tumor protein D52 (TPD52)-like protein TPD52L3/hD55 interacts with TPD52 family proteins. *Biochemical and Biophysical Research Communications*. 344:798-806.

Carroll, K.S., J. Hanna, I. Simon, J. Krise, P. Barbero, and S.R. Pfeffer. 2001. Role of Rab9 GTPase in facilitating receptor recruitment by TIP47. *Science*. 292:1373-1376.

Caswell, P., and J. Norman. 2008. Endocytic transport of integrins during cell migration and invasion. *Trends in Cell Biology*. 18:257-263.

Caswell, P.T., and J.C. Norman. 2006. Integrin trafficking and the control of cell migration. *Traffic*. 7:14-21.

Caswell, P.T., H.J. Spence, M. Parsons, D.P. White, K. Clark, K.W. Cheng, G.B. Mills, M.J. Humphries, A.J. Messent, K.I. Anderson, M.W. McCaffrey, B.W. Ozanne, and J.C. Norman. 2007. Rab25 associates with alpha 5 beta 1 integrin to promote invasive migration in 3D microenvironments. *Developmental Cell*. 13:496-510.

Catimel, B., M.X. Yin, C. Schieber, M. Condron, H. Patsiouras, J. Catimel, D. Robinson, L.S.M. Wong, E.C. Nice, A.B. Holmes, and A.W. Burgess. 2009. PI(3,4,5)P3 Interactome. *Journal of Proteome Research*. 8:3712-3726.

Chao, W.T., F. Ashcroft, A.C. Daquinag, T. Vadakkan, Z.B. Wei, P.M. Zhang, M.E. Dickinson, and J. Kunz. 2010. Type I Phosphatidylinositol

Phosphate Kinase Beta Regulates Focal Adhesion Disassembly by Promoting beta 1 Integrin Endocytosis. *Molecular and Cellular Biology*. 30:4463-4479.

Cheeseman, L.P., E.F. Harry, A.D. McAinsh, I.A. Prior, and S.J. Royle. 2013. Specific removal of TACC3-ch-TOG-clathrin at metaphase deregulates kinetochore fiber tension. *Journal of Cell Science*. 126:2102-2113.

Chen, P.I., C. Kong, X. Su, and P.D. Stahl. 2009. Rab5 Isoforms Differentially Regulate the Trafficking and Degradation of Epidermal Growth Factor Receptors. *Journal of Biological Chemistry*. 284:30328-30338.

Chen, P.I., K. Schauer, C. Kong, A.R. Harding, B. Goud, and P.D. Stahl. 2014. Rab5 Isoforms Orchestrate a "Division of Labor" in the Endocytic Network; Rab5C Modulates Rac-Mediated Cell Motility. *Plos One*. 9.

Chen, Y.Y., S. Frost, and J.A. Byrne. 2016. Dropping in on the lipid droplet-tumor protein D52 (TPD52) as a new regulator and resident protein. *Adipocyte*. 5:326-332.

Chen, Y.Y., A. Kamili, J.R. Hardy, G.E. Groblewski, K.K. Khanna, and J.A. Byrne. 2013. Tumor protein D52 represents a negative regulator of ATM protein levels. *Cell Cycle*. 12:3083-3097.

Cheng, J.P.X., and B.J. Nichols. 2016. Caveolae: One Function or Many? *Trends in Cell Biology*. 26:177-189.

Cheng, K.W., J.P. Lahad, W.L. Kuo, A. Lapuk, K. Yamada, N. Auersperg, J.S. Liu, K. Smith-McCune, K.H. Lu, D. Fishman, J.W. Gray, and G.B. Mills. 2004. The RAB25 small GTPase determines aggressiveness of ovarian and breast cancers. *Nature Medicine*. 10:1251-1256.

Chia, P.Z.C., P. Gunn, and P.A. Gleeson. 2013. Cargo trafficking between endosomes and the trans-Golgi network. *Histochemistry and Cell Biology*. 140:307-315.

Chrzanowska-Wodnicka, M., and K. Burridge. 1996. Rho-stimulated contractility drives the formation of stress fibers and focal adhesions. *Journal of Cell Biology*. 133:1403-1415.

Clouaire, T., A. Marnef, and G. Legube. 2017. Taming Tricky DSBs: ATM on duty. *DNA Repair*. 56:84-91.

Collins, B.M., A.J. McCoy, H.M. Kent, P.R. Evans, and D.J. Owen. 2002. Molecular architecture and functional model of the endocytic AP2 complex. *Cell*. 109:523-535.

Cong, L., F.A. Ran, D. Cox, S. Lin, R. Barretto, N. Habib, P.D. Hsu, X. Wu, W. Jiang, L.A. Marraffini, and F. Zhang. 2013. Multiplex Genome Engineering Using CRISPR/Cas Systems. *Science*. 339:819-823.

Conner, S.D., and S.L. Schmid. 2002. Identification of an adaptor-associated kinase, AAK1, as a regulator of clathrin-mediated endocytosis. *Journal of Cell Biology*. 156:921-929.

Danen, E.H.J., J. van Rheenen, W. Franken, S. Huveneers, P. Sonneveld, K. Jalink, and A. Sonnenberg. 2005. Integrins control motile strategy through a Rho-cofilin pathway. *Journal of Cell Biology*. 169:515-526.

Dasari, C., D.P. Yaghnam, R. Walther, and R. Ummanni. 2017. Tumor protein D52 (isoform 3) contributes to prostate cancer cell growth via targeting nuclear factor-B transactivation in LNCaP cells. *Tumor Biology*. 39.

De Franceschi, N., H. Hamidi, J. Alanko, P. Sahgal, and J. Ivaska. 2015. Integrin traffic - the update. *Journal of Cell Science*. 128:839-852.

de Marco, M.C., R. Puertollano, J.A. Martinez-Menarguez, and M.A. Alonso. 2006. Dynamics of MAL2 during glycosylphosphatidylinositol-anchored protein transcytotic transport to the apical surface of hepatoma HepG2 cells. *Traffic*. 7:61-73.

Delva, E., J.M. Jennings, C.C. Calkins, M.D. Kottke, V. Faundez, and A.P. Kowalczyk. 2008. Pemphigus vulgaris IgG-induced desmoglein-3 endocytosis and desmosomal disassembly are mediated by a clathrin- and dynamin-independent mechanism. *Journal of Biological Chemistry*. 283:18303-18313.

Derivery, E., E. Helfer, V. Henriot, and A. Gautreau. 2012. Actin Polymerization Controls the Organization of WASH Domains at the Surface of Endosomes. *Plos One*. 7.

Derivery, E., C. Sousa, J.J. Gautier, B. Lombard, D. Loew, and A. Gautreau. 2009. The Arp2/3 Activator WASH Controls the Fission of Endosomes through a Large Multiprotein Complex. *Developmental Cell*. 17:712-723.

Diaz, E., and S.R. Pfeffer. 1998. TIP47: A cargo selection device for mannose 6-phosphate receptor trafficking. *Cell*. 93:433-443.

Diekmann, Y., E. Seixas, M. Gouw, F. Tavares-Cadete, M.C. Seabra, and J.B. Pereira-Leal. 2011. Thousands of Rab GTPases for the Cell Biologist. *Plos Computational Biology*. 7.

Doherty, G.J., and H.T. McMahon. 2009. Mechanisms of Endocytosis. *Annual Review of Biochemistry*. 78:857-902.

Doray, B., P. Ghosh, J. Griffith, H.J. Geuze, and S. Kornfeld. 2002. Cooperation of GGAs and AP-1 in packaging MPRs at the trans-Golgi network. *Science*. 297:1700-1703.

Dozynkiewicz, M.A., N.B. Jamieson, I. MacPherson, J. Grindlay, P.V.E. van den Berghe, A. von Thun, J.P. Morton, C. Gourley, P. Timpson, C. Nixon, C.J. McKay, R. Carter, D. Strachan, K. Anderson, O.J. Sansom, P.T. Caswell, and J.C. Norman. 2012. Rab25 and CLIC3 Collaborate to Promote Integrin Recycling from Late Endosomes/Lysosomes and Drive Cancer Progression. *Developmental Cell*. 22:131-145.

Duleh, S.N., and M.D. Welch. 2010. WASH and the Arp2/3 Complex Regulate Endosome Shape and Trafficking. *Cytoskeleton*. 67:193-206.

Dunlop, M.H., A.M. Ernst, L.K. Schroeder, D.K. Toomre, G. Lavieu, and J.E. Rothman. 2017. Land-locked mammalian Golgi reveals cargo transport between stable cisternae. *Nature Communications*. 8.

Eathiraj, S., X.J. Pan, C. Ritacco, and D.G. Lambright. 2005. Structural basis of family-wide Rab GTPase recognition by rabenosyn-5. *Nature*. 436:415-419.

Ellis, S.J., E. Lostchuck, B.T. Goult, M. Bouaouina, M.J. Fairchild, P. Lopez-Ceballos, D.A. Calderwood, and G. Tanentzapf. 2014. The Talin Head Domain Reinforces Integrin-Mediated Adhesion by Promoting Adhesion Complex Stability and Clustering. *Plos Genetics*. 10.

Ezratty, E.J., C. Bertaux, E.E. Marcantonio, and G.G. Gundersen. 2009. Clathrin mediates integrin endocytosis for focal adhesion disassembly in migrating cells. *Journal of Cell Biology*. 187:733-747.

Ezratty, E.J., M.A. Partridge, and G.G. Gundersen. 2005. Microtubule-induced focal adhesion disassembly is mediated by dynamin and focal adhesion kinase. *Nature Cell Biology*. 7:581-U515.

Fabbri, M., S. Di Meglio, M.C. Gagliani, E. Consonni, R. Molteni, J.R. Bender, C. Tacchetti, and R. Pardi. 2005. Dynamic partitioning into lipid rafts controls the endo-exocytic cycle of the alpha L/beta(2) integrin, LFA-1, during leukocyte chemotaxis. *Molecular Biology of the Cell*. 16:5793-5803.

Fielding, A.B., and S.J. Royle. 2013. Mitotic inhibition of clathrin-mediated endocytosis. *Cellular and Molecular Life Sciences*. 70:3423-3433.

Franco, S.J., M.A. Rodgers, B.J. Perrin, J.W. Han, D.A. Bennin, D.R. Critchley, and A. Huttenlocher. 2004. Calpain-mediated proteolysis of talin regulates adhesion dynamics. *Nature Cell Biology*. 6:977-+.

Friedl, P. 2004. Prespecification and plasticity: shifting mechanisms of cell migration. *Current Opinion in Cell Biology*. 16:14-23.

Friedl, P., K.S. Zanker, and E.B. Brocker. 1998. Cell migration strategies in 3-D extracellular matrix: Differences in morphology, cell matrix interactions, and integrin function. *Microscopy Research and Technique*. 43:369-378.

Fujimoto, T., and R.G. Parton. 2011. Not Just Fat: The Structure and Function of the Lipid Droplet. *Cold Spring Harbor Perspectives in Biology*. 3.

Fujita, A., and S. Kondo. 2015. Identification of TPD54 as a candidate marker of oral epithelial carcinogenesis. *Journal of Oral and Maxillofacial Surgery Medicine and Pathology*. 27:770-774.

Funamoto, S., R. Meili, S. Lee, L. Parry, and R.A. Firtel. 2002. Spatial and temporal regulation of 3-phosphoinositides by PI 3-kinase and PTEN mediates chemotaxis. *Cell*. 109:611-623.

Gallon, M., and P.J. Cullen. 2015. Retromer and sorting nexins in endosomal sorting. *Biochemical Society Transactions*. 43:33-47.

Galvez, B.G., S. Matias-Roman, M. Yanez-Mo, M. Vicente-Manzanares, F. Sanchez-Madrid, and A.G. Arroyo. 2004. Caveolae are a novel pathway for membrane-type 1 matrix metalloproteinase traffic in human endothelial cells. *Molecular Biology of the Cell*. 15:678-687.

Ganley, I.G., K. Carroll, L. Bittova, and S. Pfeffer. 2004. Rab9 GTPase regulates late endosome size and requires effector interaction for its stability. *Molecular Biology of the Cell*. 15:5420-5430.

Garcia, C.K., K. Wilund, M. Arca, G. Zuliani, R. Fellin, M. Maioli, S. Calandra, S. Bertolini, F. Cossu, N. Grishin, R. Barnes, J.C. Cohen, and H.H. Hobbs. 2001. Autosomal recessive hypercholesterolemia caused by

mutations in a putative LDL receptor adaptor protein. *Science*. 292:1394-1398.

Gerondopoulos, A., L. Langemeyer, J.R. Liang, A. Linford, and F.A. Barr. 2012. BLOC-3 Mutated in Hermansky-Pudlak Syndrome Is a Rab32/38 Guanine Nucleotide Exchange Factor. *Current Biology*. 22:2135-2139.

Gillingham, A.K., R. Sinka, I.L. Torres, K.S. Lilley, and S. Munro. 2014. Toward a Comprehensive Map of the Effectors of Rab GTPases. *Developmental Cell*. 31:358-373.

Gomez, T.S., and D.D. Billadeau. 2009. A FAM21-Containing WASH Complex Regulates Retromer-Dependent Sorting. *Developmental Cell*. 17:699-711.

Goody, R.S., M.P. Mueller, and Y.-W. Wu. 2017. Mechanisms of action of Rab proteins, key regulators of intracellular vesicular transport. *Biological Chemistry*. 398:565-575.

Goody, R.S., A. Rak, and K. Alexandrov. 2005. The structural and mechanistic basis for recycling of Rab proteins between membrane compartments. *Cellular and Molecular Life Sciences*. 62:1657-1670.

Goto, Y., R. Nishikawa, S. Kojima, T. Chiyomaru, H. Enokida, S. Inoguchi, T. Kinoshita, M. Fuse, S. Sakamoto, M. Nakagawa, Y. Naya, T. Ichikawa, and N. Seki. 2014. Tumour-suppressive microRNA-224 inhibits cancer cell migration and invasion via targeting oncogenic TPD52 in prostate cancer. *Febs Letters*. 588:1973-1982.

Gurkan, C., H. Lapp, C. Alory, A.I. Su, J.B. Hogenesch, and W.E. Balch. 2005. Large-scale profiling of Rab GTPase trafficking networks: The membrome. *Molecular Biology of the Cell*. 16:3847-3864.

Hanahan, D., and R.A. Weinberg. 2000. The hallmarks of cancer. *Cell*. 100:57-70.

Hastie, E.L., and D.R. Sherwood. 2016. A new front in cell invasion: The invadopodial membrane. *European Journal of Cell Biology*. 95:441-448.

He, Y.C., F.S. Chen, Y. Cai, and S.H. Chen. 2015. Knockdown of tumor protein D52-like 2 induces cell growth inhibition and apoptosis in oral squamous cell carcinoma. *Cell Biology International*. 39:264-271.

Heasman, S.J., and A.J. Ridley. 2008. Mammalian Rho GTPases: new insights into their functions from in vivo studies. *Nature Reviews Molecular Cell Biology*. 9:690-701.

Heuser, J., and T. Kirchhausen. 1985. Deep-etch views of clathrin assemblies. *Journal of ultrastructure research*. 92:1-27.

Hoepfner, S., F. Severin, A. Cabezas, B. Habermann, A. Runge, D. Giilooly, H. Stenmark, and M. Zerial. 2005. Modulation of receptor recycling and degradation by the endosomal kinesin KIF16B. *Cell*. 121:437-450.

Horazdovsky, B.F., B.A. Davies, M.N.J. Seaman, S.A. McLaughlin, S. Yoon, and S.D. Emr. 1997. A sorting nexin-1 homologue, vps5p, forms a complex with vps17p and is required for recycling the vacuolar protein-sorting receptor. *Molecular Biology of the Cell*. 8:1529-1541.

Horiuchi, H., R. Lippe, H.M. McBride, M. Rubino, P. Woodman, H. Stenmark, V. Rybin, M. Wilm, K. Ashman, M. Mann, and M. Zerial. 1997. A novel Rab5 GDP/GTP exchange factor complexed to Rabaptin-5 links nucleotide exchange to effector recruitment and function. *Cell*. 90:1149-1159.

Hosoi, H., M.B. Dilling, T. Shikata, L.N. Liu, L. Shu, R.A. Ashmun, G.S. Germain, R.T. Abraham, and P.J. Houghton. 1999. Rapamycin causes poorly reversible inhibition of mTOR and induces p53-independent apoptosis in human rhabdomyosarcoma cells. *Cancer Research*. 59:886-894.

Hsu, V.W., M. Bai, and J. Li. 2012. Getting active: protein sorting in endocytic recycling. *Nature Reviews Molecular Cell Biology*. 13:1-6.

Hulce, J.J., A.B. Cognetta, M.J. Niphakis, S.E. Tully, and B.F. Cravatt. 2013. Proteome-wide mapping of cholesterol-interacting proteins in mammalian cells. *Nature Methods*. 10:259-264.

Humphries, J.D., P. Wang, C. Streuli, B. Geiger, M.J. Humphries, and C. Ballestrem. 2007. Vinculin controls focal adhesion formation by direct interactions with talin and actin. *Journal of Cell Biology*. 179:1043-1057.

Huotari, J., and A. Helenius. 2011. Endosome maturation. *Embo Journal*. 30:3481-3500.

Huttenlocher, A., and A.R. Horwitz. 2011. Integrins in Cell Migration. *Cold Spring Harbor Perspectives in Biology*. 3.

Iijima, M., Y.E. Huang, and P. Devreotes. 2002. Temporal and spatial regulation of chemotaxis. *Developmental Cell*. 3:469-478.

Ito, C., Y. Mukudai, M. Itose, K. Kato, H. Motohashi, T. Shimane, S. Kondo, and T. Shirota. 2017. Tumor Proteins D52 and D54 Have Opposite Effects on the Terminal Differentiation of Chondrocytes. *Biomed Research International*.

Iwamoto, D.V., and D.A. Calderwood. 2015. Regulation of integrin-mediated adhesions. *Current Opinion in Cell Biology*. 36:41-47.

Jacob, A., J. Jing, J. Lee, P. Schedin, S.M. Gilbert, A.A. Peden, J.R. Junutula, and R. Prekeris. 2013. Rab40b regulates trafficking of MMP2 and MMP9 during invadopodia formation and invasion of breast cancer cells. *Journal of Cell Science*. 126:4647-4658.

Jing, J., J.R. Junutula, C. Wu, J. Burden, H. Matern, A.A. Peden, and R. Prekeris. 2010. FIP1/RCP Binding to Golgin-97 Regulates Retrograde Transport from Recycling Endosomes to the trans-Golgi Network. *Molecular Biology of the Cell*. 21:3041-3053.

Johannes, L., and V. Popoff. 2008. Tracing the Retrograde Route in Protein Trafficking. *Cell*. 135:1175-1187.

Johannes, L., and W. Roemer. 2010. Shiga toxins - from cell biology to biomedical applications. *Nature Reviews Microbiology*. 8:105-116.

Johannes, L., and C. Wunder. 2011. Retrograde Transport: Two (or More) Roads Diverged in an Endosomal Tree? *Traffic*. 12:956-962.

Johansson, M., N. Rocha, W. Zwart, I. Jordens, L. Janssen, C. Kuijl, V.M. Olkkonen, and J. Neefjes. 2007. Activation of endosomal dynein motors by stepwise assembly of Rab7-RILP-p150(Glued), ORP1L, and the receptor beta III spectrin. *Journal of Cell Biology*. 176:459-471.

Jordens, I., M. Fernandez-Borja, M. Marsman, S. Dusseljee, L. Janssen, J. Calafat, H. Janssen, R. Wubbolts, and J. Neefjes. 2001. The Rab7 effector protein RILP controls lysosomal transport by inducing the recruitment of dynein-dynactin motors. *Current Biology*. 11:1680-1685.

Junutula, J.R., A.M. De Maziere, A.A. Peden, K.E. Ervin, R.J. Advani, S.M. van Dijk, J. Klumperman, and R.H. Scheller. 2004. Rab14 is involved in membrane trafficking between the Golgi complex and endosomes. *Molecular Biology of the Cell*. 15:2218-2229.

Kalaidzidis, I., M. Miaczynska, M. Brewinska-Olchowik, A. Hupalowska, C. Ferguson, R.G. Parton, Y. Kalaidzidis, and M. Zerial. 2015. APPL endosomes are not obligatory endocytic intermediates but act as stable cargo-sorting compartments. *Journal of Cell Biology*. 211:123-144.

Kamili, A., N. Roslan, S. Frost, L.C. Cantrill, D.W. Wang, A. Della-Franca, R.K. Bright, G.E. Groblewski, B.K. Straub, A.J. Hoy, Y.Y. Chen, and J.A. Byrne. 2015. TPD52 expression increases neutral lipid storage within cultured cells. *Journal of Cell Science*. 128:3223-3238.

Kato, K., Y. Mukudai, H. Motohashi, C. Ito, S. Kamoshida, T. Shimane, S. Kondo, and T. Shirota. 2017. Opposite effects of tumor protein D (TPD) 52 and TPD54 on oral squamous cell carcinoma cells. *International Journal of Oncology*. 50:1634-1646.

Kaur, S., A.B. Fielding, G. Gassner, N.J. Carter, and S.J. Royle. 2014. An unmet actin requirement explains the mitotic inhibition of clathrin-mediated endocytosis. *Elife*. 3.

Kaverina, I., O. Krylyshkina, and J.V. Small. 1999. Microtubule targeting of substrate contacts promotes their relaxation and dissociation. *Journal of Cell Biology*. 146:1033-1043.

Keil, R., and M. Hatzfeld. 2014. The armadillo protein p0071 is involved in Rab11-dependent recycling. *Journal of Cell Science*. 127:60-71.

Kelly, B.T., A.J. McCoy, K. Spate, S.E. Miller, P.R. Evans, S. Honing, and D.J. Owen. 2008. A structural explanation for the binding of endocytic dileucine motifs by the AP2 complex. *Nature*. 456:976-U981.

Keren, K., and T. Shemesh. 2017. Buckle up: Membrane tension drives lamellipodial network compression and adhesion deposition. *Journal of Cell Biology*. 216:2619-2621.

Kim, M., C.V. Carman, and T.A. Springer. 2003. Bidirectional transmembrane signaling by cytoplasmic domain separation in integrins. *Science*. 301:1720-1725.

Kinchen, J.M., and K.S. Ravichandran. 2010. Identification of two evolutionarily conserved genes regulating processing of engulfed apoptotic cells. *Nature*. 464:778-U157.

Klopper, T.H., N. Kienle, D. Fasshauer, and S. Munro. 2012. Untangling the evolution of Rab G proteins: implications of a comprehensive genomic analysis. *Bmc Biology*. 10.

Komor, A.C., A.H. Badran, and D.R. Liu. 2017. CRISPR-Based Technologies for the Manipulation of Eukaryotic Genomes. *Cell*. 168:20-36.

Kozik, P., R.W. Francis, M.N.J. Seaman, and M.S. Robinson. 2010. A Screen for Endocytic Motifs. *Traffic*. 11:843-855.

Kucera, A., M.B. Distefano, A. Berg-Larsen, F. Skjeldal, U. Repnik, O. Bakke, and C. Progida. 2016. Spatiotemporal Resolution of Rab9 and CI-MPR Dynamics in the Endocytic Pathway. *Traffic*. 17:211-229.

Kumamoto, T., N. Seki, H. Mataki, K. Mizuno, K. Kamikawaji, T. Samukawa, K. Koshizuka, Y. Goto, and H. Inoue. 2016. Regulation of TPD52 by antitumor microRNA-218 suppresses cancer cell migration and invasion in lung squamous cell carcinoma. *International Journal of Oncology*. 49:1870-1880.

Lapierre, L.A., R. Kumar, C.M. Hales, J. Navarre, S.G. Bhartur, J.O. Burnette, D.W. Provance, J.A. Mercer, M. Bahler, and J.R. Goldenring. 2001. Myosin Vb is associated with plasma membrane recycling systems. *Molecular Biology of the Cell*. 12:1843-1857.

Larocque, G., N.I. Clarke, B. Wilson, P. Caswell, and S.J. Royle. 2016. TPD54 is associated with recycling vesicles and plays a role in cell migration. *Molecular Biology of the Cell*. 27.

Laukaitis, C.M., D.J. Webb, K. Donais, and A.F. Horwitz. 2001. Differential dynamics of alpha 5 integrin, paxillin, and alpha-actinin during formation and disassembly of adhesions in migrating cells. *Journal of Cell Biology*. 153:1427-1440.

Leung, K.F., R. Baron, and M.C. Seabra. 2006. Geranylgeranylation of Rab GTPases. *Journal of Lipid Research*. 47:467-475.

Lewis, J.D., L.A. Payton, J.G. Whitford, J.A. Byrne, D.I. Smith, L. Yang, and R.K. Bright. 2007. Induction of tumorigenesis and metastasis by the murine orthologue of tumor protein D52. *Molecular Cancer Research*. 5:133-144.

Li, J., B.A. Ballif, A.M. Powelka, J. Dai, S.P. Gygi, and V.W. Hsu. 2005. Phosphorylation of ACAP1 by Akt regulates the stimulation-dependent recycling of integrin beta 1 to control cell migration. *Developmental Cell*. 9:663-673.

Li, J., Y. Li, H. Liu, Y. Liu, and B. Cui. 2017. The four-transmembrane protein MAL2 and tumor protein D52 (TPD52) are highly expressed in colorectal cancer and correlated with poor prognosis. *Plos One*. 12.

Lieu, Z.Z., and P.A. Gleeson. 2011. Endosome-to-Golgi transport pathways in physiological processes. *Histology and Histopathology*. 26:395-408.

Linder, S., C. Wiesner, and M. Himmel. 2011. Degrading Devices: Invadosomes in Proteolytic Cell Invasion. *Annual Review of Cell and Developmental Biology, Vol 27*. 27:185-211.

Lindsay, A.J., F. Jollivet, C.P. Horgan, A.R. Khan, G. Raposo, M.W. McCaffrey, and B. Goud. 2013. Identification and characterization of multiple

novel Rab-myosin Va interactions. *Molecular Biology of the Cell*. 24:3420-3434.

Linford, A., S. Yoshimura, R.N. Bastos, L. Langemeyer, A. Gerondopoulos, D.J. Rigden, and F.A. Barr. 2012. Rab14 and Its Exchange Factor FAM116 Link Endocytic Recycling and Adherens Junction Stability in Migrating Cells. *Developmental Cell*. 22:952-966.

Lippe, R., M. Miaczynska, V. Rybin, A. Runge, and M. Zerial. 2001. Functional synergy between Rab5 effector Rabaptin-5 and exchange factor Rabex-5 when physically associated in a complex. *Molecular Biology of the Cell*. 12:2219-2228.

Lobert, V.H., A. Brech, N.M. Pedersen, J. Wesche, A. Oppelt, L. Malerod, and H. Stenmark. 2010. Ubiquitination of alpha 5 beta 1 Integrin Controls Fibroblast Migration through Lysosomal Degradation of Fibronectin-Integrin Complexes. *Developmental Cell*. 19:148-159.

Luo, B.H., and T.A. Springer. 2006. Integrin structures and conformational signaling. *Current Opinion in Cell Biology*. 18:579-586.

Mai, A., S. Veltel, T. Pellinen, A. Padzik, E. Coffey, V. Marjomaki, and J. Ivaska. 2011. Competitive binding of Rab21 and p120RasGAP to integrins regulates receptor traffic and migration. *Journal of Cell Biology*. 194:291-306.

Majumdar, R., M. Sixt, and C.A. Parent. 2014. New paradigms in the establishment and maintenance of gradients during directed cell migration. *Current Opinion in Cell Biology*. 30:33-40.

Mallet, W.G., and F.R. Maxfield. 1999. Chimeric forms of furin and TGN38 are transported from the plasma membrane to the trans-Golgi network via distinct endosomal pathways. *Journal of Cell Biology*. 146:345-359.

Maritzen, T., H. Schachtner, and D.F. Legler. 2015. On the move: endocytic trafficking in cell migration. *Cellular and Molecular Life Sciences*. 72:2119-2134.

Marks, M.S., L. Woodruff, H. Ohno, and J.S. Bonifacino. 1996. Protein targeting by tyrosine- and di-leucine-based signals: Evidence for distinct saturable components. *Journal of Cell Biology*. 135:341-354.

McBride, H.M., V. Rybin, C. Murphy, A. Giner, R. Teasdale, and M. Zerial. 1999. Oligomeric complexes link Rab5 effectors with NSF and drive membrane fusion via interactions between EEA1 and syntaxin 13. *Cell*. 98:377-386.

McLauchlan, H., J. Newell, N. Morrice, A. Osborne, M. West, and E. Smythe. 1998. A novel role for Rab5-GDI in ligand sequestration into clathrin-coated pits. *Current Biology*. 8:34-45.

McMahon, H.T., and E. Boucrot. 2011. Molecular mechanism and physiological functions of clathrin-mediated endocytosis. *Nature Reviews Molecular Cell Biology*. 12:517-533.

McNally, K.E., R. Faulkner, F. Steinberg, M. Gallon, R. Ghai, D. Pim, P. Langton, N. Pearson, C.M. Danson, H. Nagele, L.L. Morris, A. Singla, B.L. Overlee, K.J. Heesom, R. Sessions, L. Banks, B.M. Collins, I. Berger, D.D. Billadeau, E. Burstein, and P.J. Cullen. 2017. Retriever is

a multiprotein complex for retromer-independent endosomal cargo recycling. *Nature Cell Biology*. 19:1214-+.

Mehta, A.D., R.S. Rock, M. Rief, J.A. Spudich, M.S. Mooseker, and R.E. Cheney. 1999. Myosin-V is a processive actin-based motor. *Nature*. 400:590-593.

Messenger, S.W., D.D.H. Thomas, M.A. Falkowski, J.A. Byrne, F.S. Gorelick, and G.E. Groblewski. 2013. Tumor protein D52 controls trafficking of an apical endolysosomal secretory pathway in pancreatic acinar cells. *American Journal of Physiology-Gastrointestinal and Liver Physiology*. 305:G439-G452.

Meyer, C., D. Zizioli, S. Lausmann, E.L. Eskelinen, J. Hamann, P. Saftig, K. von Figura, and P. Schu. 2000. mu 1A-adaptin-deficient mice: lethality, loss of AP-1 binding and rerouting of mannose 6-phosphate receptors. *Embo Journal*. 19:2193-2203.

Mierke, C.T. 2015. Physical view on migration modes. *Cell Adhesion & Migration*. 9:367-379.

Mishra, S.K., P.A. Keyel, M.J. Hawryluk, N.R. Agostinelli, S.C. Watkins, and L.M. Traub. 2002. Disabled-2 exhibits the properties of a cargo-selective endocytic clathrin adaptor. *Embo Journal*. 21:4915-4926.

Mukhopadhyay, A., X. Pan, D.G. Lambright, and H.A. Tissenbaum. 2007. An endocytic pathway as a target of tubby for regulation of fat storage. *Embo Reports*. 8:931-938.

Mukudai, Y., S. Kondo, A. Fujita, Y. Yoshihama, T. Shirota, and S. Shintani. 2013. Tumor protein D54 is a negative regulator of extracellular matrix-dependent migration and attachment in oral squamous cell carcinoma-derived cell lines. *Cellular Oncology*. 36:233-245.

Murray, D.H., M. Jahnel, J. Lauer, M.J. Avellaneda, N. Brouilly, A. Cezanne, H. Morales-Navarrete, E.D. Perini, C. Ferguson, A.N. Lupas, Y. Kalaidzidis, R.G. Parton, S.W. Grill, and M. Zerial. 2016. An endosomal tether undergoes an entropic collapse to bring vesicles together. *Nature*. 537:107-111.

Nadler, S.T., J.P. Stoehr, K.L. Schueler, G. Tanimoto, B.S. Yandell, and A.D. Attie. 2000. The expression of adipogenic genes is decreased in obesity and diabetes mellitus. *Proceedings of the National Academy of Sciences of the United States of America*. 97:11371-11376.

Nagashima, K., S. Torii, Z.H. Yi, M. Igarashi, K. Okamoto, T. Takeuchi, and T. Izumi. 2002. Melanophilin directly links Rab27a and myosin Va through its distinct coiled-coil regions. *Febs Letters*. 517:233-238.

Nalbant, P., Y.C. Chang, J. Birkenfeld, Z.F. Chang, and G.M. Bokoch. 2009. Guanine Nucleotide Exchange Factor-H1 Regulates Cell Migration via Localized Activation of RhoA at the Leading Edge. *Molecular Biology of the Cell*. 20:4070-4082.

Nekrasova, O.E., E.V. Amargo, W.O. Smith, J. Chen, G.E. Kreitzer, and K.J. Green. 2013. Desmosomal cadherins utilize distinct kinesins for assembly into desmosomes (vol 195, pg 1185, 2011). *Journal of Cell Biology*. 201:1085-1085.

Nielsen, E., F. Severin, J.M. Backer, A.A. Hyman, and M. Zerial. 1999. Rab5 regulates motility of early endosomes on microtubules. *Nature Cell Biology*. 1:376-382.

Nishimura, T., and K. Kaibuchi. 2007. Numb controls integrin endocytosis for directional cell migration with aPKC and PAR-3. *Developmental Cell*. 13:15-28.

Nobes, C.D., and A. Hall. 1995. RHO, RAC, AND CDC42 GTPASES REGULATE THE ASSEMBLY OF MULTIMOLECULAR FOCAL COMPLEXES ASSOCIATED WITH ACTIN STRESS FIBERS, LAMELLIPODIA, AND FILOPODIA. *Cell*. 81:53-62.

Nobes, C.D., and A. Hall. 1999. Rho GTPases control polarity, protrusion, and adhesion during cell movement. *Journal of Cell Biology*. 144:1235-1244.

Nottingham, R.M., I.G. Ganley, F.A. Barr, D.G. Lambright, and S.R. Pfeffer. 2011. RUTBC1 Protein, a Rab9A Effector That Activates GTP Hydrolysis by Rab32 and Rab33B Proteins. *Journal of Biological Chemistry*. 286:33213-33222.

Nottingham, R.M., G.V. Pusapati, I.G. Ganley, F.A. Barr, D.G. Lambright, and S.R. Pfeffer. 2012. RUTBC2 Protein, a Rab9A Effector and GTPase-activating Protein for Rab36. *Journal of Biological Chemistry*. 287:22740-22748.

Nourse, C.R., M.G. Mattei, P. Gunning, and J.A. Byrne. 1998. Cloning of a third member of the D52 gene family indicates alternative coding sequence usage in D52-like transcripts. *Biochimica Et Biophysica Acta-Gene Structure and Expression*. 1443:155-168.

Obata, Y., Y. Fukumoto, Y. Nakayama, T. Kuga, N. Dohmae, and N. Yamaguchi. 2010. The Lyn kinase C-lobe mediates Golgi export of Lyn through conformation-dependent ACSL3 association. *Journal of Cell Science*. 123:2649-2662.

Odorizzi, G., M. Babst, and S.D. Emr. 1998. Fab1p PtdIns(3)P 5-kinase function essential for protein sorting in the multivesicular body. *Cell*. 95:847-858.

Ohbayashi, N., M. Fukuda, and Y. Kanaho. 2017. Rab32 subfamily small GTPases: pleiotropic Rabs in endosomal trafficking. *Journal of Biochemistry*. 162:65-71.

Ohno, H., J. Stewart, M.C. Fournier, H. Bosshart, I. Rhee, S. Miyatake, T. Saito, A. Gallusser, T. Kirchhausen, and J.S. Bonifacino. 1995. INTERACTION OF TYROSINE-BASED SORTING SIGNALS WITH CLATHRIN-ASSOCIATED PROTEINS. *Science*. 269:1872-1875.

Palamidessi, A., E. Frittoli, M. Garre, M. Faretta, M. Mione, I. Testa, A. Diaspro, L. Lanzetti, G. Scita, and P.P. Di Fiore. 2008. Endocytic trafficking of Rac is required for the spatial restriction of signaling in cell migration. *Cell*. 134:135-147.

Parsons, J.T., A.R. Horwitz, and M.A. Schwartz. 2010. Cell adhesion: integrating cytoskeletal dynamics and cellular tension. *Nature Reviews Molecular Cell Biology*. 11:633-643.

Patki, V., J. Virbasius, W.S. Lane, B.H. Toh, H.S. Shpetner, and S. Corvera. 1997. Identification of an early endosomal protein regulated by phosphatidylinositol 3-kinase. *Proceedings of the National Academy of Sciences of the United States of America*. 94:7326-7330.

Paul, C.D., P. Mistriotis, and K. Konstantopoulos. 2017. Cancer cell motility: lessons from migration in confined spaces. *Nature Reviews Cancer*. 17:131-140.

Paul, N.R., G. Jacquemet, and P.T. Caswell. 2015. Endocytic Trafficking of Integrins in Cell Migration. *Current Biology*. 25:R1092-R1105.

Pearse, B.M. 1976. Clathrin: a unique protein associated with intracellular transfer of membrane by coated vesicles. *Proc Natl Acad Sci U S A*. 73:1255-1259.

Peden, A.A., E. Schonteich, J. Chun, J.R. Junutula, R.H. Scheller, and R. Prekeris. 2004. The RCP-Rab11 complex regulates endocytic protein sorting. *Molecular Biology of the Cell*. 15:3530-3541.

Pellinen, T., A. Arjonen, K. Vuoriluoto, K. Kallio, J.A.M. Fransen, and J. Ivaska. 2006. Small GTPase Rab21 regulates cell adhesion and controls endosomal traffic of beta 1-integrins. *Journal of Cell Biology*. 173:767-780.

Peplowska, K., D.F. Markgraf, C.W. Ostrowicz, G. Bange, and C. Ungermann. 2007. The CORVET tethering complex interacts with the yeast Rab5 homolog Vps21 and is involved in endo-lysosomal biogenesis. *Developmental Cell*. 12:739-750.

Petrie, R.J., N. Gavara, R.S. Chadwick, and K.M. Yamada. 2012. Nonpolarized signaling reveals two distinct modes of 3D cell migration. *Journal of Cell Biology*. 197:439-455.

Pfeffer, S.R. 2009. Multiple routes of protein transport from endosomes to the trans Golgi etwork. *Febs Letters*. 583:3811-3816.

Pfeffer, S.R. 2017. Rab GTPases: master regulators that establish the secretory and endocytic pathways. *Molecular Biology of the Cell*. 28:712-715.

Pontes, B., P. Monzo, L. Gole, A.L. Le Roux, A.J. Kosmalska, Z.Y. Tam, W.W. Luo, S. Kan, V. Viasnoff, P. Roca-Cusachs, L. Tucker-Kellogg, and N.C. Gauthier. 2017. Membrane tension controls adhesion positioning at the leading edge of cells. *Journal of Cell Biology*. 216:2959-2977.

Poppelreuther, M., B. Rudolph, C. Du, R. Grossmann, M. Becker, C. Thiele, R. Ehehalt, and J. Fullekrug. 2012. The N-terminal region of acyl-CoA synthetase 3 is essential for both the localization on lipid droplets and the function in fatty acid uptake. *Journal of Lipid Research*. 53:888-900.

Porther, N., and M. Barbieri. 2015a. Growth Factor Influences Rab5 Function in Breast Cancer. *Faseb Journal*. 29.

Porther, N., and M.A. Barbieri. 2015b. The role of endocytic Rab GTPases in regulation of growth factor signaling and the migration and invasion of tumor cells. *Small GTPases*. 6:135-144.

Poteryaev, D., S. Datta, K. Ackema, M. Zerial, and A. Spang. 2010. Identification of the Switch in Early-to-Late Endosome Transition. *Cell*. 141:497-508.

Powelka, A.M., J.L. Sun, J. Li, M.G. Gao, L.M. Shaw, A. Sonnenberg, and V.W. Hsu. 2004. Stimulation-dependent recycling of integrin beta 1 regulated by ARF6 and Rab11. *Traffic*. 5:20-36.

Progida, C., and O. Bakke. 2016. Bidirectional traffic between the Golgi and the endosomes - machineries and regulation. *Journal of Cell Science*. 129:3971-3982.

Prosseda, P.P., N. Luo, B. Wang, J.A. Alvarado, Y. Hu, and Y. Sun. 2017. Loss of OCRL increases ciliary PI(4,5)P2 in oculocerebrorenal syndrome of Lowe. *Journal of cell science*.

Proux-Gillardeaux, V., T. Galli, I. Callebaut, A. Mikhailik, G. Calothy, and M. Marx. 2003. D53 is a novel endosomal SNARE-binding protein that enhances interaction of syntaxin 1 with the synaptobrevin 2 complex in vitro. *Biochemical Journal*. 370:213-221.

Puertollano, R., R.C. Aguilar, I. Gorshkova, R.J. Crouch, and J.S. Bonifacino. 2001. Sorting of mannose 6-phosphate receptors mediated by the GGAs. *Science*. 292:1712-1716.

Puthenveedu, M.A., B. Lauffer, P. Temkin, R. Vistein, P. Carlton, K. Thorn, J. Taunton, O.D. Weiner, R.G. Parton, and M. von Zastrow. 2010. Sequence-Dependent Sorting of Recycling Proteins by Actin-Stabilized Endosomal Microdomains. *Cell*. 143:761-773.

Pylypenko, O., A. Rak, T. Durek, S. Kushnir, B.E. Dursina, N.H. Thomae, A.T. Constantinescu, L. Brunsveld, A. Watzke, H. Waldmann, R.S. Goody, and K. Alexandrov. 2006. Structure of doubly prenylated Ypt1 : GDI complex and the mechanism of GDI-mediated Rab recycling. *Embo Journal*. 25:13-23.

Rainero, E., and J.C. Norman. 2013. Late endosomal and lysosomal trafficking during integrin-mediated cell migration and invasion. *Bioessays*. 35:523-532.

Randles, M.J., M.J. Humphries, and R. Lennon. 2017. Proteomic definitions of basement membrane composition in health and disease. *Matrix Biology*. 57-58:12-28.

Rao, V.S., K. Srinivas, G.N. Sujini, and G.N.S. Kumar. 2014. Protein-protein interaction detection: methods and analysis. *International journal of proteomics*. 2014:147648.

Ratcliffe, C.D.H., P. Sahgal, C.A. Parachoniak, J. Ivaska, and M. Park. 2016. Regulation of Cell Migration and beta 1 Integrin Trafficking by the Endosomal Adaptor GGA3. *Traffic*. 17:670-688.

Ridley, A.J., M.A. Schwartz, K. Burridge, R.A. Firtel, M.H. Ginsberg, G. Borisy, J.T. Parsons, and A.R. Horwitz. 2003. Cell migration: Integrating signals from front to back. *Science*. 302:1704-1709.

Riederer, M.A., T. Soldati, A.D. Shapiro, J. Lin, and S.R. Pfeffer. 1994. LYSOSOME BIOGENESIS REQUIRES RAB9 FUNCTION AND

RECEPTOR RECYCLING FROM ENDOSOMES TO THE TRANS-GOLGI NETWORK. *Journal of Cell Biology*. 125:573-582.

Rink, J., E. Ghigo, Y. Kalaidzidis, and M. Zerial. 2005. Rab conversion as a mechanism of progression from early to late endosomes. *Cell*. 122:735-749.

Roberts, M., S. Barry, A. Woods, P. van der Sluijs, and J. Norman. 2001. PDGF-regulated rab4-dependent recycling of alpha v beta 3 integrin from early endosomes is necessary for cell adhesion and spreading. *Current Biology*. 11:1392-1402.

Roberts, M.S., A.J. Woods, T.C. Dale, P. van der Sluijs, and J.C. Norman. 2004. Protein kinase B/Akt acts via glycogen synthase kinase 3 to regulate recycling of alpha v beta 3 and alpha 5 beta 1 integrins. *Molecular and Cellular Biology*. 24:1505-1515.

Robinson, M.S., D.A. Sahlender, and S.D. Foster. 2010. Rapid Inactivation of Proteins by Rapamycin-Induced Rerouting to Mitochondria. *Developmental Cell*. 18:324-331.

Roca-Cusachs, P., A. del Rio, E. Puklin-Faucher, N.C. Gauthier, N. Biais, and M.P. Sheetz. 2013. Integrin-dependent force transmission to the extracellular matrix by alpha-actinin triggers adhesion maturation. *Proceedings of the National Academy of Sciences of the United States of America*. 110:E1361-E1370.

Rojas, R., S. Kametaka, C.R. Haft, and J.S. Bonifacino. 2007. Interchangeable but essential functions of SNX1 and SNX2 in the association of retromer with endosomes and the tracking of mannose 6-phosphate receptors. *Molecular and Cellular Biology*. 27:1112-1124.

Rojas, R., T. van Vlijmen, G.A. Mardones, Y. Prabhu, A.L. Rojas, S. Mohammed, A.J.R. Heck, G. Raposo, P. van der Sluijs, and J.S. Bonifacino. 2008. Regulation of retromer recruitment to endosomes by sequential action of Rab5 and Rab7. *Journal of Cell Biology*. 183:513-526.

Roth, T.F., and K.R. Porter. 1964. YOLK PROTEIN UPTAKE IN THE OOCYTE OF THE MOSQUITO AEDES AEGYPTI. L. *The Journal of cell biology*. 20:313-332.

Royle, S.J. 2013. Protein adaptation: mitotic functions for membrane trafficking proteins. *Nature Reviews Molecular Cell Biology*. 14:592-599.

Sahini, N., and J. Borlak. 2014. Recent insights into the molecular pathophysiology of lipid droplet formation in hepatocytes. *Progress in Lipid Research*. 54:86-112.

Santolini, E., C. Puri, A.E. Salcini, M.C. Gagliani, P.G. Pelicci, C. Tacchetti, and P.P. Di Fiore. 2000. Numb is an endocytic protein. *Journal of Cell Biology*. 151:1345-1351.

Sathasivam, P., A.M. Bailey, M. Crossley, and J.A. Byrne. 2001. The role of the coiled-coil motif in interactions mediated by TPD52. *Biochemical and Biophysical Research Communications*. 288:56-61.

Saxena, M., R. Changede, J. Hone, H. Wolfenson, and M.P. Sheetz. 2017. Force-Induced Calpain Cleavage of Talin Is Critical for Growth, Adhesion Development, and Rigidity Sensing. *Nano Lett*.

Scott, C.C., F. Vacca, and J. Gruenberg. 2014. Endosome maturation, transport and functions. *Seminars in Cell & Developmental Biology*. 31:2-10.

Seaman, M.N.J. 2004. Cargo-selective endosomal sorting for retrieval to the Golgi requires retromer. *Journal of Cell Biology*. 165:111-122.

Seaman, M.N.J., A. Gautreau, and D.D. Billadeau. 2013. Retromer-mediated endosomal protein sorting: all WASHed up! *Trends in Cell Biology*. 23:522-528.

Seaman, M.N.J., M.E. Harbour, D. Tattersall, E. Read, and N. Bright. 2009. Membrane recruitment of the cargo-selective retromer subcomplex is catalysed by the small GTPase Rab7 and inhibited by the Rab-GAP TBC1D5. *Journal of Cell Science*. 122:2371-2382.

Seaman, M.N.J., J.M. McCaffery, and S.D. Emr. 1998. A membrane coat complex essential for endosome-to-Golgi retrograde transport in yeast. *Journal of Cell Biology*. 142:665-681.

Semerdjieva, S., B. Shortt, E. Maxwell, S. Singh, P. Fonarev, J. Hansen, G. Schiavo, B.D. Grant, and E. Smythe. 2008. Coordinated regulation of AP2 uncoating from clathrin-coated vesicles by rab5 and hRME-6. *Journal of Cell Biology*. 183:499-511.

Shafaq-Zadah, M., C.S. Gomes-Santos, S. Bardin, P. Maiuri, M. Maurin, J. Iranzo, A. Gautreau, C. Lamaze, P. Caswell, B. Goud, and L. Johannes. 2016. Persistent cell migration and adhesion rely on retrograde transport of beta(1) integrin. *Nature Cell Biology*. 18:54-+.

Shahheydari, H., S. Frost, B.J. Smith, G.E. Groblewski, Y. Chen, and J.A. Byrne. 2014. Identification of PLP2 and RAB5C as novel TPD52 binding partners through yeast two-hybrid screening. *Molecular Biology Reports*. 41:4565-4572.

Shi, F., and J. Sottile. 2008. Caveolin-1-dependent beta 1 integrin endocytosis is a critical regulator of fibronectin turnover. *Journal of Cell Science*. 121:2360-2371.

Shi, F., and J. Sottile. 2011. MT1-MMP regulates the turnover and endocytosis of extracellular matrix fibronectin. *Journal of Cell Science*. 124:4039-4050.

Shin, H.W., M. Hayashi, S. Christoforidis, S. Lacas-Gervais, S. Hoepfner, M.R. Wenk, J. Modregger, S. Uttenweiler-Joseph, M. Wilm, A. Nystuen, W.N. Frankel, M. Solimena, P. De Camilli, and M. Zerial. 2005. An enzymatic cascade of Rab5 effectors regulates phosphoinositide turnover in the endocytic pathway. *Journal of Cell Biology*. 170:607-618.

Simon, N.C., and J.T. Barbieri. 2014. Exoenzyme S ADP-Ribosylates Rab5 Effector Sites To Uncouple Intracellular Trafficking. *Infection and Immunity*. 82:21-28.

Simonsen, A., J.M. Gaullier, A. D'Arrigo, and H. Stenmark. 1999. The Rab5 effector EEA1 interacts directly with syntaxin-6. *Journal of Biological Chemistry*. 274:28857-28860.

Simonsen, A., R. Lippe, S. Christoforidis, J.M. Gaullier, A. Brech, J. Callaghan, B.H. Toh, C. Murphy, M. Zerial, and H. Stenmark. 1998. EEA1 links PI(3)K function to Rab5 regulation of endosome fusion. *Nature*. 394:494-498.

Sonnichsen, B., S. De Renzis, E. Nielsen, J. Rietdorf, and M. Zerial. 2000. Distinct membrane domains on endosomes in the recycling pathway visualized by multicolor imaging of Rab4, Rab5 and Rab11. *Journal of Cell Biology*. 149:901-913.

Spangle, J.M., T.M. Roberts, and J.J. Zhao. 2017. The emerging role of PI3K/AKT-mediated epigenetic regulation in cancer. *Biochimica Et Biophysica Acta-Reviews on Cancer*. 1868:123-131.

Stehbens, S.J., M. Paszek, H. Pemble, A. Ettinger, S. Gierke, and T. Wittmann. 2014. CLASPs link focal-adhesion-associated microtubule capture to localized exocytosis and adhesion site turnover. *Nature Cell Biology*. 16:558-+.

Steinberg, F., K.J. Heesom, M.D. Bass, and P.J. Cullen. 2012. SNX17 protects integrins from degradation by sorting between lysosomal and recycling pathways. *Journal of Cell Biology*. 197:219-230.

Stenmark, H. 2009. Rab GTPases as coordinators of vesicle traffic. *Nature Reviews Molecular Cell Biology*. 10:513-525.

Sun, S.C. 2017. The non-canonical NF-kappa B pathway in immunity and inflammation. *Nature Reviews Immunology*. 17:545-558.

Swanson, J.A., and C. Watts. 1995. MACROPINOCYTOSIS. *Trends in Cell Biology*. 5:424-428.

Sweitzer, S.M., and J.E. Hinshaw. 1998. Dynamin undergoes a GTP-dependent conformational change causing vesiculation. *Cell*. 93:1021-1029.

Tadokoro, S., S.J. Shattil, K. Eto, V. Tai, R.C. Liddington, J.M. de Pereda, M.H. Ginsberg, and D.A. Calderwood. 2003. Talin binding to integrin beta tails: A final common step in integrin activation. *Science*. 302:103-106.

Teckchandani, A., E.E. Mulkearns, T.W. Randolph, N. Toida, and J.A. Cooper. 2012. The clathrin adaptor Dab2 recruits EH domain scaffold proteins to regulate integrin beta 1 endocytosis. *Molecular Biology of the Cell*. 23:2905-2916.

Temkin, P., B. Lauffer, S. Jaeger, P. Cimermancic, N.J. Krogan, and M. von Zastrow. 2011. SNX27 mediates retromer tubule entry and endosome-to-plasma membrane trafficking of signalling receptors. *Nature Cell Biology*. 13:715-U199.

Theisen, U., E. Straube, and A. Straube. 2012. Directional Persistence of Migrating Cells Requires Kif1C-Mediated Stabilization of Trailing Adhesions. *Developmental Cell*. 23:1153-1166.

Thomas, D.D.H., C.L. Frey, S.W. Messenger, B.K. August, and G.E. Groblewski. 2010a. A role for tumor protein TPD52 phosphorylation in endo-membrane trafficking during cytokinesis. *Biochemical and Biophysical Research Communications*. 402:583-587.

Thomas, D.D.H., K.M. Kaspar, W.B. Taft, N. Weng, L.A. Rodenkirch, and G.E. Groblewski. 2002. Identification of annexin VI as a Ca2+-sensitive CRHSP-28-binding protein in pancreatic acinar cells. *Journal of Biological Chemistry*. 277:35496-35502.

Thomas, D.D.H., C.L. Martin, N. Weng, J.A. Byrne, and G.E. Groblewski. 2010b. Tumor protein D52 expression and Ca2+-dependent phosphorylation modulates lysosomal membrane protein trafficking to the plasma membrane. *American Journal of Physiology-Cell Physiology*. 298:C725-C739.

Ullrich, O., S. Reinsch, S. Urbe, M. Zerial, and R.G. Parton. 1996. Rab11 regulates recycling through the pericentriolar recycling endosome. *Journal of Cell Biology*. 135:913-924.

Ullrich, O., H. Stenmark, K. Alexandrov, L.A. Huber, K. Kaibuchi, T. Sasaki, Y. Takai, and M. Zerial. 1993. RAB GDP DISSOCIATION INHIBITOR AS A GENERAL REGULATOR FOR THE MEMBRANE ASSOCIATION OF RAB PROTEINS. *Journal of Biological Chemistry*. 268:18143-18150.

Valdembri, D., and G. Serini. 2012. Regulation of adhesion site dynamics by integrin traffic. *Current Opinion in Cell Biology*. 24:582-591.

van Weering, J.R.T., P. Verkade, and P.J. Cullen. 2012. SNX-BAR-Mediated Endosome Tubulation is Co-ordinated with Endosome Maturation. *Traffic*. 13:94-107.

Vandersluijs, P., M. Hull, P. Webster, P. Male, B. Goud, and I. Mellman. 1992. THE SMALL GTP-BINDING PROTEIN RAB4 CONTROLS AN EARLY SORTING EVENT ON THE ENDOCYTIC PATHWAY. *Cell*. 70:729-740.

Vicente-Manzanares, M., X.F. Ma, R.S. Adelstein, and A.R. Horwitz. 2009. Non-muscle myosin II takes centre stage in cell adhesion and migration. *Nature Reviews Molecular Cell Biology*. 10:778-790.

Vinogradova, O., A. Velyvis, A. Velyviene, B. Hu, T.A. Haas, E.F. Plow, and J. Qin. 2002. A structural mechanism of integrin alpha(IIb)beta(3) "inside-out" activation as regulated by its cytoplasmic face. *Cell*. 110:587-597.

Wandinger-Ness, A., and M. Zerial. 2014. Rab Proteins and the Compartmentalization of the Endosomal System. *Cold Spring Harbor Perspectives in Biology*. 6.

Wang, S., Z. Ma, X. Xu, Z. Wang, L. Sun, Y. Zhou, X. Lin, W. Hong, and T. Wang. 2014a. A Role of Rab29 in the Integrity of the Trans-Golgi Network and Retrograde Trafficking of Mannose-6-Phosphate Receptor. *Plos One*. 9.

Wang, Y., C.L. Chen, Q.Z. Pan, Y.Y. Wu, J.J. Zhao, S.S. Jiang, J. Chao, X.F. Zhang, H.X. Zhang, Z.Q. Zhou, Y. Tang, X.Q. Huang, J.H. Zhang, and

J.C. Xia. 2016. Decreased TPD52 expression is associated with poor prognosis in primary hepatocellular carcinoma. *Oncotarget*. 7:6323-6334.

Wang, Z., J. Sun, Y. Zhao, W. Guo, K. Lv, and Q. Zhang. 2014b. Lentivirus-Mediated Knockdown of Tumor Protein D52-like 2 Inhibits Glioma Cell Proliferation. *Cellular and Molecular Biology*. 60:39-44.

Wassmer, T., N. Attar, M.V. Bujny, J. Oakley, C.J. Traer, and P.J. Cullen. 2007. A loss-of-function screen reveals SNX5 and SNX6 as potential components of the mammalian retromer. *Journal of Cell Science*. 120:45-54.

Wedlich-Soldner, R., and R. Li. 2003. Spontaneous cell polarization: undermining determinism. *Nature Cell Biology*. 5:267-270.

White, D.P., P.T. Caswell, and J.C. Norman. 2007. alpha V beta 3 and alpha 5B1 integrin recycling pathways dictate downstream Rho kinase signaling to regulate persistent cell migration. *Journal of Cell Biology*. 177:515-525.

Wilfling, F., A.R. Thiam, M.J. Olarte, J. Wang, R. Beck, T.J. Gould, E.S. Allgeyer, F. Pincet, J. Bewersdorf, R.V. Farese, and T.C. Walther. 2014. Arf1/COPI machinery acts directly on lipid droplets and enables their connection to the ER for protein targeting. *Elife*. 3.

Wilson, S.H.D., A.M. Bailey, C.R. Nourse, M.G. Mattei, and J.A. Byrne. 2001. Identification of MAL2, a novel member of the MAL proteolipid family, though interactions with TPD52-like proteins in the yeast two-hybrid system. *Genomics*. 76:81-88.

Woods, A.J., D.P. White, P.T. Caswell, and J.C. Norman. 2004. PKD1/PKC mu promotes alpha v beta 3 integrin recycling and delivery to nascent focal adhesions. *Embo Journal*. 23:2531-2543.

Wu, Y.W., L.K. Oesterlin, K.T. Tan, H. Waldmann, K. Alexandrov, and R.S. Goody. 2010. Membrane targeting mechanism of Rab GTPases elucidated by semisynthetic protein probes. *Nature Chemical Biology*. 6:534-540.

Wurmser, A.E., T.K. Sato, and S.D. Emr. 2000. New component of the vacuolar class C-Vps complex couples nucleotide exchange on the Ypt7 GTPase to SNARE-dependent docking and fusion. *Journal of Cell Biology*. 151:551-562.

Xu, J.P., W.M. Wang, Z.X. Zhu, Z.R. Wei, D.J. Yang, and Q.P. Cai. 2015. Tumor Protein D52-Like 2 Accelerates Gastric Cancer Cell Proliferation In Vitro. *Cancer Biotherapy and Radiopharmaceuticals*. 30:111-116.

Yamaguchi, T., N. Omatsu, A. Omukae, and T. Osumi. 2006. Analysis of interaction partners for perilipin and ADRP on lipid droplets. *Molecular and Cellular Biochemistry*. 284:167-173.

Yang, M., X.Y. Wang, J.Y. Jia, H.W. Gao, P. Chen, X.L. Sha, and S. Wu. 2015. Tumor Protein D52-Like 2 Contributes to Proliferation of Breast Cancer Cells. *Cancer Biotherapy and Radiopharmaceuticals*. 30:1-7.

Ye, F., B.G. Petrich, P. Anekal, C.T. Lefort, A. Kasirer-Friede, S.J. Shattil, R. Ruppert, M. Moser, R. Fassler, and M.H. Ginsberg. 2013. The Mechanism of Kindlin-Mediated Activation of Integrin alpha IIb beta 3. *Current Biology*. 23:2288-2295.

Yoshida, A., H. Hayashi, K. Tanabe, and A. Fujita. 2017. Segregation of phosphatidylinositol 4-phosphate and phosphatidylinositol 4,5-bisphosphate into distinct microdomains on the endosome membrane. *Biochimica Et Biophysica Acta-Biomembranes*. 1859:1880-1890.

Yu, J., S.W. Wu, and W.P. Wu. 2017. A tumor-suppressive microRNA, miRNA-485-5p, inhibits glioma cell proliferation and invasion by down-regulating TPD52L2. *American Journal of Translational Research*. 9:3336-+.

Zech, T., S.D.J. Calaminus, P. Caswell, H.J. Spence, M. Carnell, R.H. Insall, J. Norman, and L.M. Machesky. 2011. The Arp2/3 activator WASH regulates alpha 5 beta 1-integrin-mediated invasive migration. *Journal of Cell Science*. 124:3753-3759.

Zerial, M., and H. McBride. 2001. Rab proteins as membrane organizers. *Nature Reviews Molecular Cell Biology*. 2:107-117.

Zhang, Y., Q. Deng, and J.T. Barbieri. 2007. Intracellular localization of type III-delivered Pseudomonas ExoS with endosome vesicles. *Journal of Biological Chemistry*. 282:13022-13032.

Zhao, L.J., Z. Dong, S.C. Zhao, J. Xiong, and Z.G. Geng. 2017. TPD52L2 silencing inhibits lung cancer cell proliferation by cell cycle G2/M phase arrest. *International Journal of Clinical and Experimental Medicine*. 10:9785-9792.

Zhen, Y., and H. Stenmark. 2015. Cellular functions of Rab GTPases at a glance. *Journal of Cell Science*. 128:3171-3176.

Zhu, V.W., D. Upadhyay, A.B. Schrock, K. Gowen, S.M. Ali, and S.H.I. Ou. 2016. TPD52L1-ROS1, a new ROS1 fusion variant in lung adenosquamous cell carcinoma identified by comprehensive genomic profiling. *Lung Cancer*. 97:48-50.

Zolov, S.N., D. Bridges, Y. Zhang, W.-W. Lee, E. Riehle, R. Verma, G.M. Lenk, K. Converso-Baran, T. Weide, R.L. Albin, A.R. Saltiel, M.H. Meisler, M.W. Russell, and L.S. Weisman. 2012. In vivo, Pikfyve generates PI(3,5)P-2, which serves as both a signaling lipid and the major precursor for PI5P. *Proceedings of the National Academy of Sciences of the United States of America*. 109:17472-17477.

Appendix 1

TPD54 is a member of the tumor protein D52 (TPD52) family. These proteins are overexpressed in cancer and their overexpression is correlated with an aggressive, metastatic phenotype in breast cancer. In normal cells, the family members are found in association with membrane trafficking components such as clathrin, the Golgi apparatus and secretory vesicles, but very little is known about their role in membrane trafficking or how they contribute to metastasis in cancer. We used knocksideways (KS) to reroute TPD54 to mitochondria, and show that Rab4, Rab11a and Rab25 are co-rerouted. Rab5, Rab7 and Rab9 were unaffected by TPD54 KS. This implies a specific association of TPD54 with recycling vesicles. Importantly, electron microscopy of the TPD54 KS cells revealed that we reroute small vesicles to the mitochondrial surface and not just the TPD54 and Rab proteins themselves. This means that TPD54 KS is an excellent tool to rapidly and specifically inactivate the pool of TPD54-positive recycling endosomes. We highlight a functional role for TPD54 in endocytic recycling, but not endocytosis, using a transferrin recycling assay. Since recycling of integrins is crucial for cell migration, we sought to assess whether or not TPD54 plays a role in cell migration and invasion via the recycling of integrins. We show that knockdown (KD) of TPD54 significantly decreases RPE1 cell migration in 2D on fibronectin or laminin. This phenotype is seen with three independent siRNAs and can be rescued by expression of the long isoform of TPD54. A 3D migration assay in Rab25-expressing A2780 cells shows that KD of TPD54 decreases cell migration in a cell-derived matrix and also decreases invasion. Taken together, these data suggest that TPD54's role in endocytic recycling is crucial for cell migration.

TPD54 is associated with recycling vesicles and plays a role in cell migration

B1012
P1271

G. Larocque[1], N.I. Clarke[1], B. Wilson[2], P. Caswell[2] and S.J. Royle[1]

[1] Center for Mechanochemical Cell Biology, University of Warwick, United Kingdom [2] Faculty of Life Sciences, University of Manchester, United Kingdom

Aim of the project

Tumor protein D54 (TPD54) is a member of the TPD52 family and has a probable **role in membrane trafficking** (1-4), as well as in cell **adhesion and migration** in a cancer context (5). These two processes are largely influenced by the **recycling of the integrins**, the extracellular matrix receptors (6). These proteins are **recycled** in the cell via a fast pathway involving the small GTPase **Rab4**, and a slow pathway involving **Rab11 and Rab25** (7). Moreover, Rab25 has been involved in invasion and tumorogenicity through the trafficking of integrins α5β1(8). Since TPD54 has a role in cell migration on fibronectin (FN) (5), for which the main receptor is integrin α5β1, and is associated with membrane trafficking, we hypothesised that it **regulates the recycling of α5β1 integrin, residing on Rab11/Rab25/Rab4-positive recycling endosomes**. We will assess this hypothesis by checking the effect of a TPD54 KD in RPE1 cell migration. We will also look at TPD54's requirement for invasion in a breast cancer condition, using Rab25-overexpressing A2780 cells. We have seen that a KD affects the recycling pathway and we need to verify if TPD54 is linked to Rab proteins.

1. TPD54 is associated with recycling endosomes

We used the knocksideways method to assess where in the trafficking pathway TPD54 was involved. We found that it was only associated to the recycling pathway, by rerouting Rab4, Rab11a and Rab25.
An electron microscopy analysis revealed that we reroute the whole recycling vesicles, suggesting that TPD54 is tightly bound to the recycling endosomes.

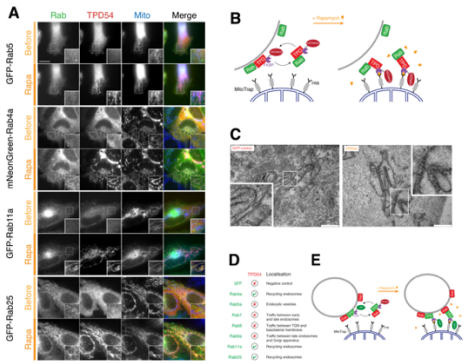

Figure 1: Rab4, Rab11 and Rab25 are rerouted to the mitochondria, along with the whole recycling vesicle, when mCherry-FKBP-TPD54 is knocked sideways. **A)** Example immunofluorescence results showing that Rab4, Rab11, Rab25 but not Rab5 are rerouted to the mitochondria, only after addition of rapamycin. Scale bar: 10 μm. **B)** Schematic of the rerouting experiment. Different Rab proteins are on specific types of vesicles, the mitochondria are labeled with a MitoTrap containing an FRB domain, and mCherry-FKBP-TPD54 is expressed in cells. Upon addition of rapamycin, the mitochondrial FRB domain and the FKBP domain will dimerise and reroute TPD54, with everything binding to it to the mitochondria. **C)** Iectron microscopy (EM) images showing that when GFP-FKBP is rerouted to the mitochondria, no vesicle is brought with the protein. When TPD54-GFP-FKBP is rerouted, so are vesicles. Scale bars: 500 nm. **D)** Only Rab4, Rab25 and Rab11 in the Rab proteins tested are associated with TPD54. **E)** Schematic representation of what is really happening by rerouting TPD54 to the mitochondria.

2. TPD54 KD reduces Tf recycling

Transferrin (Tf) is recycled through both Rab4 and Rab11 pathways. We show that TPD54 is involved in this with an uptake and recycling assay in KD cells. Preliminary data (not shown) suggest the same delay for α5β1 recycling.

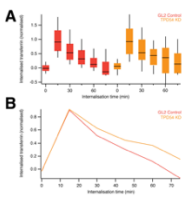

Figure 2: A TPD54 KD doesn't slow down internalisation of Tf in HeLa cells, but impairs its recycling. **A)** Boxplots showing the normalised amount of transferrin (mean pixel intensity) in GL2 control or TPD54 KD HeLa cells. Three independant repeats. Time points after incubation with Alexa-488-Tf. **B)** Median of Tf internalisation (normalised) for both GL2 control and TPD54 KD cells.

3. TPD54 KD affects RPE1 cell migration

TPD54 and integrin α5 travel on the same vesicles suggesting a possible role for TPD54 in integrin α5 recycling.

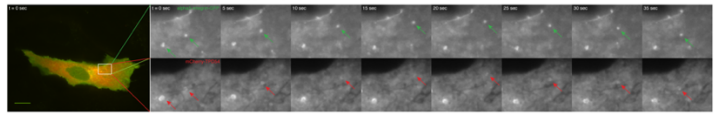

Figure 3: TPD54 coats the integrin α5-positive vesicles. **A)** RPE1 cells expressing mCherry-TPD54 and integrin α5-GFP and were imaged by light microscopy, 5 seconds per frame. mCherry-TPD54 (lower pannel, red arrow) is localised to vesicles on the membrane (the vesicles looks hollow) and integrin α5-GFP (upper pannel, green arrow) is localised in these vesicles. Scale bar: 10 μm.

We have measured the involvement of TPD54 in RPE1 cell migration by tracking them after knocking down the protein.

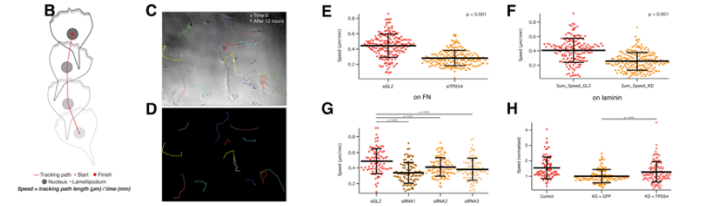

Figure 3 (continued): TPD54 coats the integrin α5-positive vesicles and is needed for RPE1 cells migration. **B)** Schematic representation showing how the tracking is done. **C)** Cells in each conditions are followed throughout the 12 h movie. **D)** From the tracks, we get information on cells coordonates and speed, from which we get data on migration such as speed and directionality. **E)** A KD of TPD54 causes a reduction of almost 50% in migration speed when migrating on fibronectin (FN). Mean and standard deviation. **F)** The migration speed is also slower in TPD54 KD cells when migrating on laminin. **G)** The migration phenotype is not siRNA depedant. **H)** The migration defect can be rescued by the transient expression of TPD54 in pIRES-EGFP vector.

4. TPD54 affects invasion

In Rab25-overexpressing cells, TPD54 colocalises with Rab25 on the leading edge of cells migrating on cell-derived-matrix.
We show that TPD54 is required for efficient invasion in collagen.

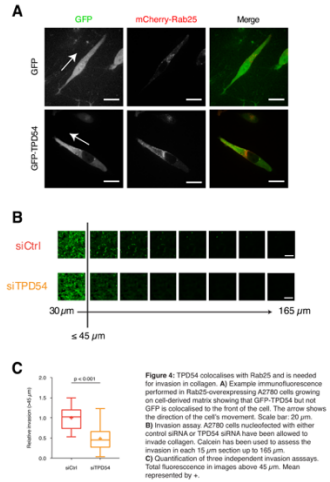

Figure 4: TPD54 colocalises with Rab25 and is needed for invasion in collagen. **A)** Example immunofluorescence performed in Rab25-overexpressing A2780 cells growing on cell-derived matrix showing that GFP-TPD54 but not GFP is colocalised to the front of the cell. The arrow shows the direction of the cell's movement. Scale bar: 20 μm. **B)** Invasion assay. A2780 cells nucleofected with either control siRNA or TPD54 siRNA have been allowed to invade collagen. Calcein has been used to assess the invasion in each 15 μm section up to 165 μm. **C)** Quantification of three independent invasion assays. Total fluorescence in images above 45 μm. Mean represented by +.

5. TPD54 KD does not phenocopy Rab4 or Rab11 KD

We compared the speed and the shape of TPD54 KD to Rab11 or Rab4 KD cells to see if the phenotype would be comparable, indicating a redudant role.
We also did Rab/TPD54 dKD to see if we would get a more severe phenotype, indicating that the two proteins are likely to be on different pathways.

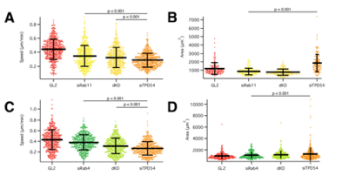

Figure 5: Rab4 or Rab11 KD RPE1 cells do not have the same phenotype as TPD54 KD cells. **A, C)** RPE1 cells were tracked during 12 hours on FN coated-dishes. The TPD54 KD cells were migrating significantly slower than the Rab11 KD (A), Rab4 KD (C) or dKD. Mean and standard deviation. **B, D)** The area of the cells was measured on the same timepoint of the migration movies for every cell. The TPD54 KD cells are significatly bigger than Rab11 KD (B), Rab4 KD (D) cells or dKD cells.

Conclusions

- TPD54 is closely involved with recycling endosomes and is important for an efficient recycling of membrane-bound proteins, like the transferrin receptor or the integrins. We still don't know the exact role of TPD54, but our data strongly suggest that it is on both the fast and the slow recycling pathway.

- The trafficking of the integrins by TPD54 makes the latter a crucial player in the cell migration pathway, given the dramatic reduction in migration speed in TPD54 KD cells. This phenotype is not tying TPD54 to only one ECM component because it is seen with both FN (generally used by motile cells) or laminin (generally used by more static cells) (9).

- Its role in migration isn't restricted in 2D migration; TPD54 is also essential for invasion in cells mimicking tumor cells, making TPD54 a potential target for cancer research.

(1)Kaur, S. et al. 2014, Elife. 3. (2)Messenger, S.W. et al. 2013, American Journal of Physiology-Gastrointestinal and Liver Physiology. 305:G439-G452. (3)Proux-Gillardeaux, V. et al. 2003, Biochemical Journal. 370:213-221. (4)Groblewski, G.E. et al. 1999, American Journal of Physiology- Gastrointestinal and Liver Physiology. 276:G219-G226. (5)Mukudai, Y. et al. 2013 Cellular Oncology. 36:233-245. (6)Caswell, P. et al. 2009, Nature reviews Molecular Cell Biology 10:843-853. (7)Paul, N.R. et al. 2015 Current Biology 25:R1092-R1105. (8)Caswell, P. et al. 2007 Developmental Cell 13: 496–510. (9)Rainero and Norman. 2013. Bioessays 35: 523-532.

Fonds de recherche Nature et technologies Québec
BSCB British Society for Cell Biology
WARWICK

Appendix 2

Table A1: Mass spectrometry analysis results

Protein name	Short name	p value	TPD54/ GFP ratio
Tumor protein D54 OS=Homo sapiens GN=TPD52L2 PE=1 SV=2 - [TPD54_HUMAN]	TPD54	0.002350471	82.49002394
Tumor protein D52 OS=Homo sapiens GN=TPD52 PE=1 SV=2 - [TPD52_HUMAN]	TPD52	0.03936578	49.67704121
Glycogen debranching enzyme OS=Homo sapiens GN=AGL PE=1 SV=3 - [GDE_HUMAN]	GDE	1.10E-07	4.175101322
Tumor protein D53 OS=Homo sapiens GN=TPD52L1 PE=1 SV=1 - [TPD53_HUMAN]	TPD53	0.003949604	9.464534208
Ras-related protein Rab-14 OS=Homo sapiens GN=RAB14 PE=1 SV=4 - [RAB14_HUMAN]	RAB14	0.000511816	6.601834833
Long-chain-fatty-acid--CoA ligase 3 OS=Homo sapiens GN=ACSL3 PE=1 SV=3 - [ACSL3_HUMAN]	ACSL3	0.005496156	7.753670482
Ras-related protein Rab-2A OS=Homo sapiens GN=RAB2A PE=1 SV=1 - [RAB2A_HUMAN]	RAB2A	0.044824451	8.724958424
Guanine nucleotide-binding protein G(I)/G(S)/G(T) subunit beta-1 OS=Homo sapiens GN=GNB1 PE=1 SV=3 - [GBB1_HUMAN]	GBB1	0.011194352	4.421704646
Bifunctional glutamate/proline--tRNA ligase OS=Homo sapiens GN=EPRS PE=1 SV=5 - [SYEP_HUMAN]	SYEP	0.007917716	3.114887967
Ras-related protein Rab-5C OS=Homo sapiens GN=RAB5C PE=1 SV=2 - [RAB5C_HUMAN]	RAB5C	0.019812876	3.370600309
Alkaline phosphatase, tissue-nonspecific isozyme OS=Homo sapiens GN=ALPL PE=1 SV=4 - [PPBT_HUMAN]	PPBT	0.002567993	2.182413263
40S ribosomal protein S4, X isoform OS=Homo sapiens GN=RPS4X PE=1 SV=2 - [RS4X_HUMAN]	RS4X	0.033696804	3.784292736
Ras GTPase-activating protein-binding protein 1 OS=Homo sapiens GN=G3BP1 PE=1 SV=1 - [G3BP1_HUMAN]	G3BP1	0.025438899	3.422136539
Desmoglein-2 OS=Homo sapiens GN=DSG2 PE=1 SV=2 - [DSG2_HUMAN]	DSG2	0.015102814	2.842562495
Histone H4 OS=Homo sapiens GN=HIST1H4A PE=1 SV=2 - [H4_HUMAN]	H4	0.012471654	2.464547853
Prohibitin-2 OS=Homo sapiens GN=PHB2 PE=1 SV=2 - [PHB2_HUMAN]	PHB2	0.033682968	3.03687628
Ras-related protein Rab-7a OS=Homo sapiens GN=RAB7A PE=1 SV=1 - [RAB7A_HUMAN]	RAB7A	0.013321094	2.362921029
40S ribosomal protein S10 OS=Homo sapiens GN=RPS10 PE=1 SV=1 - [RS10_HUMAN]	RS10	0.021373905	2.621979968
Heterogeneous nuclear ribonucleoprotein H OS=Homo sapiens GN=HNRNPH1 PE=1 SV=4 - [HNRH1_HUMAN]	HNRH1	0.016850408	2.445434717
Membrane-associated progesterone receptor component 2 OS=Homo sapiens GN=PGRMC2 PE=1 SV=1 - [PGRC2_HUMAN]	PGRC2	0.03096462	2.762257982
Polyadenylate-binding protein 1 OS=Homo sapiens GN=PABPC1 PE=1 SV=2 - [PABP1_HUMAN]	PABP1	0.004484757	1.565630998
26S proteasome non-ATPase regulatory subunit 11 OS=Homo sapiens GN=PSMD11 PE=1 SV=3 - [PSD11_HUMAN]	PSD11	0.020622572	1.748408023
14-3-3 protein epsilon OS=Homo sapiens GN=YWHAE PE=1 SV=1 - [1433E_HUMAN]	1433E	0.027397923	1.825632693
Neutral amino acid transporter B(0) OS=Homo sapiens GN=SLC1A5 PE=1 SV=2 - [AAAT_HUMAN]	AAAT	0.026642947	1.779173127
40S ribosomal protein S14 OS=Homo sapiens GN=RPS14 PE=1 SV=3 - [RS14_HUMAN]	RS14	0.043950245	1.847696312
Heat shock protein beta-1 OS=Homo sapiens GN=HSPB1 PE=1 SV=2 - [HSPB1_HUMAN]	HSPB1	0.028732263	1.571890908
Transitional endoplasmic reticulum ATPase OS=Homo sapiens GN=VCP PE=1 SV=4 - [TERA_HUMAN]	TERA	0.02772511	1.442864052
Plectin OS=Homo sapiens GN=PLEC PE=1 SV=3 - [PLEC_HUMAN]	PLEC	0.25946775	26.15472778
HLA class I histocompatibility antigen, B-8 alpha chain OS=Homo sapiens GN=HLA-B PE=1 SV=1 - [1B08_HUMAN]	1B08	0.1141289	12.07010258
Nuclease-sensitive element-binding protein 1 OS=Homo sapiens GN=YBX1 PE=1 SV=3 - [YBOX1_HUMAN]	YBOX1	0.055954635	8.417912
Poly [ADP-ribose] polymerase 1 OS=Homo sapiens GN=PARP1 PE=1 SV=4 - [PARP1_HUMAN]	PARP1	0.065113306	5.984487576
Filamin-B OS=Homo sapiens GN=FLNB PE=1 SV=2 - [FLNB_HUMAN]	FLNB	0.1021385	6.113356402
Brain acid soluble protein 1 OS=Homo sapiens GN=BASP1 PE=1 SV=2 - [BASP1_HUMAN]	BASP1	0.1672032	7.311548721
Transferrin receptor protein 1 OS=Homo sapiens GN=TFRC PE=1 SV=2 - [TFR1_HUMAN]	TFR1	0.061318159	3.700931791
Cytoplasmic dynein 1 heavy chain 1 OS=Homo sapiens GN=DYNC1H1 PE=1 SV=5 - [DYHC1_HUMAN]	DYHC1	0.17659879	5.795802399
DNA-dependent protein kinase catalytic subunit OS=Homo sapiens GN=PRKDC PE=1 SV=3 - [PRKDC_HUMAN]	PRKDC	0.088848867	4.073574297
Polypeptide N-acetylgalactosaminyltransferase 2 OS=Homo sapiens GN=GALNT2 PE=1 SV=1 - [GALT2_HUMAN]	GALT2	0.078431308	3.74449666
Keratin, type I cytoskeletal 13 OS=Homo sapiens GN=KRT13 PE=1 SV=4 - [K1C13_HUMAN]	K1C13	0.16956718	4.862172906

Histone H2A.Z OS=Homo sapiens GN=H2AFZ PE=1 SV=2 - [H2AZ_HUMAN]	H2AZ	0.19541398	5.187887248
Keratin, type I cytoskeletal 19 OS=Homo sapiens GN=KRT19 PE=1 SV=4 - [K1C19_HUMAN]	K1C19	0.24062382	5.845583475
Poly [ADP-ribose] polymerase 14 OS=Homo sapiens GN=PARP14 PE=1 SV=3 - [PAR14_HUMAN]	PAR14	0.19686858	5.09784888
Aspartyl/asparaginyl beta-hydroxylase OS=Homo sapiens GN=ASPH PE=1 SV=3 - [ASPH_HUMAN]	ASPH	0.18400952	4.691269854
Insulin-like growth factor 2 mRNA-binding protein 3 OS=Homo sapiens GN=IGF2BP3 PE=1 SV=2 - [IF2B3_HUMAN]	IF2B3	0.065951131	2.913660181
Polyadenylate-binding protein 4 OS=Homo sapiens GN=PABPC4 PE=1 SV=1 - [PABP4_HUMAN]	PABP4	0.19341166	4.750573774
Splicing factor, proline- and glutamine-rich OS=Homo sapiens GN=SFPQ PE=1 SV=2 - [SFPQ_HUMAN]	SFPQ	0.18264732	4.545313618
Voltage-dependent anion-selective channel protein 1 OS=Homo sapiens GN=VDAC1 PE=1 SV=2 - [VDAC1_HUMAN]	VDAC1	0.1636197	4.170168331
Myoferlin OS=Homo sapiens GN=MYOF PE=1 SV=1 - [MYOF_HUMAN]	MYOF	0.14887498	3.910550303
40S ribosomal protein S8 OS=Homo sapiens GN=RPS8 PE=1 SV=2 - [RS8_HUMAN]	RS8	0.076813474	2.888301234
Tubulin beta-6 chain OS=Homo sapiens GN=TUBB6 PE=1 SV=1 - [TBB6_HUMAN]	TBB6	0.19394292	4.346081482
Vesicular integral-membrane protein VIP36 OS=Homo sapiens GN=LMAN2 PE=1 SV=1 - [LMAN2_HUMAN]	LMAN2	0.069520503	2.574099676
Integrin beta-1 OS=Homo sapiens GN=ITGB1 PE=1 SV=2 - [ITB1_HUMAN]	ITB1	0.081756085	2.704716845
40S ribosomal protein S3a OS=Homo sapiens GN=RPS3A PE=1 SV=2 - [RS3A_HUMAN]	RS3A	0.079504572	2.599902303
HLA class I histocompatibility antigen, A-69 alpha chain OS=Homo sapiens GN=HLA-A PE=1 SV=2 - [1A69_HUMAN]	1A69	0.39696652	7.104442458
Signal recognition particle receptor subunit beta OS=Homo sapiens GN=SRPRB PE=1 SV=3 - [SRPRB_HUMAN]	SRPRB	0.088498011	2.620210258
60S ribosomal protein L23 OS=Homo sapiens GN=RPL23 PE=1 SV=1 - [RL23_HUMAN]	RL23	0.093564942	2.598104484
ATP synthase subunit O, mitochondrial OS=Homo sapiens GN=ATP5O PE=1 SV=1 - [ATPO_HUMAN]	ATPO	0.065734923	2.261096805
Erythrocyte band 7 integral membrane protein OS=Homo sapiens GN=STOM PE=1 SV=3 - [STOM_HUMAN]	STOM	0.11031449	2.749562864
60S ribosomal protein L18a OS=Homo sapiens GN=RPL18A PE=1 SV=2 - [RL18A_HUMAN]	RL18A	0.054852035	2.076347087
Keratin, type II cytoskeletal 8 OS=Homo sapiens GN=KRT8 PE=1 SV=7 - [K2C8_HUMAN]	K2C8	0.11560359	2.780149752
Histone H2A type 1-B/E OS=Homo sapiens GN=HIST1H2AB PE=1 SV=2 - [H2A1B_HUMAN]	H2A1B	0.38810951	6.102757506
HLA class I histocompatibility antigen, B-55 alpha chain OS=Homo sapiens GN=HLA-B PE=1 SV=1 - [1B55_HUMAN]	1B55	0.18853654	3.428412236
Talin-1 OS=Homo sapiens GN=TLN1 PE=1 SV=3 - [TLN1_HUMAN]	TLN1	0.14981109	3.008666782
Cation-independent mannose-6-phosphate receptor OS=Homo sapiens GN=IGF2R PE=1 SV=3 - [MPRI_HUMAN]	MPRI	0.14658721	2.947713797
Extended synaptotagmin-1 OS=Homo sapiens GN=ESYT1 PE=1 SV=1 - [ESYT1_HUMAN]	ESYT1	0.16446556	3.118307174
Poly [ADP-ribose] polymerase 2 OS=Homo sapiens GN=PARP2 PE=1 SV=2 - [PARP2_HUMAN]	PARP2	0.22163862	3.713459686
DNA ligase 3 OS=Homo sapiens GN=LIG3 PE=1 SV=2 - [DNLI3_HUMAN]	DNLI3	0.2448398	3.953697071
Transketolase OS=Homo sapiens GN=TKT PE=1 SV=3 - [TKT_HUMAN]	TKT	0.10105	2.424671102
Beta-1,4-galactosyltransferase 1 OS=Homo sapiens GN=B4GALT1 PE=1 SV=5 - [B4GT1_HUMAN]	B4GT1	0.16246757	3.046235093
Guanine nucleotide-binding protein G(i) subunit alpha-2 OS=Homo sapiens GN=GNAI2 PE=1 SV=3 - [GNAI2_HUMAN]	GNAI2	0.12959205	2.690956841
Tubulin alpha-1A chain OS=Homo sapiens GN=TUBA1A PE=1 SV=1 - [TBA1A_HUMAN]	TBA1A	0.38980216	5.816118547
Dolichyl-diphosphooligosaccharide--protein glycosyltransferase subunit 2 OS=Homo sapiens GN=RPN2 PE=1 SV=3 - [RPN2_HUMAN]	RPN2	0.099675447	2.365084759
Unconventional myosin-Ic OS=Homo sapiens GN=MYO1C PE=1 SV=4 - [MYO1C_HUMAN]	MYO1C	0.23421551	3.695207881
Procollagen-lysine,2-oxoglutarate 5-dioxygenase 1 OS=Homo sapiens GN=PLOD1 PE=1 SV=2 - [PLOD1_HUMAN]	PLOD1	0.13697949	2.593530586
Heat shock protein 105 kDa OS=Homo sapiens GN=HSPH1 PE=1 SV=1 - [HS105_HUMAN]	HS105	0.094613709	2.182140626
Nuclear pore complex protein Nup155 OS=Homo sapiens GN=NUP155 PE=1 SV=1 - [NU155_HUMAN]	NU155	0.18787965	2.996575556
RNA-binding protein 14 OS=Homo sapiens GN=RBM14 PE=1 SV=2 - [RBM14_HUMAN]	RBM14	0.23427267	3.403994285
Multifunctional protein ADE2 OS=Homo sapiens GN=PAICS PE=1 SV=3 - [PUR6_HUMAN]	PUR6	0.12459617	2.371814301
60S ribosomal protein L7 OS=Homo sapiens GN=RPL7 PE=1 SV=1 - [RL7_HUMAN]	RL7	0.097506054	2.092342723
DNA ligase 4 OS=Homo sapiens GN=LIG4 PE=1 SV=2 - [DNLI4_HUMAN]	DNLI4	0.1836274	2.842935502
Leucine-rich PPR motif-containing protein, mitochondrial OS=Homo sapiens GN=LRPPRC PE=1 SV=3 - [LPPRC_HUMAN]	LPPRC	0.19923094	2.961814125
Moesin OS=Homo sapiens GN=MSN PE=1 SV=3 - [MOES_HUMAN]	MOES	0.10847267	2.12636027
Ataxin-10 OS=Homo sapiens GN=ATXN10 PE=1 SV=1 - [ATX10_HUMAN]	ATX10	0.18887103	2.825951291
Vimentin OS=Homo sapiens GN=VIM PE=1 SV=4 - [VIME_HUMAN]	VIME	0.14055224	2.397165897
ADP/ATP translocase 2 OS=Homo sapiens GN=SLC25A5 PE=1 SV=7 - [ADT2_HUMAN]	ADT2	0.18112044	2.639372542
Cytoplasmic dynein 1 intermediate chain 2 OS=Homo sapiens GN=DYNC1I2 PE=1 SV=3 - [DC1I2_HUMAN]	DC1I2	0.14469066	2.331908482
40S ribosomal protein S18 OS=Homo sapiens GN=RPS18 PE=1 SV=3 - [RS18_HUMAN]	RS18	0.11440125	2.073138127

Eukaryotic translation initiation factor 3 subunit L OS=Homo sapiens GN=EIF3L PE=1 SV=1 - [EIF3L_HUMAN]	EIF3L	0.15977046	2.450446989
Lamina-associated polypeptide 2, isoform alpha OS=Homo sapiens GN=TMPO PE=1 SV=2 - [LAP2A_HUMAN]	LAP2A	0.12638932	2.129748925
Dolichol-phosphate mannosyltransferase subunit 1 OS=Homo sapiens GN=DPM1 PE=1 SV=1 - [DPM1_HUMAN]	DPM1	0.17913562	2.561190657
X-ray repair cross-complementing protein 6 OS=Homo sapiens GN=XRCC6 PE=1 SV=2 - [XRCC6_HUMAN]	XRCC6	0.1739604	2.512990984
Putative ATP-dependent RNA helicase DHX30 OS=Homo sapiens GN=DHX30 PE=1 SV=1 - [DHX30_HUMAN]	DHX30	0.18428223	2.564897797
Tubulin alpha-1B chain OS=Homo sapiens GN=TUBA1B PE=1 SV=1 - [TBA1B_HUMAN]	TBA1B	0.17285772	2.440874413
Histone H2A type 2-C OS=Homo sapiens GN=HIST2H2AC PE=1 SV=4 - [H2A2C_HUMAN]	H2A2C	0.40735894	4.75792145
NADH-cytochrome b5 reductase 3 OS=Homo sapiens GN=CYB5R3 PE=1 SV=3 - [NB5R3_HUMAN]	NB5R3	0.14771023	2.187484757
Galectin-7 OS=Homo sapiens GN=LGALS7 PE=1 SV=2 - [LEG7_HUMAN]	LEG7	0.15789968	2.250087713
Voltage-dependent anion-selective channel protein 2 OS=Homo sapiens GN=VDAC2 PE=1 SV=2 - [VDAC2_HUMAN]	VDAC2	0.15515476	2.228568125
Non-homologous end-joining factor 1 OS=Homo sapiens GN=NHEJ1 PE=1 SV=1 - [NHEJ1_HUMAN]	NHEJ1	0.15742458	2.240318416
Cyclic GMP-AMP synthase OS=Homo sapiens GN=MB21D1 PE=1 SV=2 - [CGAS_HUMAN]	CGAS	0.25774878	3.046655095
Histone H2B type 1-K OS=Homo sapiens GN=HIST1H2BK PE=1 SV=3 - [H2B1K_HUMAN]	H2B1K	0.17434146	2.355720948
DNA repair protein XRCC4 OS=Homo sapiens GN=XRCC4 PE=1 SV=2 - [XRCC4_HUMAN]	XRCC4	0.21448527	2.656043451
Ras-related protein Rab-11B OS=Homo sapiens GN=RAB11B PE=1 SV=4 - [RB11B_HUMAN]	RB11B	0.21321292	2.633028109
Succinate dehydrogenase [ubiquinone] flavoprotein subunit, mitochondrial OS=Homo sapiens GN=SDHA PE=1 SV=2 - [SDHA_HUMAN]	SDHA	0.23869087	2.811142785
Eukaryotic initiation factor 4A-I OS=Homo sapiens GN=EIF4A1 PE=1 SV=1 - [IF4A1_HUMAN]	IF4A1	0.15247563	2.132269393
Probable ATP-dependent RNA helicase DDX5 OS=Homo sapiens GN=DDX5 PE=1 SV=1 - [DDX5_HUMAN]	DDX5	0.20728475	2.543949504
Ras-related protein Rab-32 OS=Homo sapiens GN=RAB32 PE=1 SV=3 - [RAB32_HUMAN]	RAB32	0.14919734	2.099028566
Staphylococcal nuclease domain-containing protein 1 OS=Homo sapiens GN=SND1 PE=1 SV=1 - [SND1_HUMAN]	SND1	0.18414062	2.356845868
60S ribosomal protein L7a OS=Homo sapiens GN=RPL7A PE=1 SV=2 - [RL7A_HUMAN]	RL7A	0.14125836	2.018134212
FACT complex subunit SSRP1 OS=Homo sapiens GN=SSRP1 PE=1 SV=1 - [SSRP1_HUMAN]	SSRP1	0.19616824	2.37960321
Septin-2 OS=Homo sapiens GN=SEPT2 PE=1 SV=1 - [SEPT2_HUMAN]	Sep-02	0.23852962	2.672729043
Fragile X mental retardation syndrome-related protein 2 OS=Homo sapiens GN=FXR2 PE=1 SV=2 - [FXR2_HUMAN]	FXR2	0.19217999	2.281476306
Keratin, type II cytoskeletal 7 OS=Homo sapiens GN=KRT7 PE=1 SV=5 - [K2C7_HUMAN]	K2C7	0.22421588	2.508872318
Structural maintenance of chromosomes protein 4 OS=Homo sapiens GN=SMC4 PE=1 SV=2 - [SMC4_HUMAN]	SMC4	0.22913145	2.50425846
Ras-related protein Rab-1B OS=Homo sapiens GN=RAB1B PE=1 SV=1 - [RAB1B_HUMAN]	RAB1B	0.17044061	2.083286134
Replication protein A 70 kDa DNA-binding subunit OS=Homo sapiens GN=RPA1 PE=1 SV=2 - [RFA1_HUMAN]	RFA1	0.23760839	2.528431096
Zinc finger CCCH-type antiviral protein 1 OS=Homo sapiens GN=ZC3HAV1 PE=1 SV=3 - [ZCCHV_HUMAN]	ZCCHV	0.18461563	2.149109899
Matrin-3 OS=Homo sapiens GN=MATR3 PE=1 SV=2 - [MATR3_HUMAN]	MATR3	0.17046715	2.036676007
Polypyrimidine tract-binding protein 1 OS=Homo sapiens GN=PTBP1 PE=1 SV=1 - [PTBP1_HUMAN]	PTBP1	0.21080521	2.308123727
Bifunctional polynucleotide phosphatase/kinase OS=Homo sapiens GN=PNKP PE=1 SV=1 - [PNKP_HUMAN]	PNKP	0.19775239	2.195299565
LEM domain-containing protein 2 OS=Homo sapiens GN=LEMD2 PE=1 SV=1 - [LEMD2_HUMAN]	LEMD2	0.22239576	2.342138884
FACT complex subunit SPT16 OS=Homo sapiens GN=SUPT16H PE=1 SV=1 - [SP16H_HUMAN]	SP16H	0.24544333	2.471438605
CD44 antigen OS=Homo sapiens GN=CD44 PE=1 SV=3 - [CD44_HUMAN]	CD44	0.23098099	2.358525366
Poly [ADP-ribose] polymerase 9 OS=Homo sapiens GN=PARP9 PE=1 SV=2 - [PARP9_HUMAN]	PARP9	0.29851848	2.850214236
40S ribosomal protein S16 OS=Homo sapiens GN=RPS16 PE=1 SV=2 - [RS16_HUMAN]	RS16	0.25497058	2.50122375
Regulator of nonsense transcripts 1 OS=Homo sapiens GN=UPF1 PE=1 SV=2 - [RENT1_HUMAN]	RENT1	0.22090638	2.23517389
Keratin, type II cytoskeletal 3 OS=Homo sapiens GN=KRT3 PE=1 SV=3 - [K2C3_HUMAN]	K2C3	0.39299169	3.576980673
Transforming protein RhoA OS=Homo sapiens GN=RHOA PE=1 SV=1 - [RHOA_HUMAN]	RHOA	0.19688652	2.054880024
Non-POU domain-containing octamer-binding protein OS=Homo sapiens GN=NONO PE=1 SV=4 - [NONO_HUMAN]	NONO	0.21491581	2.169691626
Transcription intermediary factor 1-beta OS=Homo sapiens GN=TRIM28 PE=1 SV=5 - [TIF1B_HUMAN]	TIF1B	0.2312476	2.215016554
Inositol 1,4,5-trisphosphate receptor type 1 OS=Homo sapiens GN=ITPR1 PE=1 SV=3 - [ITPR1_HUMAN]	ITPR1	0.25832596	2.379215809
Importin-5 OS=Homo sapiens GN=IPO5 PE=1 SV=4 - [IPO5_HUMAN]	IPO5	0.28307927	2.461291276
Fragile X mental retardation syndrome-related protein 1 OS=Homo sapiens GN=FXR1 PE=1 SV=3 - [FXR1_HUMAN]	FXR1	0.23490599	2.11544379
SUN domain-containing protein 2 OS=Homo sapiens GN=SUN2 PE=1 SV=3 - [SUN2_HUMAN]	SUN2	0.26255742	2.274192396

E3 ubiquitin-protein ligase DTX3L OS=Homo sapiens GN=DTX3L PE=1 SV=1 - [DTX3L_HUMAN]	DTX3L	0.343575	2.833296889
Insulin-like growth factor 2 mRNA-binding protein 1 OS=Homo sapiens GN=IGF2BP1 PE=1 SV=2 - [IF2B1_HUMAN]	IF2B1	0.27352715	2.334237642
CAD protein OS=Homo sapiens GN=CAD PE=1 SV=3 - [PYR1_HUMAN]	PYR1	0.27306288	2.308519343
ATP-dependent RNA helicase DDX3X OS=Homo sapiens GN=DDX3X PE=1 SV=3 - [DDX3X_HUMAN]	DDX3X	0.2303322	2.007139056
Plastin-3 OS=Homo sapiens GN=PLS3 PE=1 SV=4 - [PLST_HUMAN]	PLST	0.28083777	2.297387851
CD109 antigen OS=Homo sapiens GN=CD109 PE=1 SV=2 - [CD109_HUMAN]	CD109	0.28111032	2.27685956
Eukaryotic translation initiation factor 3 subunit A OS=Homo sapiens GN=EIF3A PE=1 SV=1 - [EIF3A_HUMAN]	EIF3A	0.25509477	2.095531252
Histone H2A type 1-A OS=Homo sapiens GN=HIST1H2AA PE=1 SV=3 - [H2A1A_HUMAN]	H2A1A	0.37517393	2.83189971
Ubiquitin-like modifier-activating enzyme 1 OS=Homo sapiens GN=UBA1 PE=1 SV=3 - [UBA1_HUMAN]	UBA1	0.29258391	2.233742672
Spectrin beta chain, non-erythrocytic 1 OS=Homo sapiens GN=SPTBN1 PE=1 SV=2 - [SPTB2_HUMAN]	SPTB2	0.2727395	2.076621429
Histone H3.3C OS=Homo sapiens GN=H3F3C PE=1 SV=3 - [H3C_HUMAN]	H3C	0.27662194	2.096388775
26S proteasome non-ATPase regulatory subunit 2 OS=Homo sapiens GN=PSMD2 PE=1 SV=3 - [PSMD2_HUMAN]	PSMD2	0.29461092	2.131733619
40S ribosomal protein S3 OS=Homo sapiens GN=RPS3 PE=1 SV=2 - [RS3_HUMAN]	RS3	0.27514946	2.009751261
Keratin, type II cytoskeletal 80 OS=Homo sapiens GN=KRT80 PE=1 SV=2 - [K2C80_HUMAN]	K2C80	0.34663033	2.428337804
Serine-threonine kinase receptor-associated protein OS=Homo sapiens GN=STRAP PE=1 SV=1 - [STRAP_HUMAN]	STRAP	0.34889659	2.358988219
Arginine--tRNA ligase, cytoplasmic OS=Homo sapiens GN=RARS PE=1 SV=2 - [SYRC_HUMAN]	SYRC	0.38483357	2.557301634
3-hydroxyacyl-CoA dehydrogenase type-2 OS=Homo sapiens GN=HSD17B10 PE=1 SV=3 - [HCD2_HUMAN]	HCD2	0.32928371	2.183735519
Ras-related protein Rab-1A OS=Homo sapiens GN=RAB1A PE=1 SV=3 - [RAB1A_HUMAN]	RAB1A	0.36459032	2.395851961
Keratin, type II cytoskeletal 78 OS=Homo sapiens GN=KRT78 PE=2 SV=2 - [K2C78_HUMAN]	K2C78	0.36150655	2.254085907
Neuroblast differentiation-associated protein AHNAK OS=Homo sapiens GN=AHNAK PE=1 SV=2 - [AHNK_HUMAN]	AHNK	0.33166608	2.004544168
Keratin, type II cuticular Hb4 OS=Homo sapiens GN=KRT84 PE=2 SV=2 - [KRT84_HUMAN]	KRT84	0.40118995	2.380367531
Histone H2AX OS=Homo sapiens GN=H2AFX PE=1 SV=2 - [H2AX_HUMAN]	H2AX	0.37145334	2.124654816
Epiplakin OS=Homo sapiens GN=EPPK1 PE=1 SV=2 - [EPIPL_HUMAN]	EPIPL	0.38591927	2.197977371
Stomatin-like protein 2, mitochondrial OS=Homo sapiens GN=STOML2 PE=1 SV=1 - [STML2_HUMAN]	STML2	0.053044844	1.838392168
Ras-related protein Rab-6A OS=Homo sapiens GN=RAB6A PE=1 SV=3 - [RAB6A_HUMAN]	RAB6A	0.073765449	1.974714497
Neutral alpha-glucosidase AB OS=Homo sapiens GN=GANAB PE=1 SV=3 - [GANAB_HUMAN]	GANAB	0.082215674	1.842723471
Dolichyl-diphosphooligosaccharide--protein glycosyltransferase subunit 1 OS=Homo sapiens GN=RPN1 PE=1 SV=1 - [RPN1_HUMAN]	RPN1	0.099239729	1.987508464
RuvB-like 1 OS=Homo sapiens GN=RUVBL1 PE=1 SV=1 - [RUVB1_HUMAN]	RUVB1	0.11231224	1.952132695
Stress-70 protein, mitochondrial OS=Homo sapiens GN=HSPA9 PE=1 SV=2 - [GRP75_HUMAN]	GRP75	0.052581601	1.422412593
Cell surface glycoprotein MUC18 OS=Homo sapiens GN=MCAM PE=1 SV=2 - [MUC18_HUMAN]	MUC18	0.10686149	1.812943876
Ras-related protein Rap-1b-like protein OS=Homo sapiens PE=2 SV=1 - [RP1BL_HUMAN]	RP1BL	0.13050595	1.922200217
Extended synaptotagmin-2 OS=Homo sapiens GN=ESYT2 PE=1 SV=1 - [ESYT2_HUMAN]	ESYT2	0.11522271	1.776066235
40S ribosomal protein S5 OS=Homo sapiens GN=RPS5 PE=1 SV=4 - [RS5_HUMAN]	RS5	0.10152532	1.674739046
Glycogen [starch] synthase, muscle OS=Homo sapiens GN=GYS1 PE=1 SV=2 - [GYS1_HUMAN]	GYS1	0.13271855	1.855076489
La-related protein 1 OS=Homo sapiens GN=LARP1 PE=1 SV=2 - [LARP1_HUMAN]	LARP1	0.16587155	1.978397737
Sodium/potassium-transporting ATPase subunit alpha-1 OS=Homo sapiens GN=ATP1A1 PE=1 SV=1 - [AT1A1_HUMAN]	AT1A1	0.14374468	1.812926835
Heterogeneous nuclear ribonucleoproteins C1/C2 OS=Homo sapiens GN=HNRNPC PE=1 SV=4 - [HNRPC_HUMAN]	HNRPC	0.1107426	1.57807841
Protein DEK OS=Homo sapiens GN=DEK PE=1 SV=1 - [DEK_HUMAN]	DEK	0.16860195	1.940549549
ATP-dependent RNA helicase DDX1 OS=Homo sapiens GN=DDX1 PE=1 SV=2 - [DDX1_HUMAN]	DDX1	0.15908252	1.872398064
60S ribosomal protein L13a OS=Homo sapiens GN=RPL13A PE=1 SV=2 - [RL13A_HUMAN]	RL13A	0.12017693	1.595400989
Calnexin OS=Homo sapiens GN=CANX PE=1 SV=2 - [CALX_HUMAN]	CALX	0.16337121	1.864612646
Nuclear fragile X mental retardation-interacting protein 2 OS=Homo sapiens GN=NUFIP2 PE=1 SV=1 - [NUFP2_HUMAN]	NUFP2	0.17211224	1.905697736
Interleukin enhancer-binding factor 2 OS=Homo sapiens GN=ILF2 PE=1 SV=2 - [ILF2_HUMAN]	ILF2	0.098022483	1.433488513
Heat shock cognate 71 kDa protein OS=Homo sapiens GN=HSPA8 PE=1 SV=1 - [HSP7C_HUMAN]	HSP7C	0.12512793	1.574343702
Ubiquitin carboxyl-terminal hydrolase 5 OS=Homo sapiens GN=USP5 PE=1 SV=2 - [UBP5_HUMAN]	UBP5	0.076771058	1.273948699
60S acidic ribosomal protein P0 OS=Homo sapiens GN=RPLP0 PE=1 SV=1 - [RLA0_HUMAN]	RLA0	0.11370493	1.487470747
Calcium-binding mitochondrial carrier protein Aralar2 OS=Homo sapiens GN=SLC25A13 PE=1 SV=2 - [CMC2_HUMAN]	CMC2	0.18802901	1.914991385
40S ribosomal protein S17-like OS=Homo sapiens GN=RPS17L PE=1 SV=1 - [RS17L_HUMAN]	RS17L	0.1475994	1.665816023

Voltage-dependent anion-selective channel protein 3 OS=Homo sapiens GN=VDAC3 PE=1 SV=1 - [VDAC3_HUMAN]	VDAC3	0.10105734	1.373965117
Plasminogen activator inhibitor 1 RNA-binding protein OS=Homo sapiens GN=SERBP1 PE=1 SV=2 - [PAIRB_HUMAN]	PAIRB	0.17954947	1.833604943
Integrin alpha-V OS=Homo sapiens GN=ITGAV PE=1 SV=2 - [ITAV_HUMAN]	ITAV	0.18619382	1.872687529
26S proteasome non-ATPase regulatory subunit 5 OS=Homo sapiens GN=PSMD5 PE=1 SV=3 - [PSMD5_HUMAN]	PSMD5	0.18760984	1.877568983
Core histone macro-H2A.1 OS=Homo sapiens GN=H2AFY PE=1 SV=4 - [H2AY_HUMAN]	H2AY	0.20594357	1.978593451
60S ribosomal protein L3 OS=Homo sapiens GN=RPL3 PE=1 SV=2 - [RL3_HUMAN]	RL3	0.18883133	1.858453076
ATP synthase subunit beta, mitochondrial OS=Homo sapiens GN=ATP5B PE=1 SV=3 - [ATPB_HUMAN]	ATPB	0.13043034	1.513570923
Coatomer subunit alpha OS=Homo sapiens GN=COPA PE=1 SV=2 - [COPA_HUMAN]	COPA	0.21122155	1.971830475
Alkyldihydroxyacetonephosphate synthase, peroxisomal OS=Homo sapiens GN=AGPS PE=1 SV=1 - [ADAS_HUMAN]	ADAS	0.085902445	1.229849201
Signal transducer and activator of transcription 1-alpha/beta OS=Homo sapiens GN=STAT1 PE=1 SV=2 - [STAT1_HUMAN]	STAT1	0.19401388	1.838775709
Replication protein A 32 kDa subunit OS=Homo sapiens GN=RPA2 PE=1 SV=1 - [RFA2_HUMAN]	RFA2	0.18600518	1.791113175
40S ribosomal protein S13 OS=Homo sapiens GN=RPS13 PE=1 SV=2 - [RS13_HUMAN]	RS13	0.18409602	1.778555325
ATP synthase subunit gamma, mitochondrial OS=Homo sapiens GN=ATP5C1 PE=1 SV=1 - [ATPG_HUMAN]	ATPG	0.21382754	1.926239161
60S ribosomal protein L14 OS=Homo sapiens GN=RPL14 PE=1 SV=4 - [RL14_HUMAN]	RL14	0.14056642	1.50497021
40S ribosomal protein S6 OS=Homo sapiens GN=RPS6 PE=1 SV=1 - [RS6_HUMAN]	RS6	0.20828329	1.860927421
ATP synthase subunit alpha, mitochondrial OS=Homo sapiens GN=ATP5A1 PE=1 SV=1 - [ATPA_HUMAN]	ATPA	0.11126517	1.323526295
Guanine nucleotide-binding protein G(I)/G(S)/G(O) subunit gamma-12 OS=Homo sapiens GN=GNG12 PE=1 SV=3 - [GBG12_HUMAN]	GBG12	0.19964318	1.793716289
Eukaryotic translation initiation factor 2 subunit 3 OS=Homo sapiens GN=EIF2S3 PE=1 SV=3 - [IF2G_HUMAN]	IF2G	0.18612757	1.706244074
Eukaryotic translation initiation factor 4 gamma 1 OS=Homo sapiens GN=EIF4G1 PE=1 SV=4 - [IF4G1_HUMAN]	IF4G1	0.19971734	1.774146821
Ras-related protein Rab-3D OS=Homo sapiens GN=RAB3D PE=1 SV=1 - [RAB3D_HUMAN]	RAB3D	0.22614209	1.914315023
X-ray repair cross-complementing protein 5 OS=Homo sapiens GN=XRCC5 PE=1 SV=3 - [XRCC5_HUMAN]	XRCC5	0.2103136	1.821306667
Unconventional myosin-Ib OS=Homo sapiens GN=MYO1B PE=1 SV=3 - [MYO1B_HUMAN]	MYO1B	0.18232757	1.66409835
NAD(P) transhydrogenase, mitochondrial OS=Homo sapiens GN=NNT PE=1 SV=3 - [NNTM_HUMAN]	NNTM	0.20132735	1.761389399
CD59 glycoprotein OS=Homo sapiens GN=CD59 PE=1 SV=1 - [CD59_HUMAN]	CD59	0.18718776	1.677144411
Exportin-2 OS=Homo sapiens GN=CSE1L PE=1 SV=3 - [XPO2_HUMAN]	XPO2	0.13390695	1.374556139
Catechol O-methyltransferase OS=Homo sapiens GN=COMT PE=1 SV=2 - [COMT_HUMAN]	COMT	0.24348064	1.938957446
TAR DNA-binding protein 43 OS=Homo sapiens GN=TARDBP PE=1 SV=1 - [TADBP_HUMAN]	TADBP	0.23776747	1.892216046
Prolyl 3-hydroxylase 3 OS=Homo sapiens GN=LEPREL2 PE=1 SV=1 - [P3H3_HUMAN]	P3H3	0.19906832	1.683777736
Glycerol-3-phosphate dehydrogenase, mitochondrial OS=Homo sapiens GN=GPD2 PE=1 SV=3 - [GPDM_HUMAN]	GPDM	0.23544073	1.865795997
Ras GTPase-activating protein-binding protein 2 OS=Homo sapiens GN=G3BP2 PE=1 SV=2 - [G3BP2_HUMAN]	G3BP2	0.23502921	1.861631575
YTH domain-containing family protein 2 OS=Homo sapiens GN=YTHDF2 PE=1 SV=2 - [YTHD2_HUMAN]	YTHD2	0.20056185	1.671121531
78 kDa glucose-regulated protein OS=Homo sapiens GN=HSPA5 PE=1 SV=2 - [GRP78_HUMAN]	GRP78	0.2257794	1.7976586
Major vault protein OS=Homo sapiens GN=MVP PE=1 SV=4 - [MVP_HUMAN]	MVP	0.20431888	1.667290741
Constitutive coactivator of PPAR-gamma-like protein 1 OS=Homo sapiens GN=FAM120A PE=1 SV=2 - [F120A_HUMAN]	F120A	0.24922194	1.892209732
Reticulon-4 OS=Homo sapiens GN=RTN4 PE=1 SV=2 - [RTN4_HUMAN]	RTN4	0.18200113	1.509545944
4F2 cell-surface antigen heavy chain OS=Homo sapiens GN=SLC3A2 PE=1 SV=3 - [4F2_HUMAN]	4F2	0.19812399	1.584926209
Phosphoglycerate mutase 1 OS=Homo sapiens GN=PGAM1 PE=1 SV=2 - [PGAM1_HUMAN]	PGAM1	0.1956342	1.540499693
Inverted formin-2 OS=Homo sapiens GN=INF2 PE=1 SV=2 - [INF2_HUMAN]	INF2	0.20710793	1.595510491
Exportin-1 OS=Homo sapiens GN=XPO1 PE=1 SV=1 - [XPO1_HUMAN]	XPO1	0.22497651	1.68024423
60S ribosomal protein L5 OS=Homo sapiens GN=RPL5 PE=1 SV=3 - [RL5_HUMAN]	RL5	0.27387699	1.932268519
Putative helicase MOV-10 OS=Homo sapiens GN=MOV10 PE=1 SV=2 - [MOV10_HUMAN]	MOV10	0.21280688	1.60095925
Histone H2A type 1-H OS=Homo sapiens GN=HIST1H2AH PE=1 SV=3 - [H2A1H_HUMAN]	H2A1H	0.26999778	1.883686865
Cytosolic phospholipase A2 OS=Homo sapiens GN=PLA2G4A PE=1 SV=2 - [PA24A_HUMAN]	PA24A	0.19501606	1.499129917
Importin-7 OS=Homo sapiens GN=IPO7 PE=1 SV=1 - [IPO7_HUMAN]	IPO7	0.29176247	1.983061334
Protein disulfide-isomerase OS=Homo sapiens GN=P4HB PE=1 SV=3 - [PDIA1_HUMAN]	PDIA1	0.18899794	1.463974123
Histone H1t OS=Homo sapiens GN=HIST1H1T PE=2 SV=4 - [H1T_HUMAN]	H1T	0.20508642	1.520172697
Poly(rC)-binding protein 2 OS=Homo sapiens GN=PCBP2 PE=1 SV=1 - [PCBP2_HUMAN]	PCBP2	0.24579896	1.711636691

Vesicle-associated membrane protein-associated protein B/C OS=Homo sapiens GN=VAPB PE=1 SV=3 - [VAPB_HUMAN]	VAPB	0.22079355	1.545708608
40S ribosomal protein S15a OS=Homo sapiens GN=RPS15A PE=1 SV=2 - [RS15A_HUMAN]	RS15A	0.27632308	1.809186363
Adenylyl cyclase-associated protein 1 OS=Homo sapiens GN=CAP1 PE=1 SV=5 - [CAP1_HUMAN]	CAP1	0.25814998	1.711266837
Glypican-1 OS=Homo sapiens GN=GPC1 PE=1 SV=2 - [GPC1_HUMAN]	GPC1	0.22656547	1.549936895
Caprin-1 OS=Homo sapiens GN=CAPRIN1 PE=1 SV=2 - [CAPR1_HUMAN]	CAPR1	0.2329018	1.578041607
Sideroflexin-1 OS=Homo sapiens GN=SFXN1 PE=1 SV=4 - [SFXN1_HUMAN]	SFXN1	0.28264982	1.818921425
Ribosome-binding protein 1 OS=Homo sapiens GN=RRBP1 PE=1 SV=4 - [RRBP1_HUMAN]	RRBP1	0.30706608	1.930093334
F-box only protein 3 OS=Homo sapiens GN=FBXO3 PE=1 SV=3 - [FBX3_HUMAN]	FBX3	0.27449262	1.761151614
Leucine-rich repeat-containing protein 59 OS=Homo sapiens GN=LRRC59 PE=1 SV=1 - [LRC59_HUMAN]	LRC59	0.29507738	1.811263655
Vesicle-associated membrane protein 3 OS=Homo sapiens GN=VAMP3 PE=1 SV=3 - [VAMP3_HUMAN]	VAMP3	0.25688794	1.601485195
ATP-dependent RNA helicase A OS=Homo sapiens GN=DHX9 PE=1 SV=4 - [DHX9_HUMAN]	DHX9	0.20030099	1.353544179
Basigin OS=Homo sapiens GN=BSG PE=1 SV=2 - [BASI_HUMAN]	BASI	0.31874436	1.896294126
ATP synthase subunit g, mitochondrial OS=Homo sapiens GN=ATP5L PE=1 SV=3 - [ATP5L_HUMAN]	ATP5L	0.14977287	1.141625568
Putative RNA-binding protein Luc7-like 2 OS=Homo sapiens GN=LUC7L2 PE=1 SV=2 - [LC7L2_HUMAN]	LC7L2	0.22524558	1.435991791
60S ribosomal protein L34 OS=Homo sapiens GN=RPL34 PE=1 SV=3 - [RL34_HUMAN]	RL34	0.16966331	1.202702154
Nucleolin OS=Homo sapiens GN=NCL PE=1 SV=3 - [NUCL_HUMAN]	NUCL	0.21442354	1.379977192
Chromodomain-helicase-DNA-binding protein 1-like OS=Homo sapiens GN=CHD1L PE=1 SV=2 - [CHD1L_HUMAN]	CHD1L	0.32244527	1.867658854
Ras-related protein Rab-18 OS=Homo sapiens GN=RAB18 PE=1 SV=1 - [RAB18_HUMAN]	RAB18	0.17381731	1.207565766
Transmembrane emp24 domain-containing protein 10 OS=Homo sapiens GN=TMED10 PE=1 SV=2 - [TMEDA_HUMAN]	TMEDA	0.28179923	1.653243317
Adenosylhomocysteinase OS=Homo sapiens GN=AHCY PE=1 SV=4 - [SAHH_HUMAN]	SAHH	0.25297344	1.508388987
Integrin alpha-6 OS=Homo sapiens GN=ITGA6 PE=1 SV=5 - [ITA6_HUMAN]	ITA6	0.34726343	1.943199256
Nodal modulator 3 OS=Homo sapiens GN=NOMO3 PE=2 SV=2 - [NOMO3_HUMAN]	NOMO3	0.26104304	1.530151013
Actin, cytoplasmic 1 OS=Homo sapiens GN=ACTB PE=1 SV=1 - [ACTB_HUMAN]	ACTB	0.23447536	1.412414694
Prohibitin OS=Homo sapiens GN=PHB PE=1 SV=1 - [PHB_HUMAN]	PHB	0.20359652	1.277437685
60S ribosomal protein L6 OS=Homo sapiens GN=RPL6 PE=1 SV=3 - [RL6_HUMAN]	RL6	0.29065472	1.630348438
Integrin alpha-5 OS=Homo sapiens GN=ITGA5 PE=1 SV=2 - [ITA5_HUMAN]	ITA5	0.26785669	1.528683975
Keratin, type I cytoskeletal 17 OS=Homo sapiens GN=KRT17 PE=1 SV=2 - [K1C17_HUMAN]	K1C17	0.28784558	1.598512318
Y-box-binding protein 3 OS=Homo sapiens GN=YBX3 PE=1 SV=4 - [YBOX3_HUMAN]	YBOX3	0.34640828	1.872216321
Interferon-induced 35 kDa protein OS=Homo sapiens GN=IFI35 PE=1 SV=5 - [IN35_HUMAN]	IN35	0.35275403	1.893373995
Probable ATP-dependent RNA helicase DDX17 OS=Homo sapiens GN=DDX17 PE=1 SV=2 - [DDX17_HUMAN]	DDX17	0.33844978	1.817760759
Dolichyl-diphosphooligosaccharide--protein glycosyltransferase subunit DAD1 OS=Homo sapiens GN=DAD1 PE=1 SV=3 - [DAD1_HUMAN]	DAD1	0.26474008	1.451709
Lamin-B1 OS=Homo sapiens GN=LMNB1 PE=1 SV=2 - [LMNB1_HUMAN]	LMNB1	0.33248031	1.750707724
Programmed cell death protein 6 OS=Homo sapiens GN=PDCD6 PE=1 SV=1 - [PDCD6_HUMAN]	PDCD6	0.26656157	1.455901214
Protein-glutamine gamma-glutamyltransferase E OS=Homo sapiens GN=TGM3 PE=1 SV=4 - [TGM3_HUMAN]	TGM3	0.34885338	1.823067584
Far upstream element-binding protein 2 OS=Homo sapiens GN=KHSRP PE=1 SV=4 - [FUBP2_HUMAN]	FUBP2	0.30905116	1.622116249
60S ribosomal protein L26 OS=Homo sapiens GN=RPL26 PE=1 SV=1 - [RL26_HUMAN]	RL26	0.1960796	1.158175096
Heat shock 70 kDa protein 4L OS=Homo sapiens GN=HSPA4L PE=1 SV=3 - [HS74L_HUMAN]	HS74L	0.31450826	1.627163917
Histone-binding protein RBBP4 OS=Homo sapiens GN=RBBP4 PE=1 SV=3 - [RBBP4_HUMAN]	RBBP4	0.28347674	1.48811402
T-complex protein 1 subunit eta OS=Homo sapiens GN=CCT7 PE=1 SV=2 - [TCPH_HUMAN]	TCPH	0.24502735	1.333169697
Fragile X mental retardation protein 1 OS=Homo sapiens GN=FMR1 PE=1 SV=1 - [FMR1_HUMAN]	FMR1	0.35374239	1.791778393
Dihydrolipoyl dehydrogenase, mitochondrial OS=Homo sapiens GN=DLD PE=1 SV=2 - [DLDH_HUMAN]	DLDH	0.32233933	1.638952918
Threonine--tRNA ligase, cytoplasmic OS=Homo sapiens GN=TARS PE=1 SV=3 - [SYTC_HUMAN]	SYTC	0.33285567	1.678965871
Heterogeneous nuclear ribonucleoprotein U OS=Homo sapiens GN=HNRNPU PE=1 SV=6 - [HNRPU_HUMAN]	HNRPU	0.35369116	1.774953703
60S ribosomal protein L4 OS=Homo sapiens GN=RPL4 PE=1 SV=5 - [RL4_HUMAN]	RL4	0.32141918	1.613564465
Surfeit locus protein 4 OS=Homo sapiens GN=SURF4 PE=1 SV=3 - [SURF4_HUMAN]	SURF4	0.28882694	1.471864257
Ras-related protein Rab-8A OS=Homo sapiens GN=RAB8A PE=1 SV=1 - [RAB8A_HUMAN]	RAB8A	0.27933252	1.427756766
Proteasome activator complex subunit 2 OS=Homo sapiens GN=PSME2 PE=1 SV=4 - [PSME2_HUMAN]	PSME2	0.34178808	1.687139986
Nuclear mitotic apparatus protein 1 OS=Homo sapiens GN=NUMA1 PE=1 SV=2 - [NUMA1_HUMAN]	NUMA1	0.31525931	1.561664072
Very long-chain specific acyl-CoA dehydrogenase, mitochondrial OS=Homo sapiens GN=ACADVL PE=1 SV=1 - [ACADV_HUMAN]	ACADV	0.3577764	1.743511618

RuvB-like 2 OS=Homo sapiens GN=RUVBL2 PE=1 SV=3 - [RUVB2_HUMAN]	RUVB2	0.30422348	1.505173757
Glutamine--fructose-6-phosphate aminotransferase [isomerizing] 1 OS=Homo sapiens GN=GFPT1 PE=1 SV=3 - [GFPT1_HUMAN]	GFPT1	0.30292016	1.49150097
60S ribosomal protein L15 OS=Homo sapiens GN=RPL15 PE=1 SV=2 - [RL15_HUMAN]	RL15	0.26528853	1.339762402
Proteolipid protein 2 OS=Homo sapiens GN=PLP2 PE=1 SV=1 - [PLP2_HUMAN]	PLP2	0.31502661	1.519524023
Importin subunit beta-1 OS=Homo sapiens GN=KPNB1 PE=1 SV=2 - [IMB1_HUMAN]	IMB1	0.32649279	1.553649583
Prenylcysteine oxidase 1 OS=Homo sapiens GN=PCYOX1 PE=1 SV=3 - [PCYOX_HUMAN]	PCYOX	0.36520752	1.726209866
Trifunctional enzyme subunit beta, mitochondrial OS=Homo sapiens GN=HADHB PE=1 SV=3 - [ECHB_HUMAN]	ECHB	0.28889942	1.393326505
Heat shock 70 kDa protein 1A/1B OS=Homo sapiens GN=HSPA1A PE=1 SV=5 - [HSP71_HUMAN]	HSP71	0.28462824	1.376258325
Golgi-associated plant pathogenesis-related protein 1 OS=Homo sapiens GN=GLIPR2 PE=1 SV=3 - [GAPR1_HUMAN]	GAPR1	0.32701349	1.545735181
T-cell surface glycoprotein CD8 alpha chain OS=Homo sapiens GN=CD8A PE=1 SV=1 - [CD8A_HUMAN]	CD8A	0.25629026	1.264925815
Importin subunit alpha-1 OS=Homo sapiens GN=KPNA2 PE=1 SV=1 - [IMA1_HUMAN]	IMA1	0.4109574	1.934064613
2'-5'-oligoadenylate synthase-like protein OS=Homo sapiens GN=OASL PE=1 SV=2 - [OASL_HUMAN]	OASL	0.25579861	1.260481661
V-type proton ATPase catalytic subunit A OS=Homo sapiens GN=ATP6V1A PE=1 SV=2 - [VATA_HUMAN]	VATA	0.29824966	1.408628372
Filamin-A OS=Homo sapiens GN=FLNA PE=1 SV=4 - [FLNA_HUMAN]	FLNA	0.33482367	1.554232937
Keratin, type II cuticular Hb2 OS=Homo sapiens GN=KRT82 PE=1 SV=3 - [KRT82_HUMAN]	KRT82	0.43559697	1.995296589
Aldehyde dehydrogenase X, mitochondrial OS=Homo sapiens GN=ALDH1B1 PE=1 SV=3 - [AL1B1_HUMAN]	AL1B1	0.32441193	1.465738772
Peroxiredoxin-4 OS=Homo sapiens GN=PRDX4 PE=1 SV=1 - [PRDX4_HUMAN]	PRDX4	0.30900571	1.3944815
Ras-related protein Rab-11A OS=Homo sapiens GN=RAB11A PE=1 SV=3 - [RB11A_HUMAN]	RB11A	0.36730435	1.623831415
Mitochondrial 2-oxoglutarate/malate carrier protein OS=Homo sapiens GN=SLC25A11 PE=1 SV=3 - [M2OM_HUMAN]	M2OM	0.35808641	1.583250084
Histone H1.2 OS=Homo sapiens GN=HIST1H1C PE=1 SV=2 - [H12_HUMAN]	H12	0.38007575	1.672402686
Werner syndrome ATP-dependent helicase OS=Homo sapiens GN=WRN PE=1 SV=2 - [WRN_HUMAN]	WRN	0.34668425	1.521981801
Ras-related protein Rab-34 OS=Homo sapiens GN=RAB34 PE=1 SV=1 - [RAB34_HUMAN]	RAB34	0.3725765	1.629081797
26S protease regulatory subunit 6A OS=Homo sapiens GN=PSMC3 PE=1 SV=3 - [PRS6A_HUMAN]	PRS6A	0.30481961	1.346546479
Uncharacterized protein C9orf142 OS=Homo sapiens GN=C9orf142 PE=1 SV=2 - [CI142_HUMAN]	CI142	0.34549183	1.504387684
26S protease regulatory subunit 7 OS=Homo sapiens GN=PSMC2 PE=1 SV=3 - [PRS7_HUMAN]	PRS7	0.32604426	1.426116581
Apoptosis-inducing factor 1, mitochondrial OS=Homo sapiens GN=AIFM1 PE=1 SV=1 - [AIFM1_HUMAN]	AIFM1	0.31967157	1.392802915
GTP-binding protein SAR1a OS=Homo sapiens GN=SAR1A PE=1 SV=1 - [SAR1A_HUMAN]	SAR1A	0.28651482	1.270474693
Catenin alpha-1 OS=Homo sapiens GN=CTNNA1 PE=1 SV=1 - [CTNA1_HUMAN]	CTNA1	0.32149497	1.385570404
Ras-related protein Rab-21 OS=Homo sapiens GN=RAB21 PE=1 SV=3 - [RAB21_HUMAN]	RAB21	0.41240153	1.769031771
GTPase NRas OS=Homo sapiens GN=NRAS PE=1 SV=1 - [RASN_HUMAN]	RASN	0.37499738	1.57905874
Alpha-centractin OS=Homo sapiens GN=ACTR1A PE=1 SV=1 - [ACTZ_HUMAN]	ACTZ	0.36680722	1.537658211
Heat shock 70 kDa protein 4 OS=Homo sapiens GN=HSPA4 PE=1 SV=4 - [HSP74_HUMAN]	HSP74	0.38595843	1.604565531
Protein LYRIC OS=Homo sapiens GN=MTDH PE=1 SV=2 - [LYRIC_HUMAN]	LYRIC	0.35492986	1.472629737
Trifunctional purine biosynthetic protein adenosine-3 OS=Homo sapiens GN=GART PE=1 SV=1 - [PUR2_HUMAN]	PUR2	0.42481598	1.778862572
NADPH--cytochrome P450 reductase OS=Homo sapiens GN=POR PE=1 SV=2 - [NCPR_HUMAN]	NCPR	0.39212397	1.621765623
Keratin, type II cytoskeletal 5 OS=Homo sapiens GN=KRT5 PE=1 SV=3 - [K2C5_HUMAN]	K2C5	0.13349271	0.752727242
DnaJ homolog subfamily C member 10 OS=Homo sapiens GN=DNAJC10 PE=1 SV=2 - [DJC10_HUMAN]	DJC10	0.34391943	1.414984511
60S ribosomal protein L13 OS=Homo sapiens GN=RPL13 PE=1 SV=4 - [RL13_HUMAN]	RL13	0.43253684	1.800153146
DNA repair protein XRCC1 OS=Homo sapiens GN=XRCC1 PE=1 SV=2 - [XRCC1_HUMAN]	XRCC1	0.32530284	1.330506116
Pyruvate kinase PKM OS=Homo sapiens GN=PKM PE=1 SV=4 - [KPYM_HUMAN]	KPYM	0.33794832	1.370226957
Ras-related C3 botulinum toxin substrate 2 OS=Homo sapiens GN=RAC2 PE=1 SV=1 - [RAC2_HUMAN]	RAC2	0.31363982	1.28038519
Lysosome-associated membrane glycoprotein 2 OS=Homo sapiens GN=LAMP2 PE=1 SV=2 - [LAMP2_HUMAN]	LAMP2	0.35193005	1.419405831
Lysosome-associated membrane glycoprotein 1 OS=Homo sapiens GN=LAMP1 PE=1 SV=3 - [LAMP1_HUMAN]	LAMP1	0.34107977	1.377021807
F-actin-capping protein subunit alpha-2 OS=Homo sapiens GN=CAPZA2 PE=1 SV=3 - [CAZA2_HUMAN]	CAZA2	0.37689394	1.516186416
AP-1 complex subunit beta-1 OS=Homo sapiens GN=AP1B1 PE=1 SV=2 - [AP1B1_HUMAN]	AP1B1	0.39788201	1.604237577
6-phosphofructokinase type C OS=Homo sapiens GN=PFKP PE=1 SV=2 - [K6PP_HUMAN]	K6PP	0.42650416	1.729451276
40S ribosomal protein S9 OS=Homo sapiens GN=RPS9 PE=1 SV=3 - [RS9_HUMAN]	RS9	0.2790218	1.153108768
Importin-9 OS=Homo sapiens GN=IPO9 PE=1 SV=3 - [IPO9_HUMAN]	IPO9	0.32640061	1.31124865

Coatomer subunit gamma-1 OS=Homo sapiens GN=COPG1 PE=1 SV=1 - [COPG1_HUMAN]	COPG1	0.42210069	1.701956187
Podocalyxin OS=Homo sapiens GN=PODXL PE=1 SV=2 - [PODXL_HUMAN]	PODXL	0.28949472	1.182913354
Ras GTPase-activating-like protein IQGAP1 OS=Homo sapiens GN=IQGAP1 PE=1 SV=1 - [IQGA1_HUMAN]	IQGA1	0.41525286	1.663126807
Keratin, type II cytoskeletal 1b OS=Homo sapiens GN=KRT77 PE=2 SV=3 - [K2C1B_HUMAN]	K2C1B	0.35673195	1.413005791
F-box only protein 50 OS=Homo sapiens GN=NCCRP1 PE=1 SV=1 - [FBX50_HUMAN]	FBX50	0.34565872	1.368767857
60S ribosomal protein L22 OS=Homo sapiens GN=RPL22 PE=1 SV=2 - [RL22_HUMAN]	RL22	0.32669002	1.299402802
Glyceraldehyde-3-phosphate dehydrogenase OS=Homo sapiens GN=GAPDH PE=1 SV=3 - [G3P_HUMAN]	G3P	0.38949522	1.53652297
Calponin-2 OS=Homo sapiens GN=CNN2 PE=1 SV=4 - [CNN2_HUMAN]	CNN2	0.35988316	1.417516636
Signal recognition particle subunit SRP68 OS=Homo sapiens GN=SRP68 PE=1 SV=2 - [SRP68_HUMAN]	SRP68	0.33860081	1.319454862
Desmocollin-1 OS=Homo sapiens GN=DSC1 PE=1 SV=2 - [DSC1_HUMAN]	DSC1	0.369571	1.416788801
Lipase maturation factor 2 OS=Homo sapiens GN=LMF2 PE=1 SV=2 - [LMF2_HUMAN]	LMF2	0.38682738	1.483043354
Protein ERGIC-53 OS=Homo sapiens GN=LMAN1 PE=1 SV=2 - [LMAN1_HUMAN]	LMAN1	0.35543847	1.355816827
Alpha-enolase OS=Homo sapiens GN=ENO1 PE=1 SV=2 - [ENOA_HUMAN]	ENOA	0.38798308	1.464578119
Ketosamine-3-kinase OS=Homo sapiens GN=FN3KRP PE=1 SV=2 - [KT3K_HUMAN]	KT3K	0.36977413	1.393218637
Cytoskeleton-associated protein 4 OS=Homo sapiens GN=CKAP4 PE=1 SV=2 - [CKAP4_HUMAN]	CKAP4	0.44775572	1.717304652
Thrombospondin-1 OS=Homo sapiens GN=THBS1 PE=1 SV=2 - [TSP1_HUMAN]	TSP1	0.44380587	1.677996026
T-complex protein 1 subunit delta OS=Homo sapiens GN=CCT4 PE=1 SV=4 - [TCPD_HUMAN]	TCPD	0.36125216	1.325294909
Annexin A11 OS=Homo sapiens GN=ANXA11 PE=1 SV=1 - [ANX11_HUMAN]	ANX11	0.36752227	1.346405813
Transgelin-2 OS=Homo sapiens GN=TAGLN2 PE=1 SV=3 - [TAGL2_HUMAN]	TAGL2	0.39746037	1.454265233
Translocon-associated protein subunit alpha OS=Homo sapiens GN=SSR1 PE=1 SV=3 - [SSRA_HUMAN]	SSRA	0.38731906	1.40854017
Fatty acid synthase OS=Homo sapiens GN=FASN PE=1 SV=3 - [FAS_HUMAN]	FAS	0.45307195	1.684894605
Keratin, type I cytoskeletal 14 OS=Homo sapiens GN=KRT14 PE=1 SV=4 - [K1C14_HUMAN]	K1C14	0.12310317	0.619400214
Glutathione reductase, mitochondrial OS=Homo sapiens GN=GSR PE=1 SV=2 - [GSHR_HUMAN]	GSHR	0.41169187	1.455207217
CD97 antigen OS=Homo sapiens GN=CD97 PE=1 SV=4 - [CD97_HUMAN]	CD97	0.39592567	1.38922594
Glycogen phosphorylase, liver form OS=Homo sapiens GN=PYGL PE=1 SV=4 - [PYGL_HUMAN]	PYGL	0.40311155	1.414981231
40S ribosomal protein S19 OS=Homo sapiens GN=RPS19 PE=1 SV=2 - [RS19_HUMAN]	RS19	0.41405872	1.435811634
Plakophilin-1 OS=Homo sapiens GN=PKP1 PE=1 SV=2 - [PKP1_HUMAN]	PKP1	0.37498802	1.290345442
Proteasome activator complex subunit 3 OS=Homo sapiens GN=PSME3 PE=1 SV=1 - [PSME3_HUMAN]	PSME3	0.41495726	1.429637724
Heterogeneous nuclear ribonucleoproteins A2/B1 OS=Homo sapiens GN=HNRNPA2B1 PE=1 SV=2 - [ROA2_HUMAN]	ROA2	0.25703233	0.925334368
Heterogeneous nuclear ribonucleoprotein K OS=Homo sapiens GN=HNRNPK PE=1 SV=1 - [HNRPK_HUMAN]	HNRPK	0.44733408	1.547548637
Trifunctional enzyme subunit alpha, mitochondrial OS=Homo sapiens GN=HADHA PE=1 SV=2 - [ECHA_HUMAN]	ECHA	0.46254167	1.610428474
Splicing factor 3B subunit 3 OS=Homo sapiens GN=SF3B3 PE=1 SV=4 - [SF3B3_HUMAN]	SF3B3	0.40256545	1.358930626
Structural maintenance of chromosomes protein 2 OS=Homo sapiens GN=SMC2 PE=1 SV=2 - [SMC2_HUMAN]	SMC2	0.41226387	1.392690384
Ubiquitin carboxyl-terminal hydrolase 10 OS=Homo sapiens GN=USP10 PE=1 SV=2 - [UBP10_HUMAN]	UBP10	0.37808326	1.264795219
Fructosamine-3-kinase OS=Homo sapiens GN=FN3K PE=1 SV=1 - [FN3K_HUMAN]	FN3K	0.43861446	1.488461486
AP-2 complex subunit beta OS=Homo sapiens GN=AP2B1 PE=1 SV=1 - [AP2B1_HUMAN]	AP2B1	0.40338033	1.349584887
Glyoxylate reductase/hydroxypyruvate reductase OS=Homo sapiens GN=GRHPR PE=1 SV=1 - [GRHPR_HUMAN]	GRHPR	0.41818383	1.399105865
Homeobox protein cut-like 1 OS=Homo sapiens GN=CUX1 PE=1 SV=3 - [CUX1_HUMAN]	CUX1	0.38347408	1.265352525
Vesicle-fusing ATPase OS=Homo sapiens GN=NSF PE=1 SV=3 - [NSF_HUMAN]	NSF	0.3930468	1.293667113
6-phosphogluconate dehydrogenase, decarboxylating OS=Homo sapiens GN=PGD PE=1 SV=3 - [6PGD_HUMAN]	6PGD	0.42208573	1.399326443
Catenin beta-1 OS=Homo sapiens GN=CTNNB1 PE=1 SV=1 - [CTNB1_HUMAN]	CTNB1	0.38514623	1.262178419
Carbamoyl-phosphate synthase [ammonia], mitochondrial OS=Homo sapiens GN=CPS1 PE=1 SV=2 - [CPSM_HUMAN]	CPSM	0.48006102	1.638219649
T-complex protein 1 subunit gamma OS=Homo sapiens GN=CCT3 PE=1 SV=4 - [TCPG_HUMAN]	TCPG	0.4627831	1.558857881
Mitochondrial import inner membrane translocase subunit TIM50 OS=Homo sapiens GN=TIMM50 PE=1 SV=2 - [TIM50_HUMAN]	TIM50	0.41352266	1.35970998
Sulfide:quinone oxidoreductase, mitochondrial OS=Homo sapiens GN=SQRDL PE=1 SV=1 - [SQRD_HUMAN]	SQRD	0.42733926	1.406529914
Heterogeneous nuclear ribonucleoprotein M OS=Homo sapiens GN=HNRNPM PE=1 SV=3 - [HNRPM_HUMAN]	HNRPM	0.44794062	1.473718572
Polyubiquitin-C OS=Homo sapiens GN=UBC PE=1 SV=3 - [UBC_HUMAN]	UBC	0.21680966	0.767788446

Up-regulated during skeletal muscle growth protein 5 OS=Homo sapiens GN=USMG5 PE=1 SV=1 - [USMG5_HUMAN]	USMG5	0.40765536	1.307829206
Glutamine--tRNA ligase OS=Homo sapiens GN=QARS PE=1 SV=1 - [SYQ_HUMAN]	SYQ	0.42831463	1.38094697
Proteasome subunit alpha type-2 OS=Homo sapiens GN=PSMA2 PE=1 SV=2 - [PSA2_HUMAN]	PSA2	0.28042156	0.919069937
Protein LSM12 homolog OS=Homo sapiens GN=LSM12 PE=1 SV=2 - [LSM12_HUMAN]	LSM12	0.4261328	1.358590375
Barrier-to-autointegration factor OS=Homo sapiens GN=BANF1 PE=1 SV=1 - [BAF_HUMAN]	BAF	0.43948075	1.409171901
Zinc transporter ZIP14 OS=Homo sapiens GN=SLC39A14 PE=1 SV=3 - [S39AE_HUMAN]	S39AE	0.3979488	1.25257645
Lamina-associated polypeptide 2, isoforms beta/gamma OS=Homo sapiens GN=TMPO PE=1 SV=2 - [LAP2B_HUMAN]	LAP2B	0.50693744	1.679944591
Eukaryotic translation initiation factor 3 subunit C OS=Homo sapiens GN=EIF3C PE=1 SV=1 - [EIF3C_HUMAN]	EIF3C	0.42954728	1.34780372
Prolactin-inducible protein OS=Homo sapiens GN=PIP PE=1 SV=1 - [PIP_HUMAN]	PIP	0.39717293	1.228654859
Condensin complex subunit 3 OS=Homo sapiens GN=NCAPG PE=1 SV=1 - [CND3_HUMAN]	CND3	0.42016375	1.296561257
60S ribosomal protein L10a OS=Homo sapiens GN=RPL10A PE=1 SV=2 - [RL10A_HUMAN]	RL10A	0.4458434	1.384562239
Protein-glutamine gamma-glutamyltransferase K OS=Homo sapiens GN=TGM1 PE=1 SV=4 - [TGM1_HUMAN]	TGM1	0.42936277	1.309496488
Probable ATP-dependent RNA helicase DHX36 OS=Homo sapiens GN=DHX36 PE=1 SV=2 - [DHX36_HUMAN]	DHX36	0.39148971	1.177170597
Peroxisomal multifunctional enzyme type 2 OS=Homo sapiens GN=HSD17B4 PE=1 SV=3 - [DHB4_HUMAN]	DHB4	0.45401996	1.391206972
Serine/threonine-protein phosphatase 2A 65 kDa regulatory subunit A alpha isoform OS=Homo sapiens GN=PPP2R1A PE=1 SV=4 - [2AAA_HUMAN]	2AAA	0.46769539	1.444083136
Cation-dependent mannose-6-phosphate receptor OS=Homo sapiens GN=M6PR PE=1 SV=1 - [MPRD_HUMAN]	MPRD	0.42741072	1.283307314
40S ribosomal protein S11 OS=Homo sapiens GN=RPS11 PE=1 SV=3 - [RS11_HUMAN]	RS11	0.46316907	1.410350948
Dolichyl-diphosphooligosaccharide--protein glycosyltransferase 48 kDa subunit OS=Homo sapiens GN=DDOST PE=1 SV=4 - [OST48_HUMAN]	OST48	0.47119415	1.41214611
Protein DJ-1 OS=Homo sapiens GN=PARK7 PE=1 SV=2 - [PARK7_HUMAN]	PARK7	0.44987056	1.308557944
Heterogeneous nuclear ribonucleoprotein F OS=Homo sapiens GN=HNRNPF PE=1 SV=3 - [HNRPF_HUMAN]	HNRPF	0.49009946	1.447388034
Peroxiredoxin-6 OS=Homo sapiens GN=PRDX6 PE=1 SV=3 - [PRDX6_HUMAN]	PRDX6	0.47122976	1.371403374
Myosin-9 OS=Homo sapiens GN=MYH9 PE=1 SV=4 - [MYH9_HUMAN]	MYH9	0.4401682	1.25084526
26S protease regulatory subunit 8 OS=Homo sapiens GN=PSMC5 PE=1 SV=1 - [PRS8_HUMAN]	PRS8	0.23221841	0.7018951
Thyroid hormone receptor-associated protein 3 OS=Homo sapiens GN=THRAP3 PE=1 SV=2 - [TR150_HUMAN]	TR150	0.41714132	1.16671338
Cytochrome b-c1 complex subunit 2, mitochondrial OS=Homo sapiens GN=UQCRC2 PE=1 SV=3 - [QCR2_HUMAN]	QCR2	0.42378002	1.179882774
Clusterin OS=Homo sapiens GN=CLU PE=1 SV=1 - [CLUS_HUMAN]	CLUS	0.42993158	1.199179256
Spectrin alpha chain, non-erythrocytic 1 OS=Homo sapiens GN=SPTAN1 PE=1 SV=3 - [SPTN1_HUMAN]	SPTN1	0.45037141	1.264075582
60S ribosomal protein L8 OS=Homo sapiens GN=RPL8 PE=1 SV=2 - [RL8_HUMAN]	RL8	0.45113358	1.235375696
Torsin-1A-interacting protein 1 OS=Homo sapiens GN=TOR1AIP1 PE=1 SV=2 - [TOIP1_HUMAN]	TOIP1	0.44951752	1.215413208
Elongation factor 1-delta OS=Homo sapiens GN=EEF1D PE=1 SV=5 - [EF1D_HUMAN]	EF1D	0.1828329	0.571492578
Keratin, type I cytoskeletal 18 OS=Homo sapiens GN=KRT18 PE=1 SV=2 - [K1C18_HUMAN]	K1C18	0.54809231	1.614717483
DnaJ homolog subfamily A member 1 OS=Homo sapiens GN=DNAJA1 PE=1 SV=2 - [DNJA1_HUMAN]	DNJA1	0.49338579	1.372333226
Translocon-associated protein subunit delta OS=Homo sapiens GN=SSR4 PE=1 SV=1 - [SSRD_HUMAN]	SSRD	0.42890653	1.143427527
Leucine--tRNA ligase, cytoplasmic OS=Homo sapiens GN=LARS PE=1 SV=2 - [SYLC_HUMAN]	SYLC	0.49837571	1.380559742
Keratin, type I cytoskeletal 16 OS=Homo sapiens GN=KRT16 PE=1 SV=4 - [K1C16_HUMAN]	K1C16	0.091345742	0.39576671
Protein disulfide-isomerase A3 OS=Homo sapiens GN=PDIA3 PE=1 SV=4 - [PDIA3_HUMAN]	PDIA3	0.48780733	1.305846269
Transaldolase OS=Homo sapiens GN=TALDO1 PE=1 SV=2 - [TALDO_HUMAN]	TALDO	0.34282738	0.860028826
Heterogeneous nuclear ribonucleoprotein Q OS=Homo sapiens GN=SYNCRIP PE=1 SV=2 - [HNRPQ_HUMAN]	HNRPQ	0.4830513	1.256899936
Phosphoglycerate mutase 2 OS=Homo sapiens GN=PGAM2 PE=1 SV=3 - [PGAM2_HUMAN]	PGAM2	0.37023798	0.916039625
Kinectin OS=Homo sapiens GN=KTN1 PE=1 SV=1 - [KTN1_HUMAN]	KTN1	0.46038547	1.164067366
Ras-related protein Rap-1b OS=Homo sapiens GN=RAP1B PE=1 SV=1 - [RAP1B_HUMAN]	RAP1B	0.55255073	1.508042925
26S protease regulatory subunit 10B OS=Homo sapiens GN=PSMC6 PE=1 SV=1 - [PRS10_HUMAN]	PRS10	0.49129108	1.25537877
ELAV-like protein 1 OS=Homo sapiens GN=ELAVL1 PE=1 SV=2 - [ELAV1_HUMAN]	ELAV1	0.44800618	1.099429101
Keratin, type II cytoskeletal 2 epidermal OS=Homo sapiens GN=KRT2 PE=1 SV=2 - [K22E_HUMAN]	K22E	0.28349823	0.698321532
Prelamin-A/C OS=Homo sapiens GN=LMNA PE=1 SV=1 - [LMNA_HUMAN]	LMNA	0.52383792	1.356374581
Serum albumin OS=Homo sapiens GN=ALB PE=1 SV=2 - [ALBU_HUMAN]	ALBU	0.51879233	1.335742208
Poly [ADP-ribose] polymerase 12 OS=Homo sapiens GN=PARP12 PE=1 SV=1 - [PAR12_HUMAN]	PAR12	0.52707028	1.364851972
CTP synthase 1 OS=Homo sapiens GN=CTPS1 PE=1 SV=2 - [PYRG1_HUMAN]	PYRG1	0.55193812	1.463290008

Vasorin OS=Homo sapiens GN=VASN PE=1 SV=1 - [VASN_HUMAN]	VASN	0.47139567	1.138600016
Atlastin-3 OS=Homo sapiens GN=ATL3 PE=1 SV=1 - [ATLA3_HUMAN]	ATLA3	0.51080531	1.26483274
Glycogen phosphorylase, brain form OS=Homo sapiens GN=PYGB PE=1 SV=5 - [PYGB_HUMAN]	PYGB	0.46646819	1.110813604
UBX domain-containing protein 4 OS=Homo sapiens GN=UBXN4 PE=1 SV=2 - [UBXN4_HUMAN]	UBXN4	0.4906418	1.185262348
HLA class I histocompatibility antigen, A-68 alpha chain OS=Homo sapiens GN=HLA-A PE=1 SV=4 - [1A68_HUMAN]	1A68	0.57546055	1.484906295
Glutathione S-transferase Mu 3 OS=Homo sapiens GN=GSTM3 PE=1 SV=3 - [GSTM3_HUMAN]	GSTM3	0.39926416	0.887344261
40S ribosomal protein S2 OS=Homo sapiens GN=RPS2 PE=1 SV=2 - [RS2_HUMAN]	RS2	0.49978393	1.165146922
Neural cell adhesion molecule L1 OS=Homo sapiens GN=L1CAM PE=1 SV=2 - [L1CAM_HUMAN]	L1CAM	0.49856099	1.151141654
Golgin subfamily A member 4 OS=Homo sapiens GN=GOLGA4 PE=1 SV=1 - [GOGA4_HUMAN]	GOGA4	0.4071857	0.882566452
Peroxiredoxin-1 OS=Homo sapiens GN=PRDX1 PE=1 SV=1 - [PRDX1_HUMAN]	PRDX1	0.27986449	0.619516005
Inosine-5'-monophosphate dehydrogenase 2 OS=Homo sapiens GN=IMPDH2 PE=1 SV=2 - [IMDH2_HUMAN]	IMDH2	0.52620173	1.209231124
Kinesin-1 heavy chain OS=Homo sapiens GN=KIF5B PE=1 SV=1 - [KINH_HUMAN]	KINH	0.54202068	1.254316146
Putative nucleoside diphosphate kinase OS=Homo sapiens GN=NME2P1 PE=5 SV=1 - [NDK8_HUMAN]	NDK8	0.45559594	0.948135273
Sequestosome-1 OS=Homo sapiens GN=SQSTM1 PE=1 SV=1 - [SQSTM_HUMAN]	SQSTM	0.32427019	0.65423638
Dynactin subunit 1 OS=Homo sapiens GN=DCTN1 PE=1 SV=3 - [DCTN1_HUMAN]	DCTN1	0.53656524	1.16901546
Calcium-binding mitochondrial carrier protein SCaMC-1 OS=Homo sapiens GN=SLC25A24 PE=1 SV=2 - [SCMC1_HUMAN]	SCMC1	0.52296156	1.115189207
DNA replication licensing factor MCM7 OS=Homo sapiens GN=MCM7 PE=1 SV=4 - [MCM7_HUMAN]	MCM7	0.58941364	1.346703435
Lon protease homolog, mitochondrial OS=Homo sapiens GN=LONP1 PE=1 SV=2 - [LONM_HUMAN]	LONM	0.53718722	1.139966106
40S ribosomal protein S7 OS=Homo sapiens GN=RPS7 PE=1 SV=1 - [RS7_HUMAN]	RS7	0.55338472	1.19071066
ATP-citrate synthase OS=Homo sapiens GN=ACLY PE=1 SV=3 - [ACLY_HUMAN]	ACLY	0.58578682	1.301296614
Acetyl-CoA carboxylase 1 OS=Homo sapiens GN=ACACA PE=1 SV=2 - [ACACA_HUMAN]	ACACA	0.56680351	1.210577714
Keratin, type I cytoskeletal 10 OS=Homo sapiens GN=KRT10 PE=1 SV=6 - [K1C10_HUMAN]	K1C10	0.3969644	0.741680454
Guanine nucleotide-binding protein subunit beta-2-like 1 OS=Homo sapiens GN=GNB2L1 PE=1 SV=3 - [GBLP_HUMAN]	GBLP	0.60499746	1.336613613
Aspartate aminotransferase, mitochondrial OS=Homo sapiens GN=GOT2 PE=1 SV=3 - [AATM_HUMAN]	AATM	0.35922825	0.652047915
60S ribosomal protein L9 OS=Homo sapiens GN=RPL9 PE=1 SV=1 - [RL9_HUMAN]	RL9	0.58841944	1.246576072
Profilin-1 OS=Homo sapiens GN=PFN1 PE=1 SV=2 - [PROF1_HUMAN]	PROF1	0.3370454	0.60552062
Nicalin OS=Homo sapiens GN=NCLN PE=1 SV=2 - [NCLN_HUMAN]	NCLN	0.5609259	1.13753325
Histone H2B type 1-J OS=Homo sapiens GN=HIST1H2BJ PE=1 SV=3 - [H2B1J_HUMAN]	H2B1J	0.64215553	1.473055686
Chloride intracellular channel protein 1 OS=Homo sapiens GN=CLIC1 PE=1 SV=4 - [CLIC1_HUMAN]	CLIC1	0.58626837	1.218665711
Guanine nucleotide-binding protein G(i) subunit alpha-1 OS=Homo sapiens GN=GNAI1 PE=1 SV=2 - [GNAI1_HUMAN]	GNAI1	0.55430382	1.097007595
Serpin B5 OS=Homo sapiens GN=SERPINB5 PE=1 SV=2 - [SPB5_HUMAN]	SPB5	0.34743795	0.607487389
Catalase OS=Homo sapiens GN=CAT PE=1 SV=3 - [CATA_HUMAN]	CATA	0.59392428	1.21911949
Ribonucleoside-diphosphate reductase large subunit OS=Homo sapiens GN=RRM1 PE=1 SV=1 - [RIR1_HUMAN]	RIR1	0.30683458	0.532614963
Large neutral amino acids transporter small subunit 1 OS=Homo sapiens GN=SLC7A5 PE=1 SV=2 - [LAT1_HUMAN]	LAT1	0.16852385	0.349642712
Methionine--tRNA ligase, cytoplasmic OS=Homo sapiens GN=MARS PE=1 SV=2 - [SYMC_HUMAN]	SYMC	0.60653073	1.220020066
Polymerase delta-interacting protein 2 OS=Homo sapiens GN=POLDIP2 PE=1 SV=1 - [PDIP2_HUMAN]	PDIP2	0.41333255	0.685463022
Proteasome subunit alpha type-6 OS=Homo sapiens GN=PSMA6 PE=1 SV=1 - [PSA6_HUMAN]	PSA6	0.38445711	0.633345961
Isoleucine--tRNA ligase, cytoplasmic OS=Homo sapiens GN=IARS PE=1 SV=2 - [SYIC_HUMAN]	SYIC	0.65602249	1.415980705
60S ribosomal protein L18 OS=Homo sapiens GN=RPL18 PE=1 SV=2 - [RL18_HUMAN]	RL18	0.62966937	1.288298871
C-1-tetrahydrofolate synthase, cytoplasmic OS=Homo sapiens GN=MTHFD1 PE=1 SV=3 - [C1TC_HUMAN]	C1TC	0.33048898	0.527794677
Histone deacetylase 10 OS=Homo sapiens GN=HDAC10 PE=1 SV=1 - [HDA10_HUMAN]	HDA10	0.39788166	0.63259198
DNA replication licensing factor MCM3 OS=Homo sapiens GN=MCM3 PE=1 SV=3 - [MCM3_HUMAN]	MCM3	0.61207968	1.18605753
Heterogeneous nuclear ribonucleoprotein C-like 2 OS=Homo sapiens GN=HNRNPCL2 PE=2 SV=1 - [HNRC2_HUMAN]	HNRC2	0.60695332	1.139333499
Signal transducer and activator of transcription 3 OS=Homo sapiens GN=STAT3 PE=1 SV=2 - [STAT3_HUMAN]	STAT3	0.64929342	1.305108998
Annexin A2 OS=Homo sapiens GN=ANXA2 PE=1 SV=2 - [ANXA2_HUMAN]	ANXA2	0.51551163	0.846351872
60 kDa heat shock protein, mitochondrial OS=Homo sapiens GN=HSPD1 PE=1 SV=2 - [CH60_HUMAN]	CH60	0.54148591	0.89325964
Heat shock protein 75 kDa, mitochondrial OS=Homo sapiens GN=TRAP1 PE=1 SV=3 - [TRAP1_HUMAN]	TRAP1	0.29650393	0.450566089

Tubulin beta chain OS=Homo sapiens GN=TUBB PE=1 SV=2 - [TBB5_HUMAN]	TBB5	0.61963129	1.142470446
WD repeat-containing protein 1 OS=Homo sapiens GN=WDR1 PE=1 SV=4 - [WDR1_HUMAN]	WDR1	0.4146131	0.618557674
T-complex protein 1 subunit theta OS=Homo sapiens GN=CCT8 PE=1 SV=4 - [TCPQ_HUMAN]	TCPQ	0.45886719	0.699068228
Peptidyl-prolyl cis-trans isomerase B OS=Homo sapiens GN=PPIB PE=1 SV=2 - [PPIB_HUMAN]	PPIB	0.42119876	0.619613249
14-3-3 protein gamma OS=Homo sapiens GN=YWHAG PE=1 SV=2 - [1433G_HUMAN]	1433G	0.43765795	0.634488564
Secretory carrier-associated membrane protein 3 OS=Homo sapiens GN=SCAMP3 PE=1 SV=3 - [SCAM3_HUMAN]	SCAM3	0.65533906	1.220660172
Keratin, type II cuticular Hb6 OS=Homo sapiens GN=KRT86 PE=1 SV=1 - [KRT86_HUMAN]	KRT86	0.37114638	0.519597238
Fructose-bisphosphate aldolase A OS=Homo sapiens GN=ALDOA PE=1 SV=2 - [ALDOA_HUMAN]	ALDOA	0.41098568	0.578953665
F-box only protein 22 OS=Homo sapiens GN=FBXO22 PE=1 SV=1 - [FBX22_HUMAN]	FBX22	0.64930832	1.181936111
Cleavage and polyadenylation specificity factor subunit 7 OS=Homo sapiens GN=CPSF7 PE=1 SV=1 - [CPSF7_HUMAN]	CPSF7	0.63370556	1.105639648
2-oxoglutarate dehydrogenase, mitochondrial OS=Homo sapiens GN=OGDH PE=1 SV=3 - [ODO1_HUMAN]	ODO1	0.59354246	0.951368836
F-actin-capping protein subunit alpha-1 OS=Homo sapiens GN=CAPZA1 PE=1 SV=3 - [CAZA1_HUMAN]	CAZA1	0.65881449	1.18560838
Palladin OS=Homo sapiens GN=PALLD PE=1 SV=3 - [PALLD_HUMAN]	PALLD	0.65947926	1.184933848
Glucose-6-phosphate isomerase OS=Homo sapiens GN=GPI PE=1 SV=4 - [G6PI_HUMAN]	G6PI	0.4467901	0.611929619
Single-stranded DNA-binding protein, mitochondrial OS=Homo sapiens GN=SSBP1 PE=1 SV=1 - [SSBP_HUMAN]	SSBP	0.53708887	0.761722759
Guanine nucleotide-binding protein G(k) subunit alpha OS=Homo sapiens GN=GNAI3 PE=1 SV=3 - [GNAI3_HUMAN]	GNAI3	0.58354533	0.852590139
T-complex protein 1 subunit epsilon OS=Homo sapiens GN=CCT5 PE=1 SV=1 - [TCPE_HUMAN]	TCPE	0.54096836	0.745353117
Prostaglandin E synthase 2 OS=Homo sapiens GN=PTGES2 PE=1 SV=1 - [PGES2_HUMAN]	PGES2	0.6651386	1.098122445
Keratin, type I cuticular Ha1 OS=Homo sapiens GN=KRT31 PE=2 SV=3 - [K1H1_HUMAN]	K1H1	0.37453979	0.452157835
Cofilin-1 OS=Homo sapiens GN=CFL1 PE=1 SV=3 - [COF1_HUMAN]	COF1	0.56003851	0.755673907
Eukaryotic translation elongation factor 1 epsilon-1 OS=Homo sapiens GN=EEF1E1 PE=1 SV=1 - [MCA3_HUMAN]	MCA3	0.6844933	1.128055855
Hornerin OS=Homo sapiens GN=HRNR PE=1 SV=2 - [HORN_HUMAN]	HORN	0.56928355	0.754244865
Serine/arginine-rich splicing factor 1 OS=Homo sapiens GN=SRSF1 PE=1 SV=2 - [SRSF1_HUMAN]	SRSF1	0.64662063	0.950124183
Protein transport protein Sec24C OS=Homo sapiens GN=SEC24C PE=1 SV=3 - [SC24C_HUMAN]	SC24C	0.63349503	0.907177023
Malate dehydrogenase, mitochondrial OS=Homo sapiens GN=MDH2 PE=1 SV=3 - [MDHM_HUMAN]	MDHM	0.55887812	0.709195695
Vinculin OS=Homo sapiens GN=VCL PE=1 SV=4 - [VINC_HUMAN]	VINC	0.40473214	0.452656365
Aspartate--tRNA ligase, cytoplasmic OS=Homo sapiens GN=DARS PE=1 SV=2 - [SYDC_HUMAN]	SYDC	0.70637578	1.175183724
Protein-L-isoaspartate(D-aspartate) O-methyltransferase OS=Homo sapiens GN=PCMT1 PE=1 SV=4 - [PIMT_HUMAN]	PIMT	0.69034308	1.086295761
60S ribosomal protein L12 OS=Homo sapiens GN=RPL12 PE=1 SV=1 - [RL12_HUMAN]	RL12	0.71827245	1.202736449
Nascent polypeptide-associated complex subunit alpha OS=Homo sapiens GN=NACA PE=1 SV=1 - [NACA_HUMAN]	NACA	0.38617033	0.415461718
Annexin A1 OS=Homo sapiens GN=ANXA1 PE=1 SV=2 - [ANXA1_HUMAN]	ANXA1	0.59643072	0.764870719
Keratin, type II cytoskeletal 1 OS=Homo sapiens GN=KRT1 PE=1 SV=6 - [K2C1_HUMAN]	K2C1	0.63792229	0.861893777
Microtubule-associated protein 1B OS=Homo sapiens GN=MAP1B PE=1 SV=2 - [MAP1B_HUMAN]	MAP1B	0.69354868	1.036870111
Poly(rC)-binding protein 1 OS=Homo sapiens GN=PCBP1 PE=1 SV=2 - [PCBP1_HUMAN]	PCBP1	0.6079511	0.760102035
Carbonyl reductase [NADPH] 1 OS=Homo sapiens GN=CBR1 PE=1 SV=3 - [CBR1_HUMAN]	CBR1	0.54006416	0.59994333
Serpin H1 OS=Homo sapiens GN=SERPINH1 PE=1 SV=2 - [SERPH_HUMAN]	SERPH	0.64761192	0.847936961
40S ribosomal protein SA OS=Homo sapiens GN=RPSA PE=1 SV=4 - [RSSA_HUMAN]	RSSA	0.71979862	1.116177859
Heat shock protein HSP 90-beta OS=Homo sapiens GN=HSP90AB1 PE=1 SV=4 - [HS90B_HUMAN]	HS90B	0.73102397	1.169440417
Desmoplakin OS=Homo sapiens GN=DSP PE=1 SV=3 - [DESP_HUMAN]	DESP	0.74877942	1.259614618
7-dehydrocholesterol reductase OS=Homo sapiens GN=DHCR7 PE=1 SV=1 - [DHCR7_HUMAN]	DHCR7	0.71835762	1.101586133
T-complex protein 1 subunit beta OS=Homo sapiens GN=CCT2 PE=1 SV=4 - [TCPB_HUMAN]	TCPB	0.75569451	1.228478849
Succinyl-CoA:3-ketoacid coenzyme A transferase 1, mitochondrial OS=Homo sapiens GN=OXCT1 PE=1 SV=1 - [SCOT1_HUMAN]	SCOT1	0.60409498	0.680895843
60S ribosomal protein L27 OS=Homo sapiens GN=RPL27 PE=1 SV=2 - [RL27_HUMAN]	RL27	0.71770453	1.033389985
40S ribosomal protein S25 OS=Homo sapiens GN=RPS25 PE=1 SV=1 - [RS25_HUMAN]	RS25	0.74574256	1.141464353
Triosephosphate isomerase OS=Homo sapiens GN=TPI1 PE=1 SV=3 - [TPIS_HUMAN]	TPIS	0.62794644	0.71455233
Tubulin beta-4B chain OS=Homo sapiens GN=TUBB4B PE=1 SV=1 - [TBB4B_HUMAN]	TBB4B	0.62186915	0.69957348
Lysine--tRNA ligase OS=Homo sapiens GN=KARS PE=1 SV=3 - [SYK_HUMAN]	SYK	0.68706656	0.852195973
Lipoprotein lipase OS=Homo sapiens GN=LPL PE=1 SV=1 - [LIPL_HUMAN]	LIPL	0.75750875	1.149080423
HLA class I histocompatibility antigen, B-51 alpha chain OS=Homo sapiens GN=HLA-B PE=1 SV=1 - [1B51_HUMAN]	1B51	0.42009485	0.36007599
Filaggrin-2 OS=Homo sapiens GN=FLG2 PE=1 SV=1 - [FILA2_HUMAN]	FILA2	0.62115854	0.6468984
Elongation factor 2 OS=Homo sapiens GN=EEF2 PE=1 SV=4 - [EF2_HUMAN]	EF2	0.77235121	1.190269989
40S ribosomal protein S26 OS=Homo sapiens GN=RPS26 PE=1 SV=3 - [RS26_HUMAN]	RS26	0.74281198	1.014306028

Protein disulfide-isomerase A6 OS=Homo sapiens GN=PDIA6 PE=1 SV=1 - [PDIA6_HUMAN]	PDIA6	0.78424138	1.229492801
Elongation factor 1-alpha 1 OS=Homo sapiens GN=EEF1A1 PE=1 SV=1 - [EF1A1_HUMAN]	EF1A1	0.76924706	1.114749957
GTP-binding nuclear protein Ran OS=Homo sapiens GN=RAN PE=1 SV=3 - [RAN_HUMAN]	RAN	0.75725663	1.044285802
Thioredoxin reductase 1, cytoplasmic OS=Homo sapiens GN=TXNRD1 PE=1 SV=3 - [TRXR1_HUMAN]	TRXR1	0.77752733	1.147894501
Galectin-3-binding protein OS=Homo sapiens GN=LGALS3BP PE=1 SV=1 - [LG3BP_HUMAN]	LG3BP	0.77144569	1.11119444
L-lactate dehydrogenase B chain OS=Homo sapiens GN=LDHB PE=1 SV=2 - [LDHB_HUMAN]	LDHB	0.67996049	0.72214853
Collagen alpha-1(VIII) chain OS=Homo sapiens GN=COL8A1 PE=1 SV=2 - [CO8A1_HUMAN]	CO8A1	0.75314224	0.976013674
Microtubule-associated protein 4 OS=Homo sapiens GN=MAP4 PE=1 SV=3 - [MAP4_HUMAN]	MAP4	0.73033792	0.87513273
Annexin A5 OS=Homo sapiens GN=ANXA5 PE=1 SV=2 - [ANXA5_HUMAN]	ANXA5	0.79071581	1.141973074
Junction plakoglobin OS=Homo sapiens GN=JUP PE=1 SV=3 - [PLAK_HUMAN]	PLAK	0.79230058	1.138007819
14-3-3 protein zeta/delta OS=Homo sapiens GN=YWHAZ PE=1 SV=1 - [1433Z_HUMAN]	1433Z	0.71596527	0.780139158
Proteasome subunit alpha type-7 OS=Homo sapiens GN=PSMA7 PE=1 SV=1 - [PSA7_HUMAN]	PSA7	0.79788941	1.108739262
Keratin, type II cytoskeletal 4 OS=Homo sapiens GN=KRT4 PE=1 SV=4 - [K2C4_HUMAN]	K2C4	0.5790385	0.455494971
Alpha-actinin-1 OS=Homo sapiens GN=ACTN1 PE=1 SV=2 - [ACTN1_HUMAN]	ACTN1	0.80181926	1.084195559
Transportin-1 OS=Homo sapiens GN=TNPO1 PE=1 SV=2 - [TNPO1_HUMAN]	TNPO1	0.80804759	1.079990617
Glutathione S-transferase P OS=Homo sapiens GN=GSTP1 PE=1 SV=2 - [GSTP1_HUMAN]	GSTP1	0.75928891	0.830461741
T-complex protein 1 subunit zeta OS=Homo sapiens GN=CCT6A PE=1 SV=3 - [TCPZ_HUMAN]	TCPZ	0.81152755	1.059308788
Glucose-6-phosphate 1-dehydrogenase OS=Homo sapiens GN=G6PD PE=1 SV=4 - [G6PD_HUMAN]	G6PD	0.81647205	1.079374489
Clathrin heavy chain 1 OS=Homo sapiens GN=CLTC PE=1 SV=5 - [CLH1_HUMAN]	CLH1	0.79535979	0.950273579
Annexin A3 OS=Homo sapiens GN=ANXA3 PE=1 SV=3 - [ANXA3_HUMAN]	ANXA3	0.77714354	0.854669435
U2 small nuclear ribonucleoprotein A' OS=Homo sapiens GN=SNRPA1 PE=1 SV=2 - [RU2A_HUMAN]	RU2A	0.79543227	0.937984724
Histone deacetylase 6 OS=Homo sapiens GN=HDAC6 PE=1 SV=2 - [HDAC6_HUMAN]	HDAC6	0.82432789	1.087519528
60S ribosomal protein L11 OS=Homo sapiens GN=RPL11 PE=1 SV=2 - [RL11_HUMAN]	RL11	0.83718419	1.156734388
Tubulin alpha-1C chain OS=Homo sapiens GN=TUBA1C PE=1 SV=1 - [TBA1C_HUMAN]	TBA1C	0.19303416	0.11759222
Phenylalanine--tRNA ligase alpha subunit OS=Homo sapiens GN=FARSA PE=1 SV=3 - [SYFA_HUMAN]	SYFA	0.83705473	1.067372827
Peroxiredoxin-2 OS=Homo sapiens GN=PRDX2 PE=1 SV=5 - [PRDX2_HUMAN]	PRDX2	0.81307936	0.915036492
Emerin OS=Homo sapiens GN=EMD PE=1 SV=1 - [EMD_HUMAN]	EMD	0.84768236	1.13337495
LanC-like protein 1 OS=Homo sapiens GN=LANCL1 PE=1 SV=1 - [LANC1_HUMAN]	LANC1	0.80951667	0.881835078
26S proteasome non-ATPase regulatory subunit 1 OS=Homo sapiens GN=PSMD1 PE=1 SV=2 - [PSMD1_HUMAN]	PSMD1	0.83400893	1.021983707
Ezrin OS=Homo sapiens GN=EZR PE=1 SV=4 - [EZRI_HUMAN]	EZRI	0.82095945	0.883863518
Ubiquitin-like protein ISG15 OS=Homo sapiens GN=ISG15 PE=1 SV=5 - [ISG15_HUMAN]	ISG15	0.82079071	0.870252782
Alpha-actinin-4 OS=Homo sapiens GN=ACTN4 PE=1 SV=2 - [ACTN4_HUMAN]	ACTN4	0.8629458	1.162253814
Phosphate carrier protein, mitochondrial OS=Homo sapiens GN=SLC25A3 PE=1 SV=2 - [MPCP_HUMAN]	MPCP	0.85301244	1.067929972
Protein transport protein Sec61 subunit beta OS=Homo sapiens GN=SEC61B PE=1 SV=2 - [SC61B_HUMAN]	SC61B	0.85974902	1.016589459
Desmoglein-1 OS=Homo sapiens GN=DSG1 PE=1 SV=2 - [DSG1_HUMAN]	DSG1	0.84409022	0.883486634
Aminoacyl tRNA synthase complex-interacting multifunctional protein 2 OS=Homo sapiens GN=AIMP2 PE=1 SV=2 - [AIMP2_HUMAN]	AIMP2	0.85846728	0.958553513
Phosphoglycerate kinase 1 OS=Homo sapiens GN=PGK1 PE=1 SV=3 - [PGK1_HUMAN]	PGK1	0.86094272	0.897523259
Cell division control protein 42 homolog OS=Homo sapiens GN=CDC42 PE=1 SV=2 - [CDC42_HUMAN]	CDC42	0.90424842	0.961216456
Rho GDP-dissociation inhibitor 1 OS=Homo sapiens GN=ARHGDIA PE=1 SV=3 - [GDIR1_HUMAN]	GDIR1	0.91743696	1.013352512
Peptidyl-prolyl cis-trans isomerase A OS=Homo sapiens GN=PPIA PE=1 SV=2 - [PPIA_HUMAN]	PPIA	0.91156214	0.922416244
Dermcidin OS=Homo sapiens GN=DCD PE=1 SV=2 - [DCD_HUMAN]	DCD	0.915416	0.948884709
Elongation factor Tu, mitochondrial OS=Homo sapiens GN=TUFM PE=1 SV=2 - [EFTU_HUMAN]	EFTU	0.92033321	0.976743739
D-3-phosphoglycerate dehydrogenase OS=Homo sapiens GN=PHGDH PE=1 SV=4 - [SERA_HUMAN]	SERA	0.92613137	1.050268379
Keratin, type I cytoskeletal 9 OS=Homo sapiens GN=KRT9 PE=1 SV=3 - [K1C9_HUMAN]	K1C9	0.9270305	1.037118205
Heat shock protein HSP 90-alpha OS=Homo sapiens GN=HSP90AA1 PE=1 SV=5 - [HS90A_HUMAN]	HS90A	0.9250654	0.963735625
Sarcoplasmic/endoplasmic reticulum calcium ATPase 2 OS=Homo sapiens GN=ATP2A2 PE=1 SV=1 - [AT2A2_HUMAN]	AT2A2	0.9510445	0.97440195
Elongation factor 1-gamma OS=Homo sapiens GN=EEF1G PE=1 SV=3 - [EF1G_HUMAN]	EF1G	0.95536131	0.982077325
Rab GDP dissociation inhibitor beta OS=Homo sapiens GN=GDI2 PE=1 SV=2 - [GDIB_HUMAN]	GDIB	0.95968509	1.012138902
T-complex protein 1 subunit alpha OS=Homo sapiens GN=TCP1 PE=1 SV=1 - [TCPA_HUMAN]	TCPA	0.95989448	0.97336327
26S proteasome non-ATPase regulatory subunit 3 OS=Homo sapiens GN=PSMD3 PE=1 SV=2 - [PSMD3_HUMAN]	PSMD3	0.96060973	0.969215162
Keratin, type II cytoskeletal 6A OS=Homo sapiens GN=KRT6A PE=1 SV=3 - [K2C6A_HUMAN]	K2C6A	0.96183759	0.976063288
Translational activator GCN1 OS=Homo sapiens GN=GCN1L1 PE=1 SV=6 - [GCN1L_HUMAN]	GCN1L	0.9628855	0.976749206
Vesicle-trafficking protein SEC22b OS=Homo sapiens GN=SEC22B PE=1 SV=4 - [SC22B_HUMAN]	SC22B	0.97020113	1.022500836
Tubulin alpha-4A chain OS=Homo sapiens GN=TUBA4A PE=1 SV=1 - [TBA4A_HUMAN]	TBA4A	0.96906078	0.975549538

Hepatocyte growth factor receptor OS=Homo sapiens GN=MET PE=1 SV=4 - [MET_HUMAN]	MET	0.97391498	1.003859664
L-lactate dehydrogenase A chain OS=Homo sapiens GN=LDHA PE=1 SV=2 - [LDHA_HUMAN]	LDHA	0.9819358	1.013311145
Alpha-globin transcription factor CP2 OS=Homo sapiens GN=TFCP2 PE=1 SV=2 - [TFCP2_HUMAN]	TFCP2	0.98222518	1.009385404
Endoplasmin OS=Homo sapiens GN=HSP90B1 PE=1 SV=1 - [ENPL_HUMAN]	ENPL	0.98475915	1.00963962
Keratin, type II cytoskeletal 6B OS=Homo sapiens GN=KRT6B PE=1 SV=5 - [K2C6B_HUMAN]	K2C6B	0.98542249	0.990657468
Histone H3.1 OS=Homo sapiens GN=HIST1H3A PE=1 SV=2 - [H31_HUMAN]	H31	0.98936349	0.993920553
Ras-related protein Rab-10 OS=Homo sapiens GN=RAB10 PE=1 SV=1 - [RAB10_HUMAN]	RAB10	0.99242854	0.99921296

Appendix 3

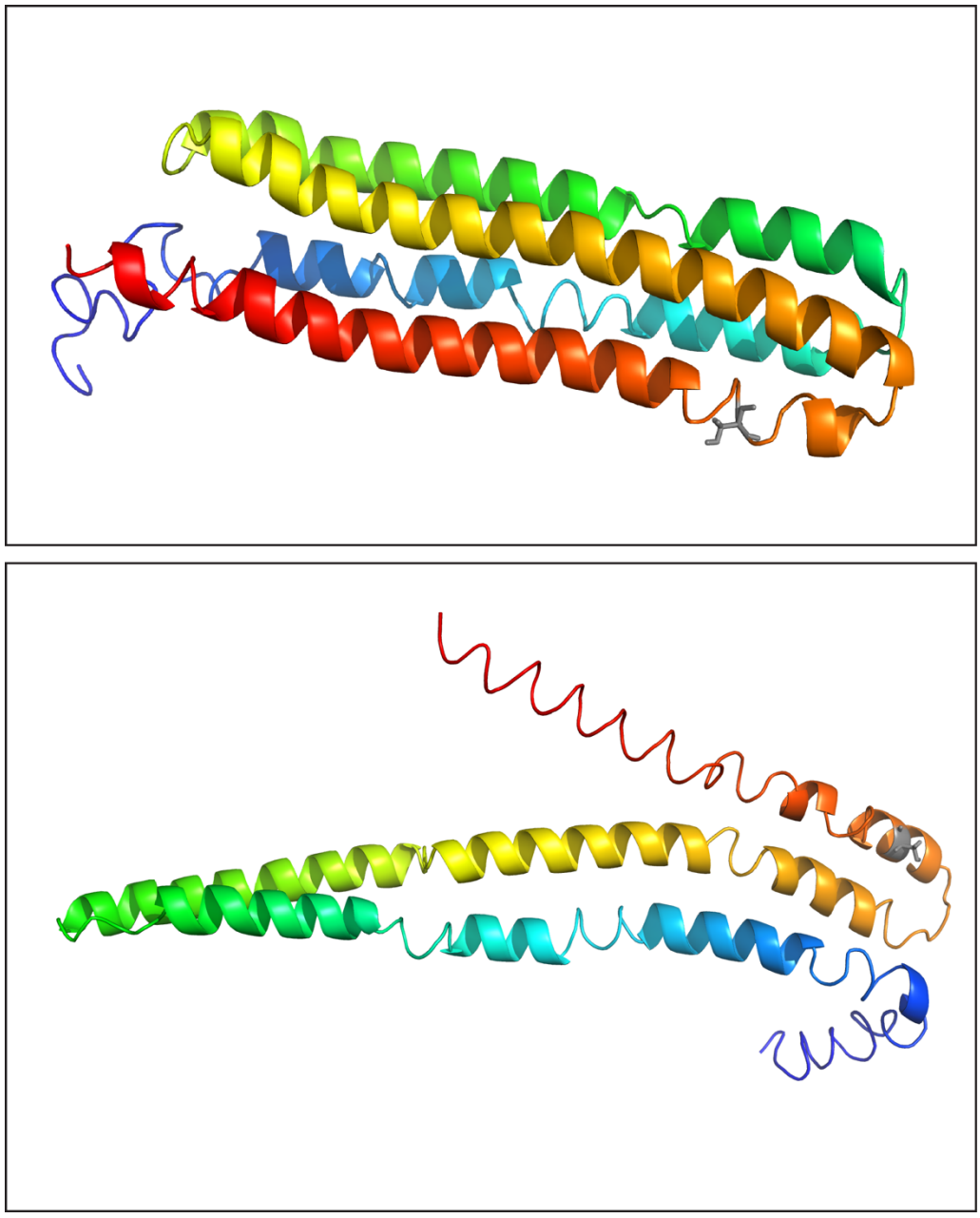

Figure A1: Two models of the 3D structure of TPD54. Upper model shows the protein with four helices, and potentially two sets of coiled-coil regions. The lower model shows two helices and one coiled-coil region. Blue is N-terminal and red is C-terminal region. Grey fragment shows the localisation of the potential phosphoserine.

Appendix 4